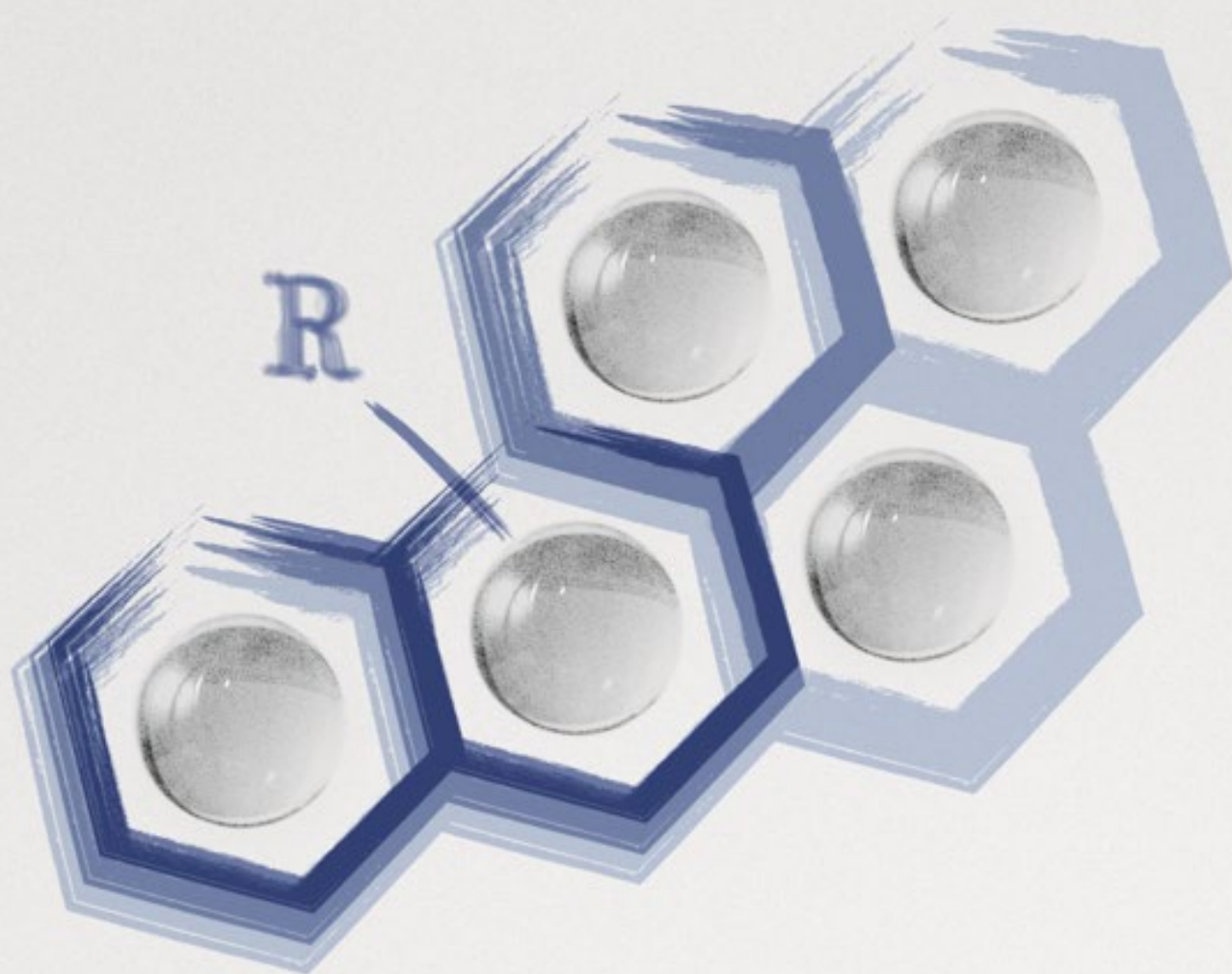


The effects of alkyl substitution on  
metabolism and resulting toxicities  
of Polycyclic Aromatic Hydrocarbons

# PAHs

that may be present in mineral oils



---

DANLEI WANG

## **Propositions**

1. The increased chances on side chain oxidation in alkyl substituted aromatic hydrocarbons do not result in reduced toxicity.  
(this thesis)
2. The use of new approach methodologies (NAMs) will drive the future hazard and risk assessment of mineral oil aromatic hydrocarbons (MOAH).  
(this thesis)
3. Strategies to efficiently reduce over-population receive insufficient scientific attention.
4. Climate change will improve social and international cooperation.
5. The fear of corona virus is more harmful than the virus itself.
6. Observing cats is a good source of creativity.

Propositions belonging to the thesis, entitled

The effects of alkylation substitution on metabolism and resulting toxicities of Polycyclic Aromatic Hydrocarbons (PAHs) that may be present in mineral oils

Danlei Wang  
Wageningen, 28 February 2022

**The effects of alkyl substitution on metabolism and  
resulting toxicities of Polycyclic Aromatic Hydrocarbons  
(PAHs) that may be present in mineral oils**

**Danlei Wang**

**Thesis committee****Promotors**

Prof. Dr I.M.C.M. Rietjens

Professor of Toxicology

Wageningen University & Research

Prof. Dr P.J. Boogaard

Special Professor, Environmental Health & Human Biomonitoring of Contaminants

Wageningen University & Research

Global Discipline Lead & Manager, Toxicology, Shell Health - Global Risk Sciences Team, SI-SHG/PT

Shell International B.V., The Hague

**Other Members:**

Dr J. Louisse, Wageningen University & Research

Dr J.C. Carrillo Palaez, Shell International B.V., The Hague

Prof. Dr A.A. Koelmans, Wageningen University & Research

Prof. Dr H. van Loveren, Maastricht University

This research was conducted under the auspices of the Graduate School VLAG (Advanced studies in Food Technology, Agrobiotechnology, Nutrition and Health Sciences)

**The effects of alkyl substitution on metabolism and  
resulting toxicities of Polycyclic Aromatic Hydrocarbons  
(PAHs) that may be present in mineral oils**

**Danlei Wang**

**Thesis**

submitted in fulfilment of the requirement for the degree of doctor

at Wageningen University

by the authority of the Rector Magnificus

Prof. Dr A.P.J. Mol,

in the presence of the

Thesis Committee appointed by the Academic Board

to be defended in public

on Monday 28 February 2022

at 4 p.m. in the Aula.

Danlei Wang

The effects of alkyl substitution on metabolism and resulting toxicities of Polycyclic Aromatic Hydrocarbons (PAHs) that may be present in mineral oils,

278 pages

PhD thesis, Wageningen University, Wageningen, NL (2022)

With references, with summary in English

DOI: <https://doi.org/10.18174/559251>

ISBN: 978-94-6447-049-9

# Table of Contents

<b>Chapter 1</b>	General Introduction .....	6
<b>Chapter 2</b>	In vitro metabolism of naphthalene and its alkylated congeners by human and rat liver microsomes via alkyl side chain or aromatic oxidation .....	48
<b>Chapter 3</b>	The effect of alkyl substitution on the oxidative metabolism and mutagenicity of phenanthrene .....	80
<b>Chapter 4</b>	The influence of alkyl substitution on the in vitro metabolism and mutagenicity of benzo[a]pyrene .....	132
<b>Chapter 5</b>	Predicting the in vivo developmental toxicity of benzo[a]pyrene (B[a]P) in rats by an in vitro-in silico approach .....	176
<b>Chapter 6</b>	General discussion and future perspectives .....	230
<b>Chapter 7</b>	Summary .....	264
<b>Appendix</b>	.....	270



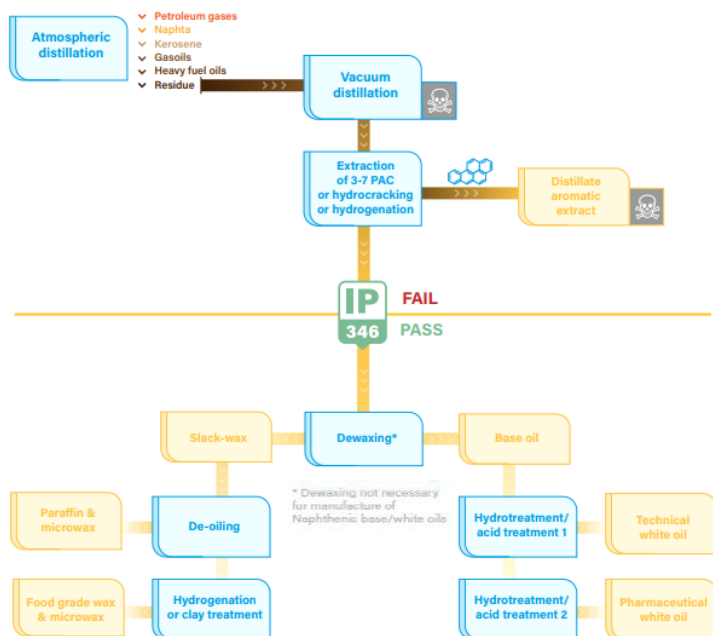


# **Chapter 1**

## **General introduction**

## 1.1 Mineral oil

Petroleum derived mineral oils are produced from crude oil through atmospheric and vacuum distillation at temperatures between 300°C and 600°C (IARC 1984, Concawe 2012) (**Figure 1**). The presence of 3- to 7-ring Polycyclic Aromatic Compounds (PACs) in mineral oils may lead to potentially genotoxic compounds and induce carcinogenicity (Mackerer, Griffis et al. 2003). The presence of undesirable carcinogenic PACs is therefore reduced or fully eliminated from mineral oils by refining processes, such as acid treatment, solvent extraction or catalytic hydrotreatment. The efficacy of these processes can be examined by the IP346 method (Concawe 1994, Carrillo, van der Wiel et al. 2019). The remaining aromatics in the refined mineral oils are highly alkylated 1- to 2-ring compounds that are generally considered safe for use in consumer products. Mineral oil applications in food production or in pharmaceuticals or cosmetic products use such highly refined and non-carcinogenic mineral oils, which are generally referred to as highly refined base oils (HRBOs) or white mineral oils and contain extremely low levels of aromatics. Mineral oils are UVCBs (substances of Unknown or Variable composition, Complex reaction products and Biological materials) by EU law (ECHA 2011) since they are constituted by large numbers of hydrocarbons. The actual composition of mineral oils varies, depending on the source of the oil and the manufacturing processes to yield the required physico-chemical specifications. The hydrocarbons in mineral oils could be described as PINA: Paraffin, Iso-Paraffin, Naphthenic or Aromatic, in other words, normal, iso- and cycloalkanes or aromatics. More specifically, paraffin and iso-paraffin are branched and unbranched alkanes; naphthenes consist of cycloalkanes, mainly cyclopentanes and cyclohexanes, alkylated and non-alkylated, mono-, di- and higher saturated ring systems; aromatics include non-substituted and alkyl-substituted mono-, di- and higher aromatic ring systems.



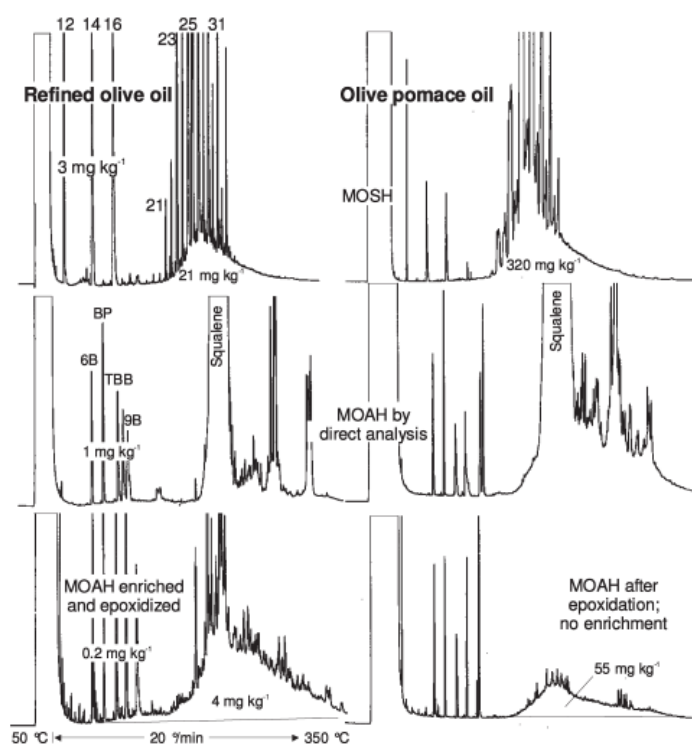
**Figure 1.** Mineral oil production process from crude oil (Concawe 2012, Carrilo, van der Wiel et al. 2019)

## 1.2 Mineral oil hydrocarbons

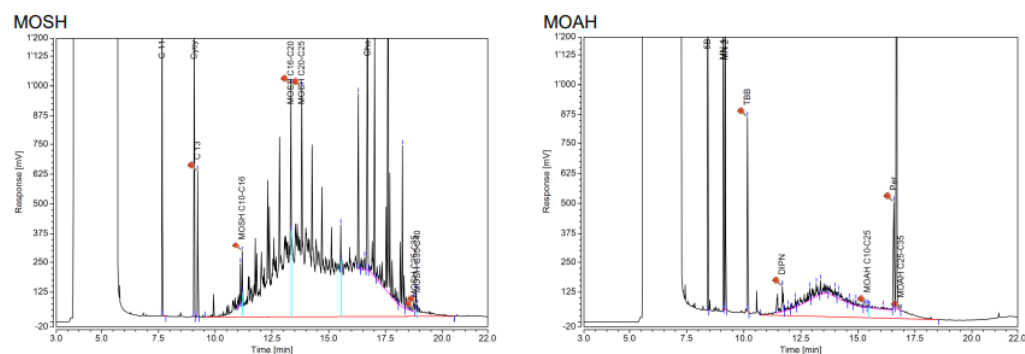
The consumption of mineral oil hydrocarbons via food and other sources is a potential safety issue (EFSA 2012). Although mineral oil applications in foods are regulated by the Joint FAO/WHO Expert Committee on Food Additives (JECFA) and European Food Safety Agency (EFSA) (JECFA 1995, Regulation 2010, Regulation 2011), mineral oil hydrocarbons present in food could originate from contamination or from mineral oils intentionally used in food production. Mineral oil hydrocarbons are hydrocarbons containing 10 to about 50 carbon atoms that do not include the naturally occurring hydrocarbons in food, nor polyolefin oligomeric hydrocarbons from plastic packaging or synthetic isoparaffins with short and long side chains (Bratinova 2019). The terminology of ‘mineral oil saturated hydrocarbons’ (MOSH) and ‘mineral oil aromatic hydrocarbons’ (MOAH) was defined based on chromatographic analyses. The terms do not



2019). Chromatographic analysis of MOSH/MOAH in food was proposed with a method based on sample epoxidation and/or enrichment followed with an online-LC-GC-FID measurement (Biedermann, Fiselier et al. 2009). Based on this method, total levels of MOSH/MOAH in edible oil and food samples contaminated with mineral oil could be characterized (**Figure 3**). JRC presented examples of MOSH/MOAH chromatograms obtained from online LC-GC analysis in rice samples with levels of 7.8mg/kg and 1.6mg/kg for total MOSH and MOAH (**Figure 4**).



**Figure 3.** Chromatograms of mineral oil contaminated samples of refined olive oil and olive pomace oil that show detection of MOSH and MOAH (Biedermann, Fiselier et al. 2009).



**Figure 4.** Chromatograms of MOSH/MOAH analysis with LC-GC in rice sample from JRC guideline (Bratinova 2019)

The MOAH fraction consists mainly of substituted aromatic hydrocarbons (Grob, Biedermann et al. 1991), but may also comprise unsubstituted polycyclic aromatic hydrocarbons (PAHs), some of which are also potential genotoxic carcinogens. This thesis focuses on compounds that may be present in MOAH since MOAH was prioritized over MOSH by the National Institute for Public Health and the Environment (RIVM) based on their potential mutagenic and carcinogenic properties.

### 1.3 Occurrence of MOAH

The presence of mineral oil in food may originate from intentional use in the food production or environmental contamination. The main sources of mineral oil presence in foods identified by EFSA include food contact materials, contaminants, food additives, processing aids, pesticides, and other uses. Quantification of MOAH in food samples indicated a background exposure to MOAH accounting for 15-30 % of the total mineral oil hydrocarbons (EFSA 2012). Sunflower oil originating from Ukraine adulterated with high levels of mineral oils as a food fraud raised concerns of public health upon consumption of mineral oil in foods. Analytical measurement of 18 adulterated sunflower oil samples indicated 17 to 37 % MOAH of the total hydrocarbons present

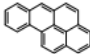
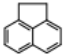
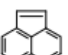
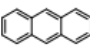
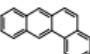
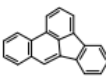
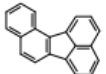
(Biedermann and Grob 2009). Among the 18 samples, remarkably high concentration of MOAH, with 1800mg/kg sample, was found in the most contaminated adulterated sunflower oil sample. From the survey studies on mineral oil in foods in two Member States, 4.5 mg/kg and 17 mg/kg MOAH was found in noodles as average and maximum concentration, respectively (EFSA 2012). Food surveys published by Foodwatch in 2015 and 2016 indicated the presence of MOAH ranging from 0.6 to 1.5 mg/kg in a series of food stuffs, including cereal products, cacao powder, chocolate products, pasta, and rice sampled from France, the Netherlands, and Germany (Foodwatch 2015, Foodwatch 2016, Foodwatch 2016). According to Foodwatch, MOAH was detected in 8 out of the 16 samples of infant and follow-up formula in France, the Netherlands, and Germany in a range of 0.5-3.0 mg/kg (Foodwatch 2019). A study conducted in China also reported that 7 out of 51 infant formula samples contained MOAH, with concentrations of 0.8 to 1.7 mg/kg (Sui, Gao et al. 2020). A Belgian market survey of mineral oil in food showed that 23 out 217 packed food samples contained high concentration of MOAH, ranging from 0.6 to 2.24 mg/kg (Van Heyst, Vanlancker et al. 2018). Edible oils were also reported to contain MOAH such as cocoa butter, sunflower oil and palm oil (Stauff, Schnapka et al. 2020). A survey from Food Standards Australia New Zealand (FSANZ) suggested that MOAH in food packaging was detected with concentrations ranging from 11 to 9600 mg/kg in 90% of the 56 samples analyzed, while 92% of these 56 food samples contained MOAH at or lower than the Limit of Quantification (LOQ) of 10 mg/kg (FSANZ 2018).

#### **1.4 Current risk assessment on MOAH**

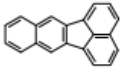
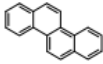
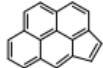
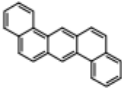
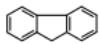
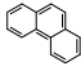
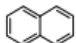
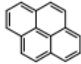

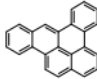
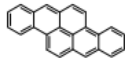
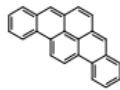
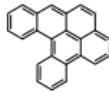
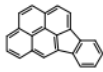
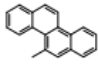
The aromatic hydrocarbons in the food chain that have been studied and evaluated are generally pyrogenic PAHs that can be formed at higher temperatures and during combustion (EFSA 2008). Some PAHs are known to be genotoxic carcinogens in experimental animals and have been listed

as priority aromatic hydrocarbons for risk assessment upon dietary consumption in human by the Scientific Committee on Food (SCF) (**Table 1**). In contrast, the PAHs present in petroleum-derived products, including mineral oils, are typically highly alkylated, and referred to as petrogenic PAHs. Petrogenic PAHs are currently barely studied (Concawe 2017). The petrogenic PAHs in food which are not alkylated ('naked') or only methylated are potentially mutagenic and carcinogenic as suggested by EFSA (2012). The possible genotoxicity and carcinogenicity of MOAH and its occurrence in foods makes it an emerging topic of concern in modern food safety.

**Table 1.** PAHs that were selected by the SCF, the Grimmer Institute and EPA with cancer classification according to IARC (Boogaard 2012).

Name	IARC classification	SCF	Grimmer	EPA	Structure
Benzo[ <i>a</i> ]pyrene	1	+	+	+	
Acenaphthene	3	-	—	+	
Acenaphthylene	-	-	—	+	
Anthracene	3	-	+	+	
Benz[ <i>a</i> ]anthracene	2B	+	+	+	
Benzo[ <i>b</i> ]fluoranthrene	2B	+	+	+	
Benzo[ <i>j</i> ]fluoranthrene	2B	+	+	-	



Benzo[k]fluoranthrene	2B	+	+	+	
Chrysene	2B	+	+	+	
Cyclopenta[cd]pyrene	2A	+	+	-	
Dibenz[a,h]anthracene	2A	+	+	+	
Fluorene	3	-	-	+	
Phenanthrene	3	-	+	+	
Naphthalene	2B	-	-	+	
Pyrene	3	-	+	+	
Benzo[g,h,i]perylene	3	+	+	+	
Dibenzo[a,e]pyrene	3	+	-	-	
Dibenzo[a,h]pyrene	2B	+	-	-	
dibenzo[a,i]pyrene	2B	+	-	-	
dibenzo[a,l]pyrene	2A	+	-	-	
Indeno[1,2,3-cd]pyrene	2B	+	+	+	
5-Methyl-chrysene	2B	+	-	-	

Limited comparable studies on the Absorption, Distribution, Metabolism and Excretion (ADME) of non-alkylated and related methylated PAHs in experimental animals or human have been reported. Phenanthrene, anthracene, benzo[a]pyrene (B[a]P) and 2,6-dimethylnaphthalene (DMN), 7,12-dimethylbenz[a]anthracene (DMBA) are readily absorbed through the intestine of rats (Laher, Rigler et al. 1984, Rahman, Barrowman et al. 1986) indicating that methyl substitution of these PAH has limited influence on their gastrointestinal absorption. PAHs are highly lipophilic compounds that distribute over all lipid-rich tissues (IPCS 1998). Similarly, in another study substituted PAHs including 1,6-DMN and 7,12-DMBA were shown to distribute into adipose tissue, liver, kidney and other examined tissues (Flesher 1967, Kilanowicz, Sapota et al. 2002). It is expected that a similar distribution pattern will be observed for other alkylated aromatic hydrocarbons. Metabolic activation of aromatic hydrocarbons to reactive metabolites is essential for their genotoxic and potentially carcinogenic effects as well as their developmental toxicity. Metabolic studies on some short-chain alkylated naphthalene and 7,12-DMBA suggested that short-chain alkylated MOAH are metabolized by cytochrome P450 (CYP) enzymes via alkyl side chain hydroxylation to alcoholic metabolites and/or aromatic ring oxidation to phenols and diols. Some of the formed metabolites reflect bioactivation and are involved in the toxicities of the alkyl substituted PAHs. For example, the 3,4-dihydrodiol of 7,12-DMBA was proved to be a proximate carcinogenic metabolite in rodents (Wislocki, Gadek et al. 1980). The metabolites from CYP mediated metabolism can be subsequently conjugated via glucuronidation and sulfation and excreted via urine and feces.

Genotoxicity of mineral oil can be assessed with the so-called modified Ames test that was specially developed to test the mutagenicity of petroleum-derived base oils, which are essentially mineral oils (Blackburn, Deitch et al. 1986, Concawe 2012, ASTM 2014). Mineral oils are

extracted with DMSO to concentrate the polycyclic organic compounds into the DMSO prior to the reverse mutation assay (Natusch and Tomkins 1978). Studies on mineral oil extracts and mineral oil fractions in the modified Ames test and DNA adduct formation suggested that the genotoxicity of petroleum substances is mainly induced by 3- to 7-ring aromatics (Roy, Johnson et al. 1988, Ingram, Scammells et al. 1994, Ingram, Phillips et al. 1995, Ingram, Phillips et al. 2000, Mackerer, Griffis et al. 2003). Dermal carcinogenicity induced by mineral oil has been demonstrated in mouse skin painting assay (Twort and Twort 1931, Smith, Sunderland et al. 1951, Roy, Johnson et al. 1988, Blackburn, Roy et al. 1996). A highly significant correlation was found between the mutagenicity index (MI) and dermal carcinogenicity in mouse skin-painting bioassays (Concawe 2012), therefore the modified Ames test is considered a predictive indicator for carcinogenic petroleum derived products.

Since MOAH is not a distinct chemical entity, dose-response data for carcinogenicity via oral route exposure cannot be obtained. Current hazard evaluation of the MOAH fraction is based on the carcinogenicity observed for individual non-alkylated PAHs and alkylated PAHs via inhalation and oral exposure in experimental animals. Several in vivo studies on the carcinogenicity of non-substituted PAHs in experimental animals are available. For a number of them IARC considered the available evidence sufficient to classify them as probable (IARC Class 2A) or possible (IARC Class 2B) carcinogens, including Benz[a]anthracene (BaA), benzo[b]fluoranthene, benzo[j]fluoranthene benzo[k]fluoranthene, chrysene (CHR), cyclopenta[cd]pyrene, dibenz[a,h]anthracene, dibenzo[a,h]pyrene, dibenzo[a,i]pyrene, dibenzo[a,l]pyrene, indeno[1,2,3-cd]pyrene (IP) and 5-methyl-chrysene (**Table 1**). In addition, B[a]P was classified as a human carcinogen (IARC Class I). Some evidence for carcinogenic potential of alkylated aromatic hydrocarbons has been summarized in **Table 2**.

In addition, developmental toxicity is of concern for some petroleum substances associated with the presence of PACs, in particular polycyclic aromatic hydrocarbons (PAHs), in these products. Heavy and poorly refined petroleum substances, with a substantial amount of 3- to 7-ring PAHs are able to induce developmental toxicity in experimental animals (Feuston and Mackerer , Feuston, Kerstetter et al. 1989, Feuston, Low et al. 1994, Hoberman, Christian et al. 1995, Feuston, Hamilton et al. 1996). In contrast, petroleum substances containing no PAHs and no aromatics, e.g. highly refined base oil (HRBO) and synthetic analogues of petroleum substances such as gas-to-liquid (GTL) products tested negative in prenatal development toxicity studies (Mobil 1987, Boogaard, Carrillo et al. 2017). Thus, developmental toxicity as observed with some heavier petroleum substances has been associated with the presence of mainly 3- to 7-ring polycyclic aromatic hydrocarbons (PAHs), in these products (Murray, Roth Rn Fau - Nicolich et al. , Tsitou, Heneweer et al. 2015, Kamelia, Louisse et al. 2017).

**Table 2.** An overview of in vivo studies of alkylated aromatic hydrocarbons that showed carcinogenic potential in experimental animals

Compound	Species	Exposure	Dose	Cancer endpoint	Reference
1-methylnaphthalene	Male B6C3F1 mice	81 weeks diet	0, 750, 1500 mg/kg	Lung adenomas and adenocarcinoma (benign)	(Murata, Denda et al. 1993)
2-methylnaphthalene	Male B6C3F1 mice	81 weeks diet	0, 750, 1500 mg/kg	Lung adenomas and carcinoma (benign)	(Murata, Denda et al. 1997)
1,4-dimethylphenanthrene	CrI:CD/1 (ICR)BR mice	10 days skin	0.3mg	Skin tumor initiator	(LaVoie, Bedenko et al. 1982)
4,10-dimethylphenanthrene					
7-methylbenzanthracene; 8-methylbenzanthracene; 12-methylbenzanthracene; 6-methylbenzanthracene; 9-methylbenzanthracene; 7,12-DMBA	CrI: CD-1 mice	21 weeks skin	7, 24, 97µg*	Skin tumor initiator	(Wislocki, Fiorentini et al. 1982)
7,12-DMBA	hr/hr Oslo mice	80weeks skin	51.2µg	Skin tumor initiator	(Iversen 1989)
1-Methyl-B[a]P; 2-Methyl-B[a]P; 3-Methyl-B[a]P; 4-Methyl-B[a]P; 5-Methyl-B[a]P; 6-Methyl-B[a]P; 11-Methyl-B[a]P; 12-Methyl-B[a]P;	Female Sencar mice	15weeks Skin	53µg*	Skin tumor initiator	(Iyer, Lyga et al. 1980)
1,2-Dimethyl-B[a]P 1,6-Dimethyl-B[a]P 3,6-Dimethyl-B[a]P 4,5-Dimethyl-B[a]P					

\*marked doses were recalculated as mass (µg) from the moles (nmol)

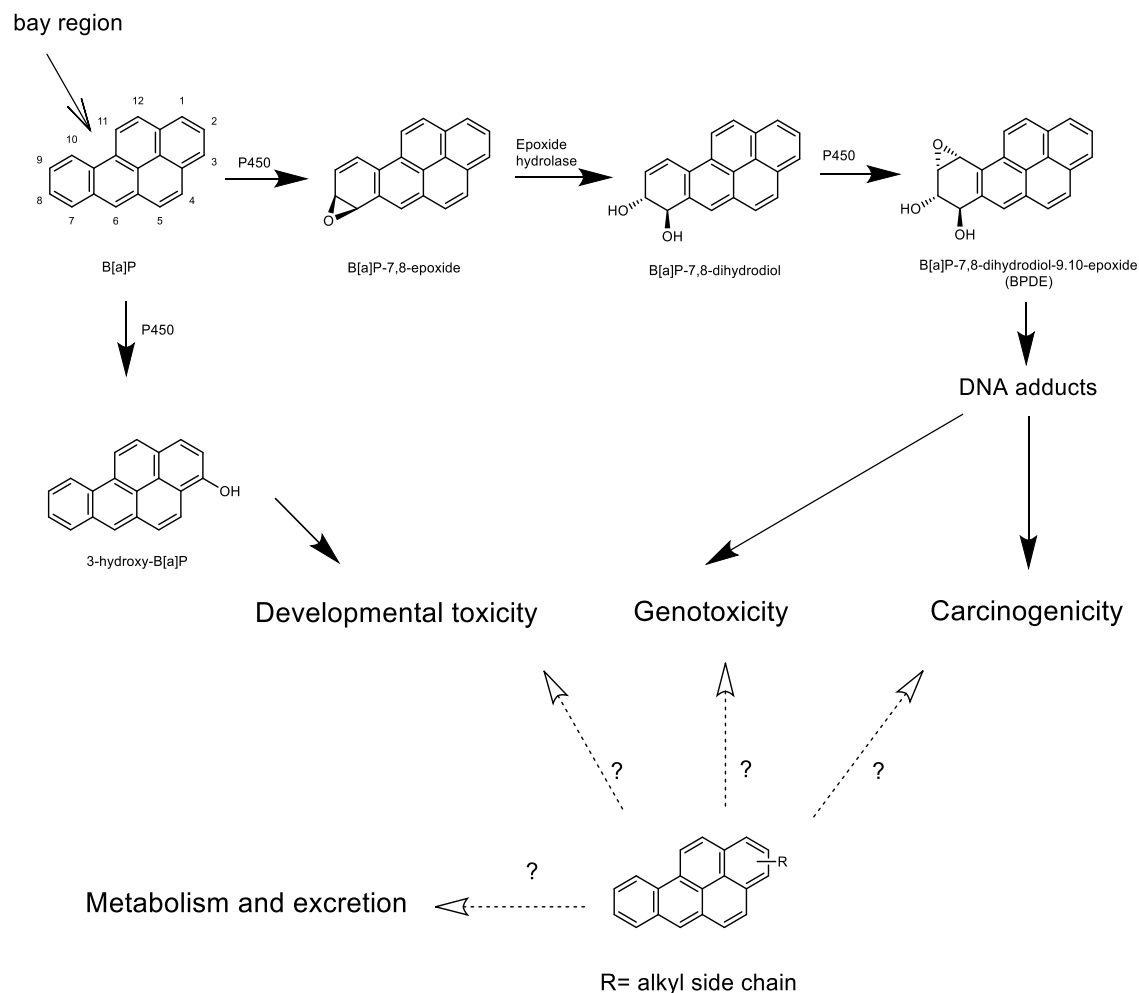
The risk characterization for genotoxic carcinogens is commonly based on the Margin of Exposure (MOE) approach (EFSA 2005). To calculate the MOE a Reference Point (RP) such as the lower confidence limit of the benchmark dose causing 10% tumor incidence above background values (BMDL<sub>10</sub>) or a T25 (dose causing 25% tumor incidence) can be used as point of departure. The CONTAM Panel characterized the risk of the “naked” PAHs in food using the MOE calculated for marker PAHs such as B[a]P, PAH2 (sum of B[a]P and chrysene), PAH4 (PAH2 plus two other model PAHs) or PAH8 (PAH4 plus 4 other model PAHs) (EFSA 2008). The MOE values for the four categories of PAH were calculated from the dietary exposure to consumers and the BMDL<sub>10</sub> values derived from carcinogenicity studies on two coal tar mixtures described by Culp et al. (Culp, Gaylor et al. 1998, EFSA 2008). The resulting MOEs for the average consumers were higher than 10,000 indicating a low concern for consumer health. With respect to high consumer exposure to the four categories of PAHs, the MOEs were close or lower than 10,000 indicating a potential health concern. However, dose response data on the carcinogenicity of neither MOAH nor mineral oils are available to derive a BMDL<sub>10</sub> or T25. Due to the potential risk of exposure to MOAH for the general public, the CONTAM Panel considered exposure to MOAH via food to be of concern based on the possible carcinogenic risk.

As a risk management action, the Federal Ministry of Food and Agriculture of Germany submitted recently a proposal to regulate MOAH in foods and food contact materials to the World Trade Organization (WTO) (FMFA 2021). It entails a restriction of the presence of MOAH in the scope of food contact paper, paperboard or cardboard made of recycled paper to a level of less than 0.5 mg/kg of food and 0.15 mg/kg of food simulants.

## 1.5 Aim of this thesis and underlying hypotheses

Considering that the lack of toxicological data prevents a proper risk assessment of alkylated PAH, which are representative constituents of MOAH, the aim of the present project is to obtain a better insight in (1) the relative metabolic bioactivation and detoxification and (2) the genotoxic potential of naked versus alkylated PAHs that may be present in mineral oils, and (3) to develop physiologically-based kinetic (PBK) model facilitated quantitative in vitro-in vivo-extrapolation (QIVIVE) models for selected PAHs to provide a basis for risk assessment of MOAH using new approach methodologies (NAMs).

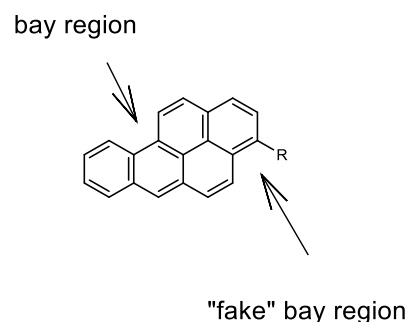
More than 98% of MOAH are highly alkylated aromatic hydrocarbons that have been barely studied (Grob, Biedermann et al. 1991), therefore the current assessment on MOAH is based on the non-substituted PAHs. One of the well-known genotoxic and carcinogenic PAHs is B[a]P that has been extensively studied in vitro and in vivo. B[a]P is known to be bioactivated to a bay region dihydrodiol-epoxide, characterized as (+) anti-B[a]P-7,8-dihydrodiol-9,10-epoxide (BPDE) that is DNA reactive and induces carcinogenicity (Sims, Grover et al. 1974, Jerina, Sayer et al. 1980) (**Figure 5**). In addition, a bioactivation pathway for the observed in-vivo prenatal developmental toxicity of B[a]P was proposed to be associated with its metabolism to 3-hydroxy-B[a]P mediated by P450 enzymes (Bui, Tran et al. 1986, Archibong, Inyang et al. 2002, Kamelia, de Haan et al. 2020). However, it is not clear if alkyl substitution of B[a]P and PAHs in general will result in the same metabolic pathway and toxicities including genotoxicity, carcinogenicity and developmental toxicity as observed for the naked analogues.



**Figure 5.** Proposed metabolic activation pathways of B[a]P for genotoxicity, carcinogenicity and developmental toxicity. Schematic view of questions on toxicities that may be induced by alkyl substitution of B[a]P as an example of alkylated PAHs

Although on thermodynamic grounds it is expected that alkylated PAH will undergo oxidative metabolism on the alkyl side chains rather than on the condensed aromatic rings - thus facilitating their excretion rather than their bioactivation to DNA reactive metabolites - there are regulatory concerns that alkylated PAH pose a greater genotoxic hazard than naked PAHs. For example, when alkyl substitution of PAH introduces fake bay region(s) (**Figure 6**), it is hypothesized that the presence of extra “fake” bay region(s) may increase the genotoxic potential of PAHs.





**Figure 6.** Demonstration of “fake” bay region with an example of alkyl substituted B[a]P. R = alkyl side chain

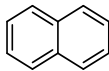
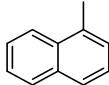
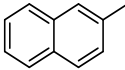
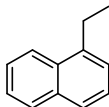
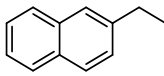
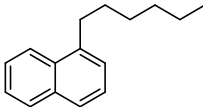
## 1.6 Model compounds

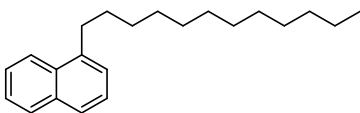
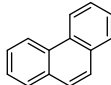
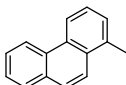
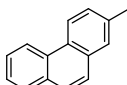
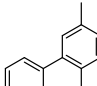
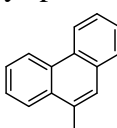
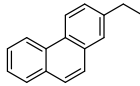
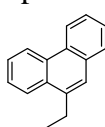
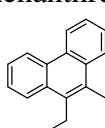
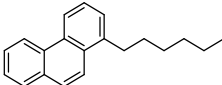
To investigate the relative balance between detoxification and bioactivation upon metabolism, in the present thesis the oxidative metabolism of naked PAH was compared to that of the corresponding alkylated compounds. To this end, individual PAHs and their alkylated congeners were tested. Although metabolic activation of PAHs proceeds by oxidation directly on the aromatic ring, alkylated PAH can also undergo metabolic activation on the alkyl group (Myers, Ali et al. 2007, Flesher and Lehner 2016). This may affect their ultimate (geno)toxic and carcinogenic potential. Most studies on metabolic activation of alkylated PAHs available so far focused on mono-methylated compounds (Flesher and Lehner 2016, Huang, Mesaros et al. 2017). Metabolism of longer chain mono- and poly-substituted PAHs has not yet been investigated despite the fact that these compounds are the predominant aromatics present in mineral oils on the EU market and represent most of the MOAH fraction. There is some evidence that the substitution position, ring number and chain length of short-chain alkylated PAHs indeed may affect the metabolic activation and as a consequence influence the potential for (geno)toxicity of the compound (Hecht, Amin et al. 1985, Flesher and Lehner 2016).

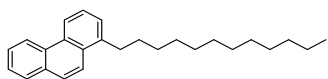
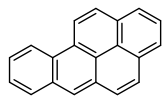
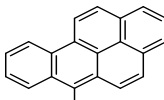
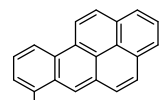
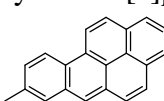
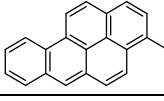
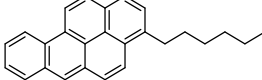
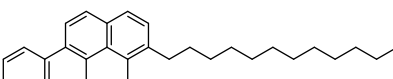
High-priority PAHs have been designated by the EU SCF, the USA Environmental Protection Agency (EPA) and the Grimmer Institute (Grimmer, Jacob et al. 1997, Lerda 2011). These PAH have been listed with their cancer classification according to IARC (IARC 2010) in **Table 1** (Boogaard 2012). Naphthalene, phenanthrene and B[a]P and their alkyl substituents were selected as model compounds based on structural and biological interests. Naphthalene is a two-ring aromatic hydrocarbon (**Table 1**) listed as a priority aromatic by the EPA. Based on its carcinogenicity observed in animals and insufficient human data, naphthalene was classified as possibly carcinogenic to humans (Group 2B) by IARC. Despite the lack of genotoxic potential, naphthalene and its alkyl substituents are good model compounds to study the oxidative metabolism pattern of PAHs as alkyl substituted 1- and 2-ring aromatics are highly abundant in highly refined mineral oils. Custom-synthesized hexyl- and commercially available methyl-, ethyl- and dodecyl- naphthalenes were investigated for their oxidative metabolism (**Table 3**). Phenanthrene is a three-ring PAH with a bay region, prioritized by the EPA and the Grimmer Institute. Phenanthrene itself was found to be non-genotoxic and classified as a Group 3 carcinogen by IARC based on inadequate data in experimental animals (**Table 1**). However, it is the smallest PAH with a bay region which makes phenanthrene and its alkylated analogues interesting for studies of possible metabolic activation and mutagenicity. Therefore, phenanthrene, commercially available methyl-substituted phenanthrenes as well as custom-synthesized 1-n-hexyl and 1-n-dodecyl substituted phenanthrenes were selected as model compounds (**Table 3**). B[a]P is a five-ring PAH that has been extensively studied in the past decades and was prioritized by the SCF, the Grimmer institute and the EPA and was classified by IARC as a Group 1 carcinogen (**Table 1**). Bioactivation leading to mutagenicity, carcinogenicity and developmental toxicity have been reported in experimental animals as well as in in vitro bioassays and may also be relevant to human (Yang, McCourt et al. 1977, Gelboin 1980, Kamelia, de Haan et al. 2020). B[a]P and twelve of its

monomethyl substituted analogues showed positive mutagenic potential upon bioactivation in bacterial reverse mutation studies (Peilu Chui 1982, Santella, Kinoshita et al. 1982, Utesch, Glatt et al. 1987). To investigate the effect of methyl substitution that introduces artificial bay region(s) in B[a]P on its metabolism and mutagenic potential, four methyl substituted congeners of B[a]P, 3-, 6-, 7- and 8-methyl-B[a]P, were selected as model compounds (**Table 3**). In addition, custom synthesized 3-n-hexyl- and 3-n-dodecyl-B[a]P were included as model compounds to investigate the effect of chain length on the metabolic oxidation of alkylated PAHs (**Table 3**).

**Table 3.** Non-substituted (‘naked’) and alkyl-substituted aromatic hydrocarbons selected as model compounds for the present thesis

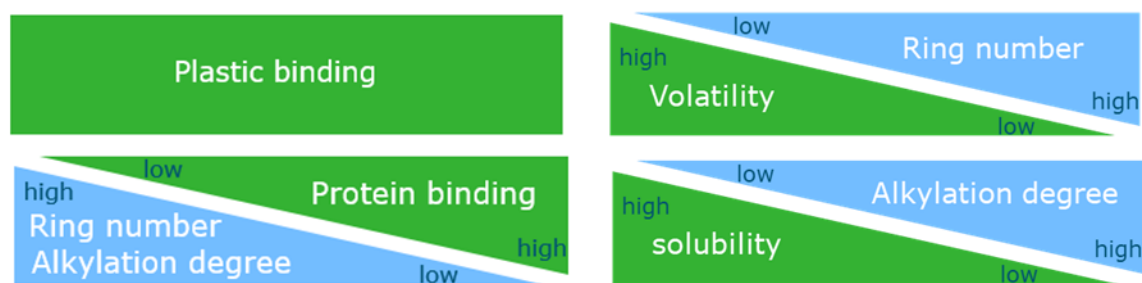
Chemical name and structure	CAS number	Boiling point	Molecular weight	Formula
2-ring non-substituted and alkyl-substituted aromatic hydrocarbons in <b>Chapter 2</b>				
naphthalene 	91-20-3	217.9°C	128.17g/mol	C <sub>10</sub> H <sub>8</sub>
1-methyl-naphthalene 	90-12-0	240-243°C	142.2 g/mol	C <sub>11</sub> H <sub>10</sub>
2-methyl-naphthalene 	91-57-6	241.1°C	142.2 g/mol	C <sub>11</sub> H <sub>10</sub>
1-ethyl-naphthalene 	1127-76-0	258.6 °C	156.22 g/mol	C <sub>12</sub> H <sub>12</sub>
2-ethyl-naphthalene 	939-27-5	258 °C	156.22 g/mol	C <sub>12</sub> H <sub>12</sub>
1-n-hexyl-naphthalene 	2876-53-1	322 °C	212.33 g/mol	C <sub>16</sub> H <sub>20</sub>

1-n-dodecyl-naphthalene 	38641-16-6	415°C	296.49 g/mol	C <sub>22</sub> H <sub>32</sub>
3-ring non-substituted and alkyl-substituted PAHs in <b>Chapter 3</b>				
phenanthrene 	85-01-8	340°C	178.23 g/mol	C <sub>14</sub> H <sub>10</sub>
1-methyl-phenanthrene 	832-69-9	354-355°C	192.26 g/mol	C <sub>15</sub> H <sub>12</sub>
2-methyl-phenanthrene 	2531-84-2	353°C	192.26 g/mol	C <sub>15</sub> H <sub>12</sub>
3-methyl-phenanthrene 	832-71-3	350°C	192.26 g/mol	C <sub>15</sub> H <sub>12</sub>
9-methyl-phenanthrene 	883-20-5	354°C	192.26 g/mol	C <sub>15</sub> H <sub>12</sub>
2-ethyl-phenanthrene 	2531-84-2	363°C	206.28 g/mol	C <sub>16</sub> H <sub>14</sub>
9-ethyl-phenanthrene 	3674-75-7	364°C	206.28 g/mol	C <sub>16</sub> H <sub>14</sub>
9-ethyl-10-methyl-phenanthrene 	17024-02-1	381°C	220.31 g/mol	C <sub>17</sub> H <sub>16</sub>
1-n-hexyl-phenanthrene 	-	415°C	262.39 g/mol	C <sub>20</sub> H <sub>22</sub>

1-n-dodecyl-phenanthrene 	-	491°C	346.55 g/mol	C <sub>26</sub> H <sub>34</sub>
5-ring non-substituted and alkyl-substituted PAHs in <b>Chapter 4</b>				
benzo[a]pyrene 	50-32-8	495°C	252.31 g/mol	C <sub>20</sub> H <sub>12</sub>
6-methyl-benzo[a]pyrene 	2381-39-7	510°C	266.33 g/mol	C <sub>21</sub> H <sub>14</sub>
7-methyl-benzo[a]pyrene 	63041-77-0	510°C	266.33 g/mol	C <sub>21</sub> H <sub>14</sub>
8-methyl-benzo[a]pyrene 	63041-76-9	510°C	266.33 g/mol	C <sub>21</sub> H <sub>14</sub>
3-methyl-benzo[a]pyrene 	16757-81-6	510°C	266.33 g/mol	C <sub>21</sub> H <sub>14</sub>
3-n-hexyl-benzo[a]pyrene 	-	-	336.5 g/mol	C <sub>26</sub> H <sub>24</sub>
3-n-dodecyl-benzo[a]pyrene 	-	-	420.6 g/mol	C <sub>32</sub> H <sub>36</sub>

The physical properties of the selected model aromatic hydrocarbons vary based on the ring number and alkylation degree (**Figure 7**). The selected naphthalene, phenanthrene, B[a]P and their alkyl substituents may bind to plastics which makes Eppendorf tubes unsuitable as experimental containers. The aromatic hydrocarbons with low ring number such as naphthalene and its alkylated analogues are highly volatile compounds with high vapor pressure in spite of their relatively high boiling points. The aromatic hydrocarbons with longer alkyl-substituents, such as n-hexyl- and n-

dodecyl- side chains have low solubility in Dimethylsulfoxide (DMSO). Tetrahydrofuran (THF) is a less polar solvent than DMSO and can dissolve aromatics with longer alkyl-substituents to allow their testing in in vitro bioassay systems. Last but not the least, some 5-ring aromatic hydrocarbons, such as B[a]P and its congeners and lower ring number aromatic hydrocarbons with a long alkyl side chain may bind to microsomal protein. All these characteristics have to be taken into account when designing the experiments described in the present thesis. In the next sections it is described in some more detail how this was done.



**Figure 7.** Properties of the selected aromatic hydrocarbons to be considered when defining the experimental conditions for the in vitro studies of the present thesis

## 1.7 Methodology

### 1.7.1 Microsomal incubations

The oxidative metabolism of the non-substituted aromatic hydrocarbons for which alkylated (methylated) counterparts are available (**Table 3**) were tested by incubation with rat and human hepatic microsomes, both with and without a metabolic activation system present. The model compounds comprised non-substituted and alkyl-substituted 2-ring, 3-ring and 5-ring aromatic hydrocarbons. Attention was given to the nature of the alkyl chain since this was expected to be an important factor influencing the metabolic pathways. Glass vials or glass tubes were used for incubation. Under atmospheric pressure and with an incubation temperature of 37°C, the glass

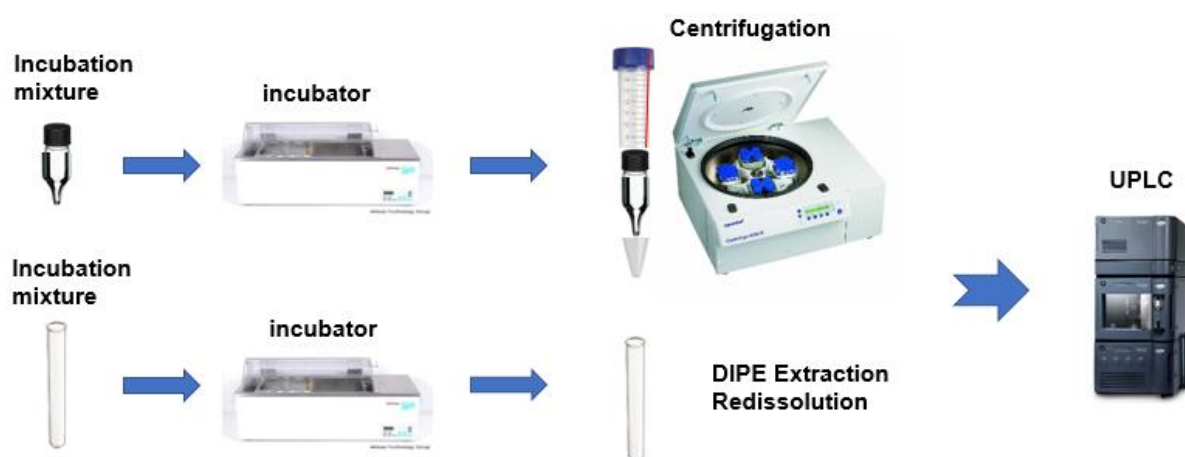
experimental containers were capped to prevent evaporation of the test compounds with low ring number. DMSO was used as the solvent for the alkyl-substituted naphthalene, phenanthrene and B[a]P with side chain lengths up to C3. THF was selected as the solvent for hexylated and dodecylated naphthalene, phenanthrene and B[a]P. The binding between microsomal protein and some selected aromatic hydrocarbons interferes with detection of the test compounds and their metabolites in the incubation mixture. Therefore, organic solvent extraction with diisopropylether (DIPE) was applied to break the binding between the test compounds and the microsomal proteins.

The test compound concentration-dependent formation of the oxidative metabolites in the incubation mediated by cytochrome P450 enzymes from rats and human were measured and characterized based on Michaelis-Menten kinetics. Due to the complex properties of the selected model compounds, the incubation was performed using two approaches (**Figure 8a**). In the first approach, centrifugation was applied to incubation mixtures of naphthalene and phenanthrene and their alkylated analogues with side chain lengths up to C3. After the incubation mixture was incubated for the optimized time, the glass vials were placed into plastic tubes that could be centrifuged. The supernatant of the incubation mixture was analyzed using Ultra Performance Liquid Chromatography (UPLC). In the second approach, extraction with the organic solvent DIPE was applied to incubations with B[a]P and its alkylated analogues as well as to the incubations with n-hexyl- and n-dodecyl-substituted naphthalene and phenanthrene. The extraction solvent was subsequently evaporated with a stream of nitrogen and the residue was re-dissolved in methanol and analyzed with UPLC. Metabolite identification was achieved either by Gas Chromatography Triple Quadrupole Mass Spectrometry (GC-MS/MS) analysis or by co-elution and comparison of UV spectra when reference chemicals were available. For GC-MS/MS analysis (**Figure 8b**), the incubation mixture was incubated at the concentration where the Michaelis Menten curve starts to

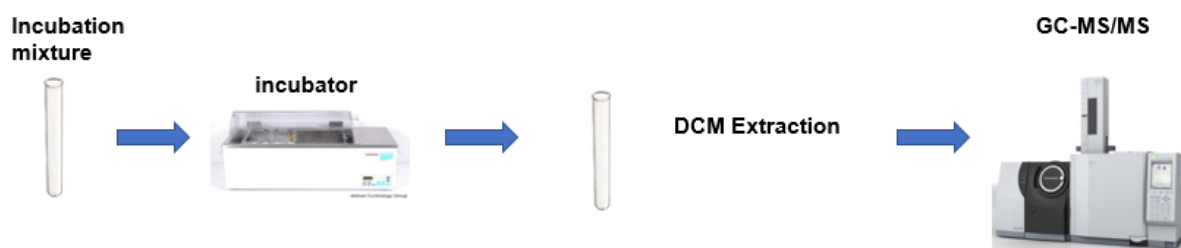
saturate and the optimized incubation time, followed by dichloromethane (DCM) extraction. The DCM extracts were analyzed by GC-MS/MS to obtain detailed mass spectra of the formed metabolites.

#### Microsomal incubation

(a)



(b)



**Figure 8.** A schematic overview of the methodology used for the microsomal incubations followed by (a) quantification with UPLC or (b) metabolite identification with GC-MS/MS

#### 1.7.2 Ames test

The Ames test (the bacterial reverse mutation assay) is accepted by regulatory authorities as an in vitro genetic toxicity screening assay for chemicals in adherence of the OECD guideline 471 (Ames,



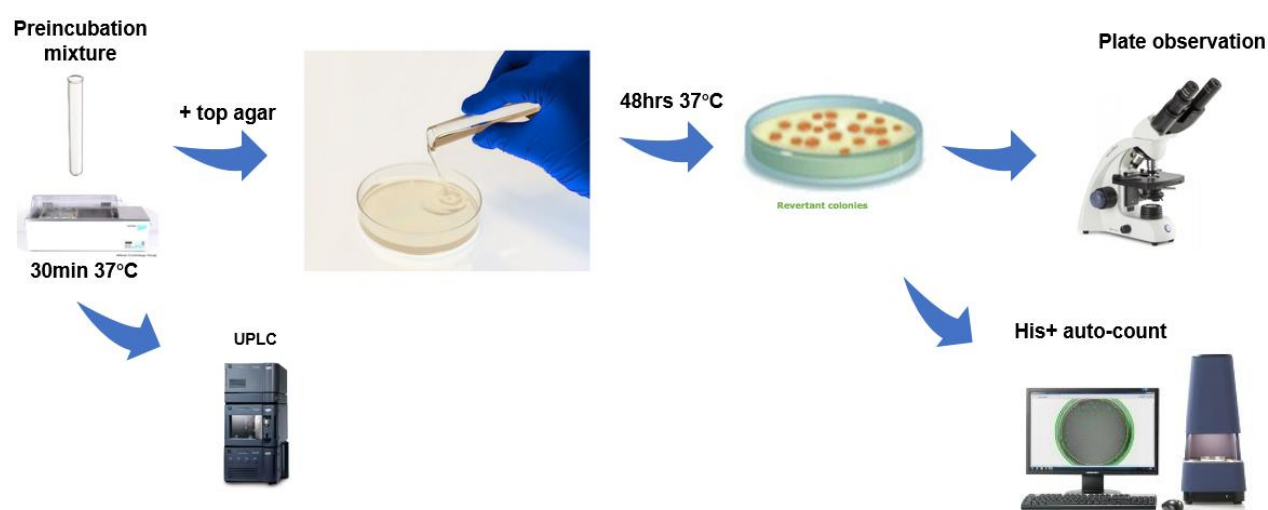
McCann et al. 1975, OECD 1997). The commonly used bacterial strains of *Salmonella typhimurium* in the assay are genetically modified to inactivate a gene involved in synthesis of histidine. When the bacterial strain is exposed to a mutagen, mutation may reverse the inability of the bacteria to synthesize histidine and thus allow growth of revertant colonies which can be observed and quantified. Using different strains of *S. typhimurium*, different types of mutation can be detected such as base-pair substitution and frameshift mutations. Some chemicals have to be bioactivated to become mutagenic and the Ames test is therefore performed with and without a mammalian metabolic system generally by adding liver S9 homogenate and the co-factors for oxidative metabolism.

In the present study, the effect of alkyl substitution on the mutagenicity of PAHs was assessed in the standard Ames test with preincubation (Yahagi, Degawa et al. 1975) (**Figure 9**). The tested compounds include phenanthrene and four methyl-substituted phenanthrenes and B[a]P and four methyl-substituted B[a]P. Each individual model compound was tested in the absence and presence of a metabolic system that consisted of an NADPH-generating system and Arocolor 1254 induced rat liver S9 homogenate. A mixture composed of S9-mix or phosphate buffer, a bacterial culture of the TA98 or TA100 tester strain ( $10^8$  cells/mL final concentration) and the test compound or the solvent was preincubated for 30min at 37°C. After the pre-incubation period, top agar was added to the preincubation mixture and poured onto selective Minimal Glucose Agar (MGA) plates. After solidification of the top agar, the plates were inverted and incubated in the dark at  $37^\circ\text{C} \pm 1.0^\circ\text{C}$  for  $48 \pm 4$ h. After incubation, the bacterial background lawn was checked under a microscope. Chemical precipitation on the agar plate was checked. The revertant colonies ( $\text{His}^+$ ) were automatically counted.

Any increase in the total number of revertants should be evaluated for its biological relevance including by a comparison of the results with the historical control data range. A test item is considered positive (mutagenic) in the test if the total number of revertants in tester strain TA100 is greater than two times the concurrent control, and if the total number of revertants in tester strain TA98 is greater than three times the concurrent control (Hamel, Roy et al. 2016, Levy, Zeiger et al. 2019).

The incubation mixture was analyzed with UPLC to obtain the metabolic profile that the bacterial strains were exposed to. The preincubation mixture, with exclusion of the bacteria and with and without a metabolic activation system was incubated separately from the actual Ames test. After 48 hours of incubation, this preincubation mixture was centrifuged (at 5000rpm / 4000×g, for 10 min), extracted with DIPE and the extract was analyzed for phenanthrene analogues and B[a]P analogues as described in section 1.7.1.

#### Ames test



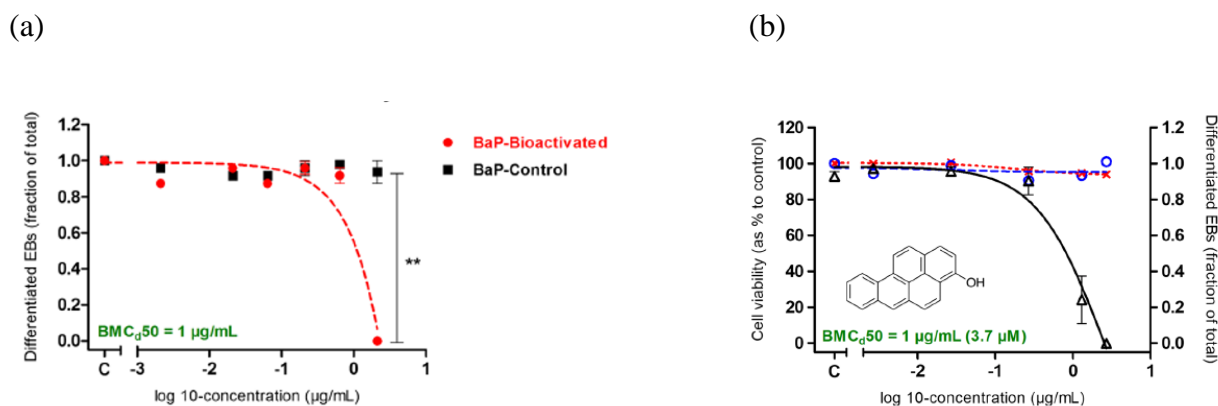
**Figure 9.** Schematic view of Ames test with preincubation method as applied in this thesis

### **1.7.3 PBK modeling - facilitated QIVIVE**

The REACH (Registration, Evaluation, Authorization, and Restriction of Chemical) legislation has been issued by the European Commission (EC) in 2006 aiming at greater protection of human health and the environment from the risks of chemical exposure (EC 2006). It requires all chemical substances that are produced in or put onto the market of the EU at a volume of  $\geq 100$  tonnes/year to be evaluated for their effect on prenatal development (ECHA 2009). This includes  $\pm 186$  currently active registered EINECS numbers of petroleum substances. Given the large number of experimental animals potentially needed for safety testing of chemical substances according to the current OECD 414 guideline (OECD 2018), REACH also promotes and supports the use of alternative testing strategies for the hazard assessment of chemical substances in order to reduce the number of tests on animals (ECHA 2014). Thus, the development and application of alternative testing strategies for assessing the developmental toxicity of highly complex petroleum substances are highly relevant and important. In the long run, this may reduce animal experimentation and resources needed to study the developmental toxicity of highly complex petroleum substances by the application of the 3Rs (Reduction, Replacement, and Refinement) principle of animal use in toxicological research.

The Embryonic Stem cell Test (EST) is widely used and validated as an in vitro alternative testing strategy to detect developmental toxicity hazards by the European Center for the Validation of Alternative Methods (ECVAM 2002, Genschow, Spielmann et al. 2004). The mouse embryonic stem cell line ES-D3 derived from blastocysts of a 129S2/SvPas mouse is typically used in the EST. The differentiation of these ES-D3 cells proceeds via the formation of so called embryoid bodies (EBs) that are able to spontaneously differentiate into any cell type of the three germ layers (endoderm, mesoderm, and ectoderm), including cardiomyocytes. The ability of chemicals to

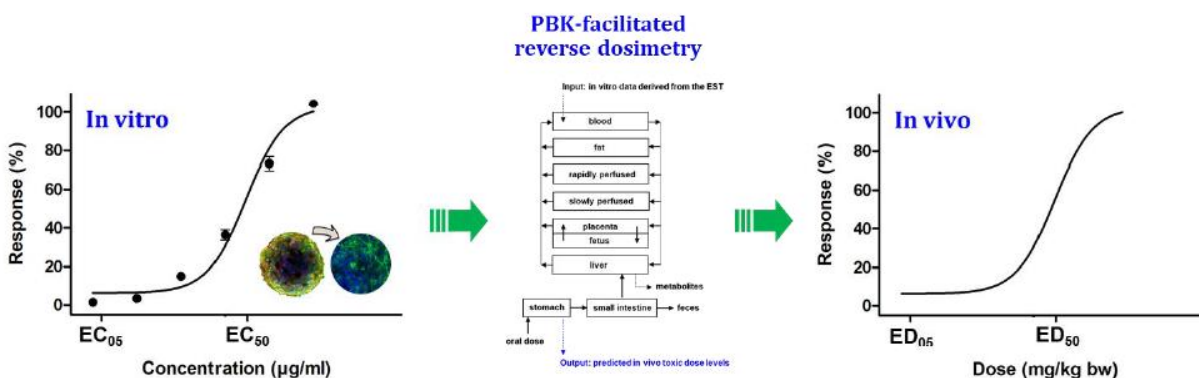
inhibit the differentiation of ES-D3 cells into contracting cardiomyocytes is exploited as the endpoint of this assay and allows to evaluate possible developmental toxicity in vitro. The EST was proved to adequately assess developmental toxicity of extracts of PAH-containing petroleum substances since the in vitro results showed a strong correlation with the prenatal developmental toxicity potencies observed in vivo (Kamelia, Louisse et al. 2017). This study suggested that the presence of 3- to 7- ring PAHs plays an important role in determining prenatal developmental toxicity of petroleum substances. Furthermore, it was found that B[a]P needs to be bioactivated to 3-hydroxybenzo[a]pyrene (3-OHB[a]P) to induce positive effects in the EST (Kamelia, de Haan et al. 2020). Dose response curves in the EST were generated for B[a]P in the presence and absence of a bioactivation system and for 3-OHB[a]P. The derived Benchmark Concentration  $BMC_{d50}$  that corresponds to 50% inhibition of ES-D3 cell differentiation into beating cardiomyocytes for bioactivated B[a]P was 1  $\mu\text{g/mL}$  (**Figure 10a**) and for 3-OHB[a]P it was also 1  $\mu\text{g/mL}$  (**Figure 10b**).



**Figure 10.** Concentration dependent effect of (a) B[a]P and (b) 3-OHB[a]P showing that not B[a]P or any of its other metabolites but 3-OHB[a]P is mainly responsible for the in vitro developmental toxicity detected in the EST (Kamelia, de Haan et al. 2020).

Developmental toxicity observed in vitro does not always reflect the in vivo embryotoxicity since toxicokinetics are excluded in in vitro models. Inclusion of the toxicokinetics of test substances by

applying physiologically based kinetic (PBK) modeling enables extrapolation of the obtained in vitro results to the in vivo situation (Rietjens, Louisse et al. 2011). A PBK model is a set of differential equations that together describe the ADME characteristics of a compound within an organism (Rietjens, Louisse et al. 2011). In a PBK model, a human or animal body is represented by several compartments representing tissues and organs (**Figure 11**). The physiologically-relevant concentration-dependent kinetics for metabolism and circulation of a model compound can be described in silico with a PBK model, together with the concentration(s) of its active metabolite(s) in the target organ of interest for a certain dose, time point and route of administration (Rietjens, Louisse et al. 2011). Moreover, PBK modeling allows translation of in vitro concentration-dependent responses, for example in the EST, into in vivo dose-responses using the so-called reverse dosimetry approach (Strikwold, Woutersen et al. 2012, Louisse, Wust et al. 2017). Proofs of principle for the use of PBK modeling facilitated reverse dosimetry for QIVIVE have been demonstrated for different compounds causing developmental toxicity (Louisse, Gonen et al. 2011, Strikwold, Spenkelink et al. 2013, Li, Zhang et al. 2017).



**Figure 11.** Scheme of QIVIVE using an in vitro concentration response curve derived from the EST and PBK modeling facilitated reverse dosimetry to predict an in vivo dose response curve for developmental toxicity.

In the present study, an in-silico approach of using PBK modelling facilitated reverse dosimetry was developed to predict developmental toxicity of a selected five ring PAH, B[a]P. The developed in vitro-in silico QIVIVE approach serves as a basis for a better risk assessment of petrogenic PAHs and supports the application of the 3Rs principle under the REACH regulation. The kinetic parameter values for metabolism of B[a]P and conjugation of 3-OHB[a]P in rats were determined in vitro. The blood concentrations of the B[a]P and 3-OHB[a]P via intravenous, intratracheal and oral exposure routes were simulated in the PBK model and were properly evaluated with in vivo kinetic data. The in vitro concentration-dependent response data for 3-OHB[a]P (Kamelia, de Haan et al. 2020) in the EST were translated into in vivo dose response data for its parent compound B[a]P using the PBK model facilitated reverse dosimetry approach. The predicted in vivo response data can be compared to the data reported in in vivo studies to evaluate the adequacy of the approach.

## **Outline of the thesis**

**Chapter 1** of this thesis provides background information of MOAH presence in food, societal relevance to the public health, aim and hypotheses of the thesis as well as a short description of the methodology applied.

**Chapter 2** describes the oxidative metabolism of a two-ring aromatic hydrocarbon, naphthalene, and its alkylated analogues, by rat and human liver microsomes in vitro. The effect of alkylation of naphthalene on a potential metabolic shift in its metabolism from aromatic ring to aliphatic side chain oxidation is characterized.

**Chapter 3** evaluates the possible effects of alkylation on the bioactivation and the genotoxic potency of a three-ring aromatic hydrocarbon, phenanthrene, by studying metabolism and genotoxicity of phenanthrene and some of its alkylated analogues. The oxidative metabolites of phenanthrene itself and those of the alkylated phenanthrenes were identified to characterize the effect of alkyl substitution on the metabolic pattern and the resulting mutagenicity.

**Chapter 4** investigates the mutagenicity and metabolic activation of a five-ring aromatic hydrocarbon, B[a]P, by studying metabolism and genotoxicity of B[a]P and some of its selected alkylated analogues. The metabolite profiles of B[a]P and its alkyl substituted B[a]Ps were characterized to reveal the effect of alkyl substitution on metabolism of B[a]P by rat and human liver microsomes and the resulting mutagenicity.

**Chapter 5** explores the possibility of PBK modelling facilitated QIVIVE in prediction of developmental toxicity for B[a]P that provides a proof of principle of applying this in vitro–in silico approach for evaluating developmental toxicity of B[a]P, in order to investigate if this NAM would provide a promising strategy for predicting the developmental toxicity of related PAHs, without the need for extensive animal testing.

**Chapter 6** of the thesis presents the overall discussion of the results obtained and also presents some future perspectives for the field of metabolism, bioactivation and toxicity of alkylated PAHs present in MOAH.

## Reference

- Ames, B. N., J. McCann and E. Yamasaki (1975). "Methods for detecting carcinogens and mutagens with the Salmonella/mammalian-microsome mutagenicity test." Mutat Res **31**(6): 347-364.
- Archibong, A. E., F. Inyang, A. Ramesh, M. Greenwood, T. Nayyar, P. Kopsombut, D. B. Hood and A. M. Nyanda (2002). "Alteration of pregnancy related hormones and fetal survival in F-344 rats exposed by inhalation to benzo(a)pyrene." Reprod Toxicol **16**(6): 801-808.
- ASTM (2014). Standard Test Method for Determining Carcinogenic Potential of Virgin Base Oils in Metalworking Fluids. **E1687-10**.
- BfR (2012). Determination of hydrocarbons from mineral oil (MOSH & MOAH) or plastics (POSH & PAO) in packaging materials and dry foodstuffs by solid phase extraction and GC-FID
- Biedermann, M., K. Fiselier and K. Grob (2009). "Aromatic hydrocarbons of mineral oil origin in foods: method for determining the total concentration and first results." J Agric Food Chem **57**(19): 8711-8721.
- Biedermann, M. and K. Grob (2009). "How “white” was the mineral oil in the contaminated Ukrainian sunflower oils?" European Journal of Lipid Science and Technology **111**(4): 313-319.
- Blackburn, G. R., R. A. Deitch, C. A. Schreiner and C. R. Mackerer (1986). "Predicting carcinogenicity of petroleum distillation fractions using a modified Salmonella mutagenicity assay." Cell Biol Toxicol **2**(1): 63-84.
- Blackburn, G. R., T. A. Roy, W. T. Bleicher, M. V. Reddy and C. R. Mackerer (1996). "Comparison of Biological and Chemical Predictors of Dermal Carcinogenicity of Petroleum Oils." Polycyclic Aromatic Compounds **11**(1-4): 201-210.
- Boogaard, P. (2012). Biomonitoring of Exposure to Polycyclic Aromatic Hydrocarbons. **1**: 338-359.



Boogaard, P. J., J. C. Carrillo, L. G. Roberts and G. F. Whale (2017). "Toxicological and ecotoxicological properties of gas-to-liquid (GTL) products. 1. Mammalian toxicology." Crit Rev Toxicol **47**(2): 121-144.

Bratinova, S. (2019). Guidance on sampling, analysis and data reporting for the monitoring of mineral oil hydrocarbons in food and food contact materials. J. R. Centre.

Bui, Q. Q., M. B. Tran and W. L. West (1986). "A comparative study of the reproductive effects of methadone and benzo[a]pyrene in the pregnant and pseudopregnant rat." Toxicology **42**(2-3): 195-204.

Carrillo, J. C., A. van der Wiel, D. Danneels, O. Kral and P. J. Boogaard (2019). "The selective determination of potentially carcinogenic polycyclic aromatic compounds in lubricant base oils by the DMSO extraction method IP346 and its correlation to mouse skin painting carcinogenicity assays." Regul Toxicol Pharmacol **106**: 316-333.

Concawe (1994). The use of dimethyl sulphoxide (DMSO) extract by the IP 346 method as an indicator of the carcinogenicity of lubricant base oils and distillate aromatic extracts. Brussels.

Concawe (2012). Use of the modified Ames test as an indicator of the carcinogenicity of residue aromatic extracts. Brussels.

Concawe (2017). PAH integrated exposure modelling. Brussels.

Culp, S. J., D. W. Gaylor, W. G. Sheldon, L. S. Goldstein and F. A. Beland (1998). "A comparison of the tumors induced by coal tar and benzo[a]pyrene in a 2-year bioassay." Carcinogenesis **19**(1): 117-124.

EC (2006). C1 REGULATION (EC) No 1907/2006 OF THE EUROPEAN PARLIAMENT AND OF THE COUNCIL.

ECHA (2009). "Information requirements for repeated dose toxicity and reproductive toxicity-substances over 100 (and 1000) tonnes.".

ECHA (2011). Characterisation, chemical representation and modelling of UVCB substances.

ECHA (2014). "The use of alternatives to testing on animals for REACH."

ECVAM (2002). The Use of Scientifically-Validated In Vitro Tests for Embryotoxicity.

EFSA (2005). "Opinion of the Scientific Committee on a request from EFSA related to A Harmonised Approach for Risk Assessment of Substances Which are both Genotoxic and Carcinogenic." EFSA Journal **3**(10): 282.

EFSA (2008). "Polycyclic Aromatic Hydrocarbons in Food - Scientific Opinion of the Panel on Contaminants in the Food Chain." EFSA Journal **6**(8): 724.

EFSA (2012). "Scientific Opinion on Mineral Oil Hydrocarbons in Food." EFSA Journal **10**(6): 2704.

FMFA (Federal Ministry of Food and Agriculture) (2021). Twenty-Second Ordinance amending the Consumer Goods Ordinance. Fedral Ministry of Food and Agriculture.

Feuston, M. H., C. E. Hamilton and C. R. Mackerer (1996). "Systemic and developmental toxicity of dermally applied distillate aromatic extract in rats." Fundam Appl Toxicol **30**(2): 276-284.

Feuston, M. H., S. L. Kerstetter, E. J. Singer and M. A. Mehlman (1989). "Developmental toxicity of Clarified Slurry Oil applied dermally to rats." Toxicol Ind Health **5**(3): 587-599.

Feuston, M. H., L. K. Low, C. E. Hamilton and C. R. Mackerer (1994). "Correlation of systemic and developmental toxicities with chemical component classes of refinery streams." Fundam Appl Toxicol **22**(4): 622-630.

Feuston, M. H. and C. R. Mackerer "Developmental toxicity of clarified slurry oil, syntower bottoms, and distillate aromatic extract administered as a single oral dose to pregnant rats." (0098-4108 (Print)).

Flesher, J. W. (1967). "Distribution of radioactivity in the tissues of rats after oral administration of 7,12-dimethylbenz(A)anthracene-3H." Biochem Pharmacol **16**(9): 1821-1831.

Flesher, J. W. and A. F. Lehner (2016). "Structure, function and carcinogenicity of metabolites of methylated and non-methylated polycyclic aromatic hydrocarbons: a comprehensive review." Toxicology Mechanisms and Methods **26**(3): 151-179.

Foodwatch (2015). Besmetting van ons voedsel met minerale oliën. Resultaten van de foodwatch Test. .

Foodwatch (2016). MINERALÖLE IN SCHOKOLADEN-WEIHNACHTSMÄNNERN.

Foodwatch (2016). Mineröl in Schokoladen-Osterhasen.

Foodwatch (2019). International test of various canned baby milk products for their content of mineral oil hydrocarbons (MOSH/MOAH).

FSANZ (2018). Mineral oil hydrocarbons in food and food packaging. F. S. A. N. Zealand.

Gelboin, H. V. (1980). "Benzo[alpha]pyrene metabolism, activation and carcinogenesis: role and regulation of mixed-function oxidases and related enzymes." Physiol Rev **60**(4): 1107-1166.

Genschow, E., H. Spielmann, G. Scholz, I. Pohl, A. Seiler, N. Clemann, S. Bremer and K. Becker (2004). "Validation of the embryonic stem cell test in the international ECVAM validation study on three in vitro embryotoxicity tests." Altern Lab Anim **32**(3): 209-244.

Grimmer, G., J. Jacob and K. W. Naujack (1997). "Atmospheric emission of polycyclic aromatic hydrocarbons in sampling areas of the German environmental specimen bank. Method for the precise measurement of gaseous and particle-associated polycyclic aromatic hydrocarbons in the sub-nanogram range using deuterated internal standards." Chemosphere **34**(9): 2213-2226.

Grob, K., M. Biedermann, A. Artho and J. Egli (1991). "Food contamination by hydrocarbons from packaging materials determined by coupled LC-GC." Z Lebensm Unters Forsch **193**(3): 213-219.

Hamel, A., M. Roy and R. Proudlock (2016). Chapter 4 - The Bacterial Reverse Mutation Test. Genetic Toxicology Testing. R. Proudlock. Boston, Academic Press: 79-138.

Hecht, S. S., S. Amin, A. A. Melikian, E. J. Lavoie and D. Hoffmann (1985). Effects of Methyl and Fluorine Substitution on the Metabolic Activation and Tumorigenicity of Polycyclic Aromatic Hydrocarbons. Polycyclic Hydrocarbons and Carcinogenesis, American Chemical Society. **283**: 85-105.

Hoberman, A. M., M. S. Christian, S. Lovre, R. Roth and F. Koschier (1995). "Developmental toxicity study of clarified slurry oil (CSO) in the rat." Fundam Appl Toxicol **28**(1): 34-40.

Huang, M., C. Mesaros, L. C. Hackfeld, R. P. Hodge, I. A. Blair and T. M. Penning (2017). "Potential Metabolic Activation of Representative Alkylated Polycyclic Aromatic Hydrocarbons 1-Methylphenanthrene and 9-Ethylphenanthrene Associated with the Deepwater Horizon Oil Spill in Human Hepatoma (HepG2) Cells." Chem Res Toxicol **30**(12): 2140-2150.

IARC (1984). Polynuclear aromatic hydrocarbons, Part 2, carbon blacks, mineral oils (lubricant base oils and derived products) and some nitroarenes. Lyon, France. **33**: 1-440.

IARC (2010). Some Non-Heterocyclic Polycyclic Aromatic Hydrocarbons and Some Related Exposures. Lyon, France. **92**.

Ingram, A. J., J. C. Phillips and S. Davies (2000). "DNA adducts produced by oils, oil fractions and polycyclic aromatic hydrocarbons in relation to repair processes and skin carcinogenesis." J Appl Toxicol **20**(3): 165-174.

Ingram, A. J., J. C. Phillips and R. Lee (1995). "DNA adduct formation by mineral oils and their fractions as indicated by 32P-postlabelling: Is adduct formation truly indicative of carcinogenic potential?" Journal of Applied Toxicology **15**(4): 275-283.

Ingram, A. J., D. V. Scammells and K. May (1994). "An investigation of the main mutagenic components of a carcinogenic oil by fractionation and testing in the modified ames assay." Journal of Applied Toxicology **14**(3): 173-179.

IPCS (1998). Selected Non-heterocyclic Polycyclic Aromatic Hydrocarbons.

Iversen, O. H. (1989). "Studies of the carcinogenesis and tumorigenesis of skin applications of dodecylbenzene on hairless mice." Br J Ind Med **46**(9): 608-616.

Iyer, R. P., J. W. Lyga, J. A. Secrist, 3rd, G. H. Daub and T. J. Slaga (1980). "Comparative tumor-initiating activity of methylated benzo(a)pyrene derivatives in mouse skin." Cancer Res **40**(4): 1073-1076.

JECFA (1995). Evaluation of Certain Food Additives and Contaminants. J. F. W. E. C. o. F. Additives. Geneva.

Jerina, D. M., J. M. Sayer, D. R. Thakker, H. Yagi, W. Levin, A. W. Wood and A. H. Conney (1980). Carcinogenicity of Polycyclic Aromatic Hydrocarbons: The Bay-Region Theory, Dordrecht, Springer Netherlands.

Kamelia, L., L. de Haan, B. Spenkelink, B. Bruyneel, H. B. Ketelslegers, P. J. Boogaard and I. Rietjens (2020). "The role of metabolism in the developmental toxicity of polycyclic aromatic hydrocarbon-containing extracts of petroleum substances." J Appl Toxicol **40**(3): 330-341.

Kamelia, L., J. Louisse, L. de Haan, I. Rietjens and P. J. Boogaard (2017). "Prenatal developmental toxicity testing of petroleum substances: Application of the mouse embryonic stem cell test (EST) to compare in vitro potencies with potencies observed in vivo." Toxicol In Vitro **44**: 303-312.

Kilanowicz, A., A. Sapota and B. Czerski (2002). "Disposition and metabolism of 1,6-dimethylnaphthalene in rats." Toxicol Lett **134**(1-3): 227-235.

Laher, J. M., M. W. Rigler, R. D. Vetter, J. A. Barrowman and J. S. Patton (1984). "Similar bioavailability and lymphatic transport of benzo(a)pyrene when administered to rats in different amounts of dietary fat." J Lipid Res **25**(12): 1337-1342.

LaVoie, E. J., V. Bedenko, L. Tulley-Freiler and D. Hoffmann (1982). "Tumor-initiating activity and metabolism of polymethylated phenanthrenes." Cancer Res **42**(10): 4045-4049.

Lerda, D. (2011). Polycyclic Aromatic Hydrocarbons (PAHs) Factsheet. E. C. J. R. Centre. Geel, Belgium.

Levy, D. D., E. Zeiger, P. A. Escobar, A. Hakura, B. M. van der Leede, M. Kato, M. M. Moore and K. I. Sugiyama (2019). "Recommended criteria for the evaluation of bacterial mutagenicity data (Ames test)." Mutat Res Genet Toxicol Environ Mutagen **848**: 403074.

Li, H., M. Zhang, J. Vervoort, I. M. Rietjens, B. van Ravenzwaay and J. Louisse (2017). "Use of physiologically based kinetic modeling-facilitated reverse dosimetry of in vitro toxicity data for prediction of in vivo developmental toxicity of tebuconazole in rats." Toxicol Lett **266**: 85-93.

Louisse, J., S. Gonen, I. M. Rietjens and M. Verwei (2011). "Relative developmental toxicity potencies of retinoids in the embryonic stem cell test compared with their relative potencies in in vivo and two other in vitro assays for developmental toxicity." Toxicol Lett **203**(1): 1-8.

Louisse, J., R. C. I. Wust, F. Pistollato, T. Palosaari, M. Barilari, P. Macko, S. Bremer and P. Prieto (2017). "Assessment of acute and chronic toxicity of doxorubicin in human induced pluripotent stem cell-derived cardiomyocytes." Toxicol In Vitro **42**: 182-190.

Mackerer, C. R., L. C. Griffis, J. S. Grabowski, Jr. and F. A. Reitman (2003). "Petroleum mineral oil refining and evaluation of cancer hazard." Appl Occup Environ Hyg **18**(11): 890-901.

Mobil (1987). Stock 461 rat teratology study.

Murata, Y., A. Denda, H. Maruyama and Y. Konishi (1993). "Chronic toxicity and carcinogenicity studies of 1-methylnaphthalene in B6C3F1 mice." Fundam Appl Toxicol **21**(1): 44-51.

Murata, Y., A. Denda, H. Maruyama, D. Nakae, M. Tsutsumi, T. Tsujiuchi and Y. Konishi (1997). "Chronic toxicity and carcinogenicity studies of 2-methylnaphthalene in B6C3F1 mice." Fundam Appl Toxicol **36**(1): 90-93.

Murray, F. J., M. J. Roth Rn Fau - Nicolich, T. M. Nicolich Mj Fau - Gray, B. J. Gray Tm Fau - Simpson and B. J. Simpson "The relationship between developmental toxicity and aromatic-ring class profile of high-boiling petroleum substances." (1096-0295 (Electronic)).

Myers, S. R., M. Y. Ali, T. Wright and C. Cunningham (2007). "BENZO(A)PYRENE METABOLISM: ROLE OF BIOALKYLATION." Polycyclic Aromatic Compounds **27**(4): 339-359.

Natusch, D. F. S. and B. A. Tomkins (1978). "Isolation of polycyclic organic compounds by solvent extraction with dimethyl sulfoxide." Analytical Chemistry **50**(11): 1429-1434.

OECD (1997). OECD Guideline for Testing of Chemicals, Genetic Toxicology No. 471. Paris.

OECD (2018). "OECD 414 Guideline for testing of chemicals: prenataldevelopmental toxicity study.".

Peilu Chui, S. K. Y. (1982). A structure-activity relationship study of monomethylbenzo[a]pyrenes by the use of Salmonella Typhimurium tester strain TA100 and by analysis of metabolite formation. Polynuclear Aromatic Hydrocarbons: Physical and Biological Chemistry: 193-200.

Rahman, A., J. A. Barrowman and A. Rahimtula (1986). "The influence of bile on the bioavailability of polynuclear aromatic hydrocarbons from the rat intestine." Can J Physiol Pharmacol **64**(9): 1214-1218.

Regulation, C. (2010). Commission Regulation (EU) No 37/2010 on pharmacologically active substances and their classification regarding maximum residue limits in foodstuffs of animal origin.

Regulation, C. (2011). Commission Regulation (EU) No 10/2011 on plastic materials and articles intended to come into contact with food.

Rietjens, I. M., J. Louisse and A. Punt (2011). "Tutorial on physiologically based kinetic modeling in molecular nutrition and food research." Mol Nutr Food Res **55**(6): 941-956.

- Roy, T. A., S. W. Johnson, G. R. Blackburn and C. R. Mackerer (1988). "Correlation of mutagenic and dermal carcinogenic activities of mineral oils with polycyclic aromatic compound content." Fundam Appl Toxicol **10**(3): 466-476.
- Santella, R., T. Kinoshita and A. M. Jeffrey (1982). "Mutagenicity of Some Methylated Benzo[a]Pyrene Derivatives." Mutation Research **104**(4-5): 209-213.
- Sims, P., P. L. Grover, A. Swaisland, K. Pal and A. Hewer (1974). "Metabolic activation of benzo(a)pyrene proceeds by a diol-epoxide." Nature **252**(5481): 326-328.
- Smith, W. E., D. A. Sunderland and K. Sugiura (1951). "Experimental analysis of the carcinogenic activity of certain petroleum products." AMA Arch Ind Hyg Occup Med **4**(4): 299-314.
- Stauff, A., J. Schnapka, F. Heckel and R. Matissek (2020). "Mineral Oil Hydrocarbons (MOSH/MOAH) in Edible Oils and Possible Minimization by Deodorization Through the Example of Cocoa Butter." European Journal of Lipid Science and Technology **122**(7): 1900383.
- Strikwold, M., B. Spenkelink, R. A. Woutersen, I. M. Rietjens and A. Punt (2013). "Combining in vitro embryotoxicity data with physiologically based kinetic (PBK) modelling to define in vivo dose-response curves for developmental toxicity of phenol in rat and human." Arch Toxicol **87**(9): 1709-1723.
- Strikwold, M., R. A. Woutersen, B. Spenkelink, A. Punt and I. M. Rietjens (2012). "Relative embryotoxic potency of p-substituted phenols in the embryonic stem cell test (EST) and comparison to their toxic potency in vivo and in the whole embryo culture (WEC) assay." Toxicol Lett **213**(2): 235-242.
- Sui, H., H. Gao, Y. Chen, R. Ke, H. Zhong, Q. Zhong, Z. Liu and Y. Song (2020). "Survey of mineral oil hydrocarbons in infant formula from the Chinese market." Food Addit Contam Part A Chem Anal Control Expo Risk Assess **37**(6): 1040-1048.



Tsitou, P., M. Heneweer and P. J. Boogaard (2015). "Toxicogenomics in vitro as an alternative tool for safety evaluation of petroleum substances and PAHs with regard to prenatal developmental toxicity." Toxicol In Vitro **29**(2): 299-307.

Twort, C. C. and J. M. Twort (1931). The carcinogenic potency of mineral oils. S.l, s.n.

Utesch, D., H. Glatt and F. Oesch (1987). "Rat hepatocyte-mediated bacterial mutagenicity in relation to the carcinogenic potency of benz(a)anthracene, benzo(a)pyrene, and twenty-five methylated derivatives." Cancer Res **47**(6): 1509-1515.

Van Heyst, A., M. Vanlancker, J. Vercammen, K. Van den Houwe, B. Mertens, M. Elskens and E. Van Hoeck (2018). "Analysis of mineral oil in food: results of a Belgian market survey." Food Addit Contam Part A Chem Anal Control Expo Risk Assess **35**(10): 2062-2075.

Wislocki, P. G., K. M. Fiorentini, P. P. Fu, S. K. Yang and A. Y. Lu (1982). "Tumor-initiating ability of the twelve monomethylbenz[a]anthracenes." Carcinogenesis **3**(2): 215-217.

Wislocki, P. G., K. M. Gadek, M. W. Chou, S. K. Yang and A. Y. Lu (1980). "Carcinogenicity and mutagenicity of the 3,4-dihydrodiols and other metabolites of 7,12-dimethylbenz(a)anthracene and its hydroxymethyl derivatives." Cancer Res **40**(10): 3661-3664.

Yahagi, T., M. Degawa, Y. Seino, T. Matsushima and M. Nagao (1975). "Mutagenicity of carcinogenic azo dyes and their derivatives." Cancer Lett **1**(2): 91-96.

Yang, S. K., D. W. McCourt, J. C. Leutz and H. V. Gelboin (1977). "Benzo[a]pyrene diol epoxides: mechanism of enzymatic formation and optically active intermediates." Science **196**(4295): 1199-1201.



## **Chapter 2**

# **In vitro metabolism of naphthalene and its alkylated congeners by human and rat liver microsomes via alkyl side chain or aromatic oxidation**

Danlei Wang, Ben Bruyneel, Lenny Kamelia, Sebastiaan Wesseling, Ivonne M.C.M. Rietjens,  
Peter J. Boogaard

Published in Chemico-Biological Interactions (2020) 315: 108905

## **Abstract**

Mineral oils widely are applied in food production and processing and may contain polycyclic aromatic hydrocarbons (PAHs). The PAHs that may be present in mineral oils are typically alkylated, and have been barely studied. Metabolic oxidation of the aromatic ring is a key step to form DNA-reactive PAH metabolites, but may be less prominent for alkylated PAHs since alkyl substituents would facilitate side chain oxidation as an alternative. The current study investigates this hypothesis of preferential side chain oxidation at the cost of aromatic oxidation using naphthalene and a series of its alkyl substituted analogues as model compounds. The metabolism was assessed by measuring metabolite formation in rat and human liver microsomal incubations using UPLC and GC-MS/MS. The presence of an alkyl side chain markedly reduced aromatic oxidation for all alkyl-substituted naphthalenes that were converted. 1-n-Dodecyl-naphthalene was not metabolized under the experimental conditions applied. With rat liver microsomes for 1-methyl-, 2-methyl-, 1-ethyl-, and 2-ethyl- naphthalene, alkyl side chain oxidation was preferred over aromatic oxidation. With human liver microsomes this was the case for 2-methyl-, and 2-ethyl-naphthalene. It is concluded that addition of an alkyl substituent in naphthalene shifts metabolism in favor of alkyl side chain oxidation at the cost of aromatic ring oxidation. Furthermore, alkyl side chains of 6 or more carbon atoms appeared to seriously hamper and reduce overall metabolism, metabolic conversion being no longer observed with the C12 alkyl side chain. In summary, alkylation of PAHs likely reduces their chances of aromatic oxidation and bioactivation.

## 1. Introduction

Mineral oils are applied in food production processes and applications, such as food packaging material, food additives, processing aids and machine lubricants. Hydrocarbons that may be present in mineral oils have been reported as an emerging food safety issue by the European Food Safety Authority (EFSA) [1]. The presence of mineral oil derived aromatic hydrocarbons is considered a potential concern because of the mutagenicity and carcinogenicity of some PAHs with three or more, non- or simple- alkylated, aromatic rings [1]. A key step in formation of the DNA reactive genotoxic metabolites of PAHs is metabolic bioactivation of the aromatic hydrocarbons via aromatic ring oxidation by cytochrome P450 enzymes [2]. However, this aromatic oxidation and bioactivation has been primarily studied for unsubstituted ('naked') PAHs, also referred to as pyrogenic PAHs because they are typical for coal-derived products and combustion products. In contrast, the PAHs present in petroleum-derived substances, also referred to as petrogenic PAHs, are primarily alkylated PAHs [3], for which the knowledge on metabolism is limited, although it may be hypothesized that alkylation may influence metabolism of the aromatic hydrocarbons.

To get more insight into cytochrome P450-mediated oxidative metabolism of alkylated PAHs that may be present in mineral oils, the aim of the present study was to characterize the relative aromatic and alkyl side chain oxidation of a series of alkylated naphthalene congeners. It has been reported that naphthalene is metabolized to trans-1,2-dihydro-1,2-naphthalenediol, 1-naphthol and 2-naphthol, all metabolites resulting from aromatic oxidation, by cytochromes P450 in incubations with pooled human liver microsomes [4]. The P450 isoform CYP1A2 was identified as the most efficient enzyme in production of 1,2-dihydro-1,2-naphthalenediol and 1-naphthol, and CYP3A4 was the most effective enzyme for 2-naphthol production [4]. However, data on metabolic kinetics of alkylated naphthalenes are limited and the oxidation pattern of naphthalene substituted with longer alkyl chains is still unclear.

Based on the available literature [5] and thermodynamic grounds, it can be hypothesized that alkylated PAHs will undergo oxidative metabolism on the alkyl side chain more easily than on the condensed aromatic rings, facilitating their excretion and detoxification over their potential bioactivation. The present study investigates the hypothesis on preferential side chain oxidation at the cost of aromatic oxidation using naphthalene and a series of its alkyl substituted analogues as the model compounds. To this end, the oxidative metabolism of 1-methylnaphthalene, 2-methylnaphthalene, 1-ethylnaphthalene, 2-ethylnaphthalene, 1-n-hexylnaphthalene and 1-n-dodecylnaphthalene in human and rat hepatic microsomal incubations was characterized, and the kinetics and metabolic efficiencies for formation of the different metabolites were quantified.

## **2. Materials and methods**

### **2.1 Chemicals and reagents**

Naphthalene ( $\geq 99\%$ ), and 1-methylnaphthalene ( $\geq 94\%$ ) were purchased from Merck (Darmstadt, Germany). 2-methylnaphthalene ( $\geq 97\%$ ), 1-ethylnaphthalene ( $\geq 97\%$ ), 2-ethylnaphthalene ( $\geq 99\%$ ), and the reference standards 1-naphthol ( $\geq 99\%$ ), 1-(hydroxymethyl) naphthalene ( $\geq 98\%$ ), 2-(hydroxymethyl) naphthalene ( $\geq 98\%$ ), 1-(1-hydroxyethyl) naphthalene ( $\geq 99\%$ ), 2-(1-hydroxyethyl) naphthalene ( $\geq 98\%$ ), and 2-(hydroxyethyl) naphthalene ( $\geq 98\%$ ), and also tetrahydrofuran ( $\geq 99.9\%$ ), and trifluoroacetic acid ( $\geq 99\%$ ), were purchased from Sigma-Aldrich (St.Louis, USA). 1-n-hexylnaphthalene ( $\geq 99.3\%$ ) was synthesized by the Biochemical Institute for Environmental Carcinogens (Großhansdorf, Germany). 1-n-dodecylnaphthalene ( $\geq 95\%$ ) was purchased from Combi-Blocks (San Diego, USA). Acetonitrile was bought from Biosolve (Dieuze, France).  $\alpha$ -naphthaflavone was obtained from Acros (New Jersey, USA). Dimethyl sulfoxide (DMSO) and  $\text{K}_2\text{HPO}_4 \cdot 3\text{H}_2\text{O}$  were supplied by Merck (Darmstadt, Germany). NADPH was

obtained from Carbosynth (Berkshire, UK). Gentest™ pooled male Sprague Dawley rat liver microsomes (RLM) and Ultrapool™ human liver microsomes (HLM) 150 with a protein concentration of 20 mg/ml were supplied by Corning (New York, USA), and the latter contained cytochrome P450 liver enzymes of 150 individuals.

## **2.2 In vitro incubations of naphthalene and its alkylated congeners with human and rat liver microsomes**

Microsomal oxidation of naphthalene and its alkylated congeners by HLM and RLM was investigated. An overall 200 µl incubation system consisted of potassium phosphate buffer (0.1 M, pH 7.4), 5 mM MgCl<sub>2</sub>, HLM/RLM at a final microsomal protein concentration of 0.5 mg/ml, 1 mM NADPH, and each of the individual test compounds at concentrations ranging from 0 to 600 µM. Test compounds were naphthalene, 1-methylnaphthalene, 2-methylnaphthalene, 1-ethylnaphthalene, 2-ethylnaphthalene, 1-n-hexylnaphthalene and 1-n-dodecylnaphthalene. The final concentration of substrate solvent, either DMSO or tetrahydrofuran (the latter used for 1-n-hexylnaphthalene and 1-n-dodecylnaphthalene due to their low solubility in DMSO), in the incubation mixture was 1% (v/v), which did not affect the enzymatic activity of rat liver microsomes [6]. The incubation mixtures were prepared and incubated in glass vials to avoid plastic binding of the substrates. The glass vials were capped to prevent substrate loss due to volatility. After pre-incubation of the incubation mixture at 37°C for 1 min, the enzymatic reaction was initiated by adding microsomes to the incubation mixture which was subsequently incubated at 37°C for 10 min. The reaction was terminated by adding 100 µl ice-cold acetonitrile followed by vortexing. After 5 min centrifugation at 5000 rpm, 4°C, the supernatant was collected for ultra-performance liquid chromatography (UPLC) analysis. However, concentrations of the metabolites of two of the test substrates, 1-n-hexylnaphthalene and 1-n-dodecylnaphthalene, in the supernatant

appeared too low to detect metabolism due to binding to microsomal protein. Therefore, a diisopropylether (DIPE) extraction of the metabolites was performed after the reaction was stopped by the addition of 20  $\mu$ l 10% HClO<sub>4</sub>. The incubation mixture (total volume of 220  $\mu$ l) was extracted three times with 1 ml DIPE. Each time, the upper layer was collected and the combined DIPE fractions were subsequently vaporized under a nitrogen stream. The residues were dissolved in 100  $\mu$ l methanol and analyzed by UPLC.

To investigate the species differences between HLM and RLM, an inhibition study of CYP1A in incubations of naphthalene, 1-methylnaphthalene and 1-ethylnaphthalene was performed. An overall 200  $\mu$ l incubation system consisted of potassium phosphate buffer (0.1 M, pH 7.4), 5 mM MgCl<sub>2</sub>, HLM/RLM at a final microsomal protein concentration of 0.5 mg/ml, 1 mM NADPH, 1  $\mu$ M  $\alpha$ -naphthoflavone (an inhibitor of CYP1A), and each of the individual test compounds at a concentration of approximately the same value as K<sub>M</sub>. The test concentration of each substrate was 60  $\mu$ M for HLM and 200  $\mu$ M for RLM. The incubation was performed by the same procedure as described above, with an incubation time of 10 min at 37°C. The reaction was stopped by addition of 100  $\mu$ l ice-cold acetonitrile followed by vortexing and a 5-min centrifugation at 5000 rpm at 4°C, the supernatant was collected for ultra-performance liquid chromatography (UPLC) analysis.

### **2.3 UPLC analysis**

The metabolites formed were analyzed and quantified using an Acquity UPLC system equipped with a photodiode array (PDA) detector (Waters, Milford, MA). The metabolites and their parent compound were separated on a reverse phase Acquity UPLC® BEH C18 column (21  $\times$  50 mm, 1.7  $\mu$ m, Waters, Milford, MA) and detected at wavelength ranging from 190 nm to 400 nm. Eluent A was nano-pure water containing 0.1% trifluoroacetic acid (v/v), and eluent B was acetonitrile containing 0.1% trifluoroacetic acid (v/v). The gradient elution started from 90% A and 10% B



applied from 0.0 min to 0.5 min, which was changed to 10% A and 90% B from 0.5 to 12.5 min and then kept at 10% A and 90% B from 12.5 min to 13.5 min, changed back to 90% A and 10% B from 13.5 to 14.5 min and then maintained at the starting conditions from 14.5 min until 17 min. The total run time was 17 min using a flow rate of 0.6 ml/min. The temperature of the column was set at 40°C and the autosampler at 10°C during the UPLC analysis. The injection volume was 3.5 µl. Metabolites were quantified using their peak area at the wavelength specified in Table 1, using calibration curves of available reference compounds. Metabolites were identified by comparing the retention time (RT) and wavelength spectra to reference standard chemicals on UPLC. When reference standard chemicals were not available commercially, metabolite identification by GC-MS/MS was performed. The unknown minor metabolites were categorized by concerning elution time and mass spectra both on UPLC and GC-MS/MS.

#### **2.4 Metabolite identification by GC-MS/MS**

To prepare samples for metabolite identification by GC-MS/MS, each individual substrate (300 µM final concentration) was incubated in a volume of 400 µl in potassium phosphate buffer (0.1 M, pH 7.4) containing 5 mM MgCl<sub>2</sub>, HLM/RLM at a final microsomal protein concentration of 1 mg/ml, and 1 mM NADPH at 37°C for 10 min. After incubation, the incubation mixture was centrifuged for 5 min at 5000 rpm and 4°C. The supernatant of the incubation mixture was transferred to a fresh vial and extracted 3 times with 100 µl dichloromethane (DCM) followed by vortexing. DCM phase containing the substrate and metabolites was separated from the aqueous mixture. The organic (lower) phase was collected from each extraction, combined and used for GC-MS/MS measurement. The spectra of each metabolite obtained from measurement were compared with mass spectra data center NIST library (14, 14s, 17-1, 17-2, 17s) installed in GCMS solution software Version 4.45 (Shimadzu, Japan).

The metabolites formed from naphthalene, 1-methylnaphthalene, 2-methylnaphthalene, 1-ethylnaphthalene, 2-ethylnaphthalene and 1-n-hexylnaphthalene were analyzed using a Shimadzu GC-MS/MS system consisting of GC-2010 Plus coupled with Mass spectrometer TQ8040 (Shimadzu, Japan). A 30 m capillary column with 0.25 mm diameter (SH-Rxi-5ms, Shimadzu, Japan) was used to separate the metabolites upon injection of 1  $\mu$ l of the extract with split ratio of 20:1, using a constant flow of helium gas (1 ml/min). The column oven temperature started at 80°C and 1-min hold, increased to 280°C at a rate of 40°C/min from 1 min to 6 min, followed by 2 min hold at 280°C. The total run time was 8 min and electron ionization (70eV) was used to generate the ions of metabolites for mass spectrometric detection.

## **2.5 Data analysis**

The metabolite concentrations were quantified by UPLC and used to calculate velocity of the enzymatic reaction in pmol/min/mg microsomal protein. The kinetic parameters  $K_M$  and  $V_{max}$  were obtained using a nonlinear regression (curve fit) applying the Michaelis Menten equation in GraphPad Prism 5 (San Diego, USA). Some kinetic curves seemed to be better fitted by other modelling approaches, such as substrate inhibition and sigmoidal models, however the outcome parameters from fits were not realistic. Michaelis Menten approach gave basically an equally good fit, with more realistic parameters and was therefore applied as a first approximation to describe the metabolism in terms of  $V_{max, app.}$  and  $K_{M, app.}$ . The intrinsic clearance ( $Cl_{int}$ ) was calculated as  $V_{max}$  divided by  $K_M$  to compare the metabolic efficiency of formation of the different metabolites.

## **3. Results**

### **3.1 Microsomal metabolism of naphthalene and its alkyl substituted analogues**

The substrate concentration-dependent metabolite formation of naphthalene, 1-methylnaphthalene, 2-methylnaphthalene, 1-ethylnaphthalene, 2-ethylnaphthalene and 1-n-hexylnaphthalene by both

HLM and RLM is presented in **Figure 1**. Since inhibition was apparent at higher concentrations in the microsomal incubations with 1-hexylnaphthalene, these concentrations were excluded on the Michalis-Menten analysis and for the calculation of  $V_{\max, \text{app}}$  and  $K_{M, \text{app}}$ . 1-n-Dodecyl naphthalene was not metabolized under the experimental conditions applied. The kinetic parameters including  $K_{M, \text{app}}$ ,  $V_{\max, \text{app}}$  and  $Cl_{\text{int}}$ , derived from modelling the data are presented in **Table 1**.

Two metabolites were detected in metabolic incubations of naphthalene with both HLM and RLM (**Figure 1**) and were identified as 1-naphthol and 1,2-dihydro-1,2-naphthalenediol. The dihydrodiol was the most abundant metabolite formed by HLM, while 1-naphthol was the primary metabolite formed by RLM. The  $Cl_{\text{int}}$  for 1,2-dihydro-1,2-naphthalenediol formation by HLM was significantly higher than that by RLM, but for 1-naphthol formation the  $Cl_{\text{int}}$  by HLM and RLM were similar (**Table 1**).

The primary metabolites formed by both HLM and RLM from the investigated alkylated naphthalenes were alcohols, which are more polar than the parent compounds. The most abundant metabolites formed by HLM and RLM from 1-methylnaphthalene, 2-methylnaphthalene, 1-ethylnaphthalene, and 2-ethylnaphthalene were identified as metabolites resulting from side-chain oxidation being 1-(hydroxymethyl)naphthalene, 2-(hydroxymethyl)naphthalene, 1-(1-hydroxyethyl)naphthalene, and 2-(1-hydroxyethyl)naphthalene, respectively (**Figure 1**), as demonstrated by co-elution and similar absorbance spectra as the reference standards in the UPLC analysis.

Minor metabolites of 1-methylnaphthalene, 2-methylnaphthalene, 1-ethylnaphthalene, 2-ethylnaphthalene, and 1-n-hexylnaphthalene were characterized by comparing mass spectra of these metabolites obtained using GC-MS/MS to those of reference spectra in the NIST library. Two metabolites of 1-methylnaphthalene eluting at 2.14 min and 2.18 min (**Table 1**) were characterized

as dihydro-1-methylnaphthalenediols based on their molecular ion peak of  $m/z$  176 and a similar fragmentation pattern in the mass spectra as observed for 1,2-dihydro-naphthalenediol. Three minor 1-methylnaphthalene metabolites with retention time of 4.30 min, 4.59 min and 4.95 min (**Table 1**) were tentatively identified as 1-methylnaphthols based on their molecular ion peak of  $m/z$  158 and MS spectra comparable to reference spectra in the NIST library.

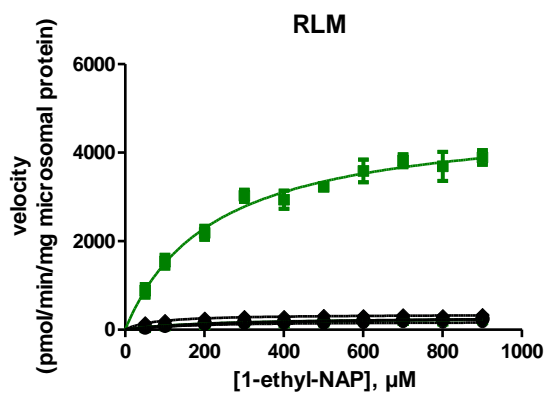
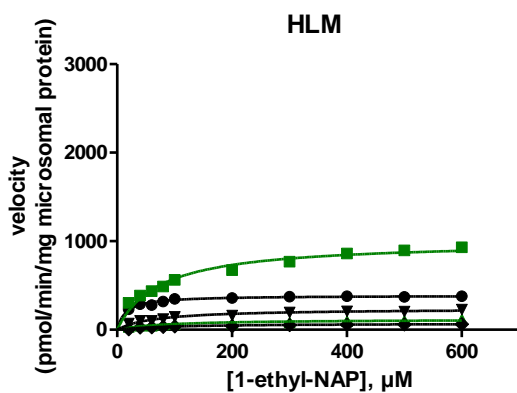
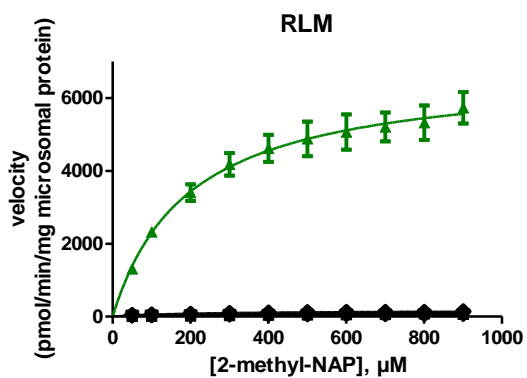
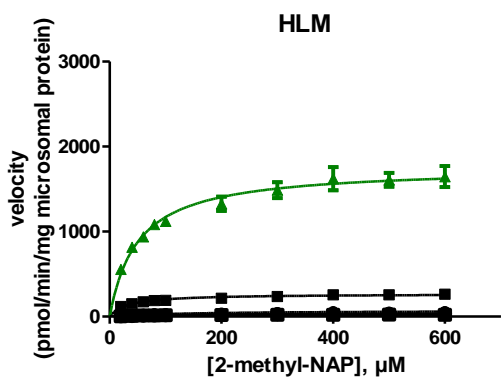
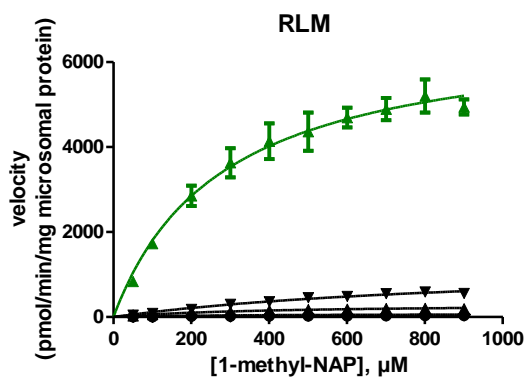
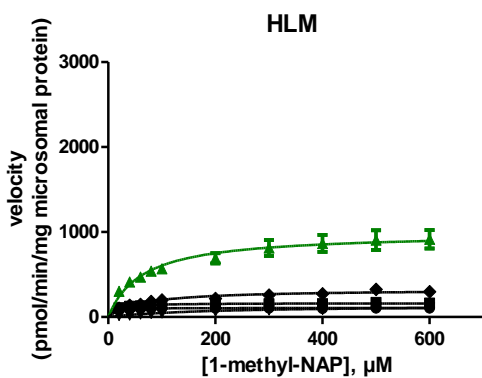
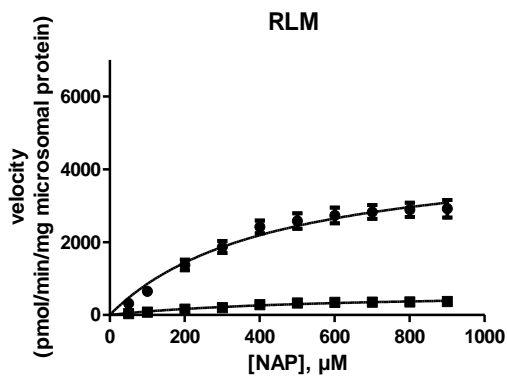
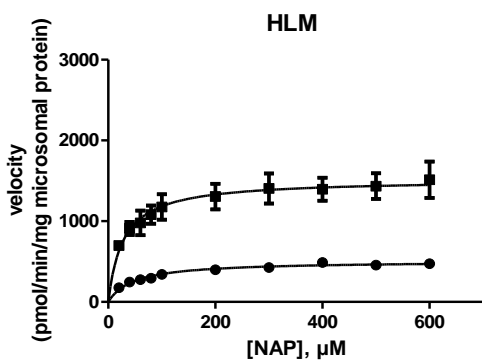
The minor metabolites formed from 2-methylnaphthalene (**Table 1**) eluting at 1.70 min, 1.96 min and 2.25 min were characterized as dihydro-2-methylnaphthalenediols with a molecular ion peak of  $m/z$  176, and three 2-methylnaphthalene dihydrodiols with  $m/z$  176, including the 3,4-dihydrodiol, the 5,6-dihydrodiol and the 7,8-dihydrodiol, in line with what was reported previously for conversion of 2-methylnaphthalene in rat liver microsomal incubations [7]. In the present study, formation of 5,6-dihydro-2-methylnaphthalenediol was observed only at high concentrations of 600 $\mu$ M 2-methylnaphthalene incubated with RLM.

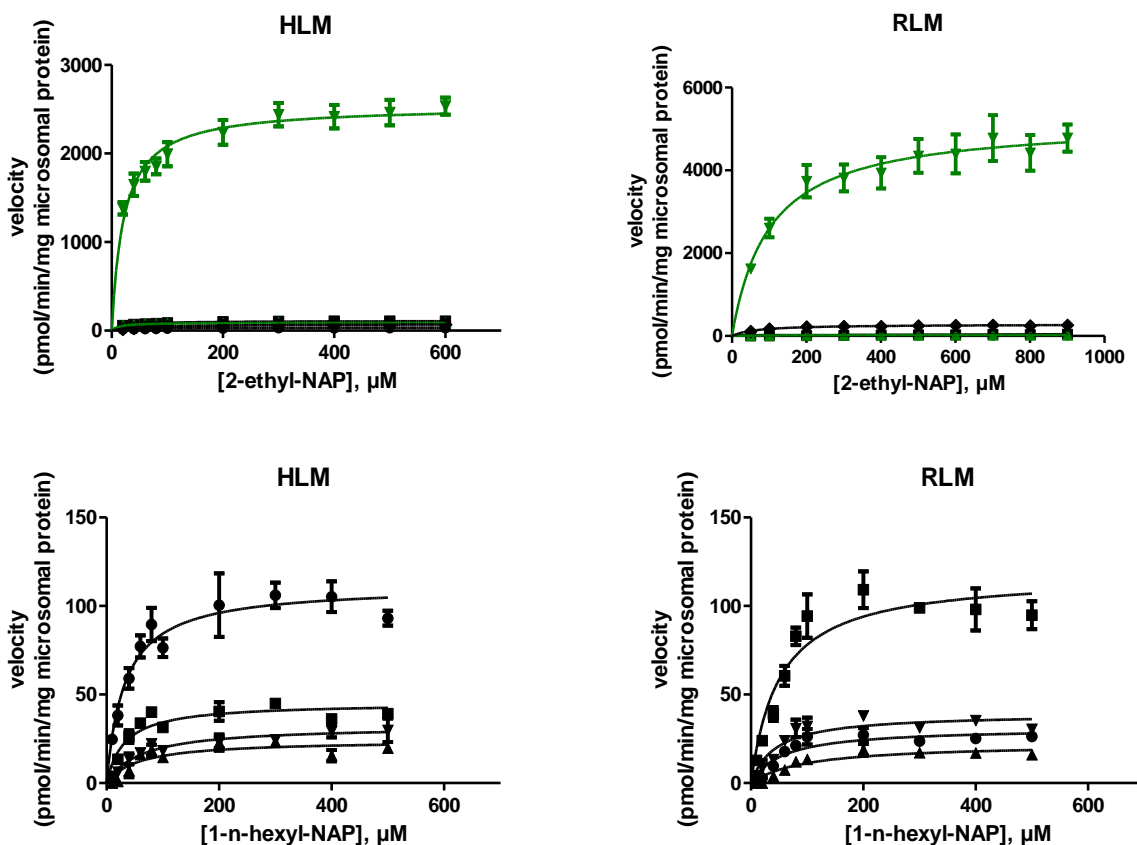
Among the five minor metabolites of 1-ethylnaphthalene, the metabolite eluting at 2.96 min was identified as dihydro-1-ethylnaphthalenediol based on its  $m/z$  190 and its fragmentation pattern being similar to those of an available reference compound. Furthermore, the mass spectra of the metabolite with retention time 3.97 min and a base peak of  $m/z$  155 and a molecular ion peak of  $m/z$  170, suggested it to be 1-naphthylmethylketone because these mass spectra characteristics were similar to those of 2-naphthylmethylketone (a metabolite of 2-ethylnaphthalene, *vide infra*) in the NIST library. Two additional metabolites with retention time of 5.29 min and 5.34 min and a base peak of  $m/z$  157 were assigned as 1-ethylnaphthols. The metabolite with retention time of 6.65min was not found in GC-MS analysis so assigned as unknown.

The 3 metabolites of 2-ethylnaphthalene eluting at 2.64 min, 3.04 min and 3.08 min were characterized as dihydro-2-ethylnaphthalenediols with a molecular ion peak of  $m/z$  190. The

metabolite of 2-ethylnaphthalene with retention time of 3.91 min showed a base peak of  $m/z$  127 and a molecular ion peak of  $m/z$  172 in the mass spectra, while the metabolite co-eluted with the reference compound 2-hydroxyethylnaphthalene on UPLC and its MS spectrum also matched the spectrum of 2-hydroxyethylnaphthalene in the NIST library. An additional metabolite of 2-ethylnaphthalene was detected at the GC with retention time of 5.5 min. This metabolite was not observed in the UPLC chromatogram. A molecular peak of  $m/z$  170 and a base peak of  $m/z$  127 of this additional metabolite observed in the mass spectrum, matched the mass spectrum of 2-naphthylmethylketone in the NIST library. The metabolite with retention time of 6.66min was not found in GCMS analysis so assigned as unknown.

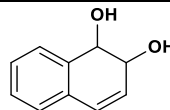
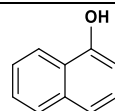
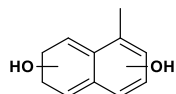
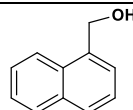
Four minor metabolites of 1-n-hexylnaphthalene with retention times ranging from 5.95 min to 6.38 min on UPLC were tentatively ascribed to different forms of 1-hexylnaphthol because of their molecular ion peak at  $m/z$  228, and a fragmentation pattern similar to other naphthols with high intensity peaks at  $m/z$  157.



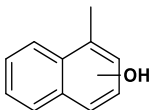
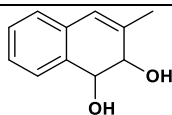
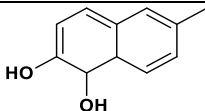
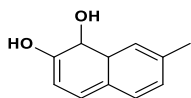
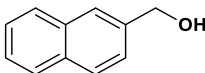
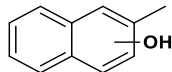


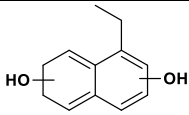
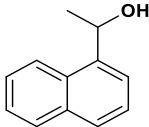
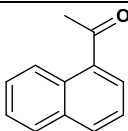
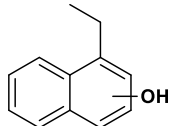
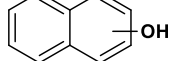
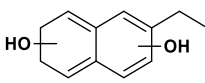
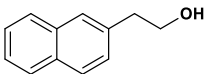
**Figure 1.** Substrate-concentration dependent metabolism of alkyl substituted naphthalenes and naphthalene itself by human and rat liver microsomes. Green line represents alkyl chain oxidation and blue line stands for aromatic ring oxidation. The figures with enlarged scale of minor metabolites are attached as Figure 1 to the supplementary materials. Abbreviation. NAP = naphthalene.

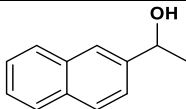
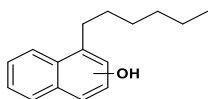
**Table 1.** The Michalis Menten parameters including  $K_{M, app}$ ,  $V_{max, app}$  and intrinsic clearance ( $Cl_{int}$ ) calculated as  $V_{max, app}/K_{M, app}$ , of the metabolites produced from alkyl substituted naphthalenes and naphthalene in human and rat microsomal incubations (Figure 1). The retention time (RT) and wavelength ( $\lambda$ ) used to identify and quantify the metabolites by UPLC-UV analysis are also presented. Results are shown as mean  $\pm$  standard error (SE) from three independent microsomal incubations. Abbreviations. ND=not detected. NM=no metabolism. NA=not applicable. app.=apparent.

Metabolites	Structure	Species	K <sub>M, app</sub> (μM)	V <sub>max, app</sub> (pmol/min/mg microsomal protein)	Cl <sub>int</sub> (V <sub>max</sub> /K <sub>M</sub> ) μl/min/mg protein
Naphthalene RT=5.59min, λ=220.7nm					
1,2-dihydro-1,2-naphthalenediol RT=1.43min,λ=215.8nm		Human	28.1 ± 7.3	1517.0 ± 78.8	54.0
		Rat	562.2 ± 238.2	634.4 ± 133.3	1.1
1-naphthol RT=3.91min, λ=211.6nm		Human	47.0 ± 7.7	507.4 ± 20.4	10.8
		Rat	436.3 ± 95.2	4578.0 ± 444.0	10.5
1-methylnaphthalene RT=6.33min, λ=223.7nm					
Dihydro-1-methylnaphthalenediol RT=2.14min, λ=217.6nm		Human	5.3 ± 1.3	107.3 ± 2.0	20.1
		Rat	ND	ND	-
Dihydro-1-methylnaphthalenediol RT=2.18 min, λ=220.7 nm		Human	11.5±4.7	163.1±8.4	14.2
		Rat	683.3±335.8	56.0±14.8	0.1
1-(hydroxymethyl)naphthalene RT=3.29min, λ=223.7nm		Human	63.5±12.3	989.6±52.7	15.6
		Rat	278.9±49.5	6823.0±437.9	24.5
1-methylnaphthol RT=4.49min, λ=228.5nm		Human	190.7±18.6	141.0±5.5	0.7
		Rat	408.7±55.0	310.5±18.0	0.8



1-methylnaphthol RT=4.59min, λ=210.4nm		Human	61.8±8.0	325.1±11.4	5.3
		Rat	1008.0±315.0	1291.0±249.8	1.3
1-methylnaphthol RT=4.95min, λ=219.4nm		Human	ND	ND	-
		Rat	295.1±160.5	76.5±15.4	0.3
2-methylnaphthalene RT=6.43min, λ=223.7nm					
3,4-dihydro-2-methylnaphthalene diol RT=1.70min, λ=224.3nm		Human	ND	ND	-
		Rat	505.8±183.3	56.4±9.7	0.1
5,6-dihydro-2-methylnaphthalenediol RT=1.96min, λ=217nm		Human	139.8±59.2	72.0±10.9	0.5
		rat	ND	ND	-
7,8-dihydro-2-methylnaphthalenediol RT=2.25min, λ=219.4nm		Human	31.4±4.3	266.8±7.7	8.5
		Rat	2542.0±1419.0	268.2±118.5	0.1
2-(hydroxymethyl)naphthalene RT=3.39min, λ=224.9nm		Human	50.4±5.9	1760.0±51.9	34.9
		Rat	194.5±36.5	6769.0±386.6	34.8
2-methylnaphthol RT=4.48min, λ=227.3nm		Human	93.6±28.7	23.5±2.2	0.3
		Rat	464.2±78.6	111.5±8.6	0.2
2-methylnaphthol RT=4.58min, λ=227.9nm		Human	88.4±17.5	35.1±2.1	0.4
		Rat	650.8±235.2	72.8±13.8	0.1
2-methylnaphthol RT=4.66min, λ=215.8nm		Human	226.5±67.5	47.68±6.0	0.2
		Rat	218.1±50.3	166.5±12.4	0.8
2-methylnaphthol RT=4.72min, λ=215.8nm		Human	66.2±17.2	25.4±1.8	0.4
		Rat	483.8±91.6	166.0±14.6	0.3
1-ethylnaphthalene RT=7.00min, Ab=224.3nm					

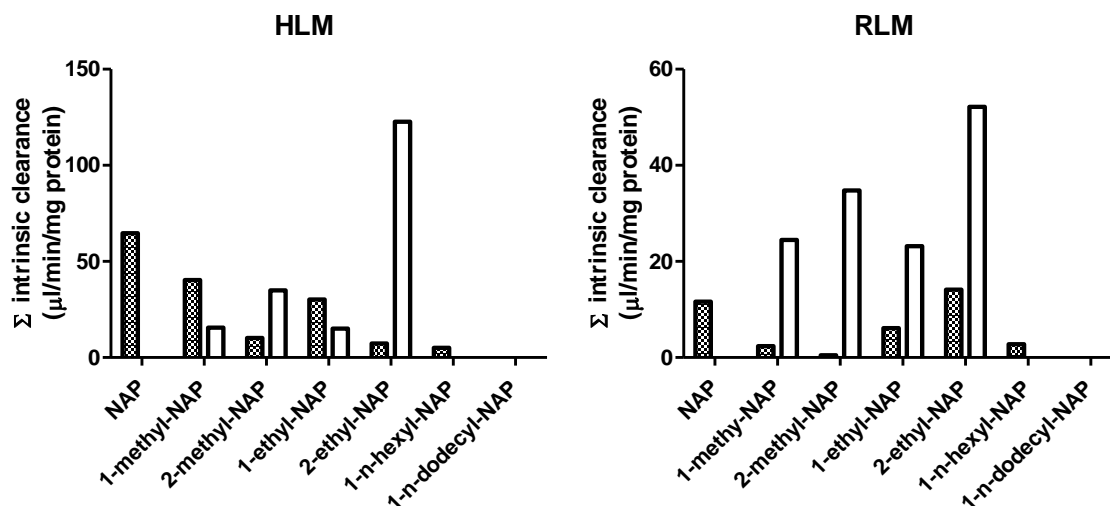
Dihydro-1-ethylnaphthalenediol RT=2.96min, λ=218.2nm		Human	14.9±2.7	386.8±10.4	25.9
		rat	140.9±62.9	186.3±21.7	1.3
1-(1-hydroxyethyl)naphthalene RT=3.92min, λ=223.7nm		Human	73.6±7.7	1001.0±30.0	13.6
		Rat	221.4±34.4	4831.0±243.2	21.8
1-naphthyl methylketone RT=3.97min, λ=224.3nm		Human	86.0±19.4	119.3±8.2	1.4
		Rat	209.7±76.5	280.3±32.3	1.3
1-ethylnaphthol RT=5.29min, λ=211nm		Human	67.3±9.5	239.7±9.5	3.6
		Rat	391.0±97.6	338.2±35.7	0.9
1-ethylnaphthol RT=5.34min, λ=224.3nm		Human	ND	ND	-
		Rat	72.1±19.1	349.8±17.6	4.9
RT=6.65min, λ=227.3nm	Unknown	Human	99.1±16.3	72.5±3.8	0.7
		Rat	226.1±83.6	291.7±35.3	1.3
2-ethylnaphthalene RT=7.11min, λ=224.9nm					
Dihydro-2-ethylnaphthalenediol RT=2.64min, λ=224.9nm		Human	ND	ND	-
		Rat	23.7±23.6	27.0±2.8	1.1
Dihydro-2-ethylnaphthalenediol RT=3.04min, λ=220nm		Human	21.9±7.2	34.4±2.0	1.6
		Rat	ND	ND	ND
Dihydro-2-ethylnaphthalenediol RT=3.08min, λ=220nm		Human	24.1±3.6	110.1±3.1	4.6
		Rat	Ambiguous	Ambiguous	-
2-(2-hydroxyethyl)naphthalene RT=3.91min, λ=224.3nm		Human	13.0±4.8	89.0±4.5	6.9
		Rat	99.8±21.6	26.5±1.3	0.3



2-(1-hydroxyethyl)naphthalene RT=3.96min, λ=224.3nm		Human	21.9±3.2	2540.0±65.1	115.9
		Rat	100.2±23.3	5200.0±268.2	51.9
RT=6.66min, λ=243.8nm	Unknown	Human	64.6±7.4	76.0±2.4	1.2
		Rat	65.7±18.7	280.9±14.5	4.3
1-n-hexylnaphthalene RT=9.58min, λ=224.9nm					
1-hexylnaphthol RT=5.95min, λ=219.4nm		Human	38.4±11.7	119.4±12.8	3.1
		Rat	119.2±55.8	48.1±12.1	0.4
Human		44.7±14.4	52.3±6.3	1.2	
Rat		110.0±30.4	178.5±25.8	1.6	
Human		139.3±87.6	40.3±14.4	0.3	
Rat		364.9±259.0	55.4±28.9	0.2	
Human		58.2±20.9	31.6±4.7	0.5	
Rat		97.3±35.4	59.7±10.9	0.6	
1-n-dodecylnaphthalene RT=12.3min, λ=224.9nm					
NM	NA	Human	-	-	-
NM		Rat	-	-	-

### 3.2 Intrinsic clearance by aromatic and alkyl side chain oxidation

Based on the kinetic data obtained, the intrinsic clearance by formation of aromatic ring versus alkyl side chain oxidation metabolites of each test compound was calculated by adding up the  $Cl_{int}$  values of the respective metabolites, and the data thus obtained are presented in **Figure 2**. The intrinsic clearance of naphthalene via aromatic ring oxidation metabolites, including 1-naphthol and dihydrodiol with HLM was 64.74  $\mu\text{l}/\text{min}/\text{mg}$  protein. In comparison, the intrinsic clearance via aromatic ring oxidation of 1-methylnaphthalene, 2-methylnaphthalene, 1-ethylnaphthalene, 2-ethylnaphthalene and 1-n-hexylnaphthalene by HLM were 1.6 to 12.7 fold lower than that for naphthalene, indicating that metabolites resulting from aromatic ring oxidation were formed relatively less efficient for alkyl substituted naphthalenes. For 1-methylnaphthalene, 1-ethylnaphthalene, 2-methylnaphthalene and 2-ethylnaphthalene this decreased intrinsic clearance via formation of metabolites resulting from aromatic ring oxidation was accompanied by a significant increase in intrinsic clearance via alkyl chain oxidation metabolites with HLM. For 2-methylnaphthalene and 2-ethylnaphthalene the intrinsic clearance via side chain oxidation even substantially exceeded that via aromatic oxidation by 3.4 and 16.8 fold, respectively.

In RLM incubations, the intrinsic clearance of naphthalene by metabolite formation from naphthalene was 11.62  $\mu\text{l}/\text{min}/\text{mg}$  protein, which is 5.6 folds lower than the intrinsic clearance observed with HLM. Also, with RLM the intrinsic clearance via aromatic ring oxidation of 1-methylnaphthalene, 2-methylnaphthalene, 1-ethylnaphthalene, 2-ethylnaphthalene and 1-n-hexylnaphthalene was reduced, being 1.4 to 7.0 fold lower than that for naphthalene. In incubations with RLM, alkyl chain oxidation dominated over aromatic ring oxidation for all alkyl substituted naphthalenes with the exception of 1-n-hexylnaphthalene.



**Figure 2.** Intrinsic clearance via aromatic ring oxidation and alkyl chain oxidation by HLM and RLM for the different model compounds.  Aromatic ring oxidation;  alkyl chain oxidation. Abbreviation. NAP = naphthalene.

### 3.3 Inhibition studies on the oxidative metabolism of on naphthalene, 1-methylnaphthalene and 1-ethylnaphthalene

To study the remarkable difference in metabolism between rat and human metabolic activity the influence of CYP1A inhibition was determined in microsomal incubations of naphthalene, 1-methylnaphthalene and 1-ethylnaphthalene by coincubation of  $\alpha$ -naphthoflavone, a specific inhibitor of CYP1A. It was shown that the formation of dihydrodiols in incubations with HLM decreased 11%–39% for the three test compounds inhibition of CYP1A (Figure 2 and Table 1 both in supplementary materials), however no differences in dihydrodiol formation by RLM was observed. Alkyl side chain oxidation on 1-methylnaphthalene and 1-ethylnaphthalene was also inhibited 14% to 28% by  $\alpha$ -naphthoflavone in incubations with HLM, while little difference in alkyl side chain oxidation upon CYP1A inhibition by rat was observed with 0-3% increase compared to the control (**Table 2**).

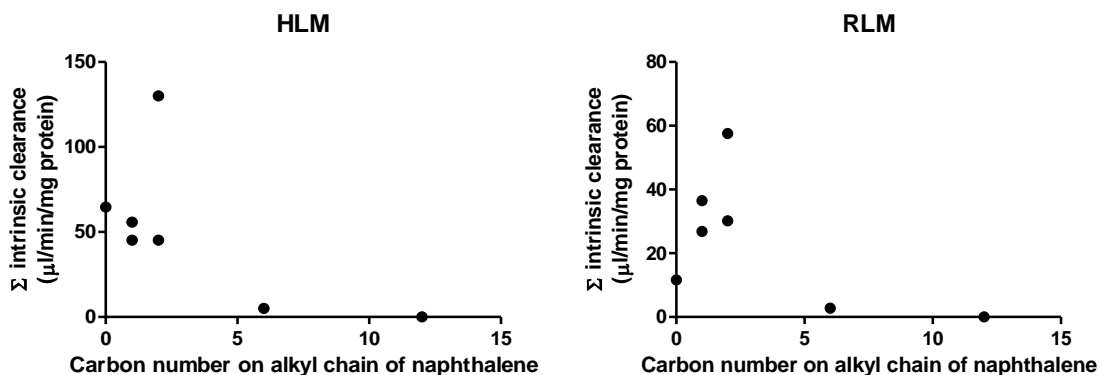
**Table 2.** Inhibition of metabolic activity of aromatic ring and alkyl chain oxidative metabolites of naked and substituted naphthalenes by  $\alpha$ -naphthoflavone. The results are expressed by percentage of control activity  $\pm$  SD. Detailed results of each metabolite can be found in Table 1 and Fig. 2 both in the supplementary material.

Substrate	Species	Aromatic ring oxidation (%)	Alkyl chain oxidation (%)
naphthalene	Human	$75 \pm 3$	0
	Rat	$114 \pm 20$	0
1-methyl-naphthalene	Human	$87 \pm 5$	$86 \pm 6$
	Rat	$94 \pm 2$	$100 \pm 11$
1-ethyl-naphthalene	Human	$86 \pm 1$	$72 \pm 6$
	Rat	$99 \pm 3$	$103 \pm 13$

### 3.4 Effect of alkyl chain length on total intrinsic clearance

**Figure 3** shows the relationship between intrinsic clearance of the alkylated naphthalenes and the number of carbon atoms in their alkyl side chain. The total intrinsic clearance was calculated by adding up the  $Cl_{int}$  values of all metabolites of the respective substrate.

The results thus obtained reveal that the total  $Cl_{int}$  of the alkylated naphthalenes by both HLM and RLM becomes less efficient with increasing side chain carbon length especially when the number of carbons in the side chain is 6 or higher (**Figure 3**). The  $Cl_{int}$  of 1-n-hexylnaphthalene (C6) was substantially lower than that of unsubstituted, methyl (C1)- or ethyl (C2)- substituted naphthalene, while 1-n-dodecylnaphthalene (C12) was not converted to a detectable level.



**Figure 3.** Relationship between total  $\text{Cl}_{\text{int}}$  of alkylated naphthalenes and the number of carbon atoms in the alkyl side chain. The intrinsic clearance was calculated by adding up the  $\text{Cl}_{\text{int}}$  values of all metabolites for the respective model compound (Table 1).

#### 4. Discussion

In the present study the biotransformation of the model compounds naphthalene and six of its alkylated analogues was studied in human and rat liver microsomal incubations to better characterize the effect of alkyl substitution on the metabolism of these aromatic hydrocarbons. This is of interest because of safety concerns regarding the presence of substituted aromatic hydrocarbons in mineral oils, and the lack of data on consequences of alkyl substitution on their metabolic fate. It was expected that alkylation would result in substantial side chain oxidation at the cost of aromatic ring oxidation. For PAHs such a metabolic switch from aromatic to side chain oxidation would shift metabolic patterns in favor of detoxification at the cost of potential bioactivation. In line with this hypothesis, alkyl chain substitution resulted in a marked reduction in the intrinsic clearance via aromatic ring oxidation as shown by the 3- to 17- fold reduction in  $\text{Cl}_{\text{int}}$  via aromatic ring oxidation as compared to this  $\text{Cl}_{\text{int}}$  for the naked parent compound naphthalene. This reduction in  $\text{Cl}_{\text{int}}$  values for aromatic oxidation was accompanied by a substantial

increase in intrinsic clearance via side chain oxidation (**Figure 2**). This increase in alkyl side chain oxidation at the cost of aromatic ring oxidation by cytochromes P450 is in line with thermodynamic considerations which predict that alkyl side chains attached to aromatic rings are more easily oxidized than the aromatic ring itself. This holds especially for the carbon atom at the benzylic position, since the radical resulting after hydrogen abstraction by the reactive high valency iron oxo intermediate of the cytochrome P450 enzyme catalyzing the reaction will be resonance stabilized by the aromatic ring. This consideration is in line with the observation that for ethyl substituted naphthalenes alkyl oxidation occurred preferentially at the benzylic carbon of the side chain. For 1-n-hexylnaphthalene side chain oxidation was not observed, which is most likely due to steric hindrance by the C6 alkyl side chain positioning the substrate within the active site of the respective P450s in such a way that the position can no longer be attacked by the activated heme cofactor. This steric hindrance may also explain the substantial reduction in total Clint with increasing alkyl chain length, resulting in substantial reduction and even no detectable substrate conversion for 1-n-hexylnaphthalene and 1-n-dodecylnaphthalene respectively.

This substantial reduction in intrinsic clearance when the length of the alkyl chain amounted to 6 or more carbon atoms is in line with data reported in a study on rat hepatic metabolism of n-alkanes which also showed that metabolic conversion decreased with increasing carbon number [8]. This study on n-alkanes reported that metabolism in rat liver microsomal incubations was no longer observed with tetradecane (C14), which is in line with the results obtained in this study for 1-n-dodecylnaphthalene (C12), especially when considering that also the carbon atoms in the naphthalene moiety would contribute to the size of the substrate dimensions. Based on these results it is tempting to speculate that alkyl substituents of substantial chain length will also prevent



metabolic conversion and thus bioactivation of alkylated substituted PAHs like phenanthrene and benzo[a]pyrene, when present in mineral oils.

The observations of the present study also match the limited data available in the literature on metabolism of alkylated naphthalenes. In rat studies, it was found that the metabolic oxidation of 2,6-diisopropylnaphthalene happens on the isopropyl side chain [9, 10]. 1-Methylnaphthalene, 2-methylnaphthalene, 1-ethylnaphthalene, 2-ethylnaphthalene, 2,7-dimethylnaphthalene were oxidized on the alkyl chain to alcohol metabolites in vitro by P450 CYP101B1 obtained from the bacteria *Nocardioides aromaticivorans* [5]. Furthermore, the metabolic oxidation of 2-methylnaphthalene and 1,6-dimethylnaphthalene by liver P450 enzymes from mice and rats respectively resulted in the formation of both aromatic ring oxidation dihydrodiols and side chain oxidation hydroxyl metabolites [11, 12]. In general, upon microsomal conversion, naphthalene and its alkylated congeners are oxidized to dihydrodiols or alcohols. These metabolites are expected to be subsequently modified by phase II enzymes to glucuronides, sulfates and UDP glucuronic acid, followed by their excretion from the body [13].

The results obtained in the present study also reveal that the metabolic conversion of the alkylated naphthalenes is not fully dominated by chemical reactivity alone, since some substrate and species-specific differences were observed pointing at an additional influence of positioning of the substrate within the active site of the P450 involved. Thus, results obtained with HLM were different from those obtained with RLM for 1-methylnaphthalene and 1-ethylnaphthalene for which the preferential side chain over aromatic ring oxidation was only observed with RLM. The outcome of the inhibition study also suggests that isoforms play an important role in dihydrodiols formation in humans but less so in rats. For the series of alkyl substituted naphthalenes as a whole, however, alkyl oxidation could easily compete with aromatic hydroxylation and showed  $Cl_{int}$

values that were 0.4- to 16.8-fold and 2.8- to 20.8-fold higher than the  $Cl_{int}$  values for aromatic hydroxylation for HLM and RLM, respectively.

Together the results of the present study support the conclusion that alkyl substitution of naphthalene results in a shift in metabolite clearance in favor of side chain oxidation at the cost of aromatic hydroxylation, while alkyl substituents with 6 or more carbon atoms may seriously reduce metabolic conversion. These conclusions are based on results obtained with a series of naphthalene model compounds. It remains to be established whether similar results would be obtained when studying the metabolism of more mineral oil relevant naked PAHs and their alkyl substituted analogues, especially including aromatic hydrocarbons with more than 3 aromatic rings. This provides an interesting topic for further research. It is expected, but remains to be demonstrated, that alkyl substituents on more “mineral oil relevant PAHs” will show similar metabolic shifts in their oxidation pattern. However, in case of PAHs with 3 or more rings, also the position of the aromatic rings with respect to one another will become a factor that may affect metabolism and toxicity. For example the toxicity of some PAHs may relate to the presence of a so-called “bay region” [14]. For alkylated PAHs this could mean that they may become more and not less toxic than their naked analogues especially when the alkyl chain would form extra (fake) bay regions thus providing extra options for formation of DNA reactive bay-region diol epoxide metabolites. Also, the species differences in metabolic clearance via aromatic ring or side chain oxidation between human and rats remains to be explored to a further extent. To evaluate the consequences of the structure of the substrates for the vivo biotransformation patterns taking also subsequent conjugation reactions into account, future studies may use cellular in vitro models and/or develop physiologically based kinetic models that describe in vivo kinetics, elucidating the consequences of our in vitro findings for the in vivo metabolite patterns in both rat and human. Finally, the

Michaelis Menten parameters obtained in the present study provide a basis for development of physiologically based kinetic (PBK) models for studies on the consequences of alkylation of aromatic hydrocarbons on the metabolic clearance and bioactivation of this important group of constituents present in mineral oils. The present study and further research will also serve as a basis for better risk assessment of mineral oil.

Nevertheless, based on the results of the present study, the main conclusion is that alkylation of PAHs likely reduces their chances on aromatic oxidation and potential bioactivation.

### **Funding information**

This work was financially supported by Concawe, and by a grant from the China Scholarship Council (No. 201807720073) to Danlei Wang.

### **Conflict of interest**

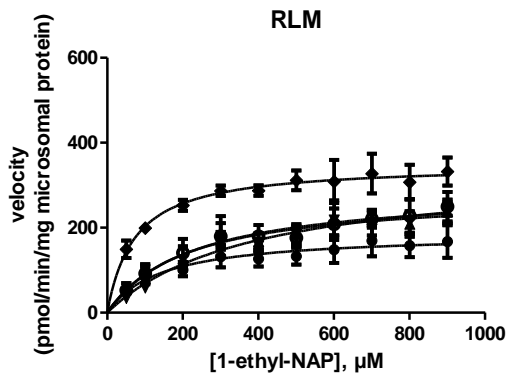
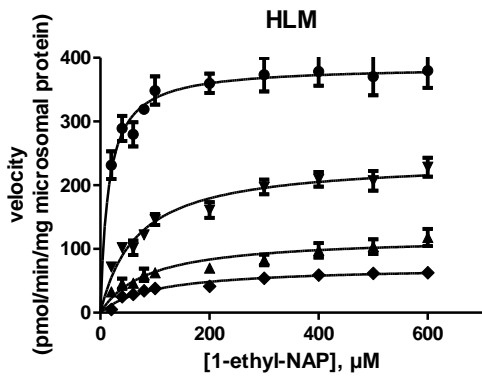
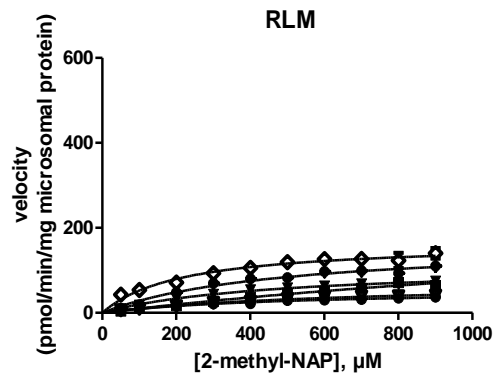
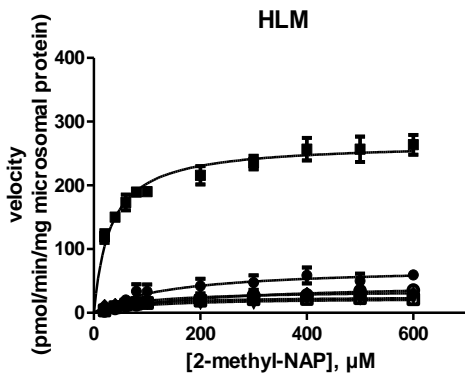
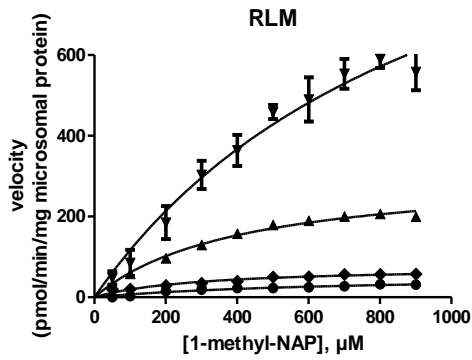
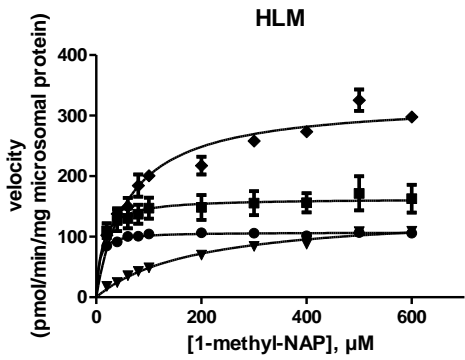
P.J.B. is employed by Shell International, a member company of Concawe, and chairman of the toxicology group of Concawe. Prof. P.J.B. is totally free (by contract) to freely design and conduct research and express his own scientific opinion without any obligation towards either Shell or Concawe. The current findings are not intended to constitute any product endorsement.

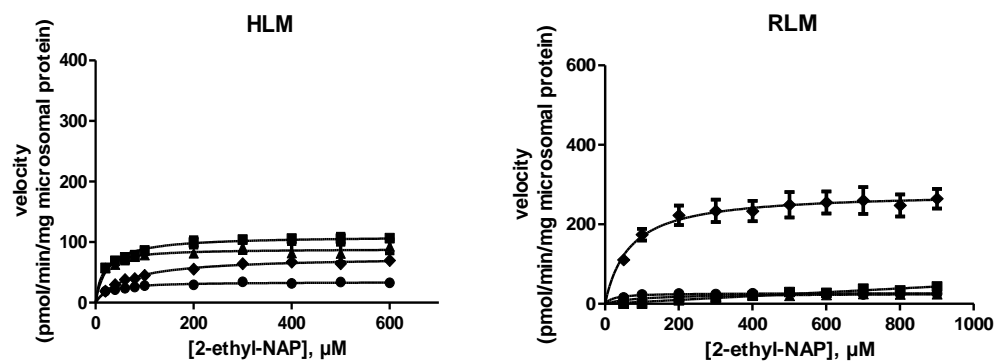
## References

- [1] Scientific Opinion on Mineral Oil Hydrocarbons in Food, EFSA Journal, 10 (2012) 2704.
- [2] B. Ewa, M.S. Danuta, Polycyclic aromatic hydrocarbons and PAH-related DNA adducts, Journal of applied genetics, 58 (2017) 321-330.
- [3] S.B. Hawthorne, D.J. Miller, J.P. Kreitinger, Measurement of total polycyclic aromatic hydrocarbon concentrations in sediments and toxic units used for estimating risk to benthic invertebrates at manufactured gas plant sites, Environmental toxicology and chemistry, 25 (2006) 287-296.
- [4] T.M. Cho, R.L. Rose, E. Hodgson, In vitro metabolism of naphthalene by human liver microsomal cytochrome P450 enzymes, Drug Metab Dispos, 34 (2006) 176-183.
- [5] E.A. Hall, M.R. Sarkar, S.G. Bell, The selective oxidation of substituted aromatic hydrocarbons and the observation of uncoupling via redox cycling during naphthalene oxidation by the CYP101B1 system, Catal Sci Technol, 7 (2017) 1537-1548.
- [6] D. Li, Y. Han, X. Meng, X. Sun, Q. Yu, Y. Li, L. Wan, Y. Huo, C. Guo, Effect of regular organic solvents on cytochrome P450-mediated metabolic activities in rat liver microsomes, Drug metabolism and disposition: the biological fate of chemicals, 38 (2010) 1922-1925.
- [7] R.K. Breger, R.F. Novak, R.B. Franklin, D. Rickert, J.J. Lech, Further Structural-Analysis of Rat-Liver Microsomal Metabolites of 2-Methylnaphthalene, Drug Metabolism and Disposition, 11 (1983) 319-323.
- [8] S.S. Anand, J.L. Campbell, J.W. Fisher, In vitro rat hepatic metabolism of n-alkanes: nonane, decane, and tetradecane, Int J Toxicol, 26 (2007) 325-329.
- [9] H. Hoke, R. Zellerhoff, Metabolism and toxicity of diisopropylnaphthalene as compared to naphthalene and monoalkyl naphthalenes: a minireview, Toxicology, 126 (1998) 1-7.

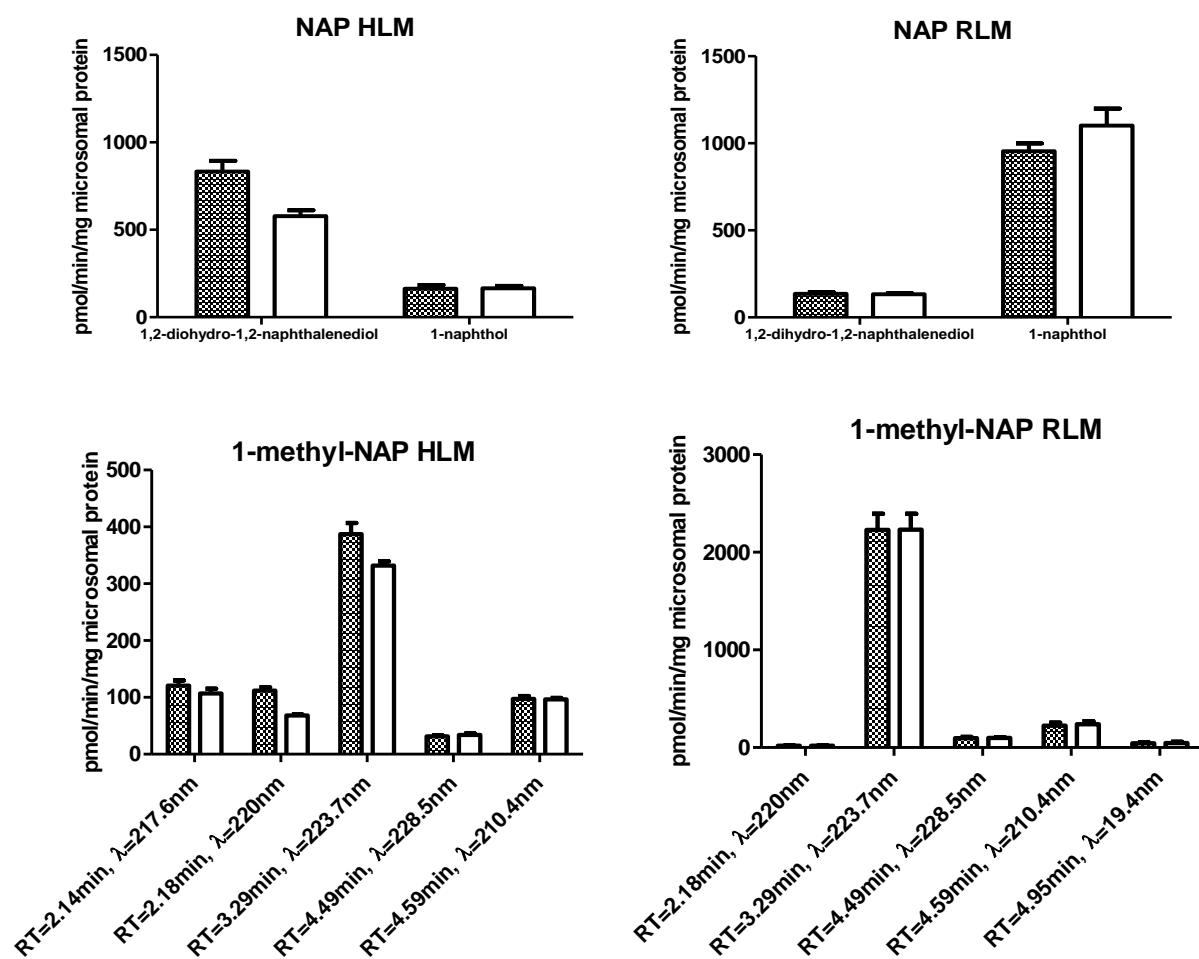
- [10] S. Kojima, T. Honda, M. Nakagawa, M. Kiyozumi, A. Takadate, Urinary metabolites of 2,6-diisopropylnaphthalene in rats, *Drug metabolism and disposition: the biological fate of chemicals*, 10 (1982) 429-433.
- [11] K.A. Griffin, C.B. Johnson, R.K. Breger, R.B. Franklin, Pulmonary toxicity, hepatic, and extrahepatic metabolism of 2-methylnaphthalene in mice, *Toxicology and applied pharmacology*, 61 (1981) 185-196.
- [12] A. Kilanowicz, A. Sapota, B. Czerski, Disposition and metabolism of 1,6-dimethylnaphthalene in rats, *Toxicology letters*, 134 (2002) 227-235.
- [13] C.Y. Lin, A.M. Wheelock, D. Morin, R.M. Baldwin, M.G. Lee, A. Taff, C. Plopper, A. Buckpitt, A. Rohde, Toxicity and metabolism of methylnaphthalenes: comparison with naphthalene and 1-nitronaphthalene, *Toxicology*, 260 (2009) 16-27.
- [14] K.P. Vijayalakshmi, C.H. Suresh, Theoretical studies on the carcinogenicity of polycyclic aromatic hydrocarbons, *J Comput Chem*, 29 (2008) 1808-1817.

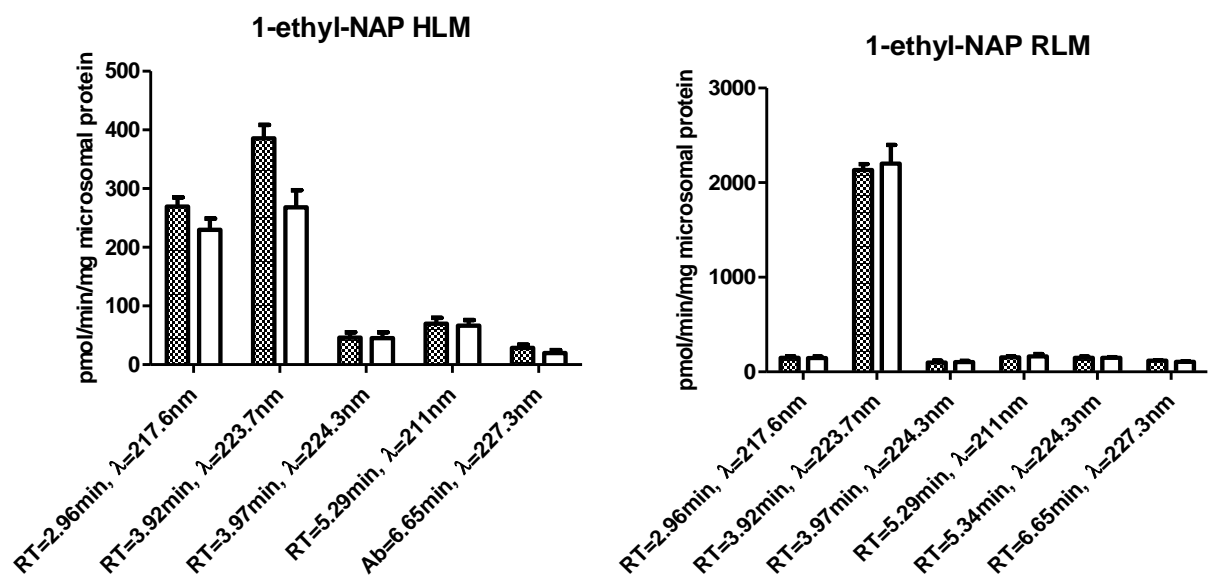
Supplementary materials





**Figure 1.** Enlarged scale of minor metabolites formed by 1-methylnaphthalene, 2-methylnaphthalene, 1-ethylnaphthalene and 2-ethylnaphthalene by HLM and RLM.





**Figure 2.** Inhibition of the formation of each metabolites of NAP, 1-methyl-NAP and 1-ethyl-NAP by HLM and RLM by CYP1A inhibitor  $\alpha$ -naphthoflavone. Metabolite names corresponding to the retention time and the wavelength can be found in Table 1 of the article. control incubation without  $\alpha$ -naphthoflavone incubation with  $\alpha$ -naphthoflavone

**Table 1.** Inhibition of metabolic activity of each metabolite formed by naphthalene, 1-methylnaphthalene and 1-ethylnaphthalene by HLM and RLM with exposure to CYP1A inhibitor  $\alpha$ - naphthoflavone.

Parent compound Metabolite	Species	Percentage of control activity $\pm$ SD
<b>Naphthalene RT=5.59min, <math>\lambda</math>=220.7nm</b>		
1,2-dihydro-1,2-naphthalenediol RT=1.43min, $\lambda$ =215.8nm	Human	70 $\pm$ 3
	Rat	98 $\pm$ 12
1-naphthol RT=3.91min, $\lambda$ =211.6nm	Human	103 $\pm$ 9
	Rat	116 $\pm$ 22



<b>1-methylnaphthalene RT=6.33min, <math>\lambda</math>=223.7nm</b>		
Dihydro-1-methylnaphthalenediol RT=2.14min, $\lambda$ =217.6nm	Human	89 $\pm$ 6
	Rat	ND
Dihydro-1-methylnaphthalenediol RT=2.18 min, $\lambda$ =220.7 nm	Human	61 $\pm$ 8
	Rat	103 $\pm$ 8
1-(hydroxymethyl)naphthalene RT=3.29min, $\lambda$ =223.7nm	Human	86 $\pm$ 6
	Rat	100 $\pm$ 1
1-methylnaphthol RT=4.49min, $\lambda$ =228.5nm	Human	109 $\pm$ 24
	Rat	103 $\pm$ 11
1-methylnaphthol RT=4.59min, $\lambda$ =210.4nm	Human	100 $\pm$ 13
	Rat	107 $\pm$ 2
1-methylnaphthol RT=4.95min, $\lambda$ =219.4nm	Human	ND
	Rat	101 $\pm$ 16
<b>1-ethylnaphthalene RT=7.00min, Ab=224.3nm</b>		
Dihydro-1-ethylnaphthalenediol RT=2.96min, $\lambda$ =218.2nm	Human	85 $\pm$ 4
	Rat	99 $\pm$ 6
1-(1-hydroxyethyl)naphthalene RT=3.92min, $\lambda$ =223.7nm	Human	69 $\pm$ 6
	Rat	103 $\pm$ 13
1-naphthyl methylketone RT=3.97min, $\lambda$ =224.3nm	Human	98 $\pm$ 3
	Rat	108 $\pm$ 19
1-ethylnaphthol RT=5.29min, $\lambda$ =211nm	Human	97 $\pm$ 18
	Rat	106 $\pm$ 16
1-ethylnaphthol RT=5.34min, $\lambda$ =224.3nm	Human	ND
	Rat	99 $\pm$ 12
RT=6.65min, $\lambda$ =227.3nm	Human	67 $\pm$ 10
	Rat	91 $\pm$ 5



## **Chapter 3**

# **The effect of alkyl substitution on the oxidative metabolism and mutagenicity of phenanthrene**

Danlei Wang, Viktoria Schramm, Jeroen Pool, Eleni Pardali, Annemarijn Brandenburg,

Ivonne M.C.M. Rietjens, Peter J. Boogaard.

Manuscript submitted to Archives of Toxicology

## Abstract

Alkyl substituted PAHs may be present in certain petroleum-derived products and in the environment and may eventually end up in consumer products, such as foodstuffs, cosmetics and pharmaceuticals. Safety concerns over possible exposure to alkylated PAHs have emerged. Bioactivation is a prerequisite for the mutagenicity and carcinogenicity of PAHs and has been extensively studied for non-substituted PAHs, while data on the bioactivation of alkyl substituted PAHs are scarce. The present study investigated the effect of alkyl substitution on the CYP 450 mediated metabolism of phenanthrene and eight of its alkylated congeners by quantifying metabolite formation in rat and human liver microsomal incubations. Furthermore, the mutagenicity of four selected methylated phenanthrenes was compared to that of phenanthrene using the Ames test. The obtained results support the hypothesis that alkyl substitution shifts the CYP 450 mediated metabolism from the aromatic ring to the alkyl side chain. Increasing the length of the alkyl-chain reduced overall metabolism with metabolic conversion for 1-n-dodecyl-phenanthrene (C12) being negligible. 1- And 9-methyl-phenanthrene, in which the methyl group generates an additional bay region-like structural motif, showed mutagenicity towards *Salmonella typhimurium* TA98 and TA 100, whereas phenanthrene and also 2- and 3-methyl-phenanthrene, without such an additional bay region-like structural motif, tested negative. It is concluded that the position of the alkylation affects the metabolism and resulting mutagenicity of phenanthrene with the mutagenicity increasing in cases where the alkyl substituent creates an additional bay-region like structural motif, in spite of the extra possibilities for side chain oxidation.

## **1. Introduction**

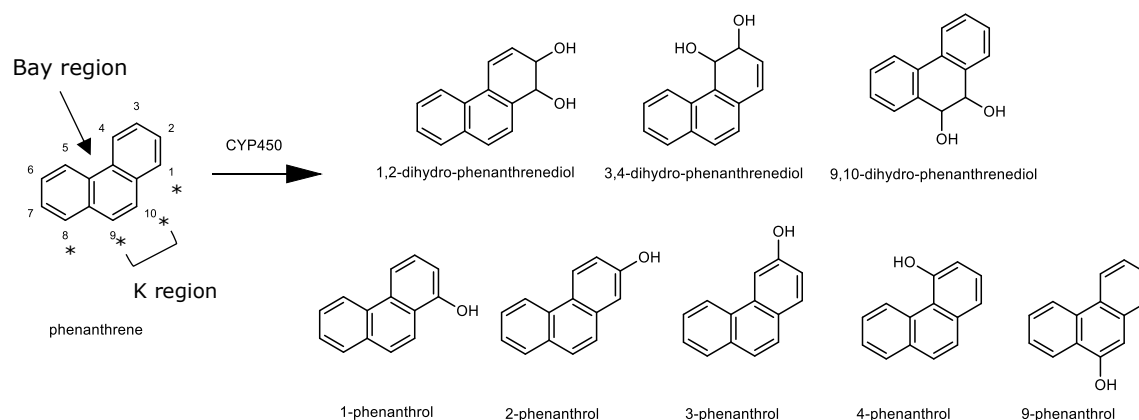
The unintentional consumption of polycyclic aromatic hydrocarbons (PAHs) via contaminated food is a general food safety issue. The PAHs present in food are typically unsubstituted as they are pyrogenic in nature, formed by incomplete heating or combustion of organic matter (EFSA 2008). However, contamination of food with petrogenic polycyclic aromatic hydrocarbons (PPAHs), which are typically alkylated, is an emerging health concern (EFSA 2012; Fengler and Gruber 2020; Grob 2018; Pirow et al. 2019; Van Heyst et al. 2018). In spite of the fact that petroleum-derived mineral oils are highly refined to eliminate undesirable substances such as mutagenic PAHs to make them compliant to EU regulations that forbid selling of carcinogenic substances to the general public (Carrillo et al. 2019), concerns about potentially carcinogenic constituents has been raised. It is known that some non-substituted and methylated polycyclic aromatic hydrocarbons with 3 to 7 fused rings are mutagenic and potentially carcinogenic (Carrillo et al. 2019). Consumer products may be contaminated with PPAH as a result of inappropriate use of mineral oils or via environmental contamination. For instance, crude oil spills, such as the Deepwater Horizon oil spill in the Gulf of Mexico, released large amounts of PPAHs into the environment (Fernando et al. 2019). In the Deepwater horizon oil spill phenanthrene and its methylated congeners were found to be amongst the most abundant PPAHs (NIST, 2012). Part of these PPAHs may be taken up by marine species and end up in the food chain via consumption of seafood which has raised concerns for human health (Pulster et al. 2020; Ylitalo et al. 2012). The current knowledge on the possible metabolic activation and genotoxicity of PAHs primarily relates to unsubstituted PAHs, which are typically of pyrogenic origin. However, the potential bioactivation due to oxidative metabolism of substituted PAHs, such as PPAHs, has not been systematically investigated.

Some unsubstituted PAHs, such as benzo[a]pyrene and dibenzo[a,l]pyrene, are bioactivated by oxidation at the “bay region” or “fjord region” to highly reactive and mutagenic dihydrodiol epoxides which may form adducts to DNA and eventually induce mutations and cancer (Boogaard 2012; Lehr et al. 1985; Tsang and Griffin 1979; Whalen et al. 1978). Information on the metabolism of PPAHs and their potential bioactivation is limited.

In our previous study, the *in vitro* hepatic biotransformation of naphthalene and alkyl substituted naphthalenes was quantified (Wang et al. 2020). It was found that alkyl substitution of naphthalene shifts metabolism towards alkyl side chain oxidation at the cost of aromatic ring oxidation. To get more insight in the metabolic transformation of alkyl substituted PAHs that may be present in mineral oils and crude oils, in the present study, the oxidative metabolism of phenanthrene and its alkylated congeners is investigated.

Phenanthrene, the smallest PAH with a bay region, was classified by IARC as group 3 (not classifiable as to its carcinogenicity to humans), based on inadequate data in experimental animals (IARC, 2010). Phenanthrene can be metabolized by cytochrome P450 enzymes from humans or rodents to 1,2-dihydrodiol-, 3,4-dihydrodiol- and 9,10-dihydrodiol-phenanthrene, and 1-, 2-, 3-, 4- and 9-phenanthrols (**Figure 1**) (Bao and Yang 1991; Chaturapit and Holder 1978; Jacob et al. 1996; Schober et al. 2010; Shou et al. 1994). However, no phenanthrene DNA adducts could be detected in Chinese hamster bone-marrow cells following *in vivo* exposure to phenanthrene (Bayer 1978). Limited data on the metabolism of alkylated congeners of phenanthrene are available. Side chain hydroxylation was reported as the major pathway of 1-methylphenanthrene and 9-ethylphenanthrene in human HepG2 cells (Huang et al. 2017). Dihydrodiols of 1-hydroxymethyl-phenanthrene, dihydrodiols of 1-methylphenanthrene, 1-hydroxymethyl-phenanthrene and 1-methylphenanthrenols were found in incubations with rat S9 fractions and 1-

methylphenanthrene (LaVoie et al. 1981). A similar metabolite profile was reported for 9-methylphenanthrene (LaVoie et al. 1981). Metabolic patterns and potential preferences for alkyl side chain oxidation or aromatic ring oxidation of other alkylated phenanthrenes, especially the ones with longer alkyl chains, are still unclear.



**Figure 1.** Reported metabolites of phenanthrene formed in microsomal incubations by P450 enzymes of humans and rodents (Bao and Yang 1991; Chaturapit and Holder 1978; Jacob et al. 1996; Schober et al. 2010; Shou et al. 1994). Each symbol \* indicates a peri position

The model compounds included in the present study were phenanthrene, 1-methylphenanthrene, 2-methylphenanthrene, 3-methylphenanthrene, 9-methylphenanthrene, 2-ethylphenanthrene, 9-ethylphenanthrene, 10-methyl-9-ethylphenanthrene, 1-n-hexylphenanthrene and 1-n-dodecylphenanthrene. The metabolic profile, kinetics and catalytic efficiency of the conversion of these model compounds in incubations with human or rat liver microsomes were characterized to better define the metabolic consequences of alkylation. In addition, some selected methylated congeners as well as unsubstituted phenanthrene were tested for their mutagenicity in the Ames test, to obtain further insight into the effect of the introduction of an additional bay region-like structural motif as a result of alkylation on the mutagenicity.

## 2. Material and Methods

### 2.1 Chemicals and reagents

Phenanthrene ( $\geq 98\%$ ), 2-ethylphenanthrene ( $\geq 98\%$ ), 9-ethylphenanthrene ( $\geq 98\%$ ), 10-methyl-9-ethylphenanthrene ( $\geq 98\%$ ), 3-(hydroxymethyl) phenanthrene ( $\geq 95.0\%$ ), 9-(hydroxymethyl) phenanthrene ( $\geq 95.0\%$ ), tetrahydrofuran ( $\geq 99.9\%$ ), trifluoroacetic acid ( $\geq 99\%$ ), methylmethanesulfonate (MMS), 2-aminoanthracene (2AA), and nitrofluorene (NF) were purchased from Sigma-Aldrich (St.Louis, USA). 1-Methylphenanthrene ( $\geq 96\%$ ) was obtained from Toronto Research Chemicals (North York, Canada). 3-Methylphenanthrene ( $\geq 98\%$ ), 1-phenanthrol ( $\geq 98\%$ ), 3-phenanthrol ( $\geq 98\%$ ), and 4-phenanthrol ( $\geq 98\%$ ) were supplied by Carbosynth (Berkshire, UK). 9-Methylphenanthrene ( $\geq 98\%$ ) and 2-methylphenanthrene ( $\geq 98\%$ ) was purchased from BOC Sciences (Hamburg, Germany). 1-n-Hexylphenanthrene ( $\geq 99.2\%$ ) and 1-n-dodecylphenanthrene ( $\geq 99.5\%$ ) were synthesized by the Biochemical Institute for Environmental Carcinogens (Großhansdorf, Germany). Acetonitrile was bought from Biosolve (Dieuze, France). Dimethyl sulfoxide (DMSO)  $K_2HPO_4 \cdot 3H_2O$ ,  $MgCl_2$ , and KCl were supplied by Merck (Darmstadt, Germany). Gentest™ pooled male Sprague Dawley rat liver microsomes (RLM) and Ultrapool™ human liver microsomes (HLM) with a protein concentration of 20 mg/ml were obtained from Corning (New York, USA), and the latter contained cytochrome P450 liver enzymes of 150 individuals. Rat liver S9 homogenate was obtained from Trinova Biochem GmbH (Giessen, Germany) and was prepared from the livers of male Sprague Dawley rats that had been injected intraperitoneally with Aroclor 1254 (500 mg/kg body weight). *Salmonella typhimurium* TA98 and TA 100 tester strains were also obtained from Trinova Biochem GmbH (Giessen, Germany). NADP and glucose-6-phosphate were supplied by Randox Laboratories Ltd. (Crumlin, UK) and Roche Diagnostics (Mannheim, Germany), respectively.



## **2.2 In vitro incubations of phenanthrene and its alkylated congeners with human and rat liver microsomes**

Microsomal oxidation of phenanthrene and its alkylated congeners by HLM and RLM was investigated in an overall 200  $\mu$ l incubation system consisting of potassium phosphate (0.1 M, pH 7.4), containing 5 mM  $MgCl_2$ , HLM/RLM at a final microsomal protein concentration of 0.5 mg/ml, 1 mM NADPH, and each of the individual test compounds at concentrations ranging from 0 to 600  $\mu$ M. Test compounds were phenanthrene, 1-methylphenanthrene, 2-methylphenanthrene, 3-methylphenanthrene, 9-methylphenanthrene, 2-ethylphenanthrene, 9-ethylphenanthrene, 10-methyl-9-ethylphenanthrene, 1-n-hexylphenanthrene and 1-n-dodecylphenanthrene. The final concentration of substrate solvent, either DMSO or tetrahydrofuran (the latter was used for 1-n-hexylphenanthrene and 1-n-dodecylphenanthrene due to their low solubility in DMSO) in the incubation mixture was 1% (v/v), which did not affect the enzymatic activity of rat liver microsomes (Li et al. 2010). The incubation mixtures were prepared and incubated in glass vials to avoid plastic binding of the substrates. The glass vials were capped to prevent substrate loss due to volatility. After pre-incubation of the incubation mixture at 37°C for 1 min, the enzymatic reaction was initiated by adding microsomes to the incubation mixture which was subsequently incubated at 37°C for 20 min. The reaction was terminated by adding 100  $\mu$ l ice-cold acetonitrile followed by vortexing. After 5 min centrifugation at 5000rpm ( $4000 \times g$ ), 4°C, the supernatant was collected for ultra-performance liquid chromatography (UPLC) analysis. However, the concentrations of the metabolites of two of the test substrates, 1-n-hexylphenanthrene and 1-n-dodecylphenanthrene, in the supernatant appeared too low to detect metabolism. Therefore, a diisopropylether (DIPE) extraction of the metabolites was performed after the reaction was stopped by the addition of 20  $\mu$ l 10%  $HClO_4$ . To this end, the incubation mixture (total volume of 220  $\mu$ l)

was extracted three times with 1 ml DIPE. Each time, the upper organic layer was collected and the DIPE was subsequently evaporated from the combined organic fractions with a gentle stream of nitrogen. The residues were dissolved in 100  $\mu$ l methanol and analyzed by UPLC.

To prepare samples for metabolite identification by GC-MS/MS, each individual test substance (200  $\mu$ M final concentration) was incubated in a volume of 400  $\mu$ l in potassium phosphate (0.1 M, pH 7.4) containing 5 mM  $\text{MgCl}_2$ , HLM or RLM at a final microsomal protein concentration of 1 mg/ml, and 1 mM NADPH at 37°C for 10 min. After incubation, the incubation mixture was centrifuged for 5 min at 5000 rpm ( $4000 \times g$ ) and 4°C. The supernatant of the incubation mixture was transferred to a fresh vial and extracted 3 times with 100  $\mu$ l dichloromethane (DCM) following vortexing. The DCM phase containing the substrate and metabolites was separated from the aqueous phase by centrifugation at 5000rpm ( $4000 \times g$ ) for 5 min. The organic (lower) phase was collected from each extraction, combined and analyzed by GC-MS/MS.

### **2.3 Bacterial reverse mutation (Ames) assay**

The mutagenicity of phenanthrene and four of its methylated analogues (1-methyl-, 2-methyl-, 3-methyl- and 9-methyl-phenanthrene) was assessed in the Ames test, a bacterial reverse mutation assay, using the TA98 and TA100 strains of *Salmonella typhimurium*. Six concentrations of each compound were tested in triplicate in the absence and presence of 5% (v/v) S9-mix prepared from the livers of Aroclor 1254 treated Sprague Dawley rats. The S9-mix contained 4mM NADP, 5.8mM glucose-6-phosphate, 0.1M sodium phosphate pH 7.4, 8mM  $\text{MgCl}_2$ , 33mM KCl and 5% S9 homogenate. Fresh bacterial cultures were prepared overnight to reach  $10^9$  cells/ml. The following solutions were pre-incubated in a rotating incubator at 70 rpm and 37°C, and contained either 0.5 ml S9-mix (in case of S9 presence) or 0.5 ml 0.1M potassium phosphate pH 7.4 (in case of S9 absence), 0.1 ml of a fresh bacterial culture ( $10^9$  cells/ml) of TA98 or TA100, and 10-100 $\mu$ g

test compound. Top agar was molten and heated to 45°C. After preincubation, the substrate solutions were added to 3 ml of the molten top agar and mixed by vortexing and the top agar mixture was poured onto a minimal glucose agar plate. After solidification of the top agar, the plates were incubated at 37°C for 48 hours. The number of revertant colonies per plate was automatically counted with the Instem Sorcerer Colony Counter (Staffordshire, UK). In absence of S9-mix, NF and MMS were tested as positive controls for incubations with TA98 and TA100, respectively. In the presence of S9-mix, 2AA was tested as a positive control in both TA98 and TA100. DMSO was tested as a solvent control in both tester strains. The mutagenicity of the test compounds was determined by the number of revertant colonies per plate and considered positive if the revertant number was increased compared to the historical control data and was also more than 3-fold or 2-fold higher than the controls for tester strain TA98 and TA100, respectively (Levy et al. 2019). The historical control data are presented in Table S1 in the supplementary material.

#### **2.4 In vitro incubations of phenanthrene and its methylated analogues with rat S9**

Since the reverse mutation assay used an S9 metabolic system instead of microsomes, for the compounds tested in the reverse mutation assay the metabolite patterns were also characterized in incubations with rat liver S9. To this end the incubation mixture of each compound tested in the reverse mutation assay with Aroclor 1254 treated rat liver S9 was analyzed by UPLC while unidentified metabolites were further analyzed by GC-MS/MS. Incubation mixtures consisting of 100 µg (1000 µM final concentration) test compound, either 0.5 ml S9-mix (in case of S9 presence) or 0.5 ml 0.1M potassium phosphate pH 7.4 (in case of S9 absence) were incubated for 48 hours at 37°C, applying the concentrations, incubation time and temperature also used in the Ames assay. After the 48-hour incubation, 250 µl acetonitrile was added to the incubation mixture followed by centrifugation at 5000rpm (4000 × g) for 5 min. The supernatant was collected for UPLC analysis.

For GC-MS/MS analysis, the incubation mixture was centrifuged for 5 min at 5000rpm ( $4000 \times g$ ) and  $4^{\circ}\text{C}$  after the 48-hour incubation. The supernatant thus obtained was transferred to a fresh vial and extracted 3 times with 100  $\mu\text{l}$  DCM following vortexing. The DCM phase, containing the substrate and its metabolites, was separated from the aqueous phase by centrifugation at  $4000 \times g$  for 5 min. The organic (lower) phase was collected, combined and analyzed by GC-MS/MS.

## **2.5 UPLC analysis**

The metabolites formed were analyzed and quantified using an Acquity UPLC system equipped with a photodiode array (PDA) detector (Waters, Milford, MA). The metabolites and their parent compound were separated on a reverse phase Acquity UPLC<sup>®</sup> BEH C18 column ( $21 \times 50$  mm,  $1.7\mu\text{m}$ , Waters, Milford, MA) and detected at wavelengths ranging from 190 nm to 400 nm. Eluent A was nano-pure water containing 0.1% trifluoroacetic acid (v/v), and eluent B was acetonitrile containing 0.1% trifluoroacetic acid (v/v). The gradient elution started from 90% A and 10% B applied from 0.0 min to 0.5 min, which was changed to 0% A and 100% B from 0.5 to 15.5 min and then kept at 0% A and 100% B from 15.5 min to 18.5 min, changed back to 90% A and 10% B from 18.5 to 18.6 min and then maintained at the starting conditions from 18.6 min until 22 min. The total run time was 22 min using a flow rate of 0.6 ml/min. The temperature of the column was set at  $40^{\circ}\text{C}$  and that of the autosampler at  $10^{\circ}\text{C}$  during the UPLC analysis. The injection volume was 3.5  $\mu\text{l}$ . Metabolites were quantified using their peak area at the wavelength specified in Table 1, using calibration curves of available reference compounds. Metabolites were identified by comparing their retention time (RT) and UV spectrum to those of reference chemicals on UPLC. When reference chemicals were not available, metabolite identification by gas chromatography-triple quadrupole mass spectrometry (GC-MS/MS) was performed. The minor metabolites were

identified by elution time and mass spectra both on UPLC and GC-MS/MS, and by comparison with available elution and spectral information from the literature.

Under the conditions used metabolite formation was linear with time and the amount of microsomal protein. The metabolite concentrations in the microsomal incubation mixtures as quantified by UPLC were used to calculate the rate of the enzymatic conversions in pmol/min/mg microsomal protein. The kinetic parameters  $K_M$  and  $V_{max}$  were obtained using a nonlinear regression curve fit applying the Michaelis Menten equation in GraphPad Prism 5 (San Diego, USA). To compare the catalytic efficiency of formation of the different metabolites the intrinsic clearance ( $Cl_{int}$ ) was calculated as  $V_{max}$  divided by  $K_M$ .

## **2.6 Metabolite identification by GC-MS/MS**

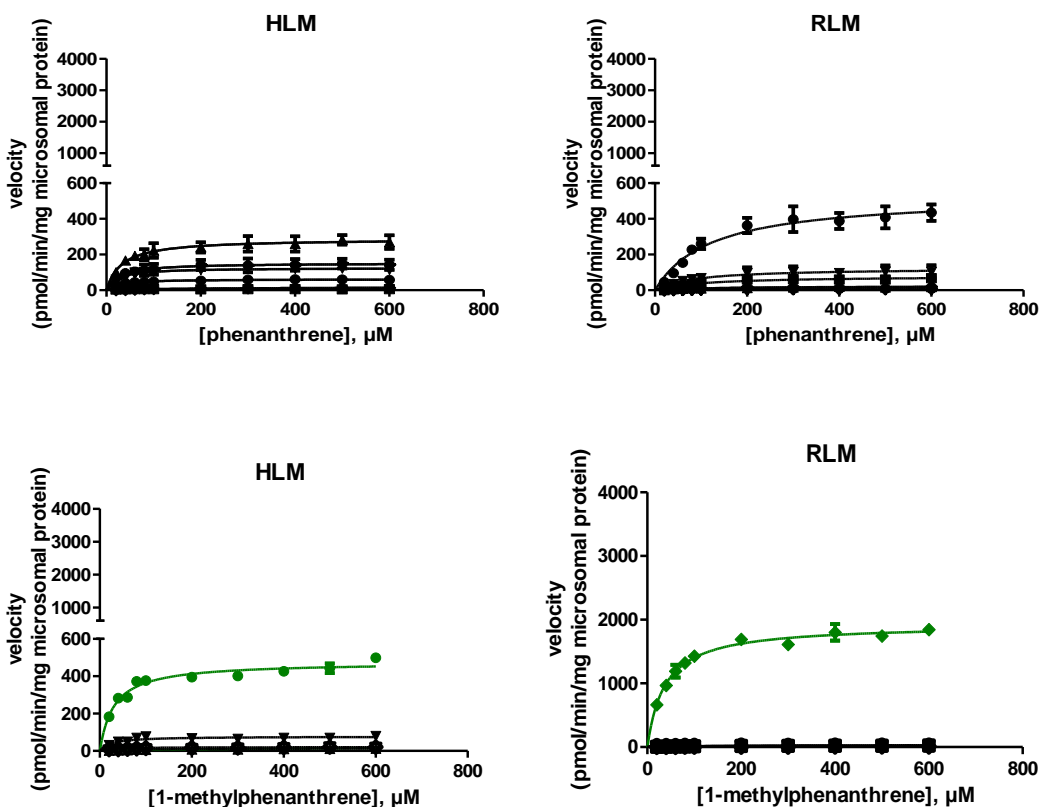
The MS spectra of all metabolites were recorded and compared to mass spectra from the NIST library (14, 14s, 17-1, 17-2, 17s) available in the GC-MS/MS solution software Version 4.45 (Shimadzu, Japan).

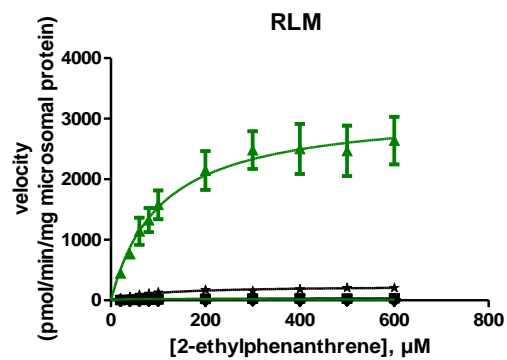
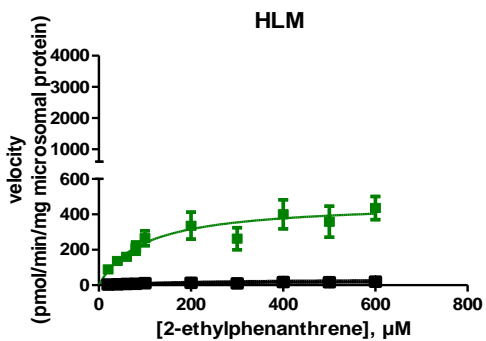
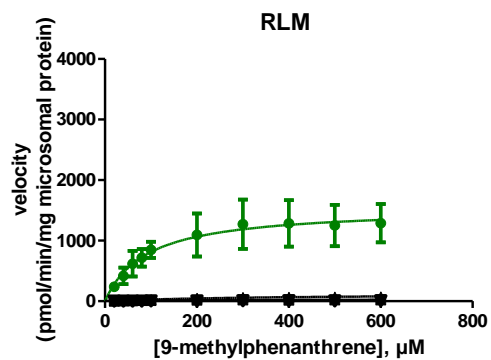
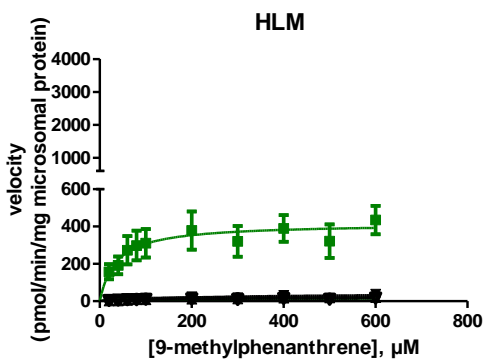
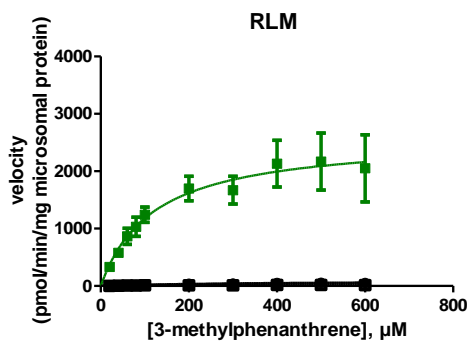
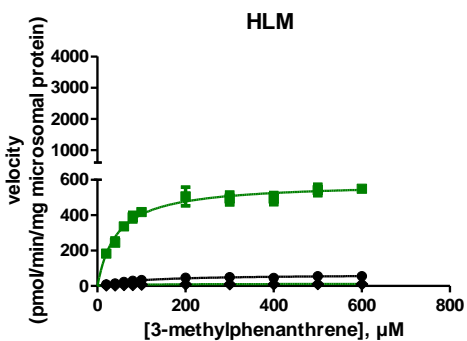
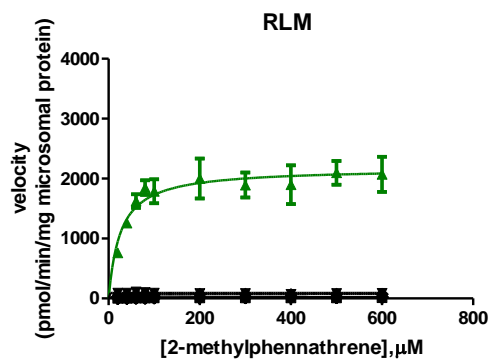
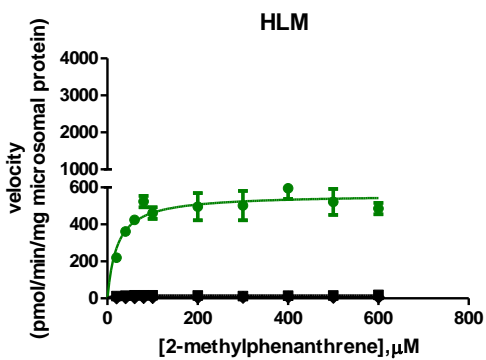
The metabolites formed from phenanthrene, 1-methylphenanthrene, 2-methylphenanthrene, 3-methylphenanthrene, 9-methylphenanthrene, 2-ethylphenanthrene, 9-ethylphenanthrene, 10-methyl-9-ethylphenanthrene, 1-n-hexylphenanthrene and 1-n-dodecylphenanthrene were analyzed using a Shimadzu GC-MS/MS system consisting of a GC-2010 Plus coupled with a mass spectrometer TQ8040 (Shimadzu, Japan). A 30 m capillary column with 0.25 mm diameter (ZB-1, Phenomenex, USA) was used to separate the metabolites upon injection of 1  $\mu$ l of the extract with splitless injection mode, using a constant flow of helium gas (1 ml/min). The column oven temperature started at 50°C and 1-min hold, increased to 300°C at a rate of 20°C/min from 1 min to 13.5 min, followed by 8.5 min hold at 300°C. The total run time was 22 min and electron ionization (70eV) was used to generate the ions of metabolites for mass spectrometric detection.

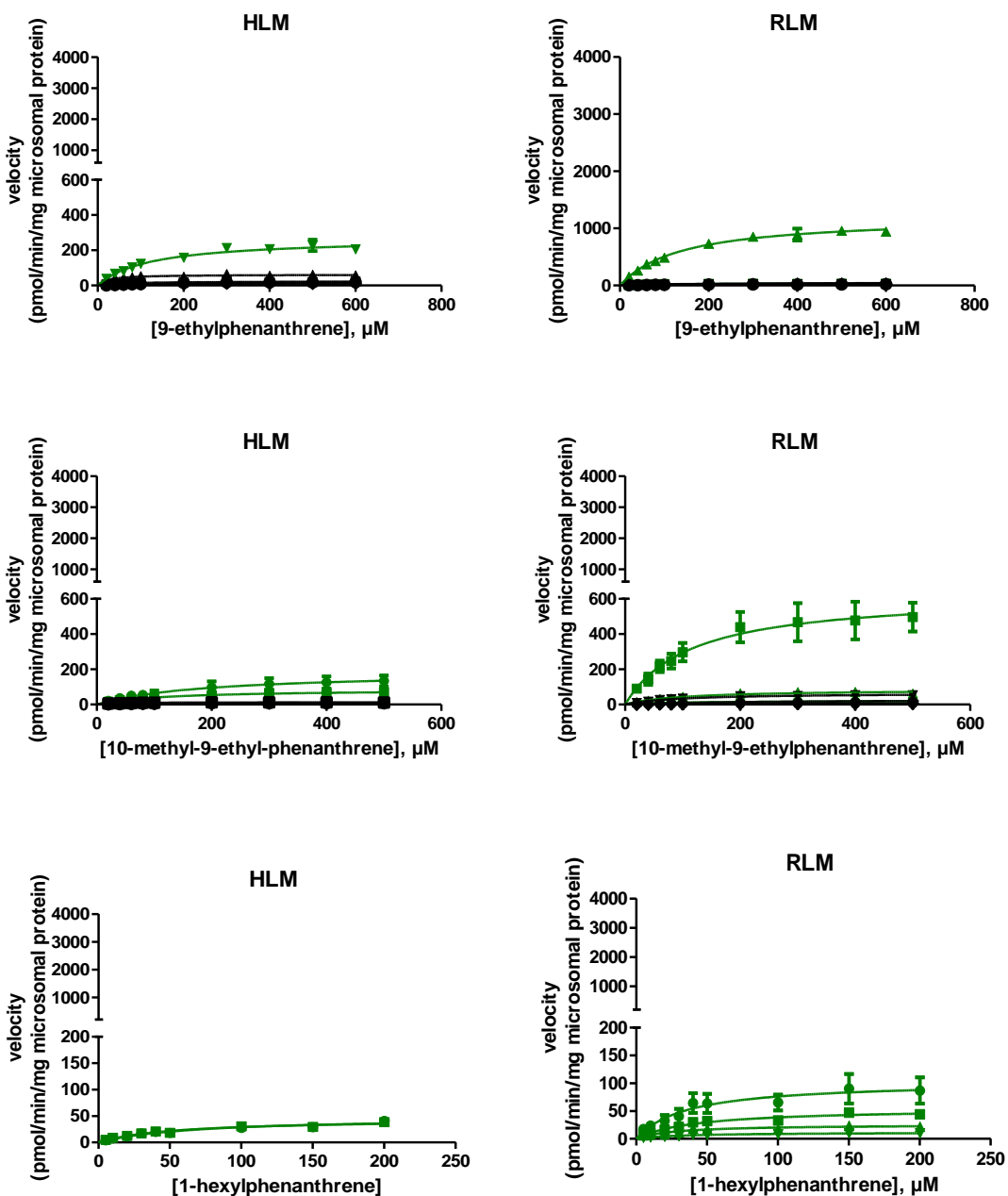
### 3. Results

#### 3.1 Microsomal metabolism of phenanthrene and its alkylated congeners

The concentration dependent rate of metabolite formation and the corresponding fitted curves representing Michaelis Menten kinetics of the metabolite formation mediated by cytochrome P450 enzymes in HLM and RLM are shown in Figure 2 for phenanthrene, 1-methylphenanthrene, 2-methylphenanthrene, 3-methylphenanthrene, 9-methylphenanthrene, 2-ethylphenanthrene, 9-ethylphenanthrene, 10-methyl-9-ethylphenanthrene and 1-n-hexylphenanthrene. No metabolic conversion was observed for 1-n-dodecylphenanthrene under the experimental conditions used. The obtained  $K_M$  and  $V_{max}$  values and the calculated  $Cl_{int}$  for formation of each metabolite derived from the curves presented in **Figure 2** are summarized in **Table 1**.



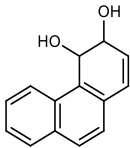
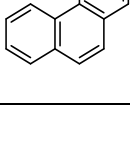
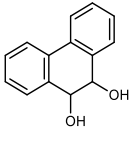
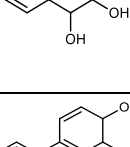
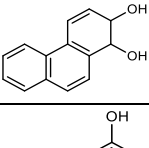
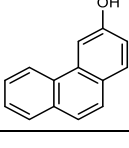


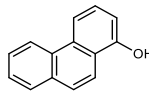
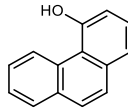
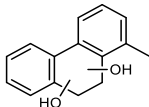
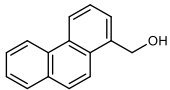
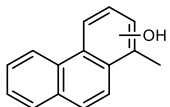


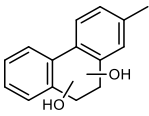
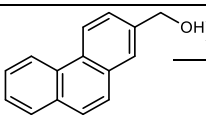
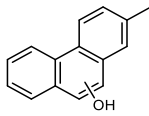
**Figure 2.** Substrate-concentration dependent metabolism of alkyl substituted phenanthrenes and phenanthrene itself by human liver microsomes (HLM) and rat liver microsomes (RLM). Green lines represent metabolite formation via alkyl chain oxidation and black lines present metabolite formation by aromatic ring oxidation. Each symbol represents experimental means and vertical bars are standard errors of the mean (n=3).

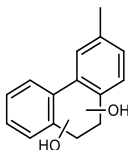
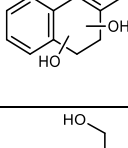
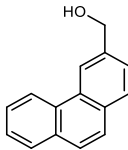
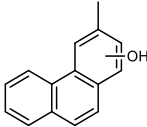
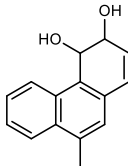
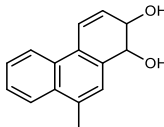
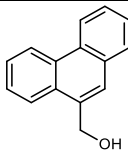


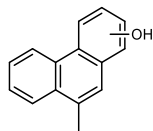
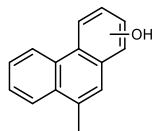
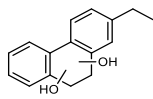
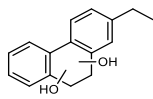
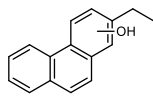
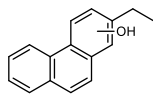
**Table 1.** The Michalis Menten parameters including  $K_M$ ,  $V_{max}$  and intrinsic clearance ( $Cl_{int}$ ) calculated as  $V_{max}/K_M$  for formation of metabolites from alkyl substituted phenanthrenes and phenanthrene in human and rat liver microsomal incubations (Figure 2). The retention time (RT) and wavelength ( $\lambda$ ) used to identify and quantify the metabolites by UPLC-UV analysis are also presented. Results are shown as mean  $\pm$  standard error of the mean (SEM) from three independent microsomal incubations. Abbreviations. ND = not detected. NM = no metabolism. NA= not applicable.

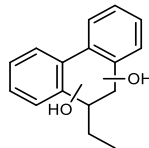
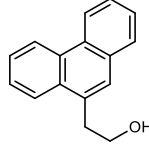
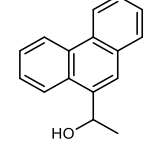
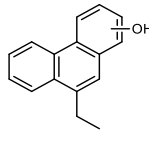
Metabolites	Structure	Species	$K_M$ ( $\mu M$ )	$V_{max}$ (pmol/min/mg microsomal protein)	$Cl_{int}$ ( $V_{max}/K_M$ ) $\mu l/min/mg$ protein
<b>Phenanthrene RT=8.21min, <math>\lambda</math>=251.1nm</b>					
3,4-dihydro-phenanthrene-diol RT=2.13min, $\lambda$ =260.2nm;		Human	22.6 $\pm$ 12.7	61.5 $\pm$ 6.3	2.7
		Rat	153.7 $\pm$ 72.4	10.3 $\pm$ 1.8	0.1
3,4-dihydro-phenanthrene-diol RT=2.24min, $\lambda$ =237.1nm		Human	8.1 $\pm$ 3.5	6.0 $\pm$ 0.3	0.7
		Rat	ND	ND	-
9,10-dihydro-phenanthrene-diol RT=3.28min, $\lambda$ =231.6nm;		Human	ND	ND	-
		Rat	84.2 $\pm$ 15.7	9.8 $\pm$ 0.6	0.1
9,10-dihydro-phenanthrene-diol RT=3.38min, $\lambda$ =209.1nm		Human	32.4 $\pm$ 9.0	287.8 $\pm$ 17.1	8.9
		Rat	121.6 $\pm$ 29.1	529.2 $\pm$ 43.2	4.4
1,2-dihydro-phenanthrene-diol RT=3.57min, $\lambda$ =237.1nm		Human	25.7 $\pm$ 12.6	152.5 $\pm$ 14.4	5.9
		Rat	104.3 $\pm$ 26.3	79.3 $\pm$ 6.5	0.8
3-phenanthrol RT=6.02min, $\lambda$ =252.9nm		Human	ND	ND	-
		Rat	103.4 $\pm$ 29.5	21.3 $\pm$ 2.0	0.2

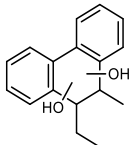
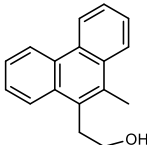
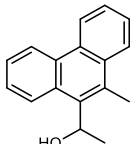
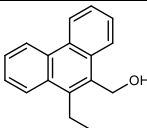
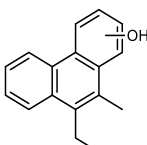
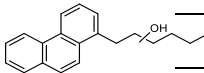
1-phenanthrol RT=6.31min, λ=251.7nm		Human	21.3±5.2	125.2±5.4	5.9
		Rat	83.6±43.1	123.9±19.2	1.5
4-phenanthrol RT=6.55min, λ=245nm		Human	188.1±104.1	18.0±3.9	0.1
		Rat	145.3±89.8	24.5±5.5	0.2
1-methylphenanthrene RT=8.99min, λ=255.3nm					
Dihydro-1-methyl-phenanthrene-diol RT=2.32min, λ=210.4nm		Human	430.8±134.7	27.5±4.6	0.1
		Rat	ND	ND	-
Dihydro-1-methyl-phenanthrene-diol RT=3.43min, λ=255.3nm		Human	ND	ND	-
		Rat	43.7±19.0	4.2±0.4	0.1
Dihydro-1-methyl-phenanthrene-diol RT=3.96min, λ=260nm		Human	ND	ND	-
		Rat	17.8±6.7	5.2±0.3	0.3
Dihydro-1-methyl-phenanthrene-diol RT=4.35min, λ=238.9nm		Human	25.1±3.3	20.6±0.5	0.8
		Rat	34.3±12.9	16.1±1.3	0.5
Dihydro-1-methyl-phenanthrene-diol RT=4.76min, λ=254.1nm		Human	ND	ND	-
		Rat	14.8±4.4	14.0±0.6	0.9
1-(hydroxymethyl) phennathrene RT=5.55min, λ=254.1nm		Human	30.5±4.1	475.3±13.2	15.6
		Rat	37.4±3.5	1926±40.3	51.5
1-methylphenanthrol RT=6.3min, λ=252.9nm		Human	107.5±18.9	14.7±0.8	0.1
		Rat	ND	ND	-
1-methylphenanthrol RT=6.80min, λ=258nm		Human	22.7±6.2	77.3±3.9	3.4
		Rat	123.0±22.4	33.1±2.1	0.3
1-methylphenanthrol		Human	ND	ND	-

RT=6.92min, $\lambda$ =249.9nm		Rat	106.5±21.5	24.0±1.6	0.2
1-methylphenanthrol RT=7.00min, $\lambda$ =258nm		Human	ND	ND	-
		Rat	93.4±21.6	17.3±1.2	0.2
1-methylphenanthrol RT=7.29min, $\lambda$ =256nm		Human	ND	ND	-
		Rat	150.2±37.6	9.0±0.8	0.1
<b>2-methylphenanthrene RT=9.05min, <math>\lambda</math>=252.9nm</b>					
Dihydro-2-methyl-phenanthrene-diol RT=3.09min, $\lambda$ =262.1nm		Human	35.9±11.9	6.4±0.5	0.2
		Rat	ND	ND	-
Dihydro-2-methyl-phenanthrene-diol RT=4.26min, $\lambda$ =212.2nm		Human	ND	ND	-
		Rat	135.8±44.5	23.1±2.7	0.2
Dihydro-2-methyl-phenanthrene-diol RT=4.42min, $\lambda$ =243.8nm		Human	ND	ND	-
		Rat	95.9±46.6	16.2±2.5	0.2
Dihydro-2-methyl-phenanthrene-diol RT=4.99min, $\lambda$ =252.9nm		Human	ND	ND	-
		Rat	141.7±43.3	12..8±1.4	0.1
2-(hydroxymethyl)-phennathrene RT=5.59min, $\lambda$ =253.5nm		Human	21.6±5.9	562.0±27.5	26.0
		Rat	25.8±7.1	2174±115.3	84.3
2-methylphenanthrol RT=6.12min, $\lambda$ =262.7nm		Human	4.9±3.2	16.3±0.8	3.3
		Rat	NA	90.7±3.8	-
2-methylphenanthrol RT=6.98min, $\lambda$ =266.9nm		Human	ND	ND	-
		Rat	15.6±4.2	76.0±3.1	4.9
2-methylphenanthrol RT=7.08min, $\lambda$ =260.8nm		Human	ND	ND	-
		Rat	39.6±13.3	11.2±0.9	0.3

3-methylphenanthrene RT=9.04min, λ=252.3nm					
Dihydro-3-methyl-phenanthrene-diol RT=4.25min, λ=210.4nm		Human	100.8±20.0	65.0±4.1	0.6
		Rat	312.5±178.2	92.3±25.1	0.3
Dihydro-3-methyl-phenanthrene-diol RT=4.42min, λ=238.9nm		Human	71.5±16.2	12.8±0.8	0.2
		Rat	121.5±29.0	20.4±1.7	0.2
3-(hydroxymethyl)-phenanthrene RT=5.62min, λ=252.9nm		Human	44.5±6.2	583.8±19.6	13.1
		Rat	120.2±41.7	2593±305	21.6
3-methylphennathrol RT=6.98min, λ=252.9nm		Human	ND	ND	-
		Rat	371.1±476.3	82.6±53.8	0.2
9-methylphenanthrene RT=9.02min, λ=252.9nm					
3,4-Dihydro-9-methyl-phenanthrene-diol RT=2.98min, λ=262.1nm		Human	55.9±23.9	26.1±3.0	0.5
		Rat	ND	ND	-
1,2-Dihydro-9-methyl-phenanthrene-diol RT=4.27min, λ=238.9nm		Human	61.8±33.7	15.6±2.4	0.3
		Rat	ND	ND	-
9-(hydroxymethyl)-phenanthrene RT=5.6min, λ=252.9nm		Human	35.3±16.3	415.9±43.9	11.8
		Rat	89.9±42.9	1543±226.6	17.2
9-methylphenanthrol RT=6.28min, λ=249.9nm		Human	278.3±145.8	27.8±6.7	0.1
		Rat	ND	ND	-

9-methylphenanthrol RT=6.73min, λ=252.9nm		Human	239.8±235.5	44.9±19.4	0.2
		Rat	226.2±99.5	27.2±5.1	0.1
9-methylphenanthrol RT=6.87min, λ=254.7nm		Human	ND	ND	-
		Rat	346.4±164.3	124.2±29.2	0.4
9-methylphenanthrol RT=7.2min, 249.9nm		Human	ND	ND	-
		Rat	445.7±463.6	41.4±23.4	0.1
9-methylphenanthrol RT=7.25min, λ=252.9nm		Human	ND	ND	-
		Rat	154.4±78.6	10.2±1.9	0.1
2-ethylphenanthrene, RT=9.84min, λ=253.5nm					
Dihydro-2-ethyl-phenanthrene-diol RT=4.6min, λ=254.1nm		Human	ND	ND	-
		Rat	25.3±23.2	33.9±11.8	1.3
Dihydro-2-ethyl-phenanthrene-diol RT=5.16min, λ=276.6nm		Human	108.3±56.2	18.4±3.2	0.2
		Rat	ND	ND	-
Dihydro-2-ethyl-phenanthrene-diol RT=5.29min, λ=241.9nm		Human	132.0±49.6	22.1±3.0	0.2
		Rat	181.7±38.3	42.9±3.5	0.2
2-(1-hydroxyethyl)-phenanthrene RT=6.21min, λ=253.5nm		Human	96.5±31.7	468.8±50.3	4.9
		Rat	105.4±27.4	3149.0±266.1	29.9
2-ethylphenanthrol RT=7.57min, λ=255.3nm		Human	ND	ND	-
		Rat	223.6±100.8	16.5±3.1	0.1
2-ethylphenanthrol RT=7.74min, λ=254.1nm		Human	ND	ND	-
		Rat	233.3±89.7	16.6±2.7	0.1
2-ethylphenanthrol		Human	ND	ND	-

RT=7.89min, $\lambda$ =254.1nm		Rat	133.2±76.4	11.8±2.4	0.1
RT=9.38min, $\lambda$ =267.6nm	Unknown	Human	205.0±85.7	37.2±6.5	0.2
		Rat	95.4±30.5	238.0±23.9	2.5
9-ethylphenanthrene RT=9.71min, $\lambda$ =252.9nm					
Dihydro-9-ethyl-phenanthrene-diol RT=3.81min, $\lambda$ =263.3nm		Human	104.6±17.3	15.2±0.8	0.1
		Rat	117.7±59.9	12.0±2.1	0.1
Dihydro-9-ethyl-phenanthrene-diol RT=3.88min, $\lambda$ =262.1nm		Human	59.1±12.4	23.5±1.4	0.4
		Rat	ND	ND	-
9-(2-hydroxyethyl)-phenanthrene RT=6.00min, $\lambda$ =253.5nm		Human	22.6±6.4	61.4±3.3	2.7
		Rat	72.9±15.2	37.0±2.26	0.5
9-(1-hydroxyethyl)-phenanthrene RT=6.20min, $\lambda$ =252.9nm		Human	122.2±22.5	267.7±17.4	2.2
		Rat	138.2±15.2	1206±47.9	8.7
9-ethylphenanthrol RT=7.42min, $\lambda$ =252.9nm		Human	159.9±34.9	12.8±1.1	0.1
		Rat	91.6±30.2	29.7±3.1	0.3
9-ethylphenanthrol RT=7.58min, $\lambda$ =254.1nm		Human	244.7±52.6	29.1±2.8	0.1
		Rat	321.4±70.5	56.6±1.8	0.2
9-ethylphenanthrol RT=7.93min, $\lambda$ =250.5nm		Human	ND	ND	-
		Rat	90.3±23.1	22.8±1.8	0.3
RT=9.35min, $\lambda$ =256.6nm	Unknown	Human	ND	ND	-
		Rat	169.0±51.7	52.7±6.2	0.3

10-methyl-9-ethyl-phenanthrene RT=10.19min, λ=255.3nm						
Dihydro-10-methyl-9-ethyl-phenanthrene-diol RT=4.29min, λ=266.3nm		Human	141.8±83.7	7.2±1.7	0.1	
		Rat	253.1±223.1	6.4±2.7	0.0	
Dihydro-10-methyl-9-ethyl-phenanthrene-diol RT=4.34min, λ=266.3		Human	102.1±70.3	10.5±2.5	0.1	
		Rat	73.7±45.0	8.09±1.6	0.1	
9-(2-hydroxyethyl)-10-methyl-phenanthrene RT=6.5min, λ=255.3nm		Human	24.7±16.5	12.9±1.8	0.5	
		Rat	88.4±39.2	21.0±3.1	0.2	
9-(1-hydroxyethyl)-10-methyl-phenanthrene RT=6.65min, λ=256nm		Human	192.4±106.8	187.1±45.2	1.0	
		Rat	114.3±4.5	630.2±81.4	5.5	
9-ethyl-10-(1-hydroxymethyl)-phenanthrene RT=6.90min, λ=256nm		Human	118.2±65.0	85.9±17.4	0.7	
		Rat	98.9±38.5	85.8±11.6	0.9	
9-ethyl-10-methyl-phenanthrol RT=7.82min, λ=255.3nm		Human	ND	ND	-	
		Rat	94.4±41.4	65.6±9.8	0.7	
9-ethyl-10-methyl-phenanthrol RT=8.3min, λ=252.3nm		Human	ND	ND	-	
		Rat	219.8±126.8	29.4±7.7	0.1	
1-n-hexyl-phenanthrene RT=12.60min, λ=256nm						
1-hydroxyhexyl-phenanthrene RT=8.45min, λ=256nm		Human	67.9±20.0	48.3±6.1	0.7	
		Rat	35.8±18.1	103.4±18.1	2.9	
1-hydroxyhexyl-phenanthrene		Human	ND	ND	-	

RT=8.58min, $\lambda$ =256nm		Rat	42.2±10.9	54.8±5.2	1.3
1-hydroxyhexyl-phenanthrene	RT=8.82min, $\lambda$ =256nm	Human	51.7±14.2	44.2±4.8	0.9
		Rat	26.6±6.0	25.6±1.8	1.0
1-hydroxyhexyl-phenanthrene	RT=9.13min, $\lambda$ =256nm	Human	ND	ND	-
		Rat	33.1±7.3	11.7±0.9	0.4
1-n-dodecyl-phenanthrene RT=16.62min, $\lambda$ =302.5nm					
NM	NA	Human	NA	NA	NA
		Rat	NA	NA	NA



Dihydro-phenanthrene-diols and phenanthrols were detected in both human and rat liver microsomal incubations of phenanthrene. Specifically, three major dihydro-phenanthrene-diols, 3,4-dihydro-phenanthrene-diol, 9,10-dihydro-phenanthrene-diol, and 1,2-dihydro-phenanthrene-diol, were characterized based on comparison with reference materials and the available literature (Bao and Yang 1991; Chaturapit and Holder 1978; Jacob et al. 1996; Schober et al. 2010; Shou et al. 1994; Sims 1970). For 3,4-dihydro-phenanthrene-diol and 9,10-dihydro-phenanthrene-diol two partially overlapping peaks, representing their respective *cis*- and *trans*-isomers, were detected at 2.13 and 2.24 min and at 3.28 and 3.38 min, respectively. Three phenanthrols were identified as 3-phenanthrol, 1-phenanthrol, and 4-phenanthrol by co-elution and identical UV spectra with the reference standards .

The oxidative metabolism of alkyl substituted phenanthrenes primarily occurred on the alkyl chain. The most abundant type of metabolites detected in both human and rat liver microsomal incubation mixtures with phenanthrenes were alcohols. The primary metabolites of 3-methylphenanthrene and 9-methylphenanthrene were identified as 3-hydroxymethyl-phenanthrene and 9-hydroxymethyl-phenanthrene, respectively, which co-eluted with the reference standards in both UPLC and GC-MS/MS analyses. The molecular ion and base peak of both 3-hydroxymethyl-phenanthrene and 9-hydroxymethyl-phenanthrene were observed at  $m/z$  208 and  $m/z$  179, respectively. A comparable mass spectrum was obtained for the primary metabolite of 1-methylphenanthrene with molecular ion at  $m/z$  208 and a base peak at  $m/z$  179 supporting its identification as 1-hydroxymethyl-phenanthrene with an identical UV spectra as reported for this compound (Huang et al. 2017). With a similar mass spectral profile, 2-hydroxymethyl-phenanthrene was identified as a primary metabolite of 2-methylphenanthrene. 2-(1-Hydroxyethyl)-phenanthrene and 9-(1-hydroxyethyl)-phenanthrene were found to be the primary metabolites of 2-ethylphenanthrene and 9-

ethylphenanthrene, respectively, with a molecular ion at  $m/z$  222 and a base peak at  $m/z$  179. In analogy with these results, the most abundant metabolite of 10-methyl-9-ethylphenanthrene was tentatively identified as 10-methyl-9-(1-hydroxyethyl)-phenanthrene with a base peak at  $m/z$  203, a molecular ion peak at  $m/z$  236 and the presence of other ion peaks at  $m/z$  179 and  $m/z$  218.

For alkylated phenanthrenes, dihydro-phenanthrene-diols and phenanthrols were minor metabolites formed in microsomal incubations with both HLM and RLM. On UPLC the most polar dihydrodiols eluted first, followed by alcohols, and subsequently by less polar phenanthrols before the parent compound eluted (**Table 1**), whereas on GC-MS/MS the parent compound with lowest boiling point eluted before the alcohols, dihydrodiols and phenanthrols. Identification of the minor metabolites was based on comparison with reference mass spectra in the NIST libraries or mass spectra of a reference compound that shared a similar structure.

Four dihydrodiols of 2-methylphenanthrene were detected at retention time 3.09 min, 4.26 min, 4.42 min and 4.99 min ionized to a molecular ion at  $m/z$  226 and a base peak at  $m/z$  165. The dihydrodiols eluting at 3.09 min and 4.26 min were identified as 3,4- and 9,10- dihydro-2-methylphenanthrene-diol based on both the retention time and comparison to the UV spectra of 3,4-dihydro-phenanthrene-diol and 9,10-dihydro-phenanthrene-diol. Three phenolic metabolites eluting at 6.12 min, 6.98 min and 7.08 min were identified as 2-methylphenanthrols.

The metabolites of 3-methylphenanthrene at retention time 4.25 min and 4.42 min were identified as dihydro-3-methylphenanthrene-diols with a molecular ion at  $m/z$  226 and a base peak at  $m/z$  165. The dihydrodiol eluting at 4.25 min was identified as 9,10-dihydro-3-methylphenanthrene-diol based on both the retention time and comparison to the UV spectrum of 9,10-dihydro-phenanthrene-diol. The metabolite of 3-methylphenanthrene eluting at 6.98 min was identified as 3-methyl-phenanthrol with a base peak at  $m/z$  208.

The metabolite of 9-methylphenanthrene eluting at 2.62 min was identified as a dihydro-9-methylphenanthrene-diol with a molecular ion at  $m/z$  226, most probably being the 3,4-dihydro-9-methylphenanthrene-diol based on both the retention time and comparison to the UV spectrum of 3,4-dihydro-phenanthrene-diol. An additional dihydrodiol was detected at retention time 4.27 min that was possibly 1,2-dihydro-9-methylphenanthrene-diol based on both the retention time and comparison of its UV spectrum to the UV spectrum of 1,2-dihydro-phenanthrene-diol. Five metabolites with retention times ranging from 6.28 to 7.25 min were identified as 9-methylphenanthrols with a base peak at  $m/z$  208 and an ion peak at  $m/z$  165.

The concentrations of the minor metabolites that were formed from 1-methylphenanthrene were too low to be quantified within the background noise of the GC-MS/MS measurements. However, based on the retention time of the metabolites formed from 3- and 9-methylphenanthrene, these minor metabolites could be tentatively identified as dihydro-1-methylphenanthrene-diols based on their retention times of 2.32 min, 3.43 min, 3.96 min, 4.35 min and 4.76 min. The metabolites formed from 1-methylphenanthrene eluting at 6.3 min to 7.29 min were tentatively assigned as 1-methylphenanthrols.

The mass spectra of the 2-ethylphenanthrene metabolites at retention times of 4.60 min, 5.16 min and 5.29 min all showed a molecular ion at  $m/z$  238 and a base peak at  $m/z$  165, and could therefore be tentatively identified as dihydro-2-ethylphenanthrene-diols. The metabolites at 7.57 min, 7.74 min and 7.89 min were tentatively identified as 2-ethylphenanthrols based on their molecular ion at  $m/z$  222 in combination with a base peak at  $m/z$  207. An additional metabolite that was tentatively identified as methyl-2-phenanthryl-ketone could not be found on UPLC but was detected by GC-MS/MS at a retention time of 12.03 min with a molecular ion at  $m/z$  220 and a

base peak at  $m/z$  205, partly overlapping with the peak of 2-(1-hydroxyethyl)-phenanthrene at 12.00 min.

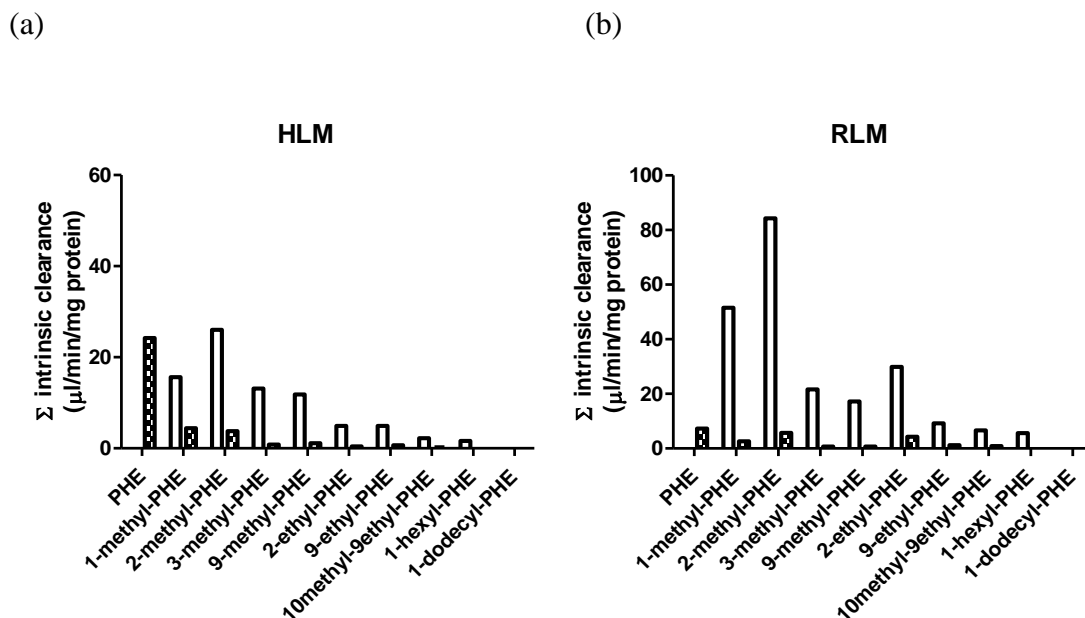
Minor metabolites of 9-ethylphenanthrene eluting at 3.81 min and 3.88 min were tentatively identified as dihydro-9-ethylphenanthrene-diols based on their molecular ions at  $m/z$  238 and base peaks at  $m/z$  165. The metabolite eluting at 6.00 min, shortly before 9-(1-hydroxyethyl)-phenanthrene was tentatively identified as 9-(2-hydroxyethyl)-phenanthrene based on a molecular ion at  $m/z$  222 and a base peak at  $m/z$  191. The metabolites at retention times of 7.42 min, 7.58 min and 7.93 min all had a molecular ion at  $m/z$  222 and a base peak at  $m/z$  207, and were identified as 9-ethylphenanthrols.

Two metabolites of 10-methyl-9-ethylphenanthrene, with retention times of 4.29 min and 4.34 min, were identified as dihydro-10-methyl-9-ethyl-phenanthrenediol with a molecular ion at  $m/z$  254 and a base peak at  $m/z$  167. The metabolite eluting at 6.5 min was identified as 10-methyl-9-(2-hydroxyethyl)-phenanthrene, an ethanol with a molecular ion at  $m/z$  236 and a base peak at  $m/z$  205. The other alcohol metabolite eluting at 6.90 min, was identified as 10-(1-hydroxymethyl)-9-ethylphenanthrene with a molecular ion at  $m/z$  236 and a base peak at  $m/z$  221. The metabolites at retention times 7.82 min and 8.30 min were identified as 10-methyl-9-ethyl-phenanthrols with a base peak at  $m/z$  236.

Four metabolites of 1-n-hexylphenanthrene eluting from 8.45 min to 9.13 min were tentatively identified as 1-n-hydroxyhexyl-phenanthrenes based on the similarity of their UV spectra to the UV spectrum of 1-n-hexyl-phenanthrene, and the fact that they were ionized to a base peak at  $m/z$  207 and showed a molecular ion at  $m/z$  278.

### 3.2 Intrinsic clearance by aromatic and alkyl side chain oxidation

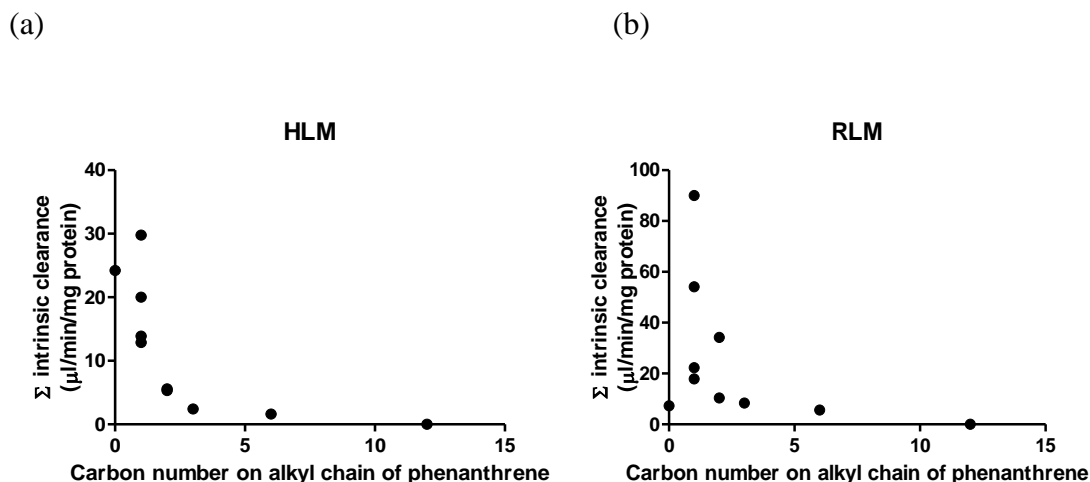
To compare the metabolic efficiency of alkyl side chain oxidation and aromatic ring oxidation of phenanthrene and its alkyl substituted analogues, the intrinsic clearance of each parent test compound via side chain metabolites and aromatic ring metabolites was calculated (**Figure 3**). The overall intrinsic clearance of phenanthrene was 24.2 and 7.3  $\mu\text{l}/\text{min}/\text{mg}$  protein when metabolized by hepatic P450 enzymes of human and rats, respectively. With increasing chain length the intrinsic clearance decreased substantially for alkylated phenanthrenes with an alkyl side chain with more than 3 carbon atoms clearance being limited or even (1-n-dodecyl-phenanthrene) not observed at all (**Figure 3**). The results presented in **Figure 3** also reveal that when phenanthrene was alkyl substituted aromatic ring oxidation was reduced in favor of alkyl side chain oxidation. When there were more than 3 carbon atoms in the alkyl side chain of the tested substrates, aromatic ring oxidation was no longer detectable. In case of HLM, the intrinsic clearance of the tested alkylated phenanthrenes for which aromatic ring oxidation was observed 5.5 to 121 times lower than that of phenanthrene. For metabolism by HLM of the tested substrates with up to 3 carbon atoms in the alkyl side chain the intrinsic clearance via alkyl side chain oxidation was 3.5 to 16.4 times greater than that via aromatic ring oxidation. RLM metabolized the alkyl chain of the alkylated phenanthrenes 1.6 to 6.1 times more efficiently than HLM. For RLM the intrinsic clearance via aromatic ring oxidation of the tested alkylated phenanthrenes was 1.3 to 10.4 fold lower than that of phenanthrene itself. For the alkylated phenanthrenes for which aromatic oxidation was still observed, the alkyl side chain oxidation was 7.0 to 30.8 times more efficient than this aromatic ring oxidation in microsomal incubations with RLM.



**Figure 3.** Intrinsic clearance via aromatic ring and alkyl chain oxidation by (a) HLM and (b) RLM for the different model compounds. Dashed bar represents aromatic ring oxidation; white bar represents alkyl chain oxidation. Abbreviation. PHE = phenanthrene.

### 3.3 Effect of alkyl chain length on total intrinsic clearance

By adding up the intrinsic clearance of all metabolites for each substrate, the total intrinsic clearance of phenanthrene with and without alkyl substitution based on side-chain carbon number was calculated. **Figure 4** presents this overall intrinsic clearance via aromatic ring and side chain oxidation as a function of the number of carbon atoms in the alkyl side chain for the different model compounds. The results thus obtained show that the metabolism of alkylated phenanthrenes by both HLM and RLM becomes less efficient with elongation of the alkyl chain, especially when the side chain carbon number was more than 3. No metabolic conversion was detected when the side chain carbon number was 12.



**Figure 4.** Relationship between total  $\text{Cl}_{\text{int}}$  of alkylated phenanthrenes and the number of carbon atoms on the alkyl side chain in metabolism with (a) HLM and (b) RLM. The intrinsic clearance was calculated by adding up the  $\text{Cl}_{\text{int}}$  values of all metabolites for the respective model compound (Table 1).

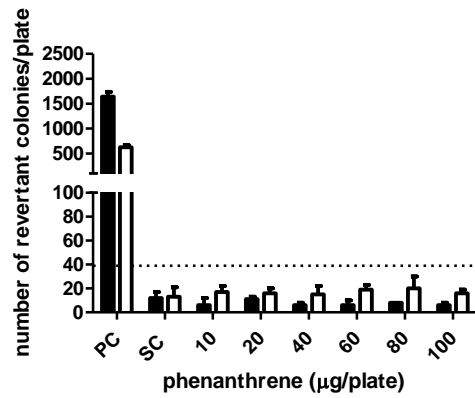
### 3.4 Mutagenicity of phenanthrene and its methylated substituents in the Ames test

The reverse mutation assay (Ames test), was used to assess the effect of methylation of phenanthrene on its mutagenicity towards *Salmonella typhimurium* tester strains TA98 and TA100. The model compounds used for these studies were non-substituted phenanthrene, phenanthrene with the methyl substitution at C1 and C9 positions generating a “fake” bay region and at C2 and C3 for which this was not the case. No precipitation was observed on the plates at the tested concentrations under microscope. None of the test compounds showed mutagenic potential in both tester strains in the absence of S9 metabolic system (Figure 5 and 6). Figure 5 and Figure 6 present the number of ( $\text{His}^+$ ) revertant colonies per plate induced by (a) phenanthrene, (b) 1-methylphenanthrene, (c) 2-methylphenanthrene, (d) 3-methylphenanthrene and (e) 9-methylphenanthrene for tester strain TA98 and TA100 respectively. No increases in the number of revertants were observed in TA 98 and TA100 upon exposure to phenanthrene in the presence of

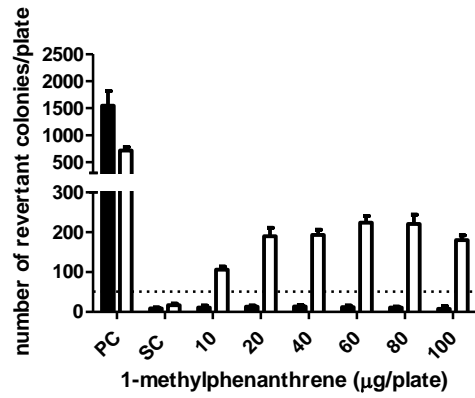
S9 metabolic system. The observed increases in the number of revertants upon exposure to 1-methylphenanthrene in the presence of an S9 metabolic activation system were up to 13.0- and 6.8-fold compared to the concurrent solvent control for tester strain TA98 and TA100, respectively. In the presence of S9 metabolic activation, for both 2-methylphenanthrene and 3-methylphenanthrene a slight dose response with 2.2- fold increase was observed in TA98, however, this was lower than the 3- fold increase required to conclude on a positive response that is biologically relevant (Levy et al. 2019) and no increased response was found in TA100 for either compound. Therefore, 2-methyl- and 3-methyl- phenanthrene were considered to be non-mutagenic in both TA98 and TA100. 2.5- Fold and 1.9-fold increases in number of revertants to the concurrent solvent control were observed for 9-methyl-PHE in TA98 and TA100 respectively, which were both lower than the 3-fold and 2-fold criteria. Close inspection of the corresponding solvent control data revealed that this was caused by the relatively high number of revertants in the concurrent solvent control in the TA98 and TA100 groups of 9-methylphenanthrene, e.g.  $23 \pm 5$  for the solvent control of 9-methylphenanthrene compared to the historical dataset with a value of  $18 \pm 6$  for TA98 (Table S1). This implies that relative to the historical control data the increase in the number of revertants of 9-methylphenanthrene are 3.2- fold and 2.0- fold and are considered to be biologically relevant and indicative of mutagenicity.



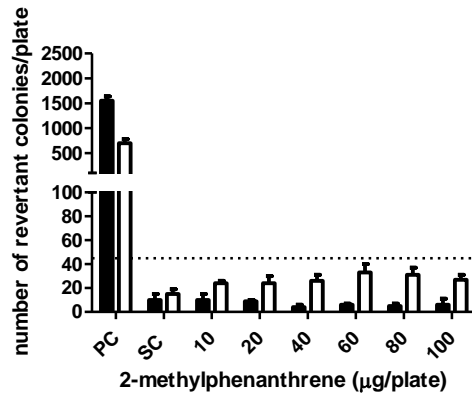
(a)



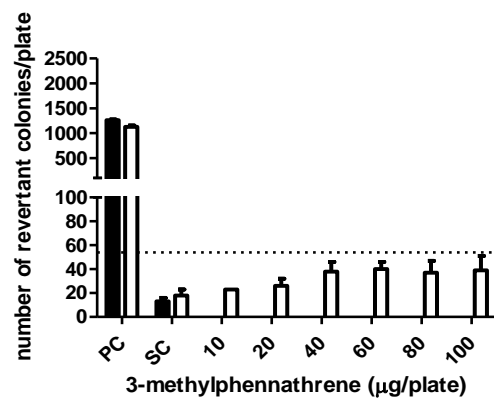
(b)



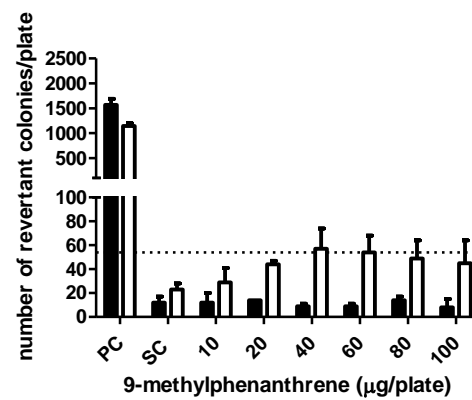
(c)



(d)



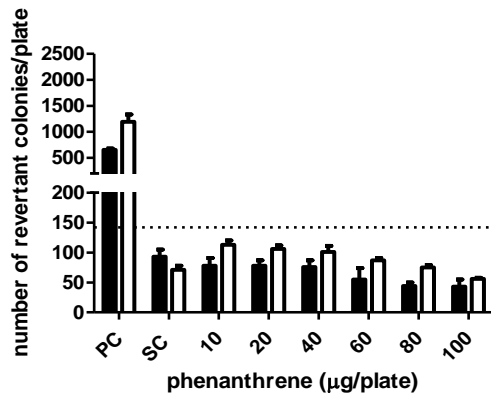
(e)



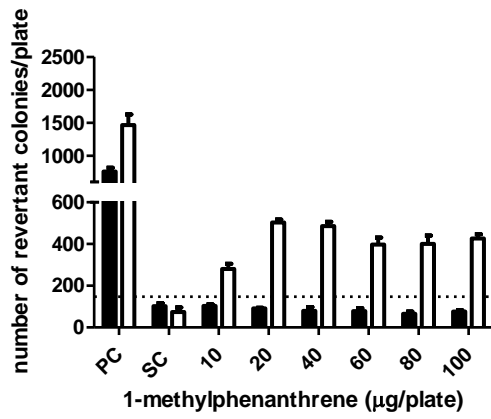
**Figure 5.** Number of revertants in *S. typhimurium* TA98 upon exposure to (a) phenanthrene (b) 1-methylphenanthrene, (c) 2-methylphenanthrene, (d) 3-methylphenanthrene and (e) 9-

methylphenanthrene in absence (black bar) and presence (white bar) of 5% S9-mix. Bars represent means and vertical bars indicate the standard deviation of the mean (n=3). The dotted horizontal line indicates 3-fold increase that is considered positive for mutagenicity. In absence of S9 mix, the test doses of 3-methyl-PHE showed cytotoxicity so no data are presented. The results of at least four analyzable doses that were non-cytotoxic were presented in Table S2 in the supplementary material showing negative results. PC = positive control, 1µg/plate 2AA with S9-mix and 10µg/plate NF without S9-mix. SC = solvent control, DMSO with and without S9-mix.

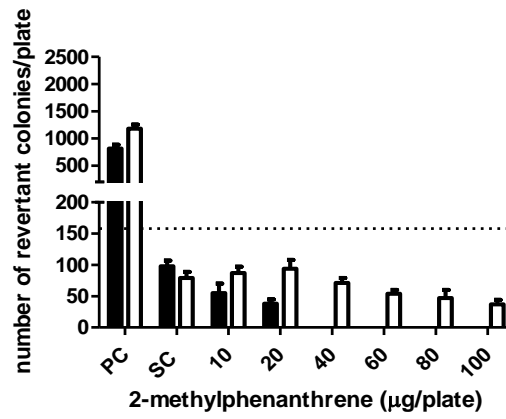
(a)



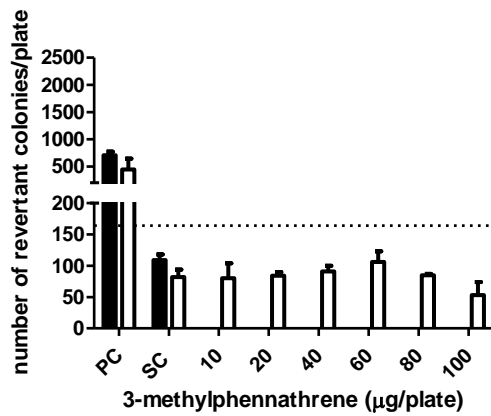
(b)



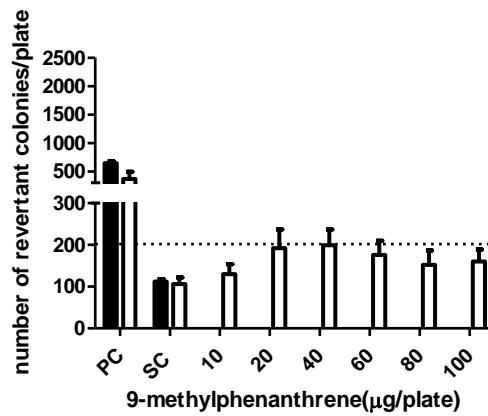
(c)



(d)



(e)



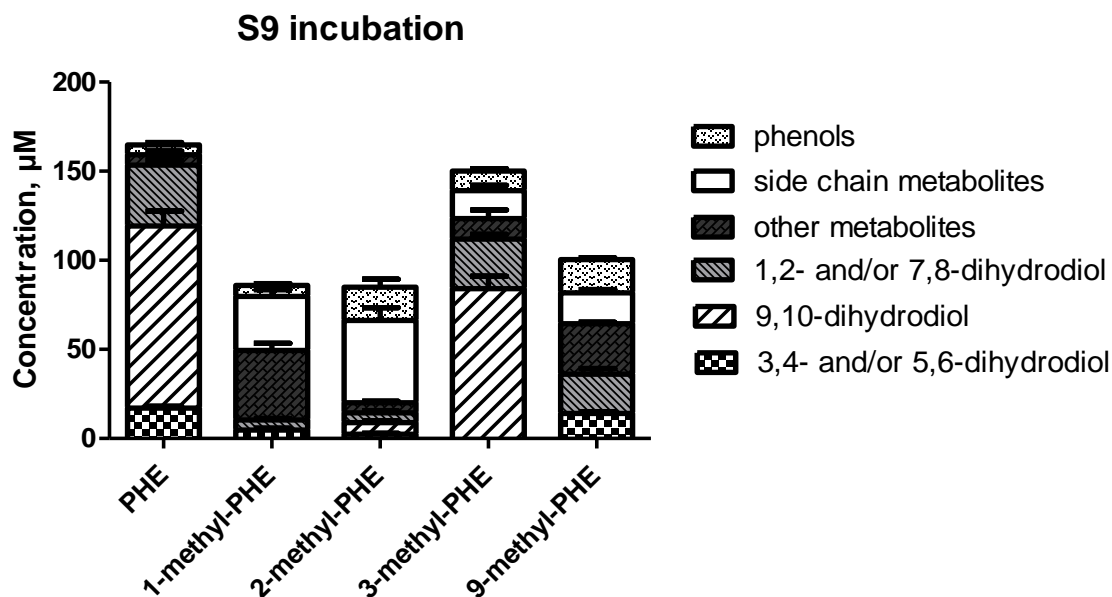
**Figure 6.** Number of revertants in *S. typhimurium* TA100 on exposure to (a) phenanthrene (b) 1-methylphenanthrene, (c) 2-methylphenanthrene, (d) 3-methylphenanthrene and (e) 9-methylphenanthrene in absence (black bar) and presence (white bar) of 5% S9-mix. The dotted horizontal line indicates 2- fold increase that is considered positive for mutagenicity. Bar represent means and vertical bars are standard deviation of the mean (n=3). In absence of S9 mix, the test doses of 2-methylphenanthrene, 3-methylphenanthrene and 9-methylphenanthrene showed cytotoxicity so no data are presented. The results of at least four analyzable lower doses that were non-cytotoxic were presented in Table S3 in the supplementary material. PC = positive control, 5µg/plate 2AA with S9-mix and 650 µg/plate MMS without S9-mix. SC = solvent control, DMSO with and without S9-mix.

### **3.5 S9 mediated metabolism of phenanthrene and its methylated analogues**

To obtain insight in the metabolic activation of the four selected methyl substituted phenanthrenes tested in the reverse mutation assay, exposure mixtures similar to those of the Ames test were analyzed by UPLC and further by GC-MS/MS for the unidentifiable metabolites. **Figure 7** shows the metabolite patterns and quantification from the incubations with phenanthrene and its four methylated phenanthrenes (tested at 1000µM a concentration being equivalent to the highest dose 100µg tested in the Ames test). Similarly to the results obtained with the microsomal incubations, metabolism of methylated phenanthrenes mediated by aroclor 1254 induced S9-mix generated dihydrodiols, alcohols and phenols (Figure S1 in supplementary material). This reveals that similar to what was already observed for the microsomal incubations, also for the S9 incubations the presence of alkyl substitution shifts the metabolism of phenanthrene in favor of side chain oxidation at the cost of aromatic oxidation. Besides, an additional type of metabolite (reflected by a peak marked with an asterisk in Figure S1 supplementary material) was identified as hydroxymethyl-

hydroxy-phenanthrene representing a further metabolite of hydroxymethyl-phenanthrene with a molecular ion at  $m/z$  226 measured by GC-MS/MS.

Three major metabolites of phenanthrene observed in the chromatogram (Figure S1 supplementary material) of the S9 incubation were identified as 3,4-dihydrodiol, 9,10-dihydrodiol and 1,2-dihydrodiol accounting for 10.5%, 62.1% and 20.7% of the total metabolite formation of phenanthrene, respectively. Formation of 1,2- and/or 7,8-dihydrodiols was found in all tested monomethylated phenanthrenes. Variation in formation of 3,4- and/or 5,6-dihydrodiols and 9,10-dihydrodiol between mutagenic phenanthrenes (1-methyl- and 9-methyl-phenanthrene) and non-mutagenic phenanthrenes (2-methyl- and 3-methylphenanthrene) was noticed (**Figure 7**). Formation of 9,10-dihydrodiol was only found in the incubations with 2-methyl and 3-methylphenanthrene at levels amounting to 7.7% and 57.7% of the metabolites formed respectively. In the S9 incubations, 3,4- and/or 5,6-dihydrodiols were formed at levels amounting to 5.5% and 12.5% of the total metabolite formation for 1-methyl- and 9-methyl-phenanthrene while at 2.2% and 0% of the total metabolite formation for 2-methyl- and 3-methyl-phenanthrene respectively.



**Figure 7.** Concentration of the metabolites formed in S9 incubation with phenanthrene and four of its methyl substituents. Each bar represents experimental means and vertical bars are standard errors of the mean (n=3).

#### 4. Discussion

The consumption of food contaminated with PPAHs from petroleum derived products or environmental sources may be of concern to human health. The hazards of PPAHs are expected to be related to bioactivation. Since data on the metabolic fate of most PPAHs, in particular alkylated PAHs, are lacking, the oxidative metabolism of phenanthrenes with various degrees of alkylation was studied to investigate the effect of the alkyl substitution. It was hypothesized that alkylation of phenanthrenes would shift to alkyl side chain oxidation at the cost of aromatic ring oxidation when compared to the non-alkylated phenanthrene. This metabolic shift would be expected to lower the chances on bioactivation to metabolites such as possibly mutagenic dihydrodiols and developmental toxicity related phenols. In line with the hypothesis, the side chain hydroxylated

metabolites of alkylated phenanthrenes were 30.9- to 3.5- fold more efficiently formed than aromatic ring oxidation metabolites by both HLM and RLM. The overall metabolism of phenanthrene with an alkyl chain with more than C6 was strongly reduced and metabolism was even absent in the case of 1-n-dodecylphenanthrene (C12). This observation may be best ascribed to possible steric hindrance by the longer alkyl chains hampering binding to the active site of the cytochrome P450 enzymes. Furthermore, metabolic oxidation primarily happened on the carbon atom at the benzylic position in case of 2-ethyl-, 9-ethyl-, and 10-methyl-9-ethyl-phenanthrenes, similar to the results obtained by microsomal incubations of 1-ethyl- and 2-ethyl-naphthalene (Wang et al. 2020). Side chain oxidation of alkylated phenanthrenes was also observed in other metabolic studies. Hydroxymethyl-phenanthrenes were detected as primary metabolites in a metabolism study with rat S9 incubations of 1-methyl-, 2-methyl, 3-methyl-, 4-methyl- and 9-methyl-phenanthrene (LaVoie et al. 1981). Side chain hydroxylation metabolites were also detected in incubations of 1-methylphenanthrene and 9-ethylphenanthrene with human hepatoma (HepG2) cells (Huang et al. 2017).

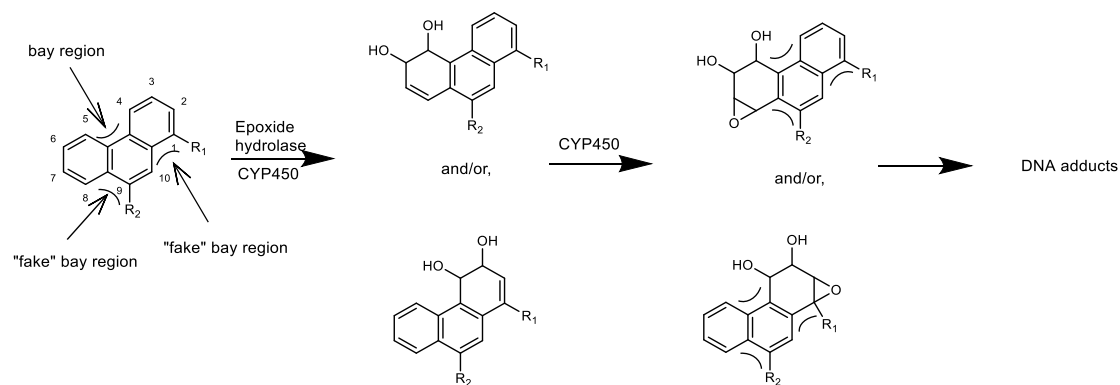
Considering that the metabolic shift from aromatic ring to side chain oxidation may reflect a shift from bioactivation to detoxification, data on the mutagenicity and tumorigenicity of these alkylated PAHs are of interest. However, data on the mutagenicity and the tumorigenicity of phenanthrene and alkyl substituted phenanthrenes are scarce. Neither phenanthrene nor its dihydrodiol metabolites were found to be mutagenic towards TA98 and TA100 tester strain of *S. typhimurium* (Bucker et al. 1979; Wood et al. 1979). This is in line with the observation in the present study that phenanthrene was tested negative for mutagenicity in both tester strains TA98 and TA100. In the present study, 1-methylphenanthrene showed 13.0- fold and 6.8- fold increase in the number of revertants compared to the concurrent solvent control when tested in the presence of metabolic

activation in TA98 and TA100, respectively. Comparable studies showed a 3.2- fold and 6- fold increase in TA98 and TA100 respectively (LaVoie et al. 1983), and an 8.4- fold and 4.1- fold increase in the same strains (Katarzyna Rudnicka 2013). In addition, 9-methylphenanthrene, the other methyl substituted phenanthrene that tested positive with 3.2- fold (TA98) and 2.0- fold (TA100) increase relative to historical controls in the present study, was previously reported to be mutagenic as reflected by a 3.0- fold increase in revertants in TA100 while testing negative (only 1.3- fold increase) in TA98 (LaVoie et al. 1983).

Considering that the possible metabolic pathway underlying mutagenicity of 1-methyl- and 9-methyl-phenanthrene could be a dihydrodiol-epoxide pathway (**Figure 8**), it can be suggested that the observed mutagenicity of 1-methyl- and 9-methyl-phenanthrene may be associated with regio- and stereo- selectivity for the possible dihydrodiol-epoxide bioactivation following the introduction of the methyl substitution. The formation of an additional bay region-like structural motif, described as “fake” bay region (**Figure 8**) upon introduction of a methyl substituent at the C1 or C9 position of phenanthrene may play a role in the observed mutagenicity. It is also of interest to note that it has been suggested before that the formation of 3,4- and/or 5,6- dihydrodiol metabolites likely reflects the bioactivation to mutagenic metabolites (LaVoie et al. 1981). This would be in line with the suggestion that methyl substitution at or near the K-region (9,10-position) of phenanthrene at its peri positions (**Figure 1**) would favor 3,4- and/or 5,6- dihydrodiol formation and mutagenicity (**Figure 5** and **6**) (LaVoie et al. 1983). Indeed for 9-methyl- and 1-methyl-phenanthrene formation of 3,4- and/or 5,6- dihydrodiol was observed, albeit to a level somewhat lower than observed for phenanthrene itself, which was tested negative for mutagenicity. Nevertheless, given the fact that methyl substitution adjacent to the K-region in 1-methyl- and 9-methyl phenanthrene forms a “fake” bay region, it implies that 3,4- and/or 5,6- dihydrodiol



formation provides increased chances of formation of a bay-region dihydrodiol-epoxide (**Figure 8**). However, in phenanthrene this 3,4- and/or 5,6 dihydrodiol formation would not result in a bay region dihydrodiol-epoxide.



**Figure 8.** Possible metabolic pathway towards bay region dihydrodiol-epoxide formation for 1-methyl- ( $R_1 = \text{CH}_3$ ) and 9-methyl- ( $R_2 = \text{CH}_3$ ) phenanthrene

Given these mutagenicity results it is also important to consider that neither phenanthrene nor its monomethylated analogues including 2-methyl- and 3-methylphenanthrene but also 1-methyl- and 9-methyl-phenanthrene were found to be active tumor initiators in mouse skin painting studies (Buening et al. 1979; LaVoie et al. 1981). This lack of tumor-initiating activity of methyl substituted phenanthrenes might be due to a relatively lower tumor inducing potency of the formed DNA adducts compared to for example the diol epoxide metabolites of benzo[a]pyrene.

Finally, it is also of interest that some authors have proposed a role for side chain hydroxylated metabolites in alkyl-substituted PAHs to play a role in their mutagenicity upon their further bioactivation by sulfotransferases to unstable DNA reactive sulfate metabolites (Huang et al. 2017). Whether for 1-methyl- and 9-methyl- phenanthrene also their side chain hydroxy metabolites play such a role remains to be investigated.

The current risk assessment of PPAHs that may be present in consumer products is based on read across to metabolic activation and formation of DNA reactive metabolites of naked PAHs due to the lack of data on PPAH themselves (Baird et al. 2007; EFSA 2012; Wickliffe et al. 2014). The results of the present study provide insight in the effect of alkylation on the oxidative metabolism of phenanthrene, and also provide kinetic parameters that may turn out to be of use for future physiologically based kinetic (PBK) models to extrapolate toxicity data obtained in vitro to in vivo taking kinetics into account. The PBK models together with in vitro concentration-response data would provide the basis of a new approach methodology (NAM) for predicting the in vivo toxicity of alkyl substituted aromatics that may be present in petroleum derived products, in line with the proof of principle predicting the developmental toxicity of benzo[a]pyrene by this in vitro - in silico approach (Wang et al. 2021).

Phenanthrene is the smallest PAH with a bay region but lacks genotoxic and carcinogenic properties observed for some bay-region PAHs with a higher number of aromatic rings, such as benzo[a]pyrene. It would be of interest for future studies to investigate whether alkylation causes similar shifts in metabolic oxidation for PAHs and PPAHs with more fused aromatic rings and in what way this influences their toxicity, as observed with naphthalene (Wang et al. 2020) and with phenanthrene in the present study. The results of the present study clearly show that the mutagenic effect depends on the site of alkylation on PAHs, with alkylation either increasing or decreasing toxicity.

Taking all together it is concluded that alkylation of PAHs favors alkyl chain oxidation at the cost of aromatic oxidation. Especially methyl substitution of phenanthrene adjacent to its K-region such as in 1-methyl- and 9-methyl-phenanthrene converted phenanthrene into mutagens towards *S. typhimurium* TA98 and TA100. The position of the alkylation affects the metabolism and resulting

mutagenicity of phenanthrene with the mutagenicity increasing in cases where the alkyl substituent creates an additional bay-region like structural motif, in spite of the extra possibilities for side chain oxidation.

## References

- Baird SJS, Bailey EA, Vorhees DJ (2007) Evaluating human risk from exposure to alkylated PAHs in an aquatic system. *Hum Ecol Risk Assess* 13(2):322-338 doi:10.1080/10807030701226277
- Bao ZP, Yang SK (1991) Liquid-Chromatographic Separation of Isomeric Phenanthrols on Monomeric and Polymeric C18 Columns. *J Chromatogr* 536(1-2):245-249 doi:10.1016/S0021-9673(01)89256-6
- Bayer U (1978) In vivo induction of sister chromatid exchanges by three polyaromatic hydrocarbons Polynuclear Aromatic Hydrocarbons. vol 3. Raven Press, New York, p 423-428
- Boogaard PJ (2012) Chapter 3F Biomonitoring of Exposure to Polycyclic Aromatic Hydrocarbons Biomarkers and Human Biomonitoring: Volume 1. vol 1. The Royal Society of Chemistry, p 338-359
- Bucker M, Glatt HR, Platt KL, et al. (1979) Mutagenicity of Phenanthrene and Phenanthrene K-Region Derivatives. *Mutation Research* 66(4):337-348 doi:10.1016/0165-1218(79)90044-2
- Buening MK, Levin W, Karle JM, Yagi H, Jerina DM, Conney AH (1979) Tumorigenicity of bay-region epoxides and other derivatives of chrysene and phenanthrene in newborn mice. *Cancer Res* 39(12):5063-8
- Carrillo JC, van der Wiel A, Danneels D, Kral O, Boogaard PJ (2019) The selective determination of potentially carcinogenic polycyclic aromatic compounds in lubricant base oils by the

DMSO extraction method IP346 and its correlation to mouse skin painting carcinogenicity assays. Regul Toxicol Pharmacol 106:316-333 doi:10.1016/j.yrtph.2019.05.012

Chaturapit S, Holder GM (1978) Studies on the hepatic microsomal metabolism of (14C) phenanthrene. Biochem Pharmacol 27(14):1865-71 doi:10.1016/0006-2952(78)90034-5

EFSA (2008) Polycyclic Aromatic Hydrocarbons in Food - Scientific Opinion of the Panel on Contaminants in the Food Chain. EFSA Journal 6(8):724 doi:10.2903/j.efsa.2008.724

EFSA (2012) Scientific Opinion on Mineral Oil Hydrocarbons in Food. EFSA Journal 10(6):2704 doi:10.2903/j.efsa.2012.2704

Fengler R, Gruber L (2020) Mineral oil migration from paper-based packaging into food, investigated by means of food simulants and model substances. Food Addit Contam Part A Chem Anal Control Expo Risk Assess:1-13 doi:10.1080/19440049.2020.1714750

Fernando H, Ju H, Kakumanu R, et al. (2019) Distribution of petrogenic polycyclic aromatic hydrocarbons (PAHs) in seafood following Deepwater Horizon oil spill. Mar Pollut Bull 145:200-207 doi:10.1016/j.marpolbul.2019.05.015

Grob K (2018) Mineral oil hydrocarbons in food: a review. Food Addit Contam Part A Chem Anal Control Expo Risk Assess 35(9):1845-1860 doi:10.1080/19440049.2018.1488185

Huang M, Mesaros C, Hackfeld LC, Hodge RP, Blair IA, Penning TM (2017) Potential Metabolic Activation of Representative Alkylated Polycyclic Aromatic Hydrocarbons 1-Methylphenanthrene and 9-Ethylphenanthrene Associated with the Deepwater Horizon Oil Spill in Human Hepatoma (HepG2) Cells. Chem Res Toxicol 30(12):2140-2150 doi:10.1021/acs.chemrestox.7b00232

- Jacob J, Raab G, Soballa V, et al. (1996) Cytochrome P450-mediated activation of phenanthrene in genetically engineered V79 Chinese hamster cells. *Environ Toxicol Pharmacol* 1(1):1-11 doi:10.1016/1382-6689(95)00003-8
- Kaden DA, Hites RA, Thilly WG (1979) Mutagenicity of soot and associated polycyclic aromatic hydrocarbons to *Salmonella typhimurium*. *Cancer Res* 39(10):4152-9
- Katarzyna Rudnicka ST, Kinga A. Budzikur, Danuta Mielżyńska-Švach, Ewa Jakimiuk, Anna Chachaj, Maciej Góra, Kamila Żelazna, Michał K. Łuczyński (2013) Assessment of mutagenic activity of methyl- and phenylphenanthrenes based on *Salmonella* test and micronucleus test. *Environmental Biotechnology* 9(2):65-71 doi:DOI: 10.14799/ebms193
- LaVoie EJ, Tulley-Freiler L, Bedenko V, Hoffman D (1981) Mutagenicity, tumor-initiating activity, and metabolism of methylphenanthrenes. *Cancer Res* 41(9 Pt 1):3441-7
- LaVoie EJ, Tulley-Freiler L, Bedenko V, Hoffmann D (1983) Mutagenicity of substituted phenanthrenes in *Salmonella typhimurium*. *Mutat Res* 116(2):91-102 doi:10.1016/0165-1218(83)90100-3
- Lehr RE, Kumar S, Levin W, et al. (1985) The Bay Region Theory of Polycyclic Aromatic Hydrocarbon Carcinogenesis. *Acs Symposium Series* 283:63-84
- Levy DD, Zeiger E, Escobar PA, et al. (2019) Recommended criteria for the evaluation of bacterial mutagenicity data (Ames test). *Mutat Res Genet Toxicol Environ Mutagen* 848:403074 doi:10.1016/j.mrgentox.2019.07.004
- Li D, Han YL, Meng XL, et al. (2010) Effect of Regular Organic Solvents on Cytochrome P450-Mediated Metabolic Activities in Rat Liver Microsomes. *Drug Metabolism and Disposition* 38(11):1922-1925 doi:10.1124/dmd.110.033894

- Pirow R, Blume A, Hellwig N, et al. (2019) Mineral oil in food, cosmetic products, and in products regulated by other legislations. *Crit Rev Toxicol* 49(9):742-789 doi:10.1080/10408444.2019.1694862
- Pulster EL, Gracia A, Armenteros M, et al. (2020) A First Comprehensive Baseline of Hydrocarbon Pollution in Gulf of Mexico Fishes. *Sci Rep-Uk* 10(1) doi:10.1038/s41598-020-62944-6
- Schober W, Pusch G, Oeder S, Reindl H, Behrendt H, Buters JT (2010) Metabolic activation of phenanthrene by human and mouse cytochromes P450 and pharmacokinetics in CYP1A2 knockout mice. *Chem Biol Interact* 183(1):57-66 doi:10.1016/j.cbi.2009.09.008
- Shou M, Korzekwa KR, Krausz KW, Crespi CL, Gonzalez FJ, Gelboin HV (1994) Regio- and stereo-selective metabolism of phenanthrene by twelve cDNA-expressed human, rodent, and rabbit cytochromes P-450. *Cancer Lett* 83(1-2):305-13 doi:10.1016/0304-3835(94)90334-4
- Sims P (1970) Qualitative and quantitative studies on the metabolism of a series of aromatic hydrocarbons by rat-liver preparations. *Biochemical Pharmacology* 19(3):795-818 doi:[https://doi.org/10.1016/0006-2952\(70\)90243-1](https://doi.org/10.1016/0006-2952(70)90243-1)
- Tsang W-S, Griffin GW (1979) The “Bay-Region” Theory of Carcinogenic Activity; Application of Perturbational Molecular Orbital Theory. In: Tsang W-S, Griffin GW (eds) *Metabolic Activation of Polynuclear Aromatic Hydrocarbons*. Pergamon, p 73-85
- Van Heyst A, Vanlancker M, Vercammen J, et al. (2018) Analysis of mineral oil in food: results of a Belgian market survey. *Food Addit Contam Part A Chem Anal Control Expo Risk Assess* 35(10):2062-2075 doi:10.1080/19440049.2018.1512758

- Wang D, Bruyneel B, Kamelia L, Wesseling S, Rietjens I, Boogaard PJ (2020) In vitro metabolism of naphthalene and its alkylated congeners by human and rat liver microsomes via alkyl side chain or aromatic oxidation. *Chem Biol Interact* 315:108905 doi:10.1016/j.cbi.2019.108905
- Wang D, Rietdijk MH, Kamelia L, Boogaard PJ, Rietjens I (2021) Predicting the in vivo developmental toxicity of benzo[a]pyrene (BaP) in rats by an in vitro-in silico approach. *Arch Toxicol* doi:10.1007/s00204-021-03128-7
- Whalen DL, Ross AM, Yagi H, Karle JM, Jerina DM (1978) Stereoelectronic factors in the solvolysis of bay region diol epoxides of polycyclic aromatic hydrocarbons. *J Am Chem Soc* 100(16):5218-5221 doi:10.1021/ja00484a058
- Wickliffe J, Overton E, Frickel S, et al. (2014) Evaluation of Polycyclic Aromatic Hydrocarbons Using Analytical Methods, Toxicology, and Risk Assessment Research: Seafood Safety after a Petroleum Spill as an Example. *Environ Health Persp* 122(1):6-9 doi:10.1289/ehp.1306724
- Wood AW, Chang RL, Levin W, et al. (1979) Mutagenicity and tumorigenicity of phenanthrene and chrysene epoxides and diol epoxides. *Cancer Res* 39(10):4069-77
- Ylitalo GM, Krahn MM, Dickhoff WW, et al. (2012) Federal seafood safety response to the Deepwater Horizon oil spill. *Proc Natl Acad Sci U S A* 109(50):20274-9 doi:10.1073/pnas.1108886109



## **Acknowledgement**

This work was financially supported by Concauwe (No. 201700093) in Belgium, and by a grant from China Scholarship Council from China (No. 201807720073) to Danlei Wang. Part of this work was supported by Operationeel Programma Kansen voor West II (EFRO) (project no KVV- 00181).

## Supplementary materials

**Table S1.** Historical control data of the solvent control of reverse mutation assay

	<b>TA98</b>		<b>TA100</b>	
<b>S9-mix</b>	-	+	-	+
<b>Range</b>	4 – 61	6 – 60	58 – 188	50 – 176
<b>Mean</b>	14	18	109	101
<b>SD</b>	5	6	19	21
<b>n</b>	2523	2528	2566	2508

SD = Standard deviation

n = Number of observations

Historical control data from experiments performed between Nov 2017 and Nov 2020.

**Table S2.** Mutagenic response of 3-methyl-PHE in the *Salmonella typhimurium* TA98 without S9-mix at lower doses that were non-cytotoxic. The results are presented as mean number of revertant colonies of 3 replicate plates and standard deviation.

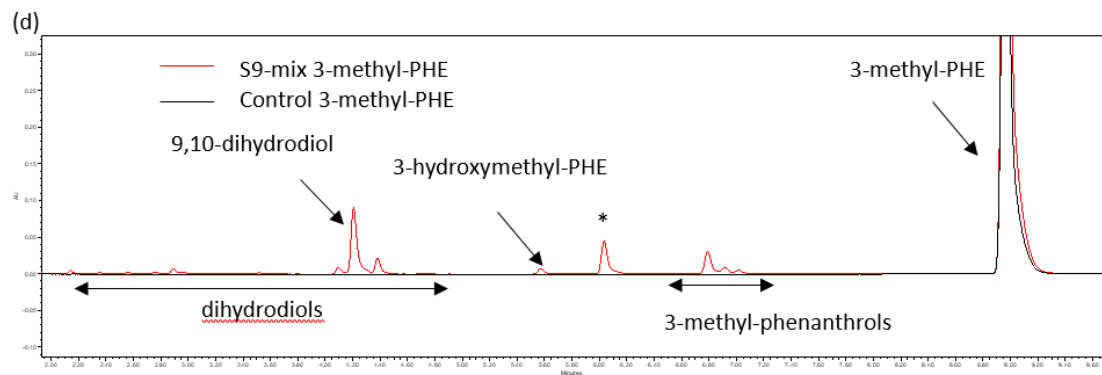
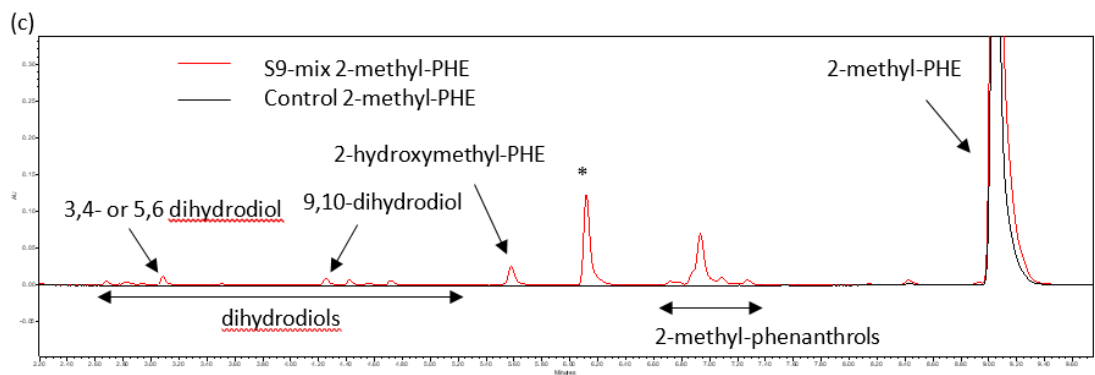
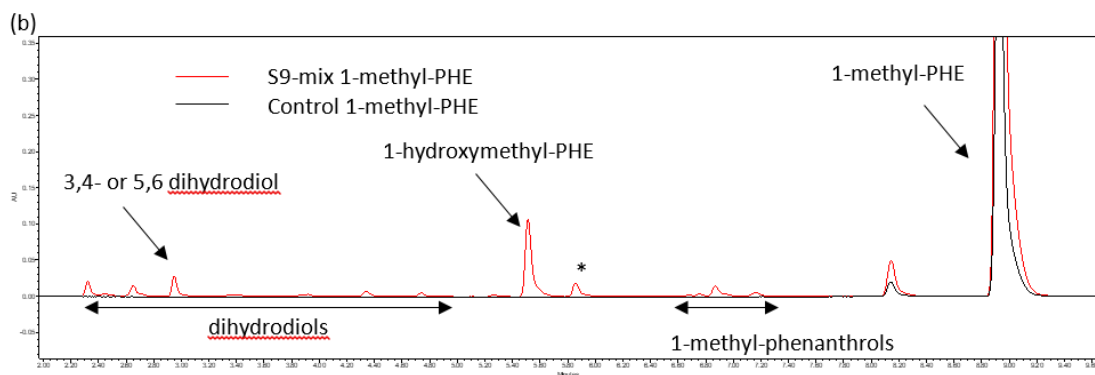
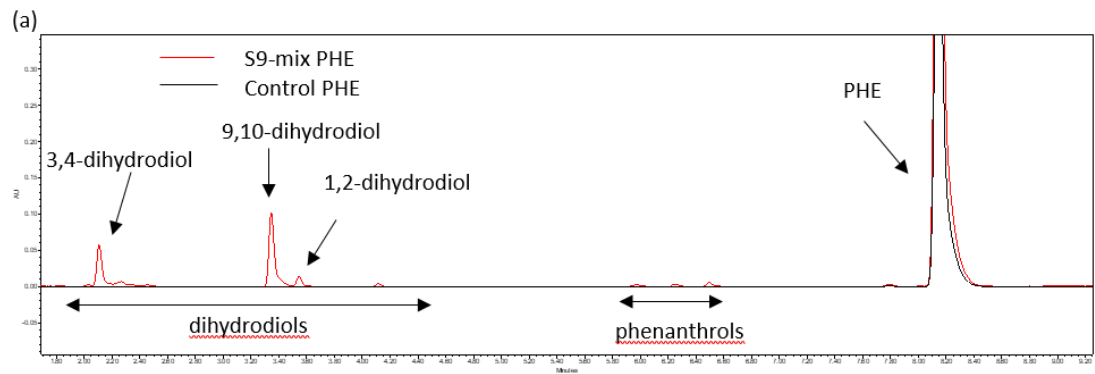
<b>Test compound</b>	<b>Dose (µg/plate)</b>	<b>His + revertant colonies TA98 without S9-mix</b>
<b>3-methyl-PHE</b>	PC	1590±295
	SC	15±4
	2	16±3
	4	17±4
	10	14±1
	20	13±2
	40	9±4 <sup>S</sup>

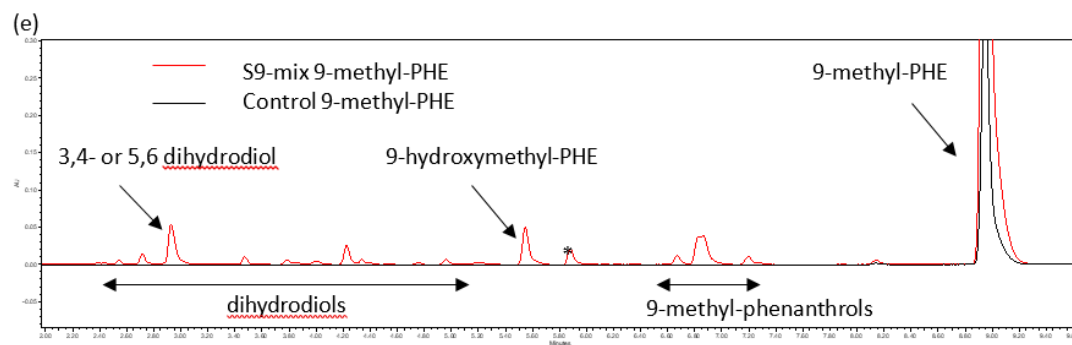
<sup>S</sup> indicates bacterial background lawn slightly reduced

**Table S3.** Mutagenic response of 2-methyl-PHE, 3-methyl-PHE and 9-methyl-PHE in the *Salmonella typhimurium* TA100 without S9-mix at lower doses that were non-cytotoxic. The results are presented as mean number of revertant colonies of 3 replicate plates and standard deviation.

Test compound	Dose (µg/plate)	His + revertant colonies TA100
		without S9-mix
2-methyl-PHE	PC	823±58
	SC	97±4
	10	106±20
	20	98±13
	40	70±8 <sup>m</sup>
3-methyl-PHE	PC	783±46
	SC	116±9
	2	112±14
	4	112±9
	10	119±11
	20	83±34
	40	75±4 <sup>m</sup>
9-methyl-PHE	PC	868±70
	SC	115±17
	2	121±7
	4	109±3
	10	105±11
	20	97±20
	40	59±40 <sup>m</sup>

<sup>m</sup> indicates bacterial background lawn moderately reduced





**Figure S1.** Relevant parts of UPLC chromatograms of incubation mixtures without and with S9-mix for (a) phenanthrene (b) 1-methylphenanthrene (c) 2-methylphenanthrene (d) 3-methylphenanthrene and (e) 9-methylphenanthrene at 254 nm wavelength. PHE = phenanthrene.



## **Chapter 4**

# **The influence of alkyl substitution on the in vitro metabolism and mutagenicity of benzo[a]pyrene**

Danlei Wang, Angelique Groot, Albrecht Seidel, Lulu Wang, Effimia Kiachaki,  
Peter J. Boogaard, Ivonne M.C.M. Rietjens

Manuscript in preparation

## **Abstract**

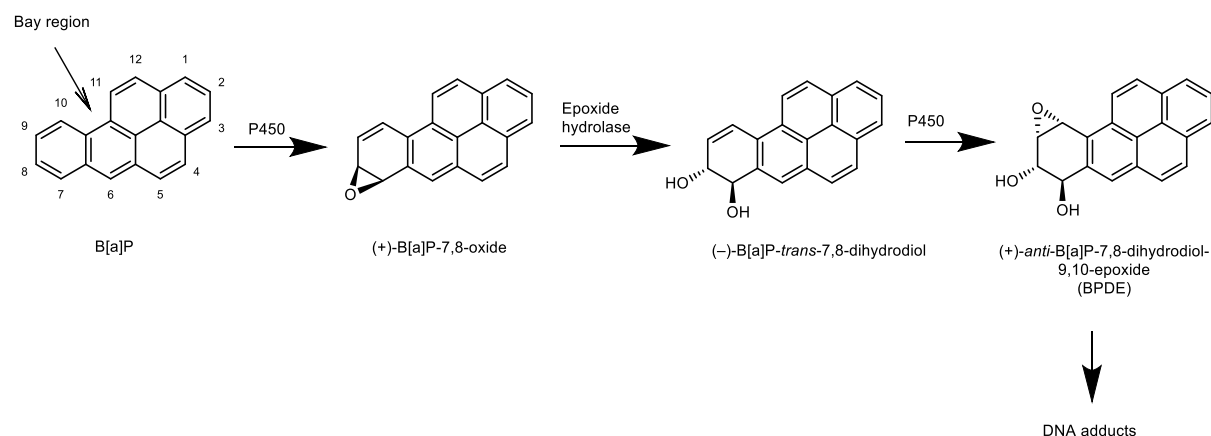
In recent years concerns over consumer exposure to mineral oil aromatic hydrocarbons (MOAH), especially those containing alkylated polycyclic aromatic hydrocarbons (PAHs), have emerged. This is especially due to the fact that some PAHs are known to be genotoxic and carcinogenic upon metabolic activation. However, available toxicological data on PAHs mainly relate to non-substituted PAHs with a lack of data on alkyl substituted PAHs. Therefore, the aim of the present study was to characterize the effect of alkyl substitution on the metabolism and mutagenicity of benzo[a]pyrene (B[a]P), a PAH known to be genotoxic and carcinogenic. To this end, the oxidative metabolism and mutagenicity of B[a]P and a series of its alkyl substituted analogues were quantified using in vitro microsomal incubations and the Ames test. The results obtained reveal that upon alkylation the metabolic oxidation shifts to the aliphatic side chain at the cost of aromatic ring oxidation. The overall metabolism, including metabolism via aromatic ring oxidation, and thus chances on bioactivation, were substantially reduced with elongation of the side chain, with metabolism of B[a]P with an alkyl substituent of > 6 C-atoms being seriously hampered. In the Ames test upon metabolic activation, methyl substitution of B[a]P resulted in an increase or decrease of the mutagenic potency depending the substitution position. The relevant pathways for mutagenicity of the selected monomethyl substituted B[a]P may involve the formation of a 7,8-dihydrodiol-9,10-epoxide, a 4,5-oxide and/or an oxidative side chain metabolite that may subsequently give rise to an unstable and reactive sulfate conjugate. It is concluded that alkylation of B[a]P does not systematically reduce its mutagenicity in spite of the metabolic shift from aromatic to side chain oxidation.



## 1. Introduction

The presence of unsubstituted ('naked') and alkylated polycyclic aromatic hydrocarbons (PAHs) in mineral oils, raised safety concerns with respect to unintentional contamination of foodstuff and other consumer products with mineral oil aromatic hydrocarbons (MOAH) <sup>1-4</sup>. Legally accepted mineral oils applied in food production, in pharmaceuticals and cosmetic products are highly refined and non-carcinogenic, and generally referred to as highly refined base oils (HRBOs) or white mineral oils. Nonetheless, unintentional or illegal use of insufficiently refined mineral oils may result in contamination of foodstuffs, pharmaceuticals or cosmetics with polycyclic aromatics from mineral oils which can chromatographically be detected and are referred to as MOAH. Some of these MOAH that can be detected in consumer products have been considered as potentially genotoxic and carcinogenic due to the presence of PAHs with 3 to 7 condensed rings with non or simple alkylation <sup>5</sup>. These PAHs generally need bioactivation to exert these adverse effects. The present study focusses on benzo[a]pyrene (B[a]P) and a series of its alkylated analogues as model compounds to study the effect of alkylation on the in vitro metabolism and mutagenicity of PAHs. B[a]P is a typical mutagenic PAH that has been classified as a Group 1 carcinogen by the International Agency for Research on Cancer (IARC) based on evidence for its carcinogenicity in experimental animals and the consideration that the compound acts through a mechanism of carcinogenicity also relevant to humans <sup>6</sup>. Bioactivation of B[a]P and other non-substituted PAHs to their genotoxic and carcinogenic metabolites was extensively studied in the past decades. These studies indicate that formation of a so-called bay region dihydrodiol-epoxide results in the most genotoxic and ultimate carcinogenic metabolite of these PAHs <sup>7,8</sup>. **Figure 1** presents the formation of such a bay region dihydrodiol-epoxide from B[a]P following conversion by cytochrome P450, epoxide hydrolase and again a cytochrome P450 mediated reaction, ultimately resulting in formation of (+) anti-B[a]P-7,8-dihydrodiol-9,10-epoxide (BPDE), one of the four potential

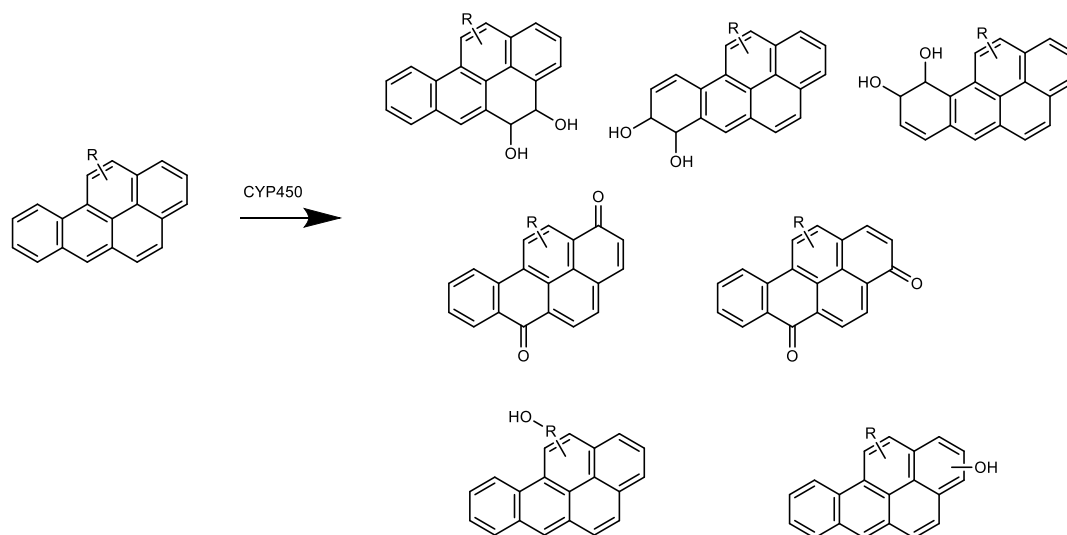
stereoisomers of B[a]P-7,8-dihydrodiol-9,10-epoxide, which was implied as the ultimate carcinogen of B[a]P<sup>9</sup>. Given that this pathway for bioactivation includes two cytochrome P450 catalyzed monooxygenation steps, and that the presence of an alkyl substituent may redirect the cytochrome P450 mediated conversion from aromatic to side chain oxidation<sup>10</sup>, it remains to be elucidated whether alkylated bay-region PAHs would be bioactivated to a similar extent as the naked analogues. Given that the PAHs present in MOAH may in part represent alkylated PAHs the aim of the present study was to quantify the effect of alkyl substitution on the in vitro metabolism and genotoxicity of PAHs using B[a]P as the model compound.



**Figure 1.** Metabolic activation pathway of B[a]P to its ultimate genotoxic and carcinogenic metabolite.

Microsomal metabolic profiles for B[a]P and two of its methylated analogues are available in literature from the 1980s, including studies on 7-methyl-B[a]P<sup>11-14</sup>, and 6-methyl-B[a]P<sup>15,16</sup>. These studies revealed that B[a]P is metabolized by rat or human liver microsomes and skin microsomes to dihydrodiols, quinones and phenols, specifically the 4,5-dihydrodiol, 7,8-dihydrodiol and 9,10-dihydrodiol of B[a]P, the 1,6-quinone, 3,6-quinone and 6-12-quinone of B[a]P, and 1-hydroxy-, 3-hydroxy- and 9-hydroxy- B[a]P (**Figure 2**)<sup>17-22</sup>. The methylated analogue 7-methyl-B[a]P was reported to be converted by polychlorinated biphenyl (PCB) induced rat liver microsomes to the

same type of metabolites and, in addition, to the metabolite resulting from side chain oxidation, 7-hydroxymethyl-B[a]P (**Figure 2**)<sup>11-13</sup>. Metabolic studies on the conversion of 6-methyl-B[a]P by 3-methylcholanthrene (3-MC) induced rat liver microsomes suggested a similar profile of metabolites with additional formation of 1-hydroxy-6-hydroxymethyl-B[a]P, 3-hydroxy-6-hydroxymethyl-B[a]P, and an unidentified ring-hydroxylated 6-methyl-B[a]P (Figure 2)<sup>15, 16</sup>. These studies identified the various type of metabolites in a qualitative way but did not quantify the level of side chain versus aromatic hydroxylation, while they also did not include a comparison of B[a]P and its methylated analogues.



**Figure 2.** A summary of the reported metabolites of B[a]P, 6-methyl and 7-methyl substituted B[a]P formed by P450 enzymes<sup>11-13, 15, 16</sup>. R = CH<sub>3</sub> substitution

With respect to the mutagenicity it appeared that methyl substitution of B[a]P may increase or decrease the response in the Ames test. The limited number of reported studies on the effect of methylation on the mutagenicity and the dermal tumor-initiating activity of B[a]P are summarized in Table 1. The effect of monomethylation of B[a]P at twelve available carbon positions was examined in an Ames test with *S. typhimurium* tester strain TA100 in the studies of Chui et al. and

Utesch et al.<sup>23, 24</sup>. Although all tested monomethyl substituted B[a]P tested positive for mutagenicity towards TA100 upon metabolic activation with rat S9 homogenate<sup>23-26</sup>, the mutagenic potency (expressed in revertants/nmol) of each monomethyl substituted B[a]P varied between studies. In the study of Chui et al., the mutagenic potency of B[a]P and the monomethyl substituted B[a]Ps towards tester strain TA100 followed the order: 9-methyl-B[a]P > 4-methyl-B[a]P > 6-methyl-B[a]P > 11-methyl-B[a]P > B[a]P > another eight monomethyl substituted B[a]Ps that showed equal or less mutagenicity compared to B[a]P itself<sup>23</sup>. The study of Utesch et al. suggested the mutagenic potency to decrease in the order 4-methyl-B[a]P > B[a]P > other eleven monomethyl substituted B[a]Ps among the twelve monomethylated B[a]Ps tested in tester strain TA100<sup>24</sup>. In line with the study of Chui et al., several other studies also reported 6-methyl-B[a]P being more mutagenic than B[a]P towards tester strain TA98 and TA100<sup>25-27</sup>. No correlation between mutagenic potency in the Ames test and the skin tumor-initiating activity reported by Iyer et al.<sup>28</sup> was found for the twelve monomethyl substituted B[a]Ps.

The present study aims to provide novel biotransformation and mutagenicity data for several selected monomethyl substituted B[a]Ps, the latter towards both tester strains TA98 and TA100 that detect frameshift mutations and base-pair mutations, respectively. In particular, the effect of methyl substitution that introduces an additional bay region-like structural motif (“fake” bay region) on the possible underlying metabolic pathways and resulting mutagenicity was explored. The reported studies suggested 6-methyl-B[a]P with two additional “fake” bay regions to be a more potent mutagen but a weaker skin tumor initiator than B[a]P. The distal substitution at the C3 position of B[a]P results in possibilities for the formation of a bay region diol-epoxide next to an additional “fake” bay region apparently resulting in lower mutagenic potency but a stronger skin tumor-initiating activity than what was observed for B[a]P. Both 8-methyl-B[a]P and 7-methyl-B[a]P in

which the methyl substituent may sterically block the formation of the bay region diol-epoxide showed less or equal mutagenic potency compared to B[a]P, and appeared inactive in tumor initiation. Taken all together these data suggest that the monomethyl substitution of B[a]P at C6, C3, C7 or the C8 position, that introduces no to two extra “fake” bay regions, provide interesting model compounds for metabolic and resulting mutagenicity studies among the twelve possible carbon positions for substitution.

To better understand the oxidative metabolism mediated by CYP enzymes of alkyl-substituted and non-substituted PAHs, the present study also characterizes the in vitro hepatic human and rat microsomal metabolism of an extended series of its alkylated analogues including in addition to B[a]P also 6-methyl-B[a]P, 7-methyl-B[a]P, 8-methyl-B[a]P, 3-methyl-B[a]P, 3-n-hexyl-B[a]P and 3-n-dodecyl-B[a]P with the latter two being specially synthesized.

**Table 1.** Overview of mutagenic potential of monomethyl substituted B[a]P and B[a]P itself in the Ames test as reported in the literature. The dose-corrected mutagenic potency of each compound is presented as the maximum value of the net increase in the number of revertants (background subtracted) divided by the dose, and expressed as revertants per nmol. The tumor-initiating activity of the monomethyl substituted B[a]Ps and of B[a]P itself, assessed in the mouse skin painting assay, is expressed as percentage of mice with tumor.

	Studies	Iyer et al. <sup>28</sup>	Bayless et al. <sup>27</sup>	Sullivan et al. <sup>14</sup>	Flesher et al <sup>29</sup>	Santella et al. <sup>25</sup>	Chui et al. <sup>23</sup>	Utesch et al. <sup>24</sup>	
		Tumor initiating	<i>S. typhimurium</i> strain						
		activity	TA98	TA98	TA98	TA100	TA100	TA100	TA100
Compound	B[a]P	67 (Potent)	38	41	13	22	88	81	34
	1-Methyl-B[a]P	80 (Potent)	-	-	-	-	-	37	11
	2-Methyl-B[a]P	38 (Weak)	-	-	-	-	-	43	18
	3-Methyl-B[a]P	76 (Potent)	-	-	-	-	-	40	26
	4-Methyl-B[a]P	67 (Potent)	-	-	-	-	-	156	59
	5-Methyl-B[a]P	27 (Weak)	-	-	-	-	-	42	11
	6-Methyl-B[a]P	24 (Weak)	173	199	97	73	341	136	32
	7-Methyl-B[a]P	0 (Inactive)	-	14	-	-	37	85	14
	8-Methyl-B[a]P	3 (Inactive)	-	-	-	-	86	88	15
	9-Methyl-B[a]P	0 (Inactive)	-	-	-	-	60	178	15
	10-Methyl-B[a]P	0 (Inactive)	-	-	-	-	23	47	8
	11-Methyl-B[a]P	90 (Very potent)	-	-	-	-	111	116	24
	12-Methyl-B[a]P	69 (Potent)	-	-	-	-	-	43	10

## 2. Material and Methods

### 2.1 Chemicals and reagents

B[a]P ( $\geq 99\%$ ), 7-methyl-B[a]P ( $\geq 98\%$ ), 8-methyl-B[a]P ( $\geq 98\%$ ), tetrahydrofuran ( $\geq 99.9\%$ ), trifluoroacetic acid ( $\geq 99\%$ ), methylmethanesulfonate (MMS), 2-aminoanthracene (2AA), and nitrofluorene (NF) were purchased from Sigma-Aldrich (St.Louis, USA). 3-Hydroxy-B[a]P was supplied by Toronto Research Chemicals (Toronto, Canada). 6-Methyl-B[a]P (99.5%) was obtained from CFW Laboratories (Newark, USA). 3-Methyl-B[a]P ( $>99\%$ ), 6-hydroxymethyl-B[a]P ( $>99\%$ ), 3-hydroxy-8-methyl-B[a]P ( $>99\%$ ), 3-n-hexyl-B[a]P ( $>99\%$ ), and 3-n-dodecyl-B[a]P ( $>99\%$ ) were synthesized by the Biochemical Institute for Environmental Carcinogens (Großhansdorf, Germany). Acetonitrile was bought from Biosolve (Dieuze, France). Dimethyl sulfoxide (DMSO),  $\text{MgCl}_2$ , KCl and  $\text{K}_2\text{HPO}_4 \cdot 3\text{H}_2\text{O}$  were supplied by Merck (Darmstadt, Germany). NADPH was obtained from Carbosynth (Berkshire, UK). Gentest™ pooled male Sprague Dawley rat liver microsomes (RLM) and Ultrapool™ human liver microsomes (HLM), both with a protein concentration of 20 mg/ml were supplied by Corning (New York, USA), the latter containing cytochrome P450 liver enzymes of 150 individuals. Aroclor 1254 induced liver S9 homogenate prepared from male Sprague Dawley rats was obtained from Trinova Biochem GmbH (Giessen, Germany). *Salmonella typhimurium* TA98 and TA100 tester strains were also obtained from Trinova Biochem GmbH (Giessen, Germany). NADP and glucose-6-phosphate were supplied by Randox Laboratories Ltd. (Crumlin, UK) and Roche Diagnostics (Mannheim, Germany), respectively.

## **2.2 In vitro incubations of B[a]P and its alkylated congeners with human and rat liver microsomes**

Microsomal incubations of B[a]P and its alkylated congeners with HLM and RLM consisted of 200  $\mu$ l incubations containing 0.1 M potassium phosphate (pH 7.4), 5 mM  $\text{MgCl}_2$ , HLM/RLM at a final microsomal protein concentration of 0.5 mg/ml, 1 mM NADPH, and each of the individual test compounds at concentrations ranging from 0 to 600  $\mu$ M. Test compounds were B[a]P, 3-methyl-B[a]P, 6-methyl-B[a]P, 7-methyl-B[a]P, 8-methyl-B[a]P, 3-n-hexyl-B[a]P and 3-n-dodecyl-B[a]P, added from 100 times concentrated stock solutions in DMSO or tetrahydrofuran (the latter was used for 1-n-hexyl-B[a]P and 1-n-dodecyl-B[a]P due to their low solubility in DMSO). The final concentration of substrate solvent, in the incubation mixture was 1% (v/v), which is known to not affect the enzymatic activity of liver microsomes<sup>30</sup>. The incubation mixtures were prepared and incubated in glass tubes to avoid plastic binding of the substrates. After pre-incubation of the incubation mixture at 37°C for 1 min, the enzymatic reaction was initiated by adding microsomes to the incubation mixture which was subsequently incubated at 37°C for 30 min. Under these conditions metabolite formation was linear with the incubation time and the microsomal protein concentration (data not shown). Because the tested substrates and their metabolites bind to microsomal protein substantially, a diisopropylether (DIPE) extraction of the metabolites was performed after the reaction was stopped by the addition of 20  $\mu$ l 10%  $\text{HClO}_4$ . The sample was subsequently extracted three times with 1 ml DIPE. Each time, the upper layer was collected and the combined DIPE fractions were subsequently vaporized under a nitrogen stream. The residues were dissolved in 100  $\mu$ l methanol and analyzed by UPLC.

The metabolite concentrations were quantified by UPLC and used to calculate the rate of the enzymatic conversion in pmol/min/mg microsomal protein. The kinetic parameters  $K_M$  and  $V_{\max}$



were obtained using a nonlinear regression (curve fit) applying the Michaelis Menten equation in GraphPad Prism 5 (San Diego, USA). The intrinsic clearance ( $Cl_{int}$ ) was calculated as  $V_{max}$  divided by  $K_M$  and used to compare the metabolic efficiency for formation of the different metabolites.

### 2.3 UPLC analysis

The metabolites formed were analyzed and quantified using an Acquity UPLC system equipped with a photodiode array (PDA) detector (Waters, Milford, MA). The metabolites and their parent compound were separated on a reverse phase Acquity UPLC® BEH C18 column (21 × 50 mm, 1.7µm, Waters, Milford, MA) and detected at a wavelength ranging from 190 nm to 400 nm. Eluent A was nano-pure water containing 0.1% trifluoroacetic acid (v/v), and eluent B was acetonitrile containing 0.1% trifluoroacetic acid (v/v). The gradient elution started from 90% A and 10% B applied from 0.0 min to 0.5 min, which was changed to 10% A and 90% B from 0.5 to 15.5 min and then kept at 10% A and 90% B from 15.5 min to 18.5 min, changed back to 90% A and 10% B from 18.51 to 22min. The total run time was 22 min using a flow rate of 0.6 ml/min. The temperature of the column was set at 40°C and the autosampler at 10°C during the UPLC analysis. The injection volume was 3.5 µl. Metabolites were quantified using their peak area at the wavelength specified in **Table 2**, using calibration curves of available reference compounds. Metabolites were identified by comparing the retention time (RT) and absorption spectra to those of reference standard chemicals. The unknown minor metabolites were tentatively identified and categorized by considering elution time on UPLC and GC-MS/MS, mass spectra and available elution and spectral information from literature as described in the result section.

### 2.4 Bacterial reverse mutation (Ames) assay

The mutagenicity of B[a]P and four of its methylated analogues including 3-methyl-B[a]P, 6-methyl-B[a]P, 7-methyl-B[a]P and 8-methyl-B[a]P was assessed in the bacterial reverse mutation

(Ames) assay using *Salmonella typhimurium* strains TA98 and TA100. Six concentrations of each compound were tested in triplicate in the absence and presence of 5% (v/v) S9-mix obtained from the livers of Aroclor 1254 treated rats. The S9-mix contained 4 mM NADP, 5.8 mM glucose-6-phosphate, 0.1 M sodium phosphate pH 7.4, 8 mM MgCl<sub>2</sub>, 33 mM KCl and 5% S9 homogenate. Fresh bacterial cultures were prepared overnight to reach 10<sup>9</sup> cells/ml. Top agar was molten and heated at 45°C. The following solutions were incubated at 70 rpm at 37°C in a shaking water bath; either 0.5 ml S9-mix (in case of S9 presence) or 0.5 ml 0.1 M phosphate pH 7.4 (in case of S9 absence), mixed with 0.1 ml of a fresh bacterial culture (10<sup>9</sup> cells/ml) of TA98 or TA100, and 2.5 – 25 µg test compound per plate. After incubation, the solutions were added to 3 ml molten top agar and mixed with vortexing. The content of the top agar tube was poured onto a minimal glucose agar plate. After solidification of the top agar, the plates were incubated at 37°C for 48 hours. The number of revertant colonies per plate was automatically counted with the Instem Sorcerer Colony Counter (Staffordshire, UK). In the absence of S9-mix, NF (10µg/plate) and MMS (650µg/plate) were tested as positive controls for incubations with TA98 and TA100, respectively. In the presence of S9-mix, 2AA (1 µg/plate and 5 µg/plate) was tested as a positive control in both TA98 and TA100. DMSO was tested as a solvent control in both tester strains. The results are considered biologically relevant for mutagenic potential when the induced increases in the number of revertant colonies are above the historical control database and more than 3-fold or 2-fold for tester strains TA98 and TA100, respectively <sup>31</sup>.

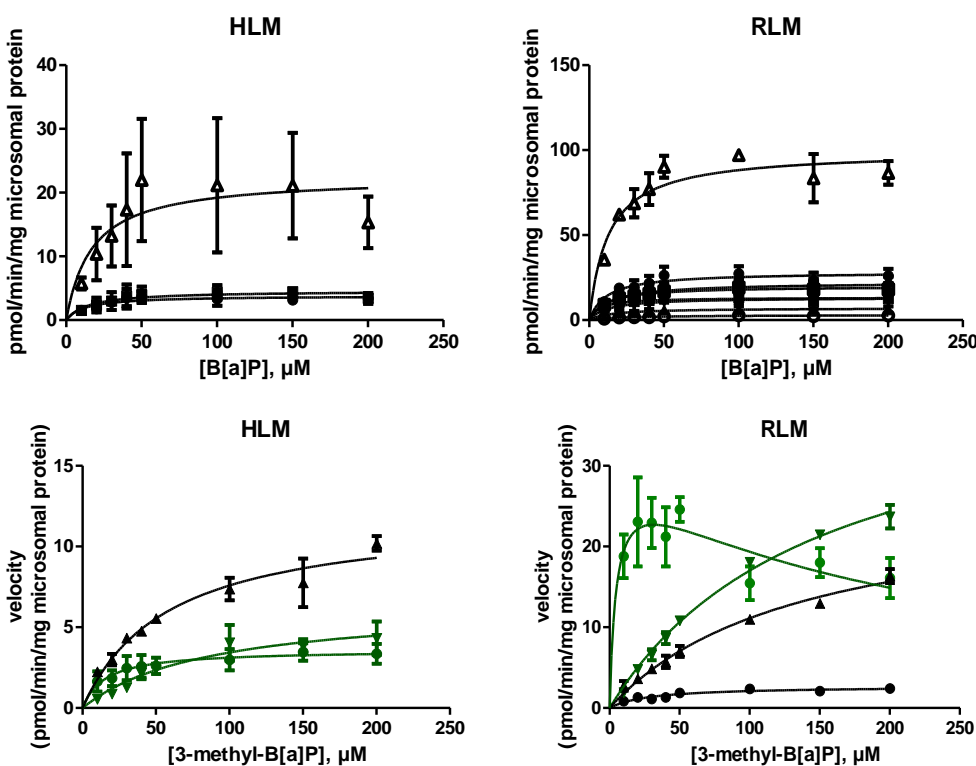
To obtain insight in the nature of the metabolites generated, additional incubations with the S9 mix were performed and analyzed as described above for the microsomal incubations. These S9 incubations had the same composition as the mixture that the bacteria were exposed to in the Ames test, and consisted of 150 µM (20 µg) test compound, 500 µl S9-mix (in the presence of metabolic activation) or 0.1 M sodium phosphate (pH 7.4) (in the absence of metabolic activation). The

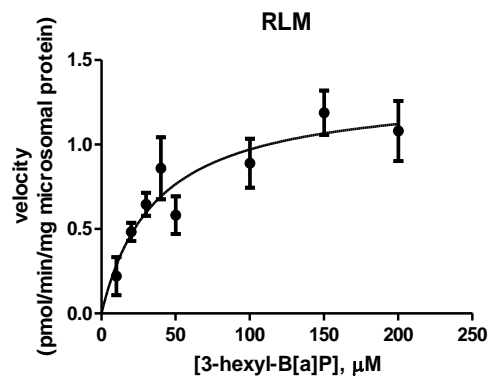
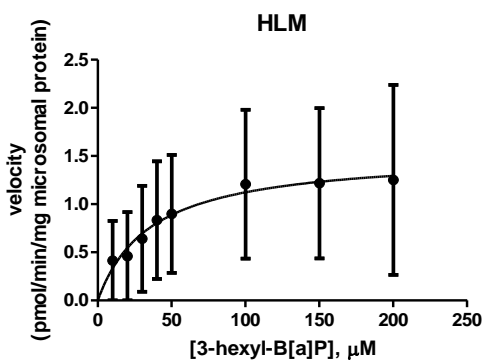
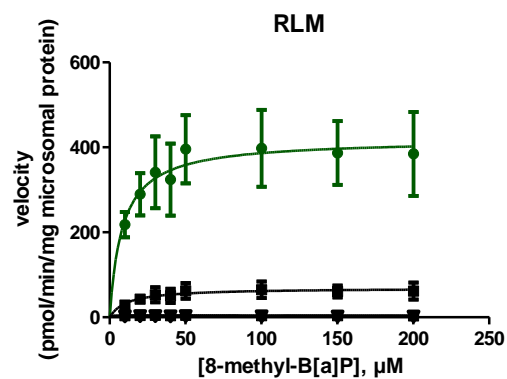
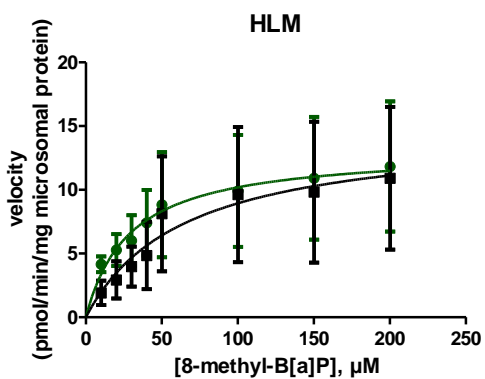
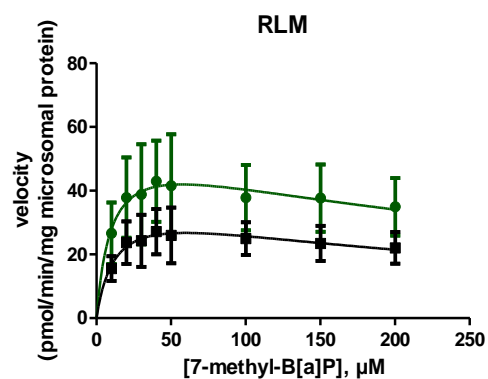
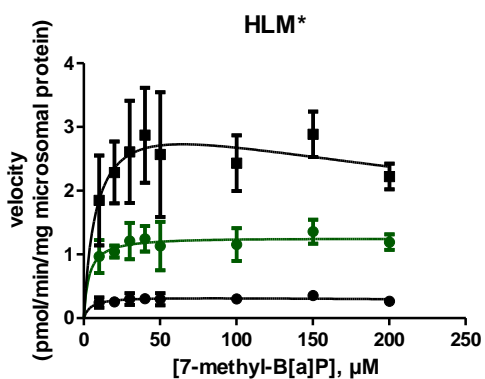
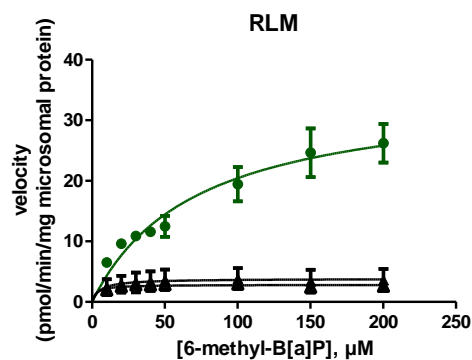
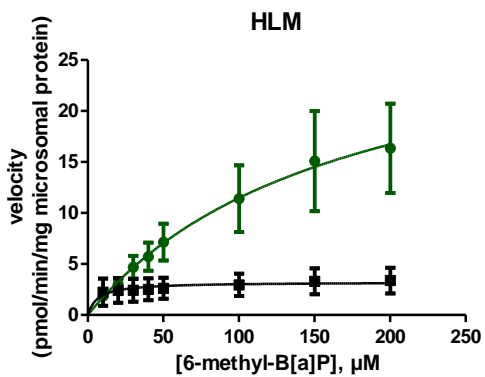
mixture was incubated at 37°C for 48 hours and subsequently treated and analyzed for metabolites formed as described above in section 2.2 and 2.3 for the microsomal incubations.

### 3. Results

#### 3.1 Microsomal metabolism of B[a]P and its alkylated analogues

The kinetics of substrate concentration dependent metabolism mediated by hepatic P450 enzymes of human and rat are shown in **Figure 3**. The results obtained reveal that most of the metabolite formations followed Michaelis Menten type saturation kinetics, in some cases substrate inhibition was observed at higher concentrations. By fitting the data to the Michaelis Menten equation, the kinetic parameters including  $K_M$ ,  $V_{max}$  and  $Cl_{int}$  for formation of each metabolite were obtained and are presented in **Table 2**.





**Figure 3.** Substrate concentration dependent metabolite formation of B[a]P and its alkyl substituted analogues by HLM and RLM. Black curves represent formation of metabolites resulting from aromatic ring oxidation and green curves present formation of metabolites from alkyl side chain oxidation. Each symbol represents experimental means and vertical bars are standard errors of the mean (n=3).

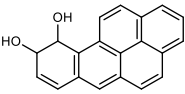
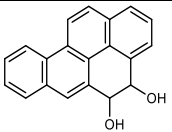
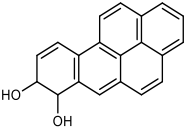
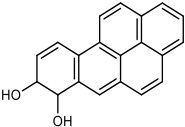
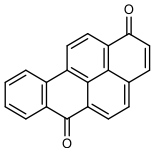
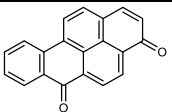
Note:

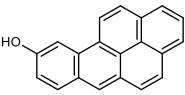
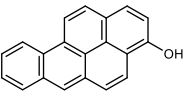
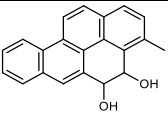
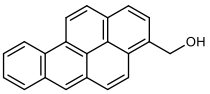
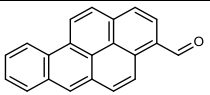
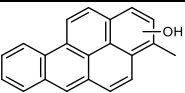
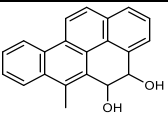
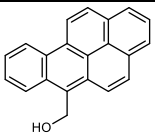
The Y-axis varies between the presented figures.

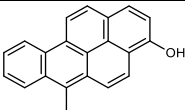
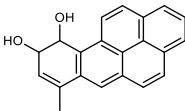
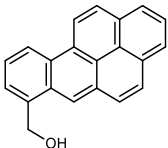
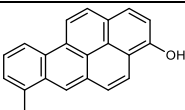
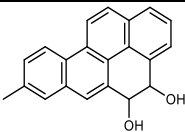
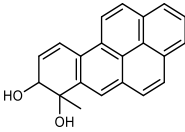
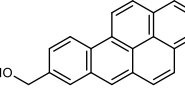
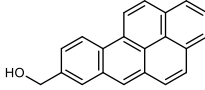
\* The figure of 7-methyl-B[a]P by HLM was obtained following 5h instead of 30min incubation.

For the metabolites showing substrate inhibition, the  $K_M$  and  $V_{max}$  of in Table 2 were obtained from Michaelis Menten fitting approach with exclusion of the concentrations that showed inhibition effect.

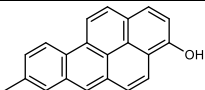
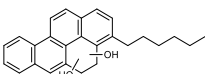
**Table 2.** The metabolite profile and corresponding Michaelis Menten parameters including  $K_M$ ,  $V_{max}$  and  $C_{lint}$  that was calculated as  $V_{max}/K_M$ . The results are shown as mean $\pm$  standard error from three independent experiments. Abbreviations: RT=retention time;  $\lambda$  = wavelength of maximum UV absorbance of the compound; ND = not detected; NM =no metabolism.

Metabolites	Structure	Species	$K_M$ ( $\mu$ M)	$V_{max}$ (pmol/min/mg microsomal protein)	$C_{lint}$ ( $V_{max}/K_M$ ) $\mu$ l/min/mg protein
<b>B[a]P RT=10.66min, <math>\lambda</math>=296.4nm</b>					
9,10-dihydro-B[a]P-diol RT=4.65min, $\lambda$ =278.6nm;		HLM	12.2 $\pm$ 8.5	3.8 $\pm$ 0.6	0.2
		RLM	11.9 $\pm$ 5.5	28.3 $\pm$ 2.8	2.4
4,5-dihydro-B[a]P-diol RT=5.69min, $\lambda$ =273.1nm		HLM	15.0 $\pm$ 11.8	4.6 $\pm$ 0.9	0.2
		RLM	6.5 $\pm$ 4.5	13.3 $\pm$ 1.4	2.0
7,8-dihydro-B[a]P-diol RT=5.79min, $\lambda$ =296.4nm		HLM	ND	ND	-
		RLM	14.6 $\pm$ 9.8	7.0 $\pm$ 1.1	0.5
7,8-dihydro-B[a]P-diol RT=5.90min, $\lambda$ =367.4nm;		HLM	ND	ND	-
		RLM	12.6 $\pm$ 10.7	13.3 $\pm$ 2.5	1.1
B[a]P-1,6-quinone RT=6.64min, $\lambda$ =219.4nm;		HLM	ND	ND	-
		RLM	14.8 $\pm$ 8.8	22.2 $\pm$ 3.2	1.5
B[a]P-3,6-quinone RT=7.19min, $\lambda$ =223.7nm;		HLM	ND	ND	-
		RLM	24.0 $\pm$ 14.4	3.0 $\pm$ 0.5	0.1

9-hydroxy-B[a]P RT=8.22min, $\lambda$ =267.6nm;		HLM	ND	ND	-
		RLM	11.4±5.2	20.0±1.9	1.8
3-hydroxy-B[a]P RT=8.51min, $\lambda$ =258.4nm;		HLM	26.4±25.9	27.0±9.1	1.0
		RLM	12.7±3.5	99.5±6.1	7.8
<b>3-methyl-B[a]P RT=11.45min, <math>\lambda</math>=301.9nm</b>					
4,5-dihydro-3-methyl-B[a]P-diol RT=4.74min, $\lambda$ =273.7nm;		HLM	ND	ND	-
		RLM	28.8±5.9	2.7±0.2	0.1
3-hydroxymethyl-B[a]P RT=7.83min, $\lambda$ =301.3nm;		HLM	15.4±7.9	3.6±0.5	0.2
		RLM	2.9±3.3	25.0±3.4	8.6
3-B[a]P-carbaldehyde RT=7.98min, $\lambda$ =226.1nm;		HLM	87.0±38.1	6.4±1.3	0.1
		RLM	149.3±19.4	42.4±3.1	0.3
Hydroxy-3-methyl-B[a]P RT=9.24min, $\lambda$ =256.6nm;		HLM	58.3±12.8	12.0±1.1	0.2
		RLM	137.4±23.0	26.4±2.4	0.2
<b>6-methyl-B[a]P RT=11.35min, <math>\lambda</math>=300nm</b>					
4,5-dihydro-6-methyl-B[a]P-diol RT=4.81min, $\lambda$ =273.1nm		HLM	ND	ND	-
		RLM	2.8±1.8	2.8±0.2	1
6-hydroxymethyl-B[a]P RT=7.68min, $\lambda$ =299.4nm		HLM	168.8±117	30.8±12.4	0.2
		RLM	71.2±19.7	35.0±4.2	0.5
3-hydroxy-6-methyl-B[a]P		HLM	6.6±8.8	3.2±0.7	0.5

RT=9.28min, $\lambda$ =264.5nm		RLM	5.4±9.1	3.8±0.9	0.7
7-methyl-B[a]P RT=11.34min, $\lambda$ =298.2nm					
9,10-dihydro-7-methyl-B[a]P-diol		HLM*	3.0±3.7	0.3±0.0	0.1
RT=5.1min, $\lambda$ =276.7nm		RLM	ND	ND	-
7-hydroxymethyl-B[a]P		HLM*	3.2±3.1	1.3±0.1	0.4
RT=7.8min, $\lambda$ =297.6nm		RLM	7.9±12.0	49.9±18.0	6.3
3-hydroxy-7-methyl-B[a]P		HLM*	3.4±4.1	2.7±0.3	0.8
RT=9.15min, $\lambda$ =268.2nm		RLM	3.4±11.5	32.3±10.4	9.5
8-methyl-B[a]P RT=11.53min, $\lambda$ =297.6nm					
4,5-dihydro-8-methyl-B[a]P-diol		HLM	ND	ND	-
RT=4.07min, $\lambda$ =274.9nm;		RLM	3.3±7.3	3.1±0.7	0.9
7,8-dihydro-8-methyl-B[a]P-diol		HLM	ND	ND	-
RT=5.56min, $\lambda$ =259nm;		RLM	2.9±5.1	5.2±1.4	1.8
7,8-dihydro-8-methyl-B[a]P-diol		HLM	ND	ND	-
RT=5.62min, $\lambda$ =259nm;		RLM	4.8±6.5	3.4±1.1	0.7
8-hydroxymethyl-B[a]P		HLM	29.1±23.3	13.2±3.3	0.5
RT=7.87min, $\lambda$ =298.2nm;		RLM	8.4±5.2	418.8±47.2	49.9



3-hydroxy-8-methyl-B[a]P		HLM	64.7±66.5	14.7±6.4	0.2
RT=9.33min, λ=258.4nm;		RLM	11.6±8.4	68.8±10.7	5.9
3-n-hexyl-B[a]P RT=14.25min, λ=302.5nm					
Dihydro-3-n-hexyl-B[a]P-diol		HLM	36.0±49.4	1.5±0.7	0.04
RT=4.70min, 247.4nm		RLM	36.7±13.1	1.3±0.2	0.04
3-dodecyl-B[a]P RT=17.45min, λ=301.9nm					
NM	-	HLM	-	-	-
NM		RLM	-	-	-

\* the data of marked HLM with 7-methyl-B[a]P was obtained following 5h incubation

The metabolites formed upon rat microsomal metabolism of B[a]P were identified and characterized in our recently published paper<sup>18</sup>. Compared to RLM, a lower number of metabolites appeared to be formed following metabolism mediated by P450 enzymes from HLM. In HLM, two dihydrodiols and a phenolic metabolite were identified as 9,10-dihydro-B[a]P-diol, 4,5-dihydro-B[a]P-diol and 3-hydroxy-B[a]P eluting at 4.65 min, 5.69 min, and 8.51 min, respectively. 7,8-Dihydro-B[a]P-diol, quinones and 9-hydroxy-B[a]P that were formed in RLM incubations were not detected in the microsomal incubation of B[a]P with HLM. Methyl substitution of B[a]P generally shifted the oxidative metabolism to the methyl side chain in incubations with both HLM and RLM. Besides the formation of dihydrodiols and phenols, side chain alcohol metabolites become the most abundant metabolites in incubations of the methyl substituted B[a]Ps with RLM but not necessarily with HLM (**Figure 3, Table 2**).

The primary metabolite, eluting at 7.68 min, that was formed in incubations of 6-methyl-B[a]P with both HLM and RLM, was characterized as 6-hydroxymethyl-B[a]P by co-elution and the same UV spectrum as that of the synthesized reference chemical. A phenolic metabolite was detected at a retention time of 9.59 min and identified as 3-hydroxy-6-methyl-B[a]P based on a similar UV spectrum as 3-hydroxy-B[a]P and 3-hydroxy-8-methyl-B[a]P. 4,5-Dihydro-6-methyl-B[a]P-diol, eluting at 4.81 min, was identified as the only dihydrodiol formed in the incubations of 6-methyl-B[a]P with RLM based on the reported spectrum of a synthetic reference standard<sup>15</sup>. No dihydrodiols of 6-methyl-B[a]P were formed in the incubation with HLM.

7-Methyl-B[a]P was metabolized to 7-hydroxymethyl-B[a]P and 3-hydroxy-7-methyl-B[a]P; both metabolites could be identified based on similarity of their reported elution and UV spectra to 7-hydroxymethyl-B[a]P and 3-hydroxy-7-methyl-B[a]P<sup>11</sup>. 7-Methyl-B[a]P was not metabolized by HLM after 30 min incubation. Upon prolonged 5 hour incubation with HLM, besides 7-hydroxymethyl-B[a]P and 3-hydroxy-7-methyl-B[a]P, an additional metabolite was detected at a

retention time of 5.1 min, which was identified as 9,10-dihydro-7-methyl-B[a]P-diol based on the spectral similarity to 9,10-dihydro-B[a]P-diol and the reported UV spectrum of 9,10-dihydro-7-methyl-B[a]P-diol <sup>11</sup>.

In RLM incubations of 8-methyl-B[a]P, three dihydrodiols eluting at 4.07 min, 5.56 min, and 5.62 min, respectively, were identified as 8-methyl-B[a]P-4,5-dihydrodiol and 8-methyl-B[a]P-7,8-dihydrodiols by comparison of their UV spectra to that of B[a]P-dihydrodiols and the reported UV spectra of 8-methyl-B[a]P-7,8-dihydrodiol <sup>32</sup>. No diols were formed in incubations of 8-methyl-B[a]P with HLM. The most abundant metabolite, eluting at 7.87 min, was identified as 8-hydroxymethyl-B[a]P. The metabolite formed in both RLM and HLM with a retention time of 9.33 min was characterized as 3-hydroxy-8-methyl-b[a]P based on comparison of its elution time and UV spectrum to the synthesized reference chemical.

Metabolite identification of 3-methyl-B[a]P was based on the comparison of retention time and UV spectrum of the metabolites to those of other methyl substituted B[a]Ps. The metabolite eluting at 4.74 min was identified tentatively as 3-methyl-B[a]P-4,5-dihydrodiol based on its UV spectrum similarity to the spectrum of 4,5-dihydrodiol-B[a]P. The metabolite at a retention time of 7.81 min was identified as 3-hydroxymethyl-B[a]P based on the effect of the hydroxylation on the retention time and UV spectrum, that was comparable to the effect of hydroxylation on the retention time and UV spectrum observed for 6-hydroxymethyl-B[a]P as compared to 6-methyl-B[a]P. The metabolite eluting at 7.95 min was tentatively identified as 3-B[a]P-carbaldehyde next to 3-hydroxymethyl-B[a]P based on the elution pattern of 1-naphthylmethylketone that was reported to elute close to 1-(1-hydroxyethyl)-naphthalene <sup>10</sup>.

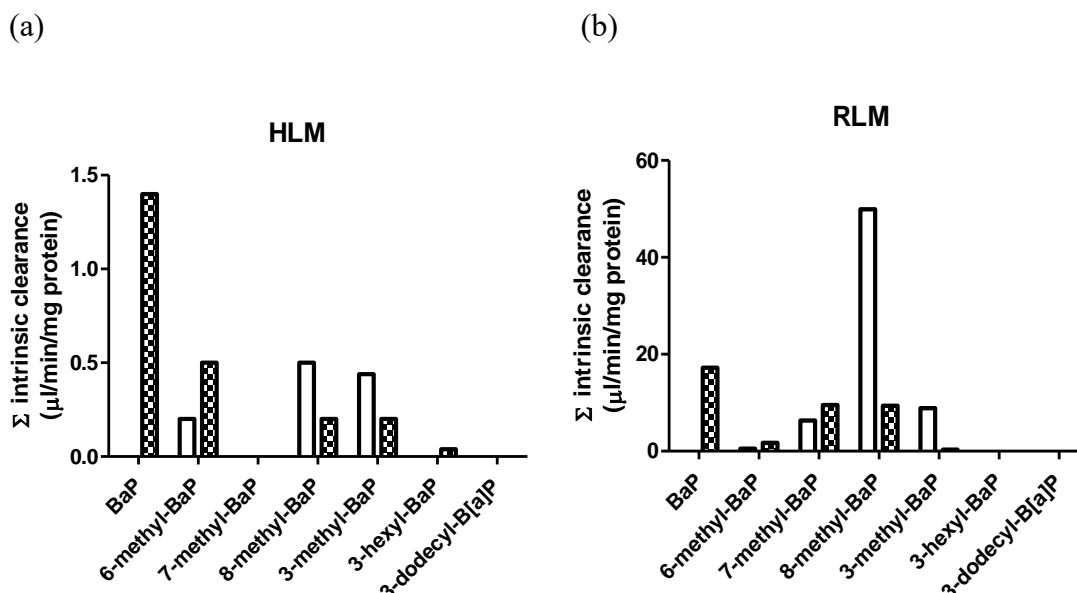
In the incubation of 3-n-hexyl-B[a]P with HLM and RLM, a common metabolite was formed eluting at 4.70 min that was tentatively identified as a dihydrodiol of 3-n-hexyl-B[a]P for eluting in the dihydrodiol region. This dihydrodiol metabolite is possibly the 4,5-dihydrodiol of 3-n-hexyl-


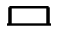
B[a]P based on the similarity of its UV spectrum to the spectrum of 4,5-dihydro-3-methyl-B[a]P-diol. 3-N-dodecyl-B[a]P was metabolized by neither HLM nor RLM under the experimental conditions applied.

### **3.2 Intrinsic clearance via side chain oxidation versus aromatic ring oxidation for B[a]P and alkyl substituted B[a]Ps**

The intrinsic clearance of B[a]P and its alkylated analogues via the different metabolites was summed up based on whether the metabolite formation represents side chain or aromatic oxidation of the tested model compounds (**Figure 4**). Generally, methyl substitution of B[a]P shifted the metabolism to methyl side chain oxidation at the cost of aromatic ring oxidation. In incubations with HLM the intrinsic clearance of aromatic ring oxidation of alkylated B[a]Ps was 2.8- to 7- fold lower compared to the that of B[a]P itself, except for 7-methyl-B[a]P for which the overall conversion by HLM within the 30 minutes incubation appeared not to result in detectable metabolite formation. The intrinsic clearance of 3-methyl- and 8-methyl- B[a]P via side chain oxidation was 2.2- to 2.5- fold higher than that via aromatic ring oxidation, except for the metabolism of 6-methyl-B[a]P via side chain oxidation which was 2.5-fold lower than that via aromatic ring oxidation. In incubations with RLM, the intrinsic clearance via aromatic ring oxidation of the methyl substituted B[a]Ps was 1.8- to 57.0- fold lower than what was observed for B[a]P itself. Side chain oxidation of 3-methyl-B[a]P and 8-methyl-B[a]P becomes the dominant pathway 29.7- and 5.3- fold higher than that observed for aromatic ring oxidation with respect to the intrinsic clearance. However, for 6-methyl- and 7-methyl-B[a]P in incubations with RLM aromatic ring oxidation was 3.4- fold and 1.5- fold higher than the side chain oxidation. 1-n-Hexyl-B[a]P was oxidized via only aromatic ring oxidation with the intrinsic clearances via aromatic ring

oxidation being were 35.0- and 430.0- fold lower than for B[a]P itself with HLM and RLM respectively.

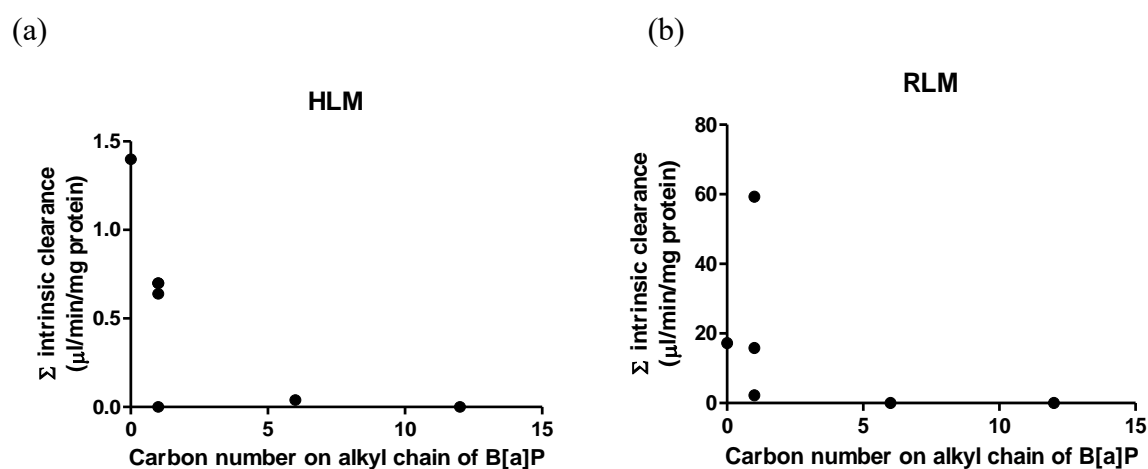


**Figure 4.** Intrinsic clearance via aromatic ring oxidation versus alkyl side chain oxidation mediated by (a) HLM and (b) RLM for B[a]P and its alkylated analogues.  Aromatic ring oxidation;  alkyl chain oxidation. Note: the Y-axis varies between the presented figures.

### 3.3 Overall intrinsic clearance of B[a]P and its alkyl substituted analogues via cytochrome P450 mediated metabolism

The overall efficiency of the liver microsomal metabolism of B[a]Ps, calculated as the sum of side chain and aromatic oxidation, appeared to depend on the species, the position of the alkyl substitution and the length of the alkyl chain. This total intrinsic clearance of B[a]P and its alkylated analogues was calculated and summarized in **Figure 5**. The intrinsic clearance of naked B[a]P metabolism by RLM was 12.3- fold higher than that observed for HLM. For the series of methylated B[a]P substrates liver microsomal metabolism by RLM was 3.1- to 84.7- fold more efficient than that observed for HLM, with the difference being greatest for 8-methyl-B[a]P. With the exception of 8-methyl-B[a]P that was metabolized 3.4- fold faster than its naked analogue by

RLM, for all other alkylated B[a]P model compounds tested metabolism was substantially less, being 1.1- to 430.0- fold lower, than what was observed for B[a]P itself. For HLM mediated metabolism, besides that 7-methyl-B[a]P was not metabolized to a detectable extent, other alkyl substituted B[a]P with alkyl chains up to and including 6 carbon atoms, were metabolized 2.0- to 35.0- fold slower than non-substituted B[a]P. By extending the incubation time to 5 hours, 7-methyl-B[a]P was metabolized with an overall intrinsic clearance of 1.3  $\mu\text{l}/\text{min}/\text{mg}$  protein by HLM. The alkyl chain length also appeared to play a role in the overall clearance via cytochrome P450 mediated conversion, since no conversion of 3-n-dodecyl-B[a]P was detected even after 5 hour incubation, neither with HLM nor with RLM.

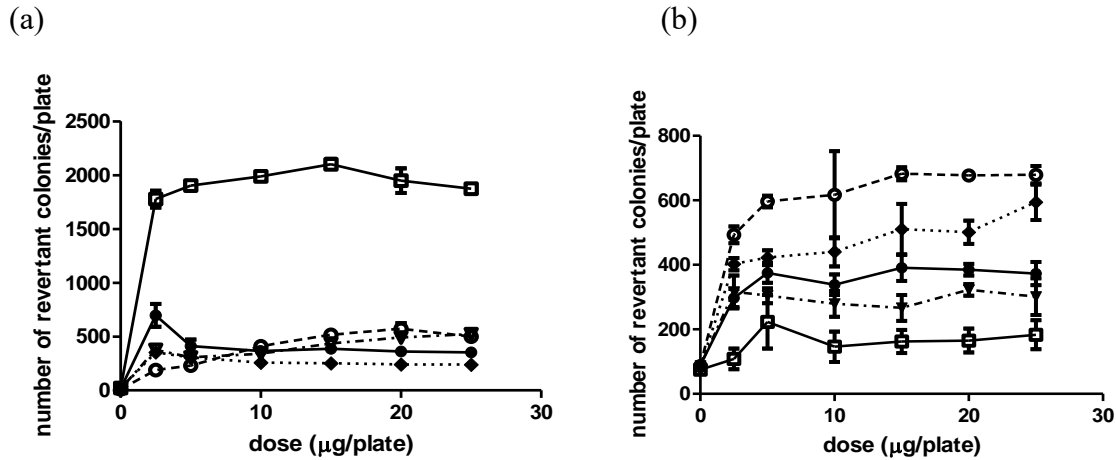


**Figure 5.** Overall intrinsic clearance of alkyl-substituted B[a]Ps in metabolism with (a) HLM (b) RLM based on the number of carbon atoms in the alkyl side chain. Note: the Y-axis varies between the presented figures.

### 3.4 Mutagenicity of B[a]P and its methyl-substituted analogues

At the tested doses of the methyl-substituted B[a]Ps and B[a]P itself, no precipitation of the compounds was observed in the Ames test. Cytotoxicity and abnormal bacterial background lawn were also not observed for all tested compounds. The dose response curves of each test compound are depicted with doses ( $\mu\text{g}/\text{plate}$ ) against observed number of revertants ( $\text{His}^+$ ) in TA98 and TA100

in the presence of S9 metabolic activation in **Figure 6a** and **Figure 6b**, respectively. The mutagenic efficacy (fold induction), calculated from the maximum increase in the number of revertants divided by the number of revertants for the solvent control, was used to judge the mutagenicity of the test compound based on the 3- fold and 2- fold criteria for TA98 and TA 100, respectively. It is concluded that B[a]P and its four methyl substituted analogues tested positive in the presence of S9 metabolic activation in both tester strains (**Table 3**). Mutagenic potency (revertants/nmol), as the maximum value of the calculated values from the net increase of the number of revertants divided by dose of each tested model compound towards tester strains TA98 and TA100 is presented in Table 3, and was used to assess the mutagenic potential of the test compounds. The observed effect of methyl substitution of B[a]P on its mutagenic potency follows the order: 6-methyl-B[a]P > B[a]P > 8-methyl-B[a]P = 7-methyl-B[a]P > 3-methyl-B[a]P towards tester strain TA98; and 3-methyl-B[a]P > 8-methyl-B[a]P > 7-methyl-B[a]P > B[a]P > 6-methyl-B[a]P towards tester strain TA100 (**Table 3**). The observed results suggests that the effect of monomethyl substitution on the mutagenic potency of B[a]P depends on the position of the substitution and the tester strain used, and not necessarily on the number of “fake” bay regions.



**Figure 6.** Number of revertants in *S. typhimurium* (a) TA98 (b) TA100 on exposure to (—●—) B[a]P, (---○---) 3-methyl-B[a]P, (—■—) 6-methyl-B[a]P, (---□---) 7-methyl-B[a]P and (····◆····) 8-methyl-B[a]P in the presence of 5% S9-mix. Each symbol represents a mean and vertical bars are the standard deviations of the mean (n=3). The mean number of revertant colonies per plate (n=15) of solvent control was  $15 \pm 5$  and  $12 \pm 4$  with and without S9-mix in tester strain TA98, respectively. 1  $\mu\text{g}/\text{plate}$  2AA with S9-mix and 10  $\mu\text{g}/\text{plate}$  NF without S9-mix that were tested as positive controls towards tester strain TA98 resulted in  $532 \pm 59$  and  $1343 \pm 117$  revertants per plate, respectively. The mean number of revertant colonies per plate (n=15) of solvent control was  $84 \pm 8$  and  $111 \pm 7$  with and without S9-mix in tester strain TA100, respectively. 5  $\mu\text{g}/\text{plate}$  2AA with S9-mix and 650  $\mu\text{g}/\text{plate}$  MMS without S9-mix that were tested as positive controls towards tester strain TA100 resulted in  $1368 \pm 168$  and  $653 \pm 67$  revertants per plate, respectively.



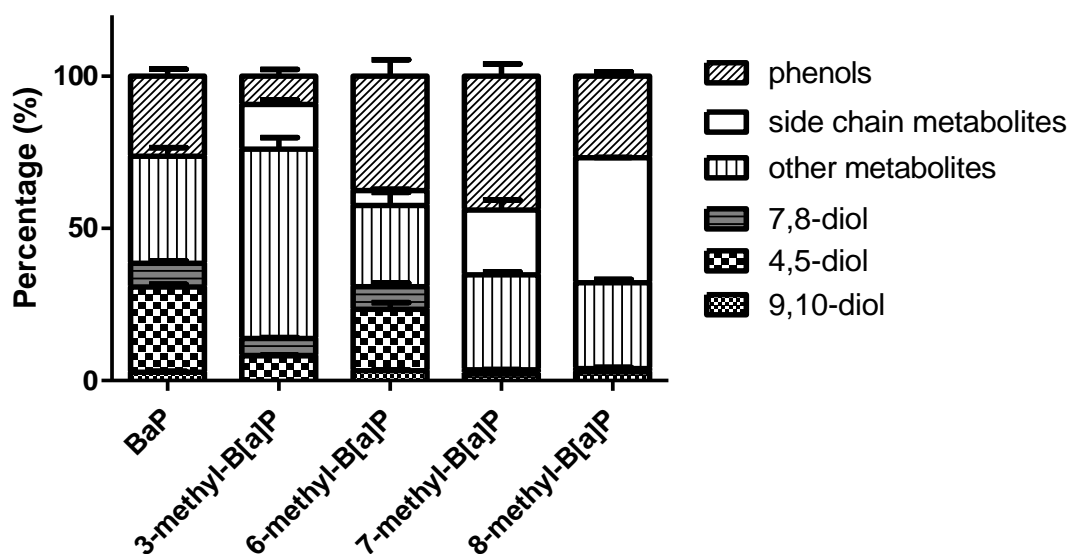
**Table 3.** Mutagenicity of benzo[a]pyrene and its monomethyl substituted analogues in the Ames test with *S. typhimurium* TA98 and TA100 in the presence of Aroclor 1254 induced rat liver S9 and NADPH-generating system. Mutagenic efficacy of each compound was calculated as the fold induction from the maximum increase in the number of revertants through dividing by the number of revertants in the solvent controls. Mutagenic potency of each compound was the maximum value of the calculated values from the net increase in number of revertants divided by the dose, expressed as revertants per nmol.

Compound	<i>S. typhimurium</i> strain			
	TA98		TA100	
	Mutagenic efficacy	Mutagenic potency	Mutagenic efficacy	Mutagenic potency
<b>B[a]P</b>	44	69	4.9	21
<b>3-methyl-B[a]P</b>	57	19	7.9	43
<b>6-methyl-B[a]P</b>	100	187	3	8
<b>7-methyl-B[a]P</b>	40	39	3.7	24
<b>8-methyl-B[a]P</b>	24	39	7.2	34

### 3.5 Liver S9 mediated metabolism of B[a]P and methyl substituted B[a]Ps

Given that in the Ames test an S9 metabolic activation system was used, the metabolite profiles of B[a]P and its methylated analogues that were tested in the Ames test were also characterized upon incubations that matched the incubation conditions of the Ames test. The chromatograms presenting the metabolic profiles of the test compounds following incubation for 48 hours with liver S9-mix used in the Ames test are presented in **Figure S1** (supplementary material). In line with the metabolites formed in the microsomal incubations, also in the incubation of B[a]P with S9-mix, dihydrodiols, quiones and phenols were formed as primary metabolites. In the S9 incubations, the metabolism of monomethyl substituted B[a]Ps again generally shifted to side chain oxidation with other metabolites including dihydrodiols, quinones and phenols being formed to a

lower extent. The concentration of especially three types of dihydrodiol metabolites formed in the S9 incubations of B[a]P and its monomethylated analogues (substrate concentration 150  $\mu$ M that is equivalent to the dose of 20  $\mu$ g in Ames test) was quantified and is presented in **Figure 7**. The total concentration of the formed metabolites varies between the methylated analogues (**Figure S2** in supplementary material). The total concentration of the formed metabolites in the S9 incubation of B[a]P was  $14.2 \pm 6.6$   $\mu$ M which was 2.4- fold, 3.7- fold, and 2.5- fold higher than the total metabolite formation for 3-methyl-, 6-methyl- and 7-methyl-B[a]P, respectively, while being 1.4- fold lower than that of 8-methyl-B[a]P (**Figure S2**). Formation of 4,5-dihydrodiol was found to be abundant in S9 incubations of B[a]P, 3-methyl- and 6-methyl-B[a]P at levels amounting to 28%, 8% and 20% of the total metabolite formation while only 0.3% and 1.1% of 4,5-dihydrodiol was found in the S9 incubations of 7-methyl- and 8-methyl-B[a]P. In the S9 incubations, 7,8-dihydrodiol metabolites were formed at levels amounting to 7.8%, 5.8%, 7.4%, 1.0% and 0% of the total formation of metabolites for B[a]P, 3-methyl-, 6-methyl-, 7-methyl- and 8-methyl-B[a]P, respectively. Formation of 9,10-dihydrodiol in the S9 incubations was on average 2.2 to 3.0 % of the total metabolite formation for B[a]P and its monomethylated analogues, except for the fact that 9,10-dihydrodiol was not formed from 3-methyl-B[a]P.



**Figure 7.** Percentage (%) of a metabolite compared to the total amount of metabolites formed in liver S9 incubations with B[a]P or four of its methylated analogues, calculated as the concentration of the respective metabolite divided by the total amount of metabolites. Each bar represents experimental means and vertical bars are standard errors of the mean (n=3). The absolute concentration ( $\mu\text{M}$ ) of the metabolites of each test compound is presented in **Figure S2** (supplementary materials).

#### 4. Discussion

The emerging concern of consumption of polycyclic aromatics, that are detectable as MOAH, via food, pharmaceuticals and cosmetics relates mainly to 3- to 7-ring PAHs with no or simple alkylation, which can possibly induce genotoxicity and carcinogenicity. So far, especially metabolism and genotoxicity of unsubstituted PAHs like B[a]P were studied, while the effect of alkylation of PAHs on their mutagenic and carcinogenic potential and relevant bioactivation pathways is far less characterized. This study investigated the effect of alkyl substitution on the in

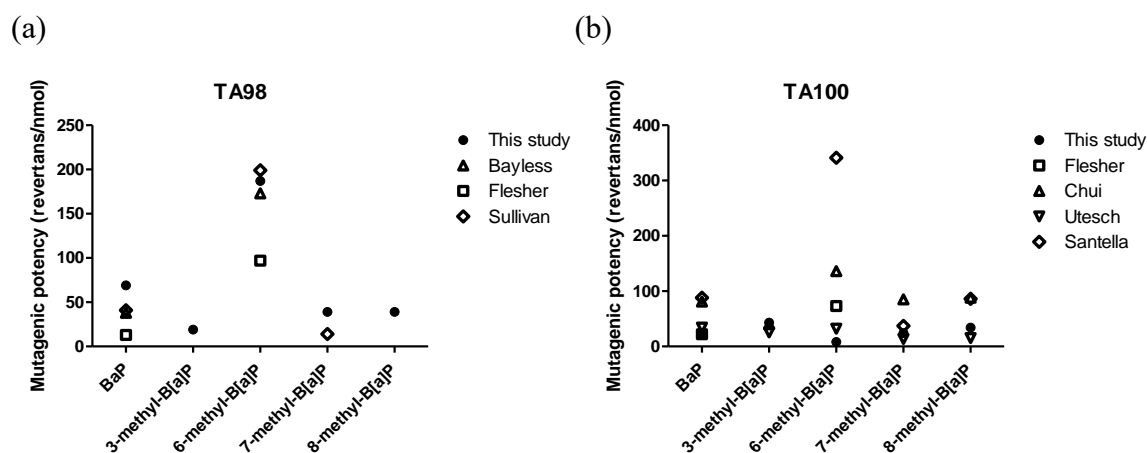
vitro metabolism and genotoxicity of B[a]P. The results obtained provide support for the hypothesis that alkylation of B[a]P shifts oxidative metabolism mediated by P450 enzymes to alkyl side chain oxidation at the cost of aromatic ring oxidation. This was the case in incubations with both HLM and RLM. A similar shift in favor of side chain oxidation at the cost of aromatic ring oxidation was previously observed for naphthalene and phenanthrene and their alkylated analogues <sup>10, 33</sup>. As genotoxicity and carcinogenicity of B[a]P, and possibly also its developmental toxicity, are considered to require metabolic activation to aromatic ring oxidative metabolites <sup>8, 18, 34</sup>, the observed metabolic shift to side chain oxidation at the cost of aromatic ring oxidation may point at lower chances of bioactivation. The results also elucidated that with an increase of the alkyl chain length, on the extent of metabolism, including metabolism via aromatic ring oxidation and thus bioactivation, was also substantially reduced. This was reflected by the limited overall metabolic efficiency for conversion of 3-n-hexyl-B[a]P that was 35- and 430- fold lower than that of B[a]P in incubations with HLM and RLM, respectively, and the fact that conversion of 3-n-dodecyl-B[a]P was not observed at all. These observations are also in line with the metabolic pattern that was observed for alkylated naphthalenes and phenanthrenes <sup>10, 33</sup>, and might be ascribed to steric hindrance hampering adequate binding of the alkylated PAHs to the active site of the cytochrome P450 isozymes involved. The observed limited metabolic conversion of 3-n-dodecyl-B[a]P seems in line with the negative mutagenic potential of a octadecyl substituted B[a]P derivative in the reverse mutation assay <sup>41</sup>.

It is also of interest that, in addition to these overall effects of alkyl substitution on the metabolic profiles of B[a]P and its methylated congeners, also some differences in metabolic profile were observed between incubations with HLM and RLM. Incubation of B[a]P and monomethylated B[a]Ps with RLM generated metabolites at higher catalytic efficiency and also generated more types of metabolites, including especially a higher level of dihydrodiols than what was observed in

incubations with HLM. Incubation of B[a]P with HLM did not generate dihydrodiol formation at all under the conditions applied. Assuming that some dihydrodiols may represent proximate mutagenic metabolites (**Figure 1**), the absence of their formation at detectable levels in incubations with HLM but not with RLM may reflect lower chances on bioactivation by HLM than RLM.

B[a]P and the selected monomethylated analogues tested positive for mutagenicity upon metabolic activation in the Ames test. The mutagenic potency (revertants/nmol) of B[a]P, 3-methyl-, 6-methyl-, 7-methyl- and 8-methyl-B[a]P towards both tester strains TA98 and TA100 is summarized across the present and historical studies in **Figure 8**<sup>14, 23-27</sup>. The overview thus obtained reveals that the methylated B[a]P analogues generally show a mutagenic potency that is within a factor of 3- fold similar to that of B[a]P with the exception of 6-methyl B[a]P, in which the substituent at C6 (meso position) introduces two “fake” bay regions, and which appeared to be more potent especially in tester strain TA98 that detects frameshift mutations, while in tester strain TA100 that detects base-pair substitutions, the results appear more variable.

All together, the mutagenic potencies of the tested monomethylated B[a]Ps observed in the present study appear to be in line with the values reported in the studies of Utesch et al.<sup>24</sup> and Flesher et al.<sup>26</sup>.

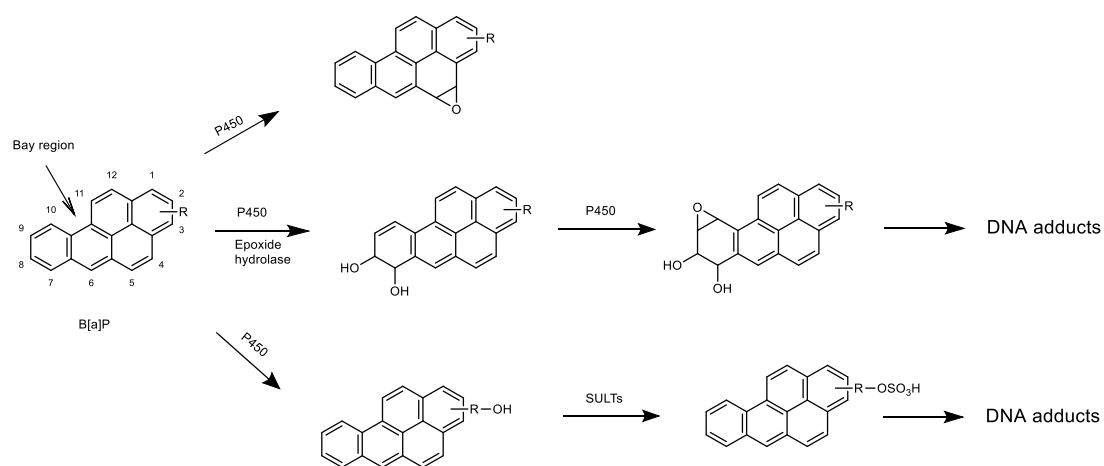


**Figure 8.** Mutagenic potential for B[a]P and four of its monomethyl substituted analogues towards (a) TA98 and (b) TA100 in the reverse mutation test obtained from of this study and literature. Each symbol represents the mutagenic potential of the corresponding compound expressed in revertants/nmol.

The dihydrodiol-epoxide pathway towards formation of the ultimate carcinogen 7,8-dihydrodiol-9,10-epoxide (**Figure 9**) may be associated also with the carcinogenicity of monomethylated B[a]P analogues. The present study showed that 7,8-dihydrodiol, the metabolite that precedes and thus reflects the chances on formation of the ultimate genotoxic metabolite 7,8-dihydrodiol-9,10-epoxide via the dihydrodiol-epoxide pathway, was detected at levels amounting to 7.8%, 5.8%, 7.4%, 1.0% and 0% of the total formation of metabolites for B[a]P, 3-methyl-, 6-methyl-, 7-methyl- and 8-methyl-B[a]P, respectively. Considering the metabolites that may contribute to the mutagenicity it is of interest to note that previous studies have shown that, when tested in the Ames test with *S. typhimurium* tester strains TA98 and TA100 in the presence of metabolic activation, 7,8-dihydro-B[a]P-diol and B[a]P-4,5-oxide were more mutagenic than B[a]P itself<sup>35, 36</sup>. It seems realistic to assume that the formation of 7,8-dihydrodiol and 4,5-oxide metabolites from the methylated B[a]P analogues (**Figure 9**) may also play a role in their mutagenicity in the Ames test. This observation is in line with the reported skin tumor initiating activity of B[a]P and 3-methyl-

B[a]P being potent, that of 6-methyl-B[a]P being weak, while 7-methyl- and 8-methyl-B[a]P, for which the results of the present study indicate formation of the 7,8-dihydrodiol and 4,5-oxide to be limited, appeared inactive in the mouse skin painting assay (**Table 1**)<sup>28</sup>. The observed formation of 7,8-dihydrodiol also indicates that the dihydrodiol-epoxide pathway may be especially relevant for B[a]P, 3-methyl- and 6-methyl B[a]P. For 1-methyl-, 6-methyl- and 7-methyl-B[a]P it was previously reported that their mutagenicity, as detected in the Ames test, remained unaffected by the addition of the epoxide hydrolase inhibitor trichloropropene oxide (TCPO), suggesting the role of the 7,8-dihydrodiol to be perhaps somewhat limited<sup>13, 27</sup>. Alternatively, 4,5-oxide metabolites of the monomethyl-B[a]Ps could possibly contribute to their in vitro mutagenicity because TCPO does not block the formation of epoxides. In the liver S9 incubations (**Figure 7**), the formation of 4,5-dihydrodiols ranged from 0.3% to 20% of the total metabolites formed for the four monomethylated B[a]P, reflecting that the formation of a 4,5-oxide metabolite can be substantial and may possibly contribute to the mutagenic potential observed in the Ames test. It is expected that the 4,5-oxide of the monomethyl substituted B[a]P may be quickly converted by epoxide hydrolase and/or excreted in the in vivo situation, preventing the in vitro mutagenicity to be displayed in vivo. Furthermore, 6-hydroxymethyl-B[a]P, formed as a side chain metabolite that appeared to be formed at a level amounting to 4.9% of the total metabolites of 6-methyl-B[a]P, showed equivalent or higher mutagenic potency compared to 6-methyl-B[a]P in both TA98 and TA100 upon S9 metabolic activation suggesting that formation of a mutagenic metabolite may even result from side chain oxidation<sup>27</sup>. It remains to be elucidated whether metabolites from side chain oxidation do play a role in the mutagenicity of other monomethylated B[a]P. The role of the meso-region side chain oxidation pathway was supported by in vivo studies. The methyl-substitution at the meso region of B[a]P, such as in 6-methyl-B[a]P, is suggested to result in methyl side chain oxidation to result in formation of 6-hydroxymethyl-B[a]P by cytochrome P450

enzymes in the present study. Subsequently, in vivo 6-hydroxymethyl-B[a]P could be conjugated by sulfotransferases to 6-[(sulfoxy)methyl]-B[a]P<sup>37</sup>. In vivo studies suggested that the sulfate ester of 6-hydroxymethyl-B[a]P forms DNA adducts and represents an ultimate genotoxic metabolite based on guanine and adenine adducts that were formed in rats and mice<sup>38, 39</sup>. It is also of interest that the tumorigenesis of monomethylated B[a]P may also relate to side chain oxidation as the benzylic ester of 6-hydroxymethyl-B[a]P was suggested to be the possible ultimate carcinogen in the in vivo mouse skin test<sup>40</sup>.



**Figure 9.** Possible metabolic pathways for genotoxicity of monomethyl-substituted B[a]P. R= CH<sub>3</sub> substitution.

The present study concludes that methyl substitution of B[a]P may alter its mutagenic potency, with the actual effect, a relatively limited increase or decrease in mutagenic potential as compared to B[a]P itself, depending on the substitution position and the tester strain used. Methylation of B[a]P shifts the metabolism to alkyl chain oxidation at the cost of aromatic ring oxidation, while elongation of the side chain reduces overall metabolism, the latter likely limiting metabolism and thus bioactivation via CYP 450 mediated reactions with alkyl chains of 6 or more carbon atoms. The relevant pathways for mutagenicity and carcinogenicity of the selected monomethyl



substituted B[a]P may involve the formation of a 7,8-dihydrodiol-9,10-epoxide, a 4,5-oxide and/or a side chain oxidative metabolite that is converted to an unstable and reactive sulfate conjugate. It is concluded that alkylation of B[a]P does not systematically reduce its mutagenicity in spite of the metabolic shift from aromatic to side chain oxidation.

## Reference

- (1) EFSA. (2012) Scientific Opinion on Mineral Oil Hydrocarbons in Food. *EFSA Journal* 10, 2704.
- (2) Grob, K. (2018) Mineral oil hydrocarbons in food: a review. *Food Addit Contam Part A Chem Anal Control Expo Risk Assess* 35, 1845-1860.
- (3) Pirow, R., Blume, A., Hellwig, N., Herzler, M., Huhse, B., Hutzler, C., Pfaff, K., Thierse, H. J., Tralau, T., Vieth, B., and Luch, A. (2019) Mineral oil in food, cosmetic products, and in products regulated by other legislations. *Crit Rev Toxicol* 49, 742-789.
- (4) D. Buijtenhuijs, B. M. v. d. V. (2019) Mineral oils in food; a review of occurrence and sources.
- (5) Mackerer, C. R., Griffis, L. C., Grabowski, J. S., Jr., and Reitman, F. A. (2003) Petroleum mineral oil refining and evaluation of cancer hazard. *Appl Occup Environ Hyg* 18, 890-901.
- (6) IARC. (2012) benzo[a]pyrene, In *Chemical Agents and Related Occupations* pp 111-138, International Agency for Research on Cancer, Lyon, France.

- (7) Jerina, D. M., Sayer, J. M., Thakker, D. R., Yagi, H., Levin, W., Wood, A. W., and Conney, A. H. (1980) Carcinogenicity of Polycyclic Aromatic Hydrocarbons: The Bay-Region Theory, pp 1-12, Springer Netherlands, Dordrecht.
- (8) Sims, P., Grover, P. L., Swaisland, A., Pal, K., and Hewer, A. (1974) Metabolic activation of benzo(a)pyrene proceeds by a diol-epoxide. *Nature* 252, 326-328.
- (9) Cheng, S. C., Hilton, B. D., Roman, J. M., and Dipple, A. (1989) DNA adducts from carcinogenic and noncarcinogenic enantiomers of benzo[a]pyrene dihydrodiol epoxide. *Chem Res Toxicol* 2, 334-340.
- (10) Wang, D., Bruyneel, B., Kamelia, L., Wesseling, S., Rietjens, I., and Boogaard, P. J. (2020) In vitro metabolism of naphthalene and its alkylated congeners by human and rat liver microsomes via alkyl side chain or aromatic oxidation. *Chem Biol Interact* 315, 108905.
- (11) Wong, T. K., Chiu, P. L., Fu, P. P., and Yang, S. K. (1981) Metabolic study of 7-methylbenzo[a]pyrene with rat liver microsomes: separation by reversed-phase and normal-phase high performance liquid chromatography and characterization of metabolites. *Chem Biol Interact* 36, 153-166.
- (12) Kinoshita, T., Konieczny, M., Santella, R., and Jeffrey, A. M. (1982) Metabolism and covalent binding to DNA of 7-methylbenzo(a)pyrene. *Cancer Res* 42, 4032-4038.
- (13) Peilu Chiu, T. K. W., Peter P. Fu, Shen K. Yang. (1982) 7-methylbenzo[a]pyrene and benzo[a]pyrene: comparative metabolic study and mutagenicity testing in Salmonella Typhimurium TA100, In *Polynuclear aromatic hydrocarbons: physical and biological chemistry* pp 183-191.

- (14) Sullivan, P. D., Ellis, L. E., Calle, L. M., and Ocasio, I. J. (1982) Chemical and enzymatic oxidation of alkylated benzo[a]pyrenes. *Chem-Biol Interact* 40, 177-191.
- (15) Hamernik, K. L., Chiu, Pei Lu, Chou, Ming W., Fu, Peter P., and Yang, Shen K. (1983) Metabolic activation of 6-methylbenzo[a]pyrene., In *Polynuclear Aromatic Hydrocarbons* (Cooke, M. D., Anthony J., Ed.).
- (16) Hamernik, K. L. (1984) The comparative study of the metabolism of 6-methylbenzo[a]pyrene and benzo[a]pyrene by rat liver microsomes, Uniformed Services University of the Health Sciences, Bethesda, Maryland.
- (17) Staretz, M. E., Murphy, S. E., Patten, C. J., Nunes, M. G., Koehl, W., Amin, S., Koenig, L. A., Guengerich, F. P., and Hecht, S. S. (1997) Comparative Metabolism of the Tobacco-Related Carcinogens Benzo[*a*]pyrene, 4-(Methylnitrosamino)-1-(3-pyridyl)-1-butanone, 4-(Methylnitrosamino)-1-(3-pyridyl)-1-butanol, and *N*'-Nitrosonornicotine in Human Hepatic Microsomes. *Drug Metabolism and Disposition* 25, 154-162.
- (18) Wang, D., Rietdijk, M. H., Kamelia, L., Boogaard, P. J., and Rietjens, I. (2021) Predicting the in vivo developmental toxicity of benzo[a]pyrene (BaP) in rats by an in vitro-in silico approach. *Arch Toxicol* 95, 3323-3340.
- (19) Sims, P. (1967) The metabolism of benzo[a]pyrene by rat-liver homogenates. *Biochem Pharmacol* 16, 613-618.
- (20) MacLeod, M. C., Levin, W., Conney, A. H., Lehr, R. E., Mansfield, B. K., Jerina, D. M., and Selkirk, J. K. (1980) Metabolism of benzo(e)pyrene by rat liver microsomal enzymes. *Carcinogenesis* 1, 165-173.

- (21) Selkirk, J. K., Croy, R. G., Whitlock, J. P., Jr., and Gelboin, H. V. (1975) In vitro metabolism of benzo(a)pyrene by human liver microsomes and lymphocytes. *Cancer Res* 35, 3651-3655.
- (22) Bickers D.R. , M. H., and Yang S.K. . (1982) Metabolism of benzo[a]pyrene by skin microsomes: comparative studies in C57BL/6N and DBA/2N mice and Sprague-Dawley rats, In *Polynuclear Aromatic Hydrocarbons: Physical and Biological Chemistry* pp 121-131.
- (23) Peilu Chui, S. K. Y. (1982) A structure-activity relationship study of monomethylbenzo[a]pyrenes by the use of Salmonella Typhimurium tester strain TA100 and by analysis of metabolite formation, In *Polynuclear Aromatic Hydrocarbons: Physical and Biological Chemistry* pp 193-200.
- (24) Utesch, D., Glatt, H., and Oesch, F. (1987) Rat hepatocyte-mediated bacterial mutagenicity in relation to the carcinogenic potency of benz(a)anthracene, benzo(a)pyrene, and twenty-five methylated derivatives. *Cancer Res* 47, 1509-1515.
- (25) Santella, R., Kinoshita, T., and Jeffrey, A. M. (1982) Mutagenicity of Some Methylated Benzo[a]Pyrene Derivatives. *Mutation Research* 104, 209-213.
- (26) Flesher, J. W., and Sydnor, K. L. (1973) Possible role of 6-hydroxymethylbenzo(a)pyrene as a proximate carcinogen of benzo(a)pyrene and 6-methylbenzo(a)pyrene. *Int J Cancer* 11, 433-437.
- (27) Bayless, J. H., Jablonski, J. E., Roach, S. M., and Sullivan, P. D. (1986) Inhibition of the mutagenicity and metabolism of 6-methyl-benzo[a]pyrene and 6-hydroxymethylbenzo[a]pyrene. *Biochem Pharmacol* 35, 2313-2322.

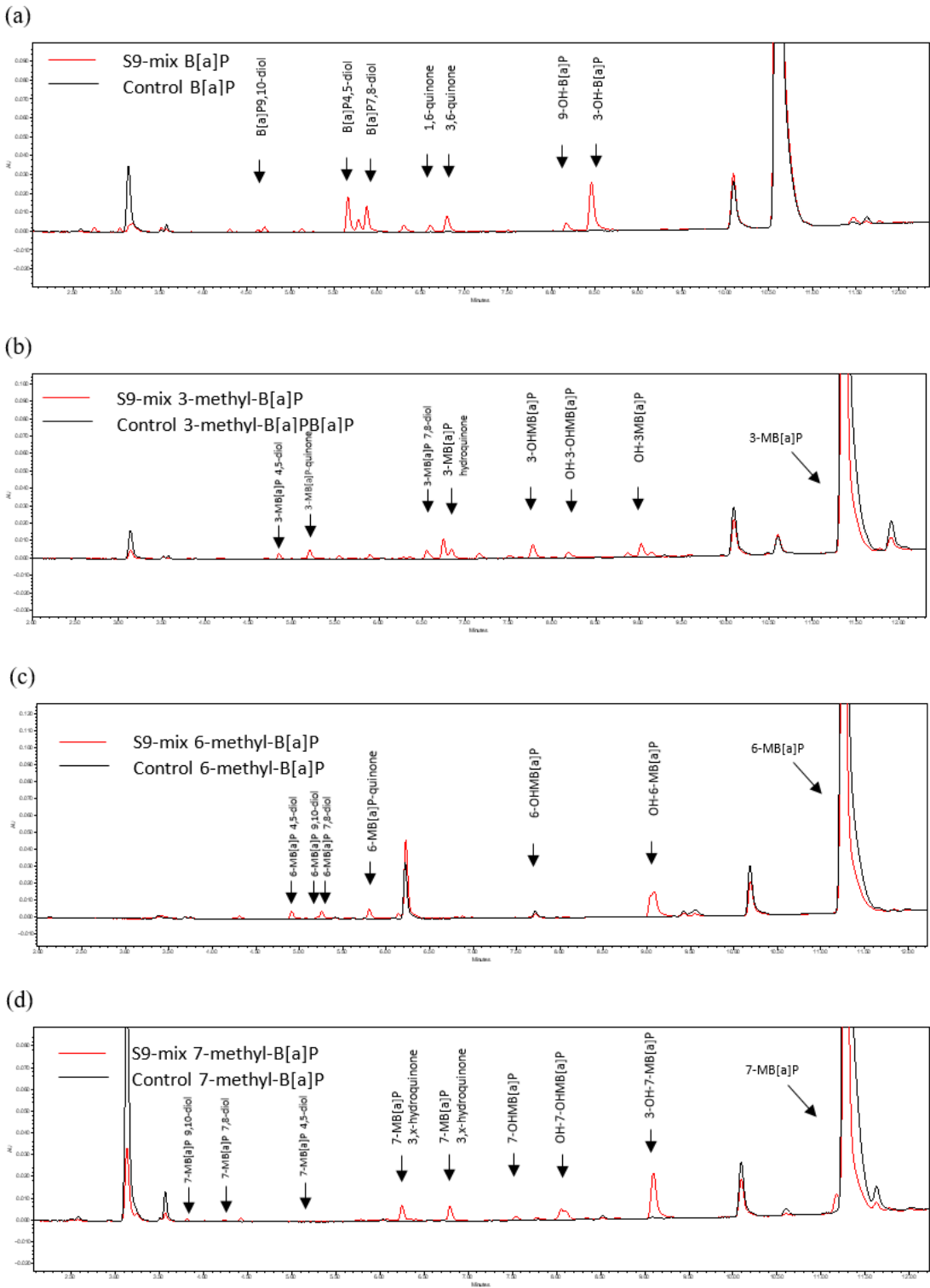
- (28) Iyer, R. P., Lyga, J. W., Secrist, J. A., 3rd, Daub, G. H., and Slaga, T. J. (1980) Comparative tumor-initiating activity of methylated benzo(a)pyrene derivatives in mouse skin. *Cancer Res* 40, 1073-1076.
- (29) J.W. Flesher, A. M. K., M. Chien, K.H. Stansbury, C. Gairola, K.L. Sydnor. (1983) Metabolic activation of carcinogenic hydrocarbons in the meso position (L region), In *Polycyclic Aromatic Hydrocarbons: Formation, Metabolism and Measurement* (Dennis, M. C. A. J., Ed.) pp 505-515, Battelle Press.
- (30) Li, D., Han, Y., Meng, X., Sun, X., Yu, Q., Li, Y., Wan, L., Huo, Y., and Guo, C. (2010) Effect of regular organic solvents on cytochrome P450-mediated metabolic activities in rat liver microsomes. *Drug Metab Dispos* 38, 1922-1925.
- (31) Hamel, A., Roy, M., and Proudlock, R. (2016) Chapter 4 - The Bacterial Reverse Mutation Test, In *Genetic Toxicology Testing* (Proudlock, R., Ed.) pp 79-138, Academic Press, Boston.
- (32) Lee, H., Sheth, J., and Harvey, R. G. (1983) Synthesis of putative oxidized metabolites of 8-methylbenzo[a]pyrene. *Carcinogenesis* 4, 1297-1299.
- (33) Wang, D., V. Schramm, J. Pool, E. Pardali, A. Brandenburg, I. M.C.M. Rietjens, P.J. Boogaard. (2021) The effect of alkyl substitution on the oxidative metabolism and mutagenicity of phenanthrene
- (34) Kamelia, L., de Haan, L., Spenkelink, B., Bruyneel, B., Ketelslegers, H. B., Boogaard, P. J., and Rietjens, I. (2020) The role of metabolism in the developmental toxicity of polycyclic aromatic hydrocarbon-containing extracts of petroleum substances. *J Appl Toxicol* 40, 330-341.

- (35) Wood, A. W., Levin, W., Lu, A. Y. H., Ryan, D., West, S. B., Yagi, H., Mah, H. D., Jerina, D. M., and Conney, A. H. (1977) Structural Requirements for Metabolic Activation of Benzo[a]Pyrene to Mutagenic Products - Effects of Modifications in 4,5-Positions, 7,8-Positions, and 9,10-Positions. *Mol Pharmacol* 13, 1116-1125.
- (36) Wislocki, P. G., Wood, A. W., Chang, R. L., Levin, W., Yagi, H., Hernandez, O., Jerina, D. M., and Conney, A. H. (1976) High mutagenicity and toxicity of a diol epoxide derived from benzo(a)pyrene. *Biochem Biophys Res Commun* 68, 1006-1012.
- (37) Flesher, J. W., Horn, J., and Lehner, A. F. (1997) 6-sulfooxymethylbenzo[a]pyrene is an ultimate electrophilic and carcinogenic form of the intermediary metabolite 6-hydroxymethylbenzo[a]pyrene. *Biochem Biophys Res Commun* 234, 554-558.
- (38) Stansbury, K. H., Flesher, J. W., and Gupta, R. C. (1994) Mechanism of aralkyl-DNA adduct formation from benzo[a]pyrene in vivo. *Chem Res Toxicol* 7, 254-259.
- (39) Rogan, E. G., Hakam, A., and Cavalieri, E. L. (1983) Structure elucidation of a 6-methylbenzo[a]pyrene-DNA adduct formed by horseradish peroxidase in vitro and mouse skin in vivo. *Chem Biol Interact* 47, 111-122.
- (40) Cavalieri, E., Roth, R., Grandjean, C., Althoff, J., Patil, K., Liakus, S., and Marsh, S. (1978) Carcinogenicity and metabolic profiles of 6-substituted benzo[a]pyrene derivatives on mouse skin. *Chem Biol Interact* 22, 53-67.
- (41) Heyst, A. V. (2019). Mineral oil migration from cardboard food contact materials: hazard identification and exposure assessment of the Belgian population. Brussel, Vrije Universiteit Brussel.

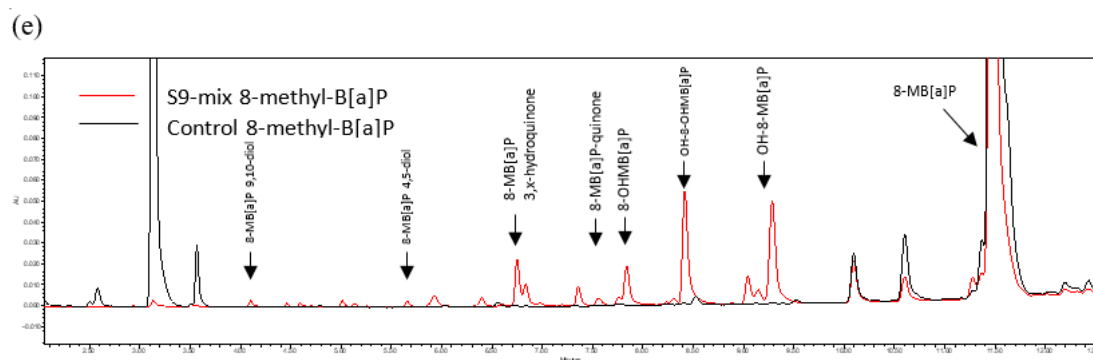
## **Acknowledgement**

This work was financially supported by Concauwe (No. 201700093) in Belgium, and by a grant from China Scholarship Council from China (No. 201807720073) to Danlei Wang. Part of this work was supported by Operationeel Programma Kansen voor West II (EFRO) (project no KVV- 00181).

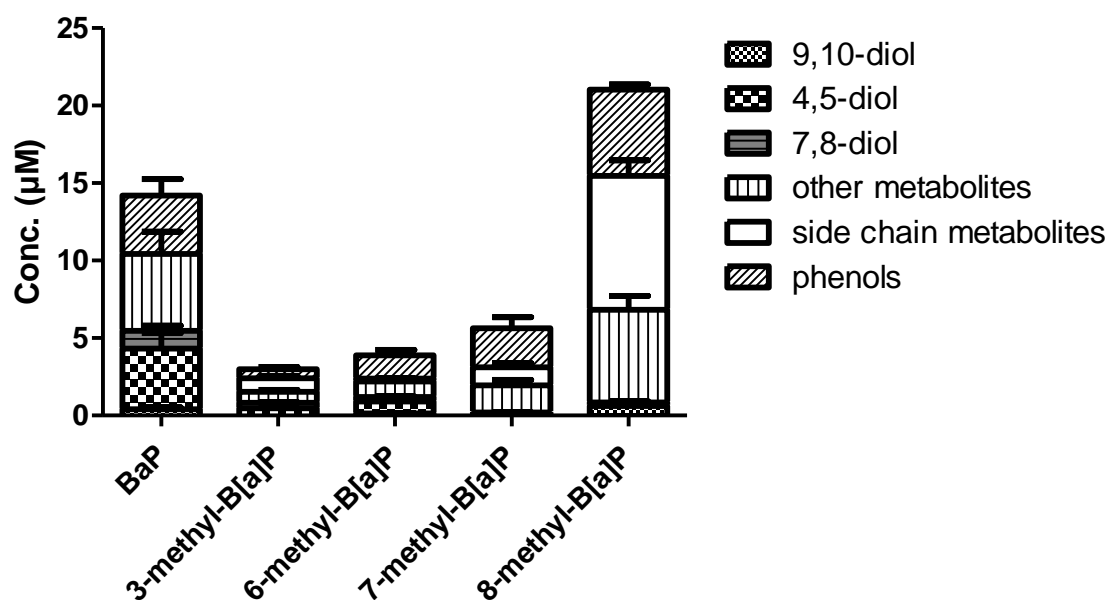
Supplementary materials







**Figure S1.** Metabolic profile of (a) B[a]P (b) 3-methyl-B[a]P (c) 6-methyl-B[a]P (d) 7-methyl-B[a]P and (e) 8-methyl-B[a]P that were formed from S9-mix or control incubation mixture that was applied to *S. typhimurium* TA98 and TA100 in the reverse mutation test. The presented chromatograms were extracted under the wavelength of 254nm.



**Figure S2.** Concentration of the metabolites formed in S9 incubation with B[a]P and four of its methyl substituents. Each bar represents experimental means and vertical bars are standard errors of the mean (n=3).



## **Chapter 5**

# **Predicting the in vivo developmental toxicity of benzo[a]pyrene (B[a]P) in rats by an in vitro-in silico approach**

Danlei Wang, Maartje H. Rietdijk, Lenny Kamelia, Peter J. Boogaard, Ivonne M.C.M. Rietjens

Published in Archives of Toxicology (2021) 95: 3323-3340

## **Abstract**

Developmental toxicity testing is an animal-intensive endpoints in toxicity testing and calls for animal-free alternatives. Previous studies showed the applicability of an in vitro – in silico approach for predicting developmental toxicity of a range of compounds, based on data from the mouse embryonic stem cell test (EST) combined with physiologically based kinetic (PBK) modelling facilitated reverse dosimetry. In the current study, the use of this approach for predicting developmental toxicity of polycyclic aromatic hydrocarbons (PAHs) was evaluated, using benzo[a]pyrene (B[a]P) as a model compound. A rat PBK model of B[a]P was developed to simulate the kinetics of its main metabolite 3-hydroxybenzo[a]pyrene (3-OHB[a]P), shown previously to be responsible for the developmental toxicity of B[a]P. Comparison to in vivo kinetic data showed that the model adequately predicted B[a]P and 3-OHB[a]P blood concentrations in the rat. Using this PBK model and reverse dosimetry, a concentration-response curve for 3-OHB[a]P obtained in the EST was translated into an in vivo dose-response curve for developmental toxicity of B[a]P in rats upon single or repeated dose exposure. The predicted half maximal effect doses (ED<sub>50</sub>) amounted to 67 and 45 mg/kg bw being comparable to the ED<sub>50</sub> derived from the in vivo dose-response data reported for B[a]P in the literature, of 29 mg/kg bw. The present study provides a proof of principle of applying this in vitro-in silico approach for evaluating developmental toxicity of B[a]P and may provide a promising strategy for predicting the developmental toxicity of related PAHs, without the need for extensive animal testing.

## **1. Introduction**

The Registration, Evaluation, Authorization and Restriction of Chemicals (REACH) legislation requires all chemical substances produced or sold within the European Union (EU) at a volume of  $\geq 100$  tonnes/year to be evaluated for developmental toxicity. Developmental toxicity testing is one of the most animal-intensive endpoints in toxicity testing, estimated to require more than 20% of all animals used for toxicity testing under REACH (Jagt et al. 2004). REACH acknowledges the need for alternative, animal-free test methods, contributing to the 3Rs (reduction, replacement and refinement) of use of experimental animals in toxicological risk assessment.

Three in vitro test methods are currently scientifically validated for developmental toxicity testing: the limb bud micro mass (MM), the whole embryo culture (WEC) and the mouse embryonic stem cell test (EST) (Genschow et al. 2004; Genschow et al. 2002). Only the EST is considered animal-free, as it makes use of the mouse embryonic stem cell line D3 (ES-D3) (Buesen et al. 2009). The differentiation assay of the EST evaluates the effect of a compound on the differentiation of ES-D3 cells into beating cardiomyocytes.

However, use of in vitro assays like the EST generates in vitro concentration-response curves while for toxicological risk assessment dose-response curves are needed since they enable definition of so-called points of departure (PoDs) to define health-based guidance values for safe human exposure. In vitro concentration-response curves can be translated into in vivo dose-response curves using physiologically based kinetic (PBK) modelling-based reverse dosimetry. This approach was previously shown to adequately predict in vivo developmental toxicity of various compounds, using concentration-response data from the EST (Li et al. 2017a; Louisse et al. 2010a; Louisse et al. 2010b; Strikwold et al. 2017). The validity of this in vitro-in silico method for polycyclic aromatic hydrocarbons (PAHs) was not yet investigated. This although PAH-containing

substances make up a large group of compounds for which REACH legislation dictates developmental toxicity testing. The aim of the present study was to evaluate the use of this in vitro-in silico approach to predict the developmental toxicity of benzo(a)pyrene (B[a]P). B[a]P was chosen as the model compound for PAHs because B[a]P is well studied, and assumed to induce developmental toxicity in rats (Archibong et al. 2002; Bui et al. 1986; Feuston et al. 1996; Feuston et al. 1989; Feuston et al. 1994; Feuston and Mackerer 1996; Hood et al. 2000; Wu et al. 2003). Furthermore, in vivo kinetic rat data are available in literature for B[a]P and its metabolite 3-hydroxybenzo[a]pyrene (3-OHB[a]P) (Marie et al. 2010; Moreau and Bouchard 2015) as well as in vivo dose-response data for reproductive toxicity of B[a]P in rats (Archibong et al. 2002; Bui et al. 1986), enabling evaluation of the predictions made by the developed in vitro-in silico approach. B[a]P is well known for its bioactivation to dihydrodiol epoxide metabolites that lead to DNA damage induced carcinogenicity. For induction of developmental toxicity, B[a]P needs bioactivation to 3-OHB[a]P as shown in previous in vitro EST studies (Kamelia et al. 2020). To facilitate the prediction of tissue concentrations for 3-OHB[a]P, a sub-model for this metabolite was included in the PBK model. Previously, PBK models for B[a]P and 3-OHB[a]P have been developed (Campbell et al. 2016; Crowell et al. 2011a; Heredia-Ortiz and Bouchard 2013; Heredia-Ortiz et al. 2011; Heredia Ortiz et al. 2014). However, these models were not applied for reverse dosimetry, leaving the question whether PBK modelling-based reverse dosimetry is suited to predict in vivo developmental toxicity of B[a]P.

To answer this question, in the present study a PBK model of B[a]P in rat was developed for predicting blood concentrations of 3-OHB[a]P. The model was used to translate concentration-response data for 3-OHB[a]P from the EST to predict an in vivo dose-response curve for

developmental toxicity of B[a]P in rats and results obtained were compared to available data in literature on kinetics and developmental toxicity of B[a]P and 3-OHB[a]P.

## **2. Material and methods**

### **2.1 Materials**

3-OHB[a]P was ordered from Toronto Research Chemicals (TRC) Canada (North York, Canada). 3'-phosphate 5'-phosphosulfate (PAPS) lithium salt was purchased from Santa Cruz Biotechnology (Dallas, Texas, United States), B[a]P, nicotinamide adenine dinucleotide phosphate (NADPH), sodium salt, sodium phosphate, sodium chloride and Trizma<sup>®</sup> base (TRIS) were purchased at Sigma-Aldrich (Zwijndrecht, The Netherlands). Uridine 5'-diphosphoglucuronic acid (UDPGA) trisodium salt was purchased from Carbosynth (Compton, United Kingdom). Pooled liver and lung S9 fractions and microsomes from male Sprague-Dawley (SD) rats were ordered from Tebu-Bio (Heerhugowaard, The Netherlands). Acetonitrile (ACN) was purchased from Biosolve (Dieuze, France). Dimethyl sulfoxide (DMSO) was obtained from Acros Organics (Geel, Belgium). Potassium hydrogen phosphate ( $K_2HPO_4$ ) and trifluoroacetic acid (TFA) were purchased from Merck (Darmstadt, Germany).

### **2.2 Method**

The PBK modelling-based reverse dosimetry approach consisted of the following steps, 1) defining a PBK model describing the kinetics of 3-OHB[a]P, the main metabolite of B[a]P, in rats, 2) determining kinetic parameter values for metabolism of B[a]P and conjugation of 3-OHB[a]P, 3) evaluation of the PBK model using in vivo kinetic literature data, 4) translation of in vitro concentration-response data for 3-OHB[a]P in the EST (Kamelia et al. 2020) into in vivo dose-

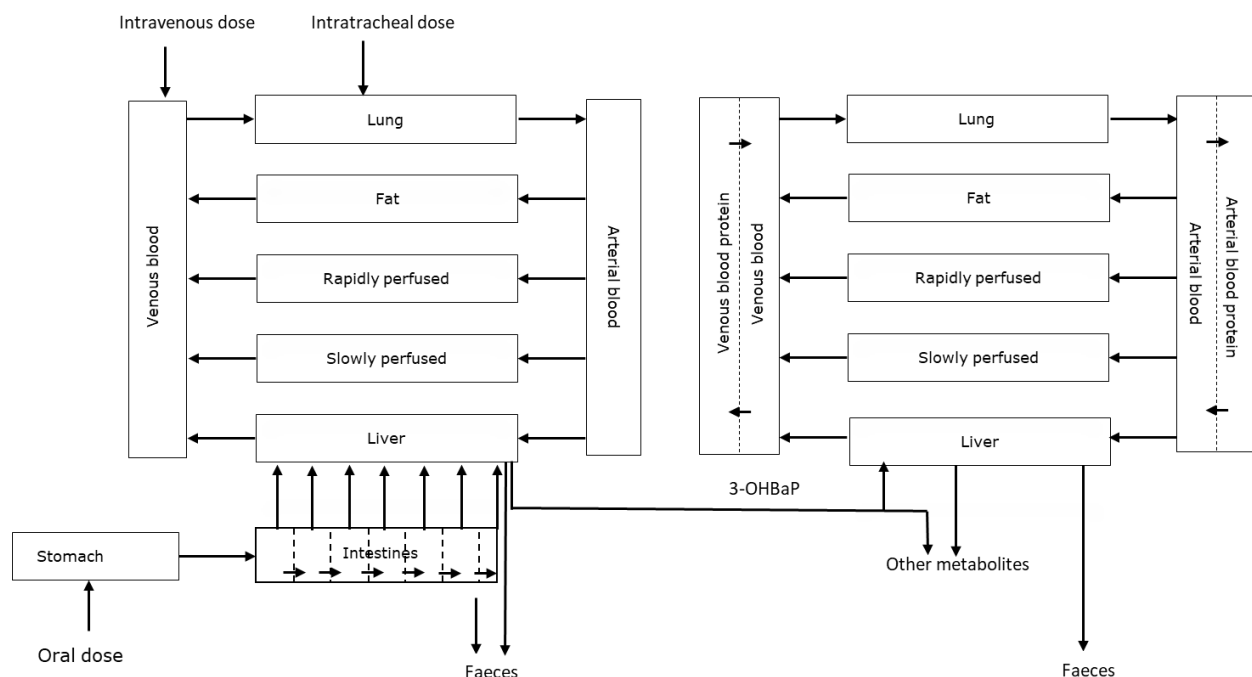
response data for developmental toxicity of B[a]P using PBK model facilitated reverse dosimetry, 5) evaluation of the predicted dose-response curve by comparison to literature reported dose-response data (Archibong et al. 2002; Bui et al. 1986).

### **2.2.1 Development of a PBK model for B[a]P and 3-OHB[a]P in rats**

The PBK model was defined based on the conceptual model for B[a]P with a submodel for 3-OHB[a]P taking into account the model codes for B[a]P PBK models that included submodels for 3-OHB[a]P reported in the literature (Campbell et al. 2016; Crowell et al. 2011b; Heredia-Ortiz and Bouchard 2013) and is presented in **Figure 1**. The conceptual PBK model for B[a]P consisted of separate compartments for venous blood, arterial blood, fat tissue, liver tissue, lung tissue, rapidly and slowly perfused tissue, stomach and intestines. 3-OHB[a]P is highly lipophilic. To prevent 3-OHB[a]P from partitioning into the fat tissue in the model simulations, it was essential to include a blood protein compartment in the model to allow binding of 3-OHB[a]P to blood protein. The unbound fraction of 3-OHB[a]P in the blood compartment was represented by the  $f_{ub, \text{ in vivo}}$ , calculated as described in section 2.2.4. The fraction of 3-OHB[a]P bound to protein in the blood protein compartment ( $f_{b, \text{ in vivo}}$ ) was calculated as 1 minus the  $f_{ub, \text{ in vivo}}$ . The intestinal compartment was divided into 7 sub compartments to describe the passage of B[a]P through the intestines upon oral exposure (Zhang et al. 2018). Conversion of B[a]P into 3-OHB[a]P and other metabolites was initially assumed to occur in the liver and lung (Heredia-Ortiz et al. 2011). Clearance of 3-OHB[a]P was assumed to result from hepatic and pulmonary conjugation (Cohen 1990; Cohen and Moore 1976). The relative contribution of pulmonary metabolism of B[a]P and 3-OHB[a]P compared to hepatic metabolism of these compounds was investigated as well. Pulmonary metabolism of B[a]P and 3-OHB[a]P quantified based on incubations of B[a]P with rat lung microsomes and 3-OHB[a]P with rat lung S9, calculated as described in section 2.2.2, was



shown to be negligible as compared to metabolism in the liver (see section 3.1) and thus not included in the PBK model. In the model it is assumed that both B[a]P and 3-OHB[a]P are eliminated to the faeces by biliary excretion.



**Figure 1.** Schematic overview of the PBK model of B[a]P containing a sub-model for 3-OHB[a]P in rats

B[a]P needs bioactivation to 3-OHB[a]P to induce developmental toxicity in vitro (Kamelia et al. 2020). Therefore, the PBK model contained a sub compartment describing the kinetics of 3-OHB[a]P, enabling prediction of blood concentrations of 3-OHB[a]P as a function of the dose of B[a]P, required for the reverse dosimetry. Based on the conceptual model the differential equations were defined and inserted in Berkley Madonna 8.3.18 (UC Berkeley, California, USA) using the Rosenbrock's algorithm for stiff systems. Model equations are included in supplementary materials 1.

The 3-OHB[a]P sub-model consisted of the same compartments as the B[a]P model, except for stomach and intestine, which were not relevant for the kinetics of 3-OHB[a]P, since 3-OHB[a]P is formed in the liver. Studies in pregnant rats have shown that the blood concentration of B[a]P in maternal and foetal blood are similar (Withey et al. 1993). The same was found for the concentration of B[a]P metabolites in maternal and foetal blood (Withey et al. 1993). It was therefore assumed that B[a]P and its metabolites readily cross the placenta and that the reproductive toxicity observed in vivo is dependent on the maternal blood concentration of 3-OHB[a]P. For this reason, separate compartments for placental and foetal tissue were not included in the model.

Physiological and anatomical parameter values were taken from literature (Brown et al. 1997; Crowell et al. 2011a) and are presented in **Table 1**.

The tissue:blood partition coefficients for B[a]P and 3-OHB[a]P were previously calculated by Crowell et al., (2011), according to the method of Poulin and Krishnan (1995) and Poulin and Theil (2002) and were applied in the current PBK model (**Table 1**).

**Table 1.** Physiological, anatomical and physicochemical parameter values for B[a]P and 3-OHB[a]P for the rat PBK model

Model parameter	Symbol	Value	Reference
<b>Physiological parameters</b>			
Body weight	BW	0.245 <sup>a</sup>	Marie et al. (2010)
<u>Fractional tissue volumes</u>			Moreau and Bouchard (2015)
Fat	VFc	0.065	
Liver	VLc	0.037	

Lung	VLuc	0.005	Crowell et al. (2011),
Arterial blood	VABc	0.0257	based on Brown et al.
Venous blood	VVBc	0.0514	(1997)
Rapidly perfused tissue	VRc	0.2159	
Slowly perfused tissue	VSc	0.6	
Cardiac output (mL/s)	QC	$15 \cdot BW^{0.74}$	
<u>Fractional tissue blood flows</u>			
Fat	QFc	0.07	
Liver	QLc	0.183	
Lung	QLuc	1	
Rapidly perfused tissue	QRc	0.4	
Slowly perfused tissue	QSc	0.347	
<b>Physicochemical parameters</b>			
<i>Benzo[a]pyrene</i>			
Molecular weight	MWBaP	252.31	
LogP		6.0	
Fraction unbound	$f_{ub}$	0.006	Calculated according to Lobell and Sivarajah (2003)
<u>Tissue:blood partition coefficients</u>			
Fat	PFBaP	496.38	Crowell et al., 2011
Liver	PLBaP	13.31	based on Poulin and
Lung	PLuBaP	13.31	Theil, 2002

Rapidly perfused tissue	PRBAP	13.31	
Slowly perfused tissue	PSBAP	6.99	
<i>3-hydroxybenzo[a]pyrene</i>			
Molecular weight	MW3OHBaP	268.3	
LogP		5.9	
Fraction unbound	$f_{ub}$	0.007	Calculated according to Lobell and Sivarajah (2003)
<u>Tissue:blood partition coefficients</u>			
Fat	PF3OHBAP	401	Crowell et al., 2011
Liver	PL3OHBAP	12.24	based on Poulin and
Lung	PLu3OHBAP	12.24	Krishnan, 1995
Rapidly perfused tissue	PR3OHBAP	12.24	
Slowly perfused tissue	P3OH BAP	6.43	

<sup>a</sup> Median of body weights of rats in these two studies

Given the nature of the in vivo data available for model evaluation, and evaluation of the predicted toxicity, the model included single and repeated intravenous, intratracheal and oral exposure to B[a]P. For oral exposure, stomach emptying and intestinal transfer of the parent compound were included. The uptake of B[a]P from the intestines to the liver was described for the 7 sub-compartments using the apparent in vivo permeability coefficient ( $P_{app, in vivo}$ ) value. The  $P_{app, in vivo}$  was derived from the in vitro  $P_{app, Caco-2}$  value for B[a]P that was previously determined in the Caco-2 model (Goth-Goldstein et al. 1999). The  $P_{app, in vivo}$  was calculated using the following

equation:  $\text{Log} (P_{\text{app, in vivo}}) = 0.6836 \times \text{Log} (P_{\text{app, Caco-2}}) - 0.5579$  (Sun et al. 2002) and applied in the model as described before (Zhang et al. 2018).

Hepatic conversion of B[a]P into 3-OHB[a]P and other metabolites was described by the  $V_{\text{max}}$  and  $K_m$ , determined in vitro using incubations with rat liver microsomes. Pulmonary metabolism of B[a]P was shown to be not relevant for the PBK model based on results from incubations with rat lung microsomes and B[a]P as described in section 2.2.2.

Clearance of 3-OHB[a]P was assumed to be the result of conjugation in liver tissue. Sulfation and glucuronidation are the main contributors to 3-OHB[a]P clearance (Cohen 1990; Cohen and Moore 1976). Based on the results of incubation experiments described in section 2.2.2, pulmonary conjugation was considered irrelevant for clearance of 3-OHB[a]P in the PBK model.  $V_{\text{max}}$  and  $K_m$  values for glucuronidation and sulfation of 3-OHB[a]P in rat liver were determined in in vitro incubations with rat liver S9, performed as described in section 2.2.2.

All in vitro  $V_{\text{max}}$  values were scaled to microsomal or S9 protein content of rat liver using the following scaling factors: 45 mg microsomal protein per gram liver tissue and 125 mg S9 protein per gram liver tissue (Houston and Galetin 2008). The scaled  $V_{\text{max}}$  values were subsequently converted to  $V_{\text{max}}$  in nmol/min/liver using the liver weight of 9.1 g, calculated from the body weight and fractional liver weight presented in **Table 1**. The  $K_m$  in vitro was assumed equal to the  $K_m$  in vivo.

## **2.2.2 Determining kinetic parameter values for metabolism of B[a]P and conjugation of 3-OHB[a]P**

### **Metabolism of B[a]P**

The formation of 3-OHB[a]P and other metabolites from B[a]P in lung and liver tissue was investigated in incubations with rat liver microsomes and rat lung microsomes. The incubation mixtures consisted of (final concentrations) 0.1 mM potassium phosphate (pH 7.4), 5 mM MgCl<sub>2</sub>, 0.5 mg/ml rat liver microsomes or 2 mg/ml rat lung microsomes, and 1 mM NADPH in conical glass vials. Incubation mixtures were pre-incubated for 1 minute, after which the reaction was initiated by the addition of B[a]P from a 100 times diluted stock solution in DMSO to reach the final volume of 200 µl (1 % DMSO v/v) with B[a]P concentrations ranging from 0 to 200 µM. The mixtures were incubated in a shaking water bath at 37 °C for 30 minutes. 20 µl ice-cold 10% (v/v) perchloric acid (HClO<sub>4</sub>) was added to terminate the reactions and the mixtures were put on ice for at least 15 minutes. Di-isopropyl ether (DIPE) was used to extract B[a]P and its metabolites from the incubation mixture. To this end, 1 ml DIPE was added to each incubation mixture, the tubes were vortexed for 20 seconds and the upper layer was collected. Extraction was performed three times. Remaining DIPE was removed by evaporation under a stream of N<sub>2</sub>. Subsequently, extracts were re-dissolved in 100 µl methanol and transferred to UPLC vials for analysis.

### **Conjugation of 3-OHB[a]P**

Incubations with rat liver and lung S9 fractions were optimized to establish linearity over time and protein concentrations for the rate of glucuronidation and sulfation of 3-OHB[a]P. The experiments performed for time optimization revealed that the pulmonary formation rate of sulfated and glucuronidated metabolites of 3-OHB[a]P was negligible compared to the formation rate of

sulfonated and glucuronidated metabolites by the liver (see section 3.2). Pulmonary conjugation was therefore considered not relevant for in vivo clearance of 3-OHB[a]P in the current PBK model and no further experiment for in vitro kinetics with lung fractions were performed.

Kinetics for 3-OHB[a]P glucuronidation, were quantified using incubations with pooled liver S9 fractions from male SD-rats. Incubation mixtures in a final volume of 200  $\mu$ l in conical glass vials consisted of (final concentrations) 0.1 mM Tris-HCl (pH 7.4), 5 mM  $MgCl_2$ , 0.1 mg/ml rat liver S9, 3 mM UDPGA and 0.025 mg/ml alamethicin.

Hepatic sulfonation of 3-OHB[a]P was evaluated using pooled liver S9 fractions of male SD-rats, in incubation mixtures with a final volume of 200  $\mu$ l in conical glass vials containing (final concentrations) 0.1 mM Tris-HCl (pH 7.4), 0.1 mg/ml rat liver S9 and 0.2 mM PAPS.

All incubation mixtures were pre-incubated for 1 minute, after which the reaction was initiated by addition of 3-OHB[a]P in final concentrations ranging from 0.01 – 50  $\mu$ M (glucuronidation) or 0.01 - 100  $\mu$ M (sulfation) added from 100 times concentrated stock solutions in DMSO to reach the final volume of 200  $\mu$ l (1 % DMSO v/v). The mixtures were incubated in a shaking water bath at 37 °C for 20 minutes (glucuronidation) or 70 minutes (sulfation). 100  $\mu$ l of ice-cold acetonitrile was added to terminate the reactions and the mixtures were put on ice for at least 15 minutes. Subsequently, the tubes were centrifuged at 4°C and 3717 g per minute for 5 minutes. The supernatant was collected and analysed by Ultra Performance Liquid Chromatography (UPLC). All incubations were performed in triplicate.

### **UPLC analysis**

The collected supernatants were analysed using a UPLC Nexera series (Shimadzu, Kyoto, Japan) to quantify the metabolites of B[a]P and the conjugates of 3-OHB[a]P formed in incubations with

rat liver microsomes and S9, respectively. The UPLC was equipped with a Photodiode Array (PDA) detector, recording wavelengths between 190 and 400nm and a Phenomenex C18 column (Phenomenex, Torrance, California, United States). The column temperature was kept at 40 °C and the auto-sampler at 4 °C during analysis. The mobile phase consisted of Nanopure water containing 0.1% (v/v) trifluoroacetic acid (TFA) (A) and acetonitrile containing 0.1% (v/v) TFA (B) at a flow rate of 0.3 ml/min. The total run time was 23 minutes and 30 seconds, starting with 10% B for 30 seconds, increasing to 100 % B in 15 minutes, maintaining this condition for 3 minutes before returning to the initial conditions of 10 % B in 30 seconds. 10 µl of sample was injected per run. Under these conditions the metabolite 3-OHB[a]P, detected at 258 nm, eluted at 10.16 minutes. For the glucuronidated and sulfonated metabolite of 3-OHB[a]P, retention time and detection wavelength were 7.5 minutes, 303.3 nm and 7.4 minutes, 301 nm respectively. The amounts of 3-OHB[a]P in the microsomal incubation sample and of glucuronidated and sulfated 3-OHB[a]P in the S9 incubation samples were quantified by integrating peak areas at their respective wavelengths using a calibration curve prepared with commercially available 3-OHB[a]P. To obtain the  $V_{\max}$  and  $K_m$  the in vitro data for the substrate concentration dependent rate of metabolite formation were fitted to the Michaelis-Menten equation using Graphpad Prism 9.0.1 for Windows (GraphPad Software, San Diego, California, USA).



**Table 2.** Summary of studies on in vivo kinetics of B[a]P and 3-OHB[a]P used for evaluation of the model predicted blood concentrations

Species	Weight (g)	Compound	Dosage	Dose (mg/kg bw)	Route of exposure	Reference
SD rat, male	260 - 290	B[a]P	Single	10	Intravenous	Marie et al., 2010
SD rat, male	200 - 250	B[a]P	Single	10	Intravenous	Moreau and Bouchard, 2015
			Single	10	Intratracheal	
			Single	10	Oral	
			Single	10	Cutaneous	

**Table 3.** Summary of the in vivo developmental toxicity study used for evaluation of predicted developmental toxicity of B[a]P using the developed PBK modelling-based reverse dosimetry approach

Species	N	Weight (g)	Route exposure	of Dosage	Dose BaP/m <sup>3</sup> )	(µg Dose bw/day)	(mg/kg Endpoint(s)	Reference
F-344 female	rat, 10	N/A	Inhalation	Repeated, 4h/day for 10 days	25, 75 or 100	4.75, 14.25 or 19 <sup>a</sup>	Foetal survival per litter Implantation sites per dam Pups per litter	Archibong et al., 2002
SD female	rat, 10- 15	225-250	Subcutaneous	Repeated Daily for 3 or 6 days		50	Implantations per litter Number of live and dead fetuses Number of resorptions	Bui et al., 1986

<sup>a</sup> Oral dose equivalent as reported by Hood et al., 2000 and Ramesh et al., 2002

### 2.2.3 PBK model evaluation and sensitivity analysis

The PBK model performance was evaluated by comparing predicted time-dependent blood concentrations of 3-OHB[a]P to reported in vivo time-dependent blood concentrations in rats after dosing B[a]P intravenously (Marie et al. 2010; Moreau and Bouchard 2015), intratracheally, and orally (Moreau and Bouchard 2015). Model development and evaluation was focussed on accurate prediction of 3-OHB[a]P, because the reverse dosimetry is based on the EST data for 3-OHB[a]P mediated induction of in vitro developmental toxicity. Further evaluation of the PBK model was done by comparing predicted dose-response data, obtained by reverse dosimetry of the EST data of 3-OHB[a]P, to in vivo dose-response data of reproductive toxicity of B[a]P in rats (Archibong et al. 2002; Bui et al. 1986), performed as described in section 2.2.5. Given the nature of the in vivo study used for evaluation of the predicted dose-response, the blood concentrations of 3-OHB[a]P were also predicted for repeated daily exposure to B[a]P, until steady state of the  $C_{\max}$  of 3-OHB[a]P was reached. An overview of the characteristics of the in vivo kinetic and dose-response studies used for model evaluation is presented in **Table 2** and **3**.

For further evaluation of the PBK model the parameters that were most influential for the prediction of the maximum blood concentration ( $C_{\max}$ ) of 3-OHB[a]P upon intravenous, intratracheal and oral exposure to B[a]P were identified by a sensitivity analysis. The sensitivity analysis was performed for intravenous, intratracheal and oral exposure. To this end, each parameter value ( $P$ ) was increased by 10% ( $P'$ ), while keeping the other parameter values constant and the total fraction of arterial and venous blood flow at 1, resulting in an initial ( $C$ ) and modified ( $C'$ ) value of the model prediction for the  $C_{\max}$  of 3-OHB[a]P. Sensitivity coefficients (SC) were calculated using the following equation:  $SC = (C' - C)/(P' - P) \times (P/C)$  (Evans and Andersen 2000). The sensitivity analysis was performed for a single dose of 10 mg/kg bw B[a]P, as this dose was applied in the

kinetic in vivo studies used for evaluation of the model predicted blood concentrations of 3-OHB[a]P (Marie et al. 2010; Moreau and Bouchard 2015). The median body weight of the rats in these kinetic in vivo studies was 0.245 kg and was applied in the model when performing the sensitivity analysis.

#### **2.2.4 Translating in vitro concentration-response data into in vivo dose-response data using PBK modelling-based reverse dosimetry**

The in vitro concentration-response curve obtained for 3-OHB[a]P in the EST (Kamelia et al. 2020) was translated into a predicted in vivo dose-response curve, using PBK modelling-based reverse dosimetry. The in vivo developmental toxicity response to B[a]P is assumed to depend on the  $C_{\max}$  of unbound 3-OHB[a]P in the maternal rat blood ( $C_{ub, in vivo}$ ). Therefore, the  $C_{ub, in vivo}$  was set equal to the concentration of unbound 3-OHB[a]P in vitro ( $C_{ub, in vitro}$ ). To correct for differences in  $f_{ub}$  between rat blood ( $f_{ub, in vivo}$ ) and the EST assay medium ( $f_{ub, in vitro}$ ), the following equation was used :

$$C_{in vivo} = \frac{C_{in vitro} * f_{ub, in vitro}}{f_{ub, in vivo}}$$

where  $C_{in vivo}$  is the total 3-OHB[a]P concentration in the maternal blood,  $C_{in vitro}$  is the total 3-OHB[a]P concentration used in vitro,  $f_{ub, in vitro}$  is the fraction unbound in the EST assay medium and  $f_{ub, in vivo}$  is the fraction unbound in rat blood.

#### **Calculating the fraction unbound ( $f_{ub}$ ) of 3-OHB[a]P in assay medium**

The  $f_{ub, in vivo}$  of 3-OHB[a]P was calculated from the LogP value of 3-OHB[a]P based on the method described previously (Lobell and Sivarajah 2003) using the QIVIVE tool of Wageningen Food Safety Research (WFSR) (<https://wfsr.shinyapps.io/wfsrqivivetools/>) (Punt et al. 2021). This in

silico method assumes the  $f_{ub, \text{ in vivo}}$  in rat plasma for rat to be the same as for human plasma. Furthermore, the  $f_{ub, \text{ in vitro}}$  values were assumed to vary linear with the protein content in the biological matrix. This assumption is supported by the linear relationship between the unbound fraction and the albumin concentration in the in vitro test system reported previously for some chlorophenols (Gulden et al. 2002). The fractions bound in vivo ( $f_{b, \text{ in vivo}}$ ) were calculated as 1 minus the  $f_{ub, \text{ in vivo}}$ . The LogP values and calculated  $f_{ub, \text{ in vivo}}$  and  $f_{b, \text{ in vivo}}$  are presented in **Table 1**.

The  $f_{ub, \text{ in vivo}}$  and  $f_{ub, \text{ in vitro}}$  depend on the protein content present in rat blood plasma and assay medium, respectively. The relative amount of protein present in the assay medium used in the EST (15% (Kamelia et al. 2020)), is approximately twice the protein content of rat blood plasma (7.5% (Torbert 1935)). Therefore, the  $f_{ub, \text{ in vitro}}$  was assumed to be half of the  $f_{ub, \text{ in vivo}}$ .

### **PBK modelling-based reverse dosimetry**

Reverse dosimetry was performed to calculate the dose of B[a]P that would give rise to the  $C_{\text{in vivo}}$  of 3-OHB[a]P obtained by setting the in vitro unbound concentrations applied in the EST equal to the unbound in vivo concentration, as described in section 2.2.4. Reverse dosimetry was performed for exposure to a single oral dose of B[a]P and for repeated daily intravenous and oral dosing. For repeated exposure, B[a]P was dosed daily until steady state of the 3-OHB[a]P blood concentration was reached. B[a]P doses were calculated using a parameter plot where the maximum blood concentration ( $C_{\text{in vivo}}$ ) of 3-OHB[a]P was plotted against the oral dose of B[a]P (mg/kg bw). In vivo dose-response data used to evaluate the model predicted dose-response curve were available from literature (Archibong et al. 2002; Bui et al. 1986), the details of these studies are summarized in **Table 3**.

### **2.2.5 Evaluation of predicted dose-dependent developmental toxicity effect**

#### **Conversion of the exposure concentration of B[a]P in air to an oral equivalent dose per kg bw**

The dose-response data predicted from the concentration-response curves derived in the EST (Kamelia et al. 2020) were compared to in vivo dose-response data for reproductive toxicity of B[a]P upon nasal inhalation (Archibong et al. 2002) and to the in vivo data for reproductive toxicity of B[a]P upon subcutaneous injection (Bui et al. 1986). The details of these studies are summarized in **Table 3**. Foetal survival, calculated as the fraction of live foetuses relative to the number of implantation sites reported in these studies, was taken as measure for in vivo reproductive toxicity. Archibong et al., (2002) exposed Fisher 344 (F-344) rats to 25, 75 or 100  $\mu\text{g B[a]P/m}^3$  via nasal inhalation, for four hours per day, from gestation day 11 to 20. Previous studies reported that the inhalation doses of 25, 75 or 100  $\mu\text{g B[a]P/m}^3$  correspond to an equivalent oral dose of 4.75, 14.25 and 19 mg/kg bw respectively (Hood et al. 2000; Ramesh et al. 2002). These oral dose equivalents in mg/kg bw were used for the comparison with model predicted dose-response data. Bui et al., (1986) exposed pregnant SD rats to 50 mg B[a]P/kg bw per day via subcutaneous injection from gestation day 6 to 8 or 6 to 11.

#### **Calculating the ED<sub>50</sub> for evaluating the predicted dose-response data**

ED<sub>50</sub> values were calculated for the predicted and reported dose-response data, using the non-linear regression with 3 parameters in Graphpad Prism version 9.0.1 for Windows (GraphPad Software, San Diego, California USA). The ED<sub>50</sub> value was calculated for the fraction differentiated into beating cardiomyocytes for the predicted dose-response data. For the in vivo studies, foetus survival (number of live foetuses as fraction of total implantations) was used as response.

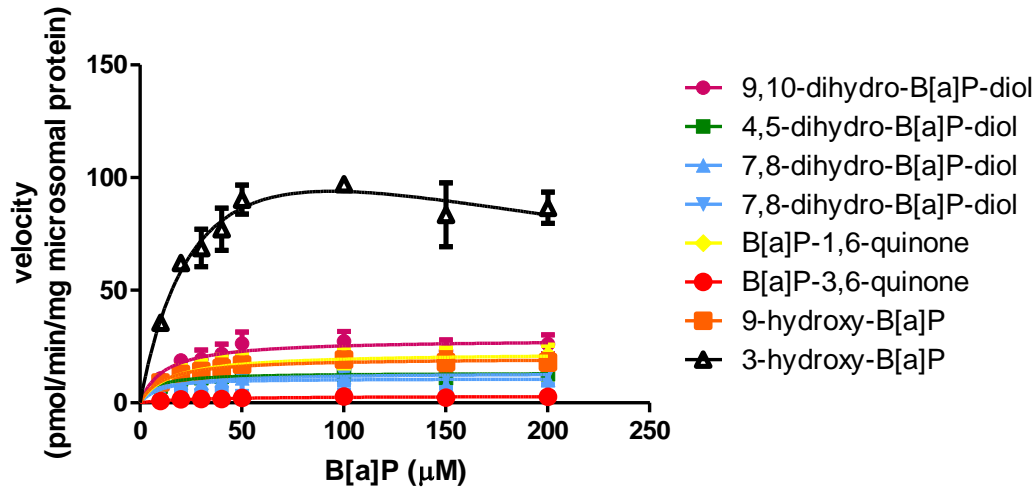
### 3. Result

#### 3.1 Development of a PBK model describing the kinetics of B[a]P and 3-OHB[a]P in rats

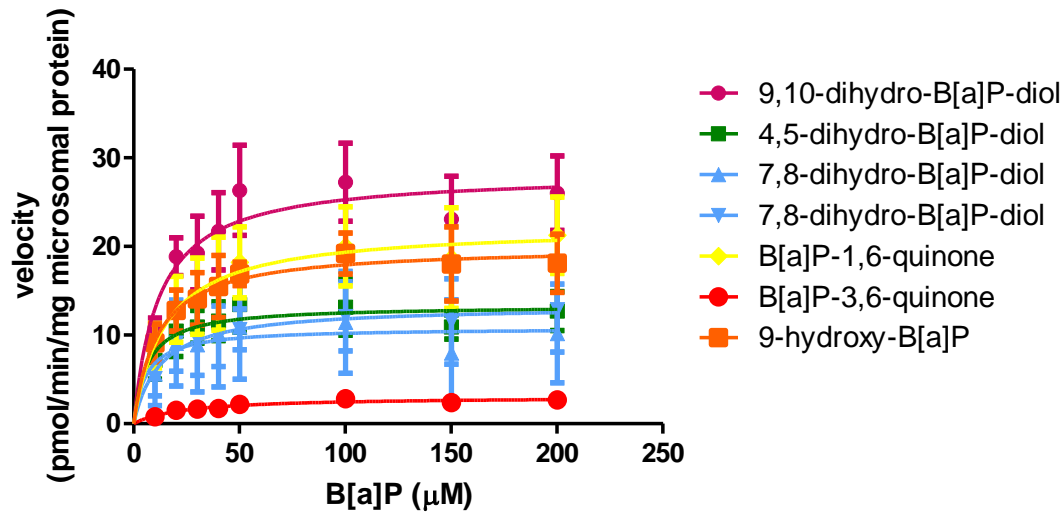
##### Kinetics of B[a]P and 3-OHB[a]P in rats

**Figure 2** presents the B[a]P concentration dependent formation of metabolites in incubations with rat liver microsomes. **Table 4** shows the kinetic parameter values,  $V_{\max}$ ,  $K_m$  and catalytic efficiency that were derived from these data. The metabolites of B[a]P were characterized based on the elution order and reference UV spectra reported in the literature (Chou 1983; Hamernik 1984; Hamernik 1983; Koehl et al. 1996; Moserova et al. 2009; Veignie et al. 2002; Yang et al. 1975) and commercially available reference chemicals. Three cis-B[a]P dihydrodiols were identified as B[a]P-9,10-dihydrodiol, B[a]P-4,5-dihydrodiol and B[a]P-7,8-dihydrodiol with identical UV spectra to those reported previously (Chou 1983; Hamernik 1984; Hamernik 1983). Another B[a]P-dihydrodiol was identified as a geometric isomer of trans-B[a]P-7,8-dihydrodiol due to spectral similarity to that of cis-B[a]P-7,8-dihydrodiol. Two quinones of B[a]P were identified as B[a]P-1,6-quinone and B[a]P-3,6-quinone with reported identical spectra (Chou 1983; Veignie et al. 2002). 9-Hydroxy-B[a]P was identified according to the reported UV wavelengths of 9-hydroxy-B[a]P (Sims 1968). 3-OHB[a]P was identified by co-elution and identical spectra to that of commercially available 3-OHB[a]P and the spectra reported by Hamernik (Hamernik 1984).

(a)



(b)

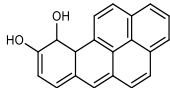
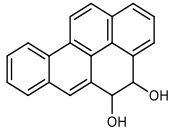
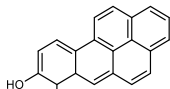
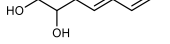
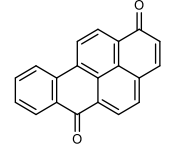
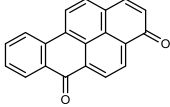
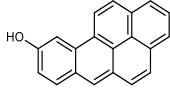
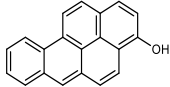


**Figure 2.** B[a]P concentration dependent formation of B[a]P metabolites in incubations with rat liver microsomes (a). Each symbol represents experimental means and vertical bars are standard errors of the mean (n=3). Triangle black line, 3-hydroxy-B[a]P; square orange line, 9-hydroxy-B[a]P; dot red line, B[a]P-3,6-quinone; diamond yellow line, B[a]P-1,6-quinone; both up and down pointing triangle blue line, 7,8-dihydro-B[a]P-diol (isomers); square green line, 4,5-dihydro-B[a]P-



diol; dot pink line, 9,10-dihydro-B[a]P-diol. To reduce overlap of the respective curves figure 1b present the data for all metabolites except 3-hydroxyBaP on a different y-axis scale.

**Table 4.** Metabolites of B[a]P formed in incubations with rat liver microsomes and the corresponding kinetic parameters.

Metabolites	Structure	$K_m$ , $\mu M$	$V_{max}$ , pmol/min/mg microsomal protein	Catalytic efficiency ( $V_{max}/K_m$ ), $\mu l/min/mg$ protein
9,10-dihydro-B[a]P-diol		11.9 $\pm$ 5.5	28.3 $\pm$ 2.8	2.4
4,5-dihydro-B[a]P-diol		6.5 $\pm$ 4.5	13.3 $\pm$ 1.4	2.0
7,8-dihydro-B[a]P-diol		14.6 $\pm$ 9.8	7.0 $\pm$ 1.1	0.5
7,8-dihydro-B[a]P-diol		12.6 $\pm$ 10.7	13.3 $\pm$ 2.5	1.1
B[a]P-1,6-quinone		14.8 $\pm$ 8.8	22.2 $\pm$ 3.2	1.5
B[a]P-3,6-quinone		24.0 $\pm$ 14.4	3.0 $\pm$ 0.5	0.1
9-hydroxy-B[a]P		11.4 $\pm$ 5.2	20.0 $\pm$ 1.9	1.8
3-hydroxy-B[a]P		34.2 $\pm$ 17.7	162.2 $\pm$ 47.6	7.8

Given these results, in the PBK model the metabolism of B[a]P was described by two Michaelis Menten equations, one to describe the bioactivation of B[a]P to 3-OHB[a]P, and the other to describe the combined conversion to all other metabolites together. **Figure 3** presents the corresponding curves and **Table 5** shows the kinetic parameter values,  $V_{max}$  and  $K_m$ , derived from these data. The  $V_{max}$  of 3-OHB[a]P formation and the  $V_{max}$  for the sum of formation of all other minor metabolites were 0.16 and 0.13 nmol/min/mg microsomal protein, respectively amounting to 4.1 and 3.3  $\mu$ mol/min/liver, when scaled to the whole liver using the scaling factor described in section 2.2.2.

**Table 5.** Kinetic parameter values for liver metabolism of B[a]P and 3-OHB[a]P in rat

	$V_{max}^a$	$K_m^b$	Scaled $V_{max}^c$	Scaled $V_{max}^d$
B[a]P to 3-OHB[a]P	0.16	34	0.44	4.1
B[a]P to other metabolites	0.13	17	0.36	3.3
	$V_{max}^e$	$K_m (\mu M)^b$	Scaled $V_{max}^c$	Scaled $V_{max}^d$
Glucuronidated 3-OHB[a]P	5.7	10	43	394
Sulfated 3-OHB[a]P	0.48	17	3.6	33

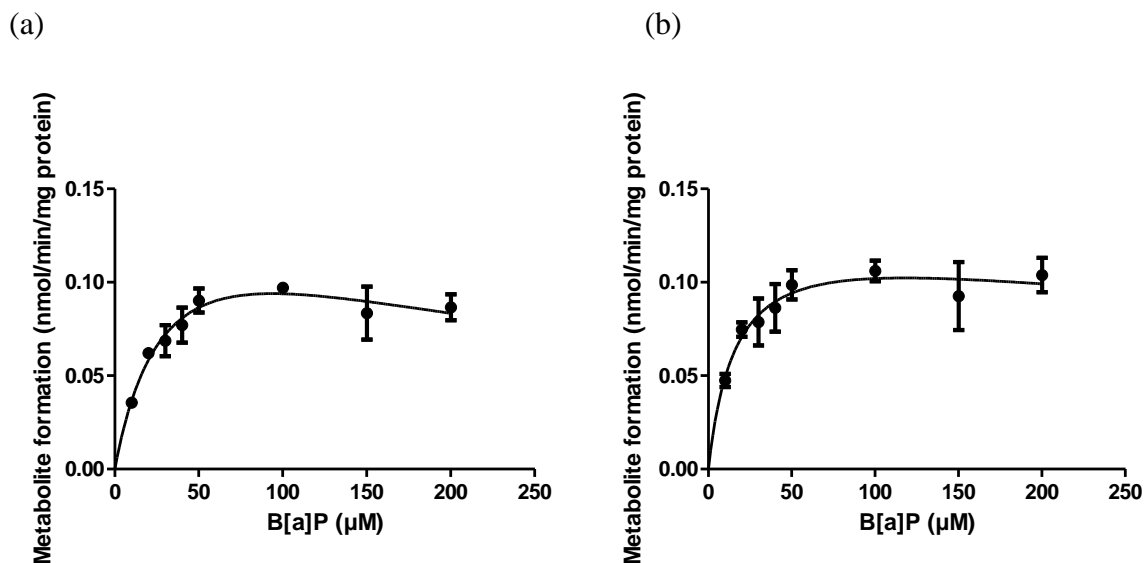
<sup>a</sup> nmol/min/mg microsomal protein

<sup>b</sup>  $\mu$ M

<sup>c</sup>  $\mu$ mol/h/g liver

<sup>d</sup>  $\mu$ mol/h/liver

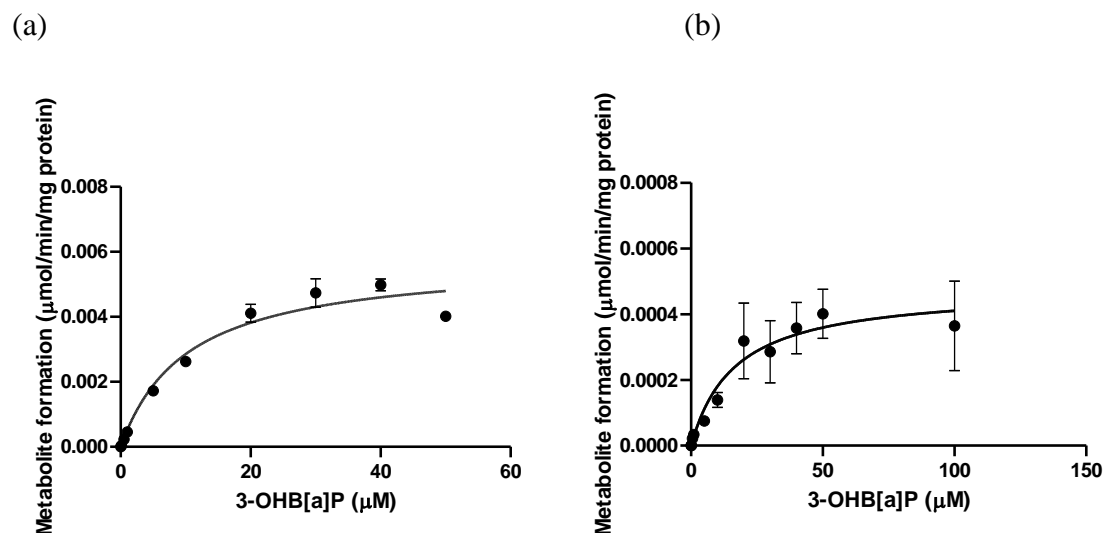
<sup>e</sup> nmol/min/mg S9 protein



**Figure 3.** Concentration-dependent oxidation of B[a]P to (a) 3-OHB[a]P and (b) sum of other metabolites in incubation with rat liver microsomes. Symbols represent the mean of three independent experiments, the error bars represent the standard error of the mean (SEM)

**Figure 4** shows the concentration dependent rate of (a) glucuronidation and (b) sulfation of 3-OHB[a]P in incubations with rat liver S9. Hepatic glucuronidation and sulfation of 3-OHB[a]P followed Michaelis-Menten kinetics. Substrate inhibition occurred at concentrations of 50 μM and higher for glucuronidation. **Table 5** shows the kinetic parameter values,  $V_{max}$  and  $K_m$ , derived from these data. Incubations of B[a]P with lung microsomes did not result in formation of detectable levels of 3-OHB[a]P, except for the incubations with the highest concentration of B[a]P (200 μM). The rate of 3-OHB[a]P formation at 200 μM B[a]P in rat lung microsomes amounted to 0.81 pmol/min/mg protein converted with a scaling factor of 3.67 mg microsomal protein/g lung and a lung weight of 1.25 g (**Table 1**) to a rate of conversion of 3.7 pmol/min/lung amounting to 0.01 % of the rate of conversion at 200 μM B[a]P in the liver of 86.6 pmol/min/mg microsomal protein, amounting to a rate of conversion of  $36.0 \times 10^3$  pmol/min/liver using the scaling factors for microsomal protein content of the liver and liver weight mentioned in section 2.2.2. Based on this

result is was concluded that 3-OHB[a]P formation from B[a]P in the lung does not add substantially to the overall 3-OHB[a]P formation and is not to be included in the PBK model.



**Figure 4.** Concentration-dependent glucuronidation (a) and sulfation (b) of 3-OHB[a]P in incubations with rat liver S9. Symbols represent the mean of three independent experiments, the error bars represent the standard error of the mean (SEM).

Incubations of 3-OHB[a]P with rat lung S9 and 50 μM 3-OHB[a]P showed that the formation rate of glucuronidated metabolites was 0.015 nmol/min/mg S9 protein, scaled to the whole lung with a scaling factor of 10.19 mg S9 protein/g lung and a lung weight of 1.25 g to a conversion rate of 0.19 nmol/min/lung. For liver, the glucuronidation rate at 50 μM 3-OHB[a]P was 4.0 nmol/min/mg S9 protein, amounting to  $4.6 \times 10^3$  nmol/min/liver, scaled to the whole liver using the scaling factor described in section 2.2.2. This implies that at 50 μM 3-OHB[a]P the pulmonary conversion rate amounted to approximately 0.04% of the hepatic conversion rate. For sulfonation, the estimated conversion rate in incubations with rat lung S9 and 50 μM 3-OHB[a]P was 0.001 nmol/min/mg S9 protein, amounting to 0.013 nmol/min/lung using the scaling factors mentioned above. For liver, the sulfation rate of 3-OHB[a]P at 50 μM 3-OHB[a]P was 0.40 nmol/min/mg

protein, scaled to the whole liver applying the scaling factors mentioned in section 2.2.2, resulting in 464 nmol/min/liver. Thus, for sulfonation, the pulmonary conversion rate is thus < 0.003% of the hepatic conversion rate. Based on these results, it was concluded that pulmonary conjugation of 3-OHB[a]P was negligible and therefore did not need to be included in the PBK model.

### 3.2 Evaluation of the PBK model and sensitivity analysis

Given that 3-OHB[a]P induces developmental toxicity in the EST (Kamelia et al. 2020) and that the aim of the present study was to translate in vitro EST data on 3-OHB[a]P to an in vivo dose-response curve for developmental toxicity of B[a]P, evaluation of the B[a]P PBK model focussed on the accuracy of predicting the 3-OHB[a]P levels. **Figure 5** presents the model predictions for B[a]P and their comparison to the literature reported values for blood B[a]P concentrations upon (a) intravenous, (b) intratracheal and (c) oral exposure. **Figure 6** shows a comparison of the predicted time-dependent blood concentrations of 3-OHB[a]P to reported in vivo time-dependent blood concentrations of 3-OHB[a]P in rats upon (a) intravenous, (b) intratracheal and (c) oral exposure to a dose of 10 mg B[a]P/kg bw/day. The data presented in Figure 5a and Figure 6a reveal that the model predictions for both B[a]P and 3-OHB[a]P match the experimental data of Marie et al. (2010) well, while the data of Moreau and Bouchard (2015), that were obtained at a similar dose level, report blood concentrations that are substantially lower than those reported by Marie et al. and/or the predictions. **Table 6** summarises the maximum blood concentrations ( $C_{\max}$ ) of 3-OHB[a]P in rat blood reported in vivo and predicted by the PBK model. Although in both experimental in vivo studies rats of the same strain were exposed intravenously to the same dose of 10 mg/kg bw/day, the predicted  $C_{\max}$  values differed. As a result the  $C_{\max}$  reported by Marie et al. (2010) was 1.1- fold higher and that of Moreau and Bouchard (2015) was 3.1- fold lower than the predicted  $C_{\max}$ . The predicted  $C_{\max}$  of 3-OHB[a]P was 4.6- and 9.6- fold higher upon

intratracheal and oral exposure to B[a]P respectively, compared to the  $C_{\max}$  of 3-OHB[a]P reported in the study of Moreau and Bouchard (2015) (Figure 6b and 6c). The study by Marie et al. (2010) did not report data for intratracheal or oral dosing, and as a result a comparison between predictions and experimental data for these routes of administration could only be made using the data of Moreau and Bouchard. When correcting these experimental data for intratracheal and oral dosing using the factor difference observed between the two experimental data sets upon intravenous dosing, the scaled experimental data of Moreau and Bouchard match the model predictions much better. The predicted  $C_{\max}$  of 3-OHB[a]P was 0.8 and 1.9 fold higher upon intratracheal and oral exposure to B[a]P respectively, compared to the scaled  $C_{\max}$  of 3-OHB[a]P reported in the study of Moreau and Bouchard (2015). The apparent discrepancy between the two available in vivo studies is not surprising considering the mean value of 3-OHB[a]P recovery in the Moreau and Bouchard study was reported to be relatively low (43% in blood).

**Table 6.** Maximum blood concentration ( $C_{\max}$ ) of 3-OHB[a]P in rat blood reported in vivo and predicted by the PBK model upon intravenous, intratracheal and oral administration of 10 mg/kg bw BaP

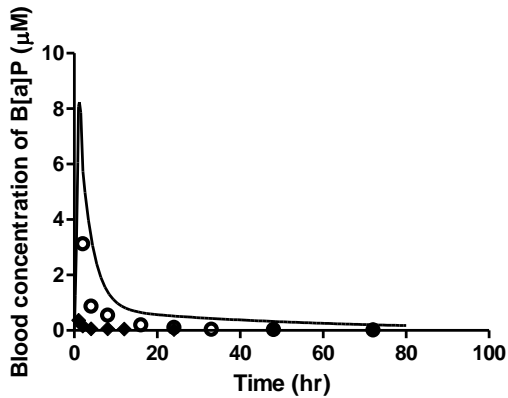
Reference	Route of exposure	$C_{\max}$ predicted ( $\mu\text{M}$ )	$C_{\max}$ reported ( $\mu\text{M}$ )	$C_{\max}$ predicted/ $C_{\max}$ reported
Moreau and Bouchard, 2015	Intravenous	0.68	0.22	3.1
Marie et al., 2010	Intravenous	0.68	0.72	0.9
Moreau and Bouchard, 2015	Intratracheal	0.65	0.14	4.6
Scaled Moreau and Bouchard, 2015	Intratracheal	0.65	0.77	0.8

Moreau and Bouchard, 2015	Oral	0.96	0.10	9.6
Scaled Moreau and Bouchard, 2015	Oral	0.96	0.51	1.9

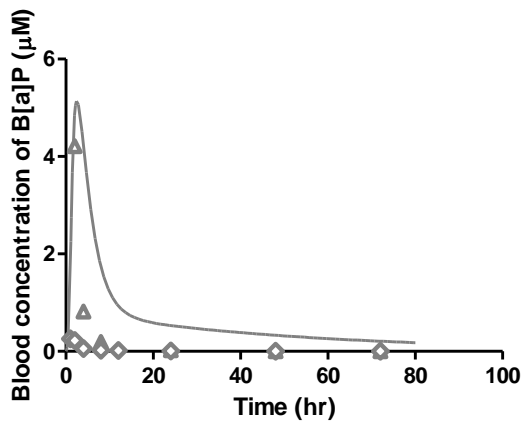
Based on these observations it was concluded that the PBK model predicted the plasma  $C_{\max}$ , for 3-OHB[a]P well enough for further use and evaluation of the PBK model by using it for PBK model based reverse dosimetry. The predictions made by the PBK model based reverse dosimetry may then also be used to further evaluate the model and its predictions.

To enable prediction of repeated dose exposures the PBK model was extended to allow repeated daily dosing. Steady state in the blood concentration of 3-OHB[a]P upon repeated exposure to B[a]P was reached after approximately 15 repetitions for all three routes of exposure. The  $C_{\max}$  values for 3-OHB[a]P predicted for repeated intravenous, intratracheal and oral exposure to B[a]P were 1.7, 1.7 and 1.4 times higher than the predicted  $C_{\max}$  values upon a single B[a]P dose for these three routes of exposure. A figure presenting the model predicted time-dependent blood concentrations for repeated intravenous, intratracheal and oral exposure to B[a]P is included in supplementary materials 2 (Figure S1).

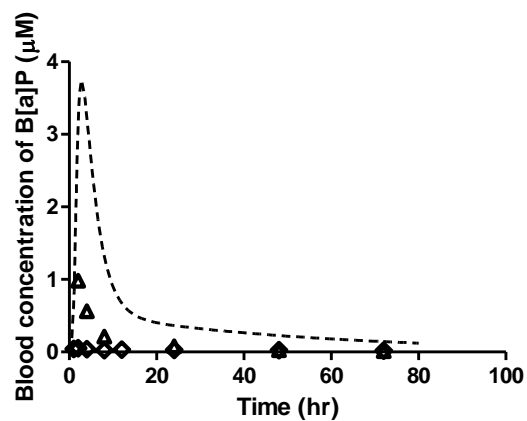
(a)



(b)



(c)

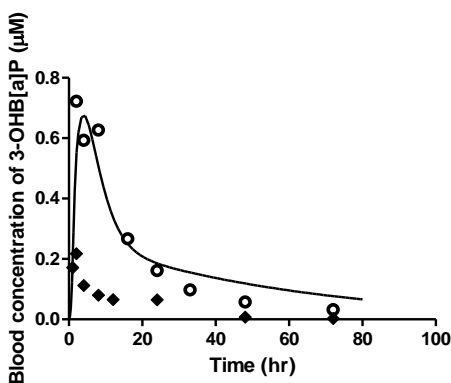


**Figure 5.** Reported and predicted blood concentrations of B[a]P in rats upon (a) intravenous, (b) intratracheal and (c) oral exposure to 10 mg/kg B[a]P in rats. Symbols represent (a) the average blood concentrations reported in the in vivo studies of Moreau and Bouchard (2015) (filled diamonds) and Marie et al. (2010) (open circles) for intravenous exposure, (b) the average blood concentrations reported in the in vivo study of Moreau and Bouchard (2015) (grey open diamonds) and scaled Moreau data (grey open triangles) upon intratracheal exposure, and (c) the average blood concentrations reported in the vivo study of Moreau and Bouchard (2015) (black open diamonds) and scaled Moreau data (black open triangles) upon oral exposure. The lines represent

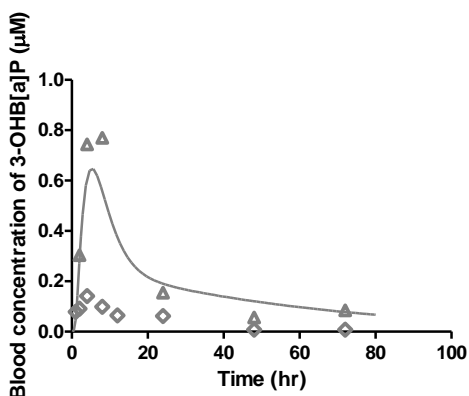


the model predicted blood concentrations upon (a) intravenous (black solid line), (b) intratracheal (grey solid line) and (c) oral (black dashed line) exposure.

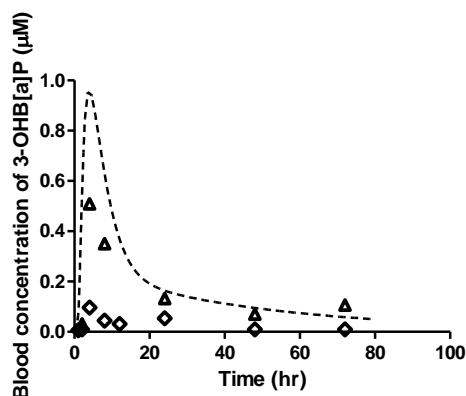
(a)



(b)



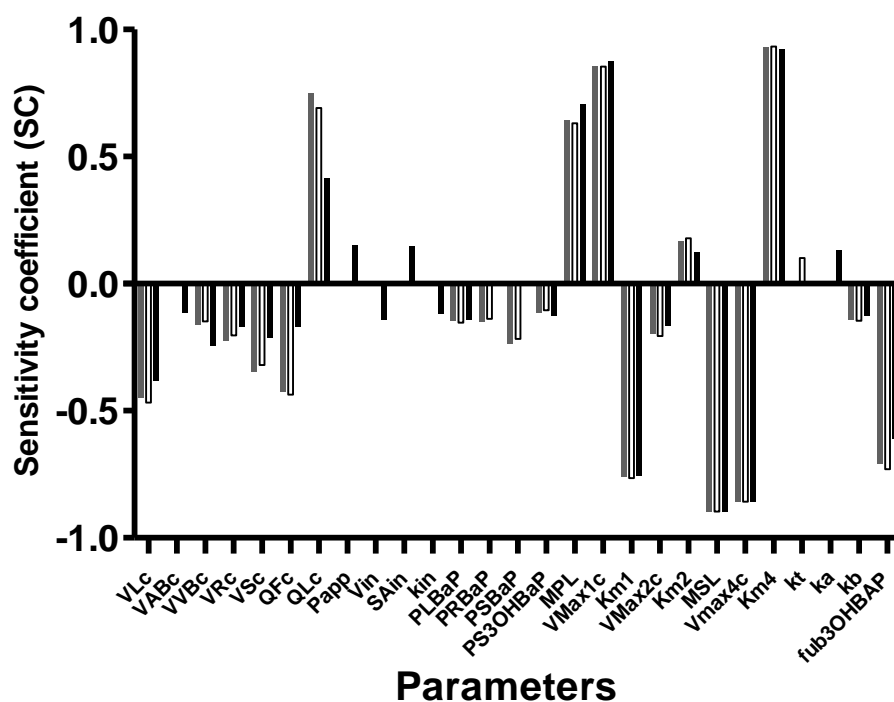
(c)



**Figure 6.** Reported and predicted blood concentrations of 3-OHB[a]P in rats upon (a) intravenous, (b) intratracheal and (c) oral exposure to 10 mg/kg B[a]P in rats. Symbols represent (a) the average blood concentrations reported in the in vivo studies of Moreau and Bouchard (2015) for intravenous (filled diamonds) and Marie et al. (2010) (open circles) for intravenous exposure. Symbols represent (b) the average blood concentrations reported in the in vivo studies of Moreau and Bouchard (2015) (grey open diamonds) and scaled Moreau data based on the folds observed in intravenous data (grey open triangles) upon intratracheal exposure. Symbols represent (c) the

average blood concentrations reported in in vivo studies of Moreau and Bouchard (2015) (black open diamonds) and scaled Moreau data based on the folds observed in intravenous data (black open triangles) upon oral exposure. The lines represent the model predicted blood concentrations upon (a) intravenous (black solid line), (b) intratracheal (grey solid line) and (c) oral (black dashed line) exposure.

A sensitivity analysis was performed to identify the parameter values that have the highest influence on the model simulations for the  $C_{\max}$  of 3-OHB[a]P in blood upon intratracheal, intravenous and oral exposure to 10 mg/kg bw B[a]P. Sensitivity coefficients with an absolute value of 0.1 and higher are shown in **Figure 7**. Parameters related to fractional blood flow to liver tissue (QLc), the fraction unbound of 3-OHB[a]P ( $f_{ub3OHB[a]P}$ ), microsomal and S9 protein content of the liver (MPL and MSL) and kinetic parameters for the metabolism of B[a]P and glucuronidation of 3-OHB[a]P ( $K_{m1}$ ,  $K_{m4}$ ,  $V_{max1c}$ ,  $V_{max4c}$ ) were found to be most influential on the simulated  $C_{\max}$  of 3-OHB[a]P.

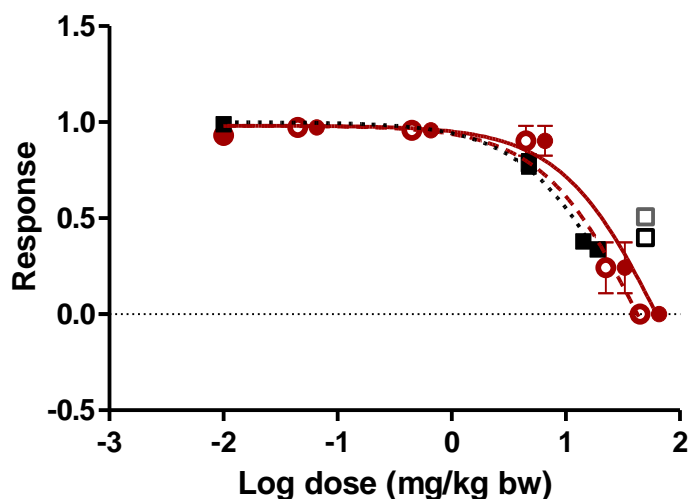


**Figure 7.** Sensitivity coefficients (SC) of PBK model parameters for the predicted C<sub>max</sub> of 3-OHB[a]P in rat blood after intravenous (grey bars), oral (black bars) or intratracheal (white bars) administration of 10 mg/kg bw B[a]P. Model parameters with an absolute SC of  $\geq 0.1$  are shown. VLC = fraction of liver tissue, VABc = fraction of arterial blood, VVBc = fraction of venous blood, VRc = fraction of rapidly perfused tissue, VSc = fraction of slowly perfused tissue, QFc = fraction of blood flow to fat, QLC = fraction of blood flow to liver, QLUc = fraction of blood flow to lung, Papp = apparent intestinal permeability coefficient in vitro obtained in the Caco-2 model, Vin = volume of each compartment of intestines, SAin = surface area intestinal compartment, kin = transfer rate to next compartment within the intestines, PLBaP = liver/blood partition coefficient of B[a]P, PRBaP = rapidly perfused tissue:blood partition coefficient of B[a]P, PSBaP = slowly perfused tissue: blood partition coefficient of B[a]P, PS3OHBaP = slowly perfused tissue:blood partition coefficient of 3-OHB[a]P, MPL = microsomal protein content in liver, Vmax1c =

maximum rate of 3-OHB[a]P formation in liver,  $K_{m1}$  = Michaelis-Menten constant for metabolism of B[a]P to 3-OHB[a]P in liver,  $V_{max2c}$  = maximum rate formation of other metabolites in liver,  $K_{m2}$  = Michaelis-Menten constant for metabolism of B[a]P to other metabolites,  $MSL$  = S9 protein content in liver,  $V_{max4c}$  = maximum rate of glucuronidation of 3-OHB[a]P formation in liver,  $K_{m4}$  = Michaelis-Menten constant for glucuronidation 3-OHB[a]P in liver,  $k_t$  = absorption constant from tracheal to lung of B[a]P,  $k_a$  = absorption constant stomach of B[a]P to GI-tract,  $k_b$  = excretion constant bile to faeces of B[a]P,  $f_{ubBaP}$  = fraction unbound of B[a]P,  $f_{ub3OHBaP}$  = fraction unbound of 3-OHB[a]P

### **3.3 Translating in vitro concentration-response data into in vivo dose-response data using PBK modelling-based reverse dosimetry**

Using the PBK model thus obtained and evaluated, the in vitro concentration-response data from the EST for 3-OHB[a]P were translated into a dose-response curve for the developmental toxicity of B[a]P, after correction for differences in free fraction of 3-OHB[a]P in vivo and in vitro. Differences in protein binding between the in vitro and in vivo situation were corrected for as described in the materials and methods section 2.2.4 with the values for  $f_{ub, \text{in vitro}}$  of 0.007 and  $f_{ub, \text{in vivo}}$  of 0.0035. This correction provides the total blood  $C_{max}$  value that matches the total in vitro concentration in the EST corrected for protein binding. Using a curve relating the PBK model predicted total blood  $C_{max}$  values of 3-OHB[a]P to the oral dose levels of B[a]P, the EST concentration-response curve for in vitro developmental toxicity of 3-OHB[a]P was converted to an in vivo dose-response curve for developmental toxicity of B[a]P. The predicted dose-response curve for single exposure to B[a]P thus obtained is shown in **Figure 8**. In addition, **Figure 8** also presents the dose-response curve predicted based on the steady state  $C_{max}$  values obtained upon repeated oral exposure to B[a]P.



**Figure 8.** Model predicted and reported in vivo dose-response curves for developmental toxicity of B[a]P in rats upon single and repeated oral exposure. The predicted dose-response curves are translated from the concentration response curve obtained in the EST for 3-OHB[a]P (Kamelia et al., 2020) representing single oral exposure (filled red circles and red solid line) and repeated oral exposure (red open circles and red dashed line). Filled black squares and dotted black line represent the in vivo data of Archibong et al., (2002), the open squares represent the data of Bui et al., (1986) for 3 day exposure (black open square) and 6 day exposure (grey open square). The error bars represent the standard error of the mean (SEM).

### **Evaluation of the PBK modelling-based reverse dosimetry based predictions**

To evaluate the predicted dose-response curves for developmental toxicity of B[a]P, **Figure 8** also presents the in vivo dose-response data on reproductive toxicity of B[a]P, represented by the foetal survival, reported in literature upon exposure of rats to B[a]P via nasal inhalation for 10 days (Archibong et al. 2002) and for subcutaneous B[a]P exposure for 3 and 6 days in rats (Bui et al. 1986). For this comparison, the inhalation dose levels in the study of Archibong et al., (2002) were

expressed in equivalent oral dose levels in mg/kg bw per day reported previously (Hood et al. 2000; Ramesh et al. 2002) (**Table 3**). Visual comparison of the dose-response curves reveals that the predicted dose response curves are in agreement with the experimental data. This further evaluates the PBK model for prediction of 3-OHB[a]P  $C_{\max}$  values upon exposure to B[a]P.

The ED<sub>50</sub> values derived from the predicted and reported dose-response curves, amount to 67 mg/kg bw for single oral exposure to B[a]P, 45 mg/kg bw per day for repeated oral exposure to B[a]P and 29 mg/kg bw per day for the reported in vivo data (Archibong et al. 2002). From the in vivo data of Bui et al., (1986) no ED<sub>50</sub> values could be calculated, but the reported effect doses are in line with the model predictions, corroborating the accuracy of the predicted dose-response curves.

#### **4. Discussion**

In vivo studies have demonstrated the reproductive toxicity of B[a]P (Archibong et al. 2002; Archibong et al. 2012; Bui et al. 1986). The aim of the present study was to evaluate the use of an in vitro- in silico approach using PBK model-facilitated reverse dosimetry for predicting the developmental toxicity of B[a]P based on in vitro toxicity data from the EST for 3-OHB[a]P, the main metabolite of B[a]P responsible for the developmental toxicity of B[a]P in the EST (Kamelia et al. 2020). The intermediate role of 3-OHB[a]P in the developmental toxicity of B[a]P also follows from the fact that B[a]P itself tested negative in the EST without bioactivation (Kamelia et al. 2020). Previous studies have shown that in vivo developmental toxicity can adequately be predicted using reverse dosimetry based on the EST for several compounds, including both compounds for which the developmental toxicity is ascribed to the parent compound itself as well as compounds for which the effect is due to a metabolite (Li et al. 2017a; Louisse et al. 2015;

Louisse et al. 2010b; Strikwold et al. 2017; Strikwold et al. 2013). So far, however, this approach has not been assessed for PAHs, although PAH-containing petroleum substances make up a large part of chemicals that require developmental toxicity testing under REACH. The current study shows that the in vitro-in silico approach is suitable for predicting developmental toxicity of B[a]P in rats, based on in vitro data of the EST for its major metabolite 3-OHB[a]P, responsible for the developmental toxicity in vitro.

For reverse dosimetry, EST data for 3-OHB[a]P and not B[a]P were used, as the ES-D3 cells of the EST appear to lack sufficient bioactivation activity to convert B[a]P into the active metabolite 3-OHB[a]P, explaining why B[a]P tested negative in the EST (Kamelia et al. 2020). Previous studies confirmed this explanation, since only pre-incubation of B[a]P with hamster liver microsomes prior to testing in the EST, resulted in a positive response that reflected the level of 3-OHB[a]P formation in the pre-incubation (Kamelia et al. 2020). These findings explicate the need for including bioactivation of B[a]P to its reactive metabolite 3-OHB[a]P, and further metabolism and clearance of 3-OHB[a]P in the quantitative in vitro – in vivo extrapolation (QIVIVE) for evaluation of the developmental toxicity of B[a]P.

The metabolism of B[a]P and 3-OHB[a]P was represented in the current PBK model by the  $V_{max}$  and  $K_m$  determined in in vitro incubations with subcellular fractions. Similar studies using rat lung microsomes revealed that pulmonary conversion of B[a]P into 3-OHB[a]P was negligible compared to the conversion in the liver. This finding was supported by previous results from microsomal incubations, showing that the metabolic rate of metabolite formation from B[a]P in rat lung was only 0.008% of liver metabolism (Prough et al. 1979). Further results obtained in the present study for conjugation of 3-OHB[a]P in incubations with rat liver and lung S9 revealed that also the conjugation of 3-OHB[a]P mainly occurs in liver. Thus in the PBK model formation and

clearance of 3-OHB[a]P was modelled in the liver compartment, while conversion in the lung was considered negligible and not included in the model code.

The PBK model developed was evaluated based on available in vivo data for 3-OHB[a]P blood concentrations as measured upon dosing 10 mg B[a]P/kg bw by various routes of administration, including intravenous, intratracheal and oral exposure (Marie et al. 2010; Moreau and Bouchard 2015). B[a]P and 3-OHB[a]P are highly lipophilic compounds, as reflected by their high LogP value. When developing the PBK model, it appeared essential to include a protein binding compartment in the blood compartment in order to prevent virtually all B[a]P to partition into the fat tissue, where it would remain unavailable for metabolism to 3-OHB[a]P. By allowing binding to blood protein, B[a]P remained in the circulation and available for metabolism in the model simulations. Evaluation of the B[a]P PBK model was focused on adequate prediction of 3-OHB[a]P levels, as 3-OHB[a]P is the main inducer of developmental toxicity in vitro and the objective of the present study was to translate in vivo EST data for 3-OHB[a]P into an in vivo dose-response curve for B[a]P (Kamelia et al. 2020). Comparison of the model predictions to the available in vivo data revealed that the model somewhat overpredicted the blood concentrations of 3-OHB[a]P reported by Moreau and Bouchard (2015), while it adequately predicted the data reported by Marie et al. (2010) and the scaled Moreau data. Given that both in vivo studies were performed in the same strain of rat, using the same route of administration and a similar B[a]P dose level, it appears that the deviations between the model predictions and the reported in vivo data may originate to a substantial extent from variants between the two experimental data sets. The results from microsomal incubation of B[a]P reveal that the  $V_{\max}$  and catalytic efficiency for formation of 3-OHB[a]P are 5.7- to 54- fold and 3.3- to 78- folds higher than for formation of the other metabolites. These results indicate that the other metabolic routes play a less prominent role than 3-OHB[a]P



formation in the metabolism of B[a]P. Furthermore, comparison of the in vitro developmental toxicity in the EST of 3-OHB[a]P and a mixture of B[a]P metabolites formed in an incubation of B[a]P with hamster liver microsomes revealed that the in vitro developmental toxicity of the mixture of B[a]P metabolites could be fully ascribed to the level of 3-OHB[a]P in this metabolite mixture (Kamelia et al. 2020). Given these results and considerations, the model was used for translation of the in vitro EST data for 3-OHB[a]P into a predicted in vivo dose response curve for developmental toxicity of B[a]P, using PBK model facilitated reverse dosimetry. The ED<sub>50</sub> values derived from the predicted in vivo dose-response curve for single and repeated oral exposure thus obtained, were in agreement with the ED<sub>50</sub> value calculated for the in vivo data of Archibong et al., 2002 and in line with the in vivo data of Bui et al., 1986. These results further support the validity of the PBK model for predicting in vivo 3-OHB[a]P blood concentrations. The results also indicate that the in vitro- in silico approach provides an adequate estimate of the developmental toxicity of B[a]P in rats. In spite of this, it is relevant to note that the EST detects development of embryonic stem cells into beating cardiomyocytes and may not reflect the specific sensitive endpoints of developmental toxicity observed upon B[a]P exposure in animal studies, such as developmental neurotoxicity (Li et al. 2012; McCallister et al. 2008; Sheng et al. 2010; Wormley et al. 2004). Inclusion of in vitro assays representing additional developmental toxicity endpoints may enhance the currently developed approach, broadening its applicability for toxicological risk assessment to an even further extent. It should be acknowledged that the endpoint characterised, the exposure regimen used and the window of sensitivity of the EST protocol may not match the exposure scenario, endpoint characterised and window of sensitivity for a compound when detecting its developmental toxicity in an in vivo study. These discrepancies may be a factor contributing to differences between predicted dose response curves and observed dose response data. Furthermore, when translating EST data to in vivo dose-response curves and comparing the predictions thus

obtained to in vivo data on developmental toxicity, it is worth to note that in vivo studies may report a variety of endpoints including for example cardiac malformations, resorptions, fetal body weight decrease, skeletal malformation, visceral malformations and also fetal deaths. In previous studies we have shown that the EST in vitro data can be used to adequately predict these different in vivo developmental toxicity endpoints (Kamelia et al. 2017; Li et al. 2016; Li et al. 2017b; Louisse et al. 2015; Louisse et al. 2010a; Louisse et al. 2011; Strikwold et al. 2017; Strikwold et al. 2012).

In conclusion, the present study shows that the developed PBK modelling-based reverse dosimetry approach can adequately predict in vivo developmental toxicity of B[a]P based on in vitro data from the EST for 3-OHB[a]P, the metabolite responsible for this adverse effect. The predicted ED<sub>50</sub> values adequately reflected the ED<sub>50</sub> value calculated from the in vivo data. This study provides a proof of principle for an integrated in vitro- in silico approach for predicting in vivo developmental toxicity of B[a]P. The method may provide a promising strategy for predicting the developmental toxicity of related polycyclic aromatic hydrocarbons (PAHs), without the need for animal testing.

## References

- Archibong AE, Inyang F, Ramesh A, et al. (2002) Alteration of pregnancy related hormones and fetal survival in F-344 rats exposed by inhalation to benzo(a)pyrene. *Reproductive toxicology* (Elmsford, NY) 16(6):801-8 doi:10.1016/s0890-6238(02)00058-8
- Archibong AE, Ramesh A, Inyang F, Niaz MS, Hood DB, Kopsombut P (2012) Endocrine disruptive actions of inhaled benzo(a)pyrene on ovarian function and fetal survival in fisher F-344 adult rats. *Reproductive toxicology* (Elmsford, NY) 34(4):635-43 doi:10.1016/j.reprotox.2012.09.003
- Brown RP, Delp MD, Lindstedt SL, Rhomberg LR, Beliles RP (1997) Physiological parameter values for physiologically based pharmacokinetic models. *Toxicol Ind Health* 13(4):407-84 doi:10.1177/074823379701300401
- Buesen R, Genschow E, Slawik B, et al. (2009) Embryonic Stem Cell Test Remastered: Comparison between the Validated EST and the New Molecular FACS-EST for Assessing Developmental Toxicity In Vitro. *Toxicological Sciences* 108(2):389-400 doi:10.1093/toxsci/kfp012
- Bui QQ, Tran MB, West WL (1986) A comparative study of the reproductive effects of methadone and benzo [a] pyrene in the pregnant and pseudopregnant rat. *Toxicology* 42(2):195-204 doi:[https://doi.org/10.1016/0300-483X\(86\)90009-0](https://doi.org/10.1016/0300-483X(86)90009-0)
- Campbell J, Franzen A, Van Landingham C, et al. (2016) Predicting lung dosimetry of inhaled particleborne benzo[a]pyrene using physiologically based pharmacokinetic modeling. *Inhal Toxicol* 28(11):520-35 doi:10.1080/08958378.2016.1214768
- Chou MW (1983) In vitro metabolism of 8- and 9-fluorobenzo[a]pyrene. In: J. CMDA (ed) *Polynuel Aromat Hydrocarbons Int Symp*, 7th. Battelle Press, Columbus, Ohio

- Cohen GM (1990) Pulmonary metabolism of foreign compounds: its role in metabolic activation. Environ Health Perspect 85:31-41 doi:10.1289/ehp.85-1568313
- Cohen GM, Moore BP (1976) Metabolism of (3H)benzo(a)pyrene by different portions of the respiratory tract. Biochem Pharmacol 25(14):1623-9 doi:10.1016/0006-2952(76)90474-3
- Crowell SR, Amin SG, Anderson KA, et al. (2011a) Preliminary physiologically based pharmacokinetic models for benzo[a]pyrene and dibenzo[def,p]chrysene in rodents. Toxicology and applied pharmacology 257(3):365-376 doi:10.1016/j.taap.2011.09.020
- Crowell SR, Amin SG, Anderson KA, et al. (2011b) Preliminary physiologically based pharmacokinetic models for benzo[a]pyrene and dibenzo[def,p]chrysene in rodents. Toxicol Appl Pharmacol 257(3):365-76 doi:10.1016/j.taap.2011.09.020
- Evans MV, Andersen ME (2000) Sensitivity analysis of a physiological model for 2,3,7,8-tetrachlorodibenzo-p-dioxin (TCDD): assessing the impact of specific model parameters on sequestration in liver and fat in the rat. Toxicological sciences : an official journal of the Society of Toxicology 54(1):71-80 doi:10.1093/toxsci/54.1.71
- Feuston MH, Hamilton CE, Mackerer CR (1996) Systemic and Developmental Toxicity of Dermally Applied Distillate Aromatic Extract in Rats. Fundamental and Applied Toxicology 30(2):276-284 doi:<https://doi.org/10.1006/faat.1996.0065>
- Feuston MH, Kerstetter SL, Singer EJ, Mehlman MA (1989) Developmental toxicity of clarified slurry oil applied dermally to rats. Toxicology and industrial health 5(3):587-599
- Feuston MH, Low LK, Hamilton CE, Mackerer CR (1994) Correlation of Systemic and Developmental Toxicities with Chemical Component Classes of Refinery Streams. Fundamental and Applied Toxicology 22(4):622-630 doi:<https://doi.org/10.1006/faat.1994.1068>

- Feuston MH, Mackerer CR (1996) Developmental toxicity of clarified slurry oil, syntower bottoms, and distillate aromatic extract administered as a single oral dose to pregnant rats. *Journal of toxicology and environmental health* 49(1):45-66
- Genschow E, Spielmann H, Scholz G, et al. (2004) Validation of the embryonic stem cell test in the international ECVAM validation study on three in vitro embryotoxicity tests. *Alternatives to laboratory animals : ATLA* 32(3):209-44 doi:10.1177/026119290403200305
- Genschow E, Spielmann H, Scholz G, et al. (2002) The ECVAM international validation study on in vitro embryotoxicity tests: results of the definitive phase and evaluation of prediction models. European Centre for the Validation of Alternative Methods. *Alternatives to laboratory animals : ATLA* 30(2):151-76 doi:10.1177/026119290203000204
- Goth-Goldstein R, Holman H-YN, Russell ML (1999) In vitro model for intestinal uptake of benzo(a)pyrene. Berkeley Lab, <https://indoor.lbl.gov/publications/vitro-model-intestinal-uptake>
- Gulden M, Morchel S, Tahan S, Seibert H (2002) Impact of protein binding on the availability and cytotoxic potency of organochlorine pesticides and chlorophenols in vitro. *Toxicology* 175(1-3):201-13 doi:10.1016/s0300-483x(02)00085-9
- Hamernik KL (1984) A comparative study of the metabolism of 6-methylbenzo[a]pyrene and benzo[a]pyrene by rat liver microsomes. Uniformed Services University of the Health Sciences
- Hamernik KLC, Pei Lu, Chou, Ming W., Fu, Peter P., and Yang, Shen K. (1983) Metabolic Activation of 6-methylbenzo[a]pyrene. . In: Cooke MD, Anthony J. (ed) *Polynucl Aromat Hydrocarbons Int Symp*, 7th. Battelle Press, Columbus, Ohio. , p 583-597

- Heredia-Ortiz R, Bouchard M (2013) Understanding the linked kinetics of benzo(a)pyrene and 3-hydroxybenzo(a)pyrene biomarker of exposure using physiologically-based pharmacokinetic modelling in rats. *Journal of pharmacokinetics and pharmacodynamics* 40(6):669-82 doi:10.1007/s10928-013-9338-9
- Heredia-Ortiz R, Bouchard M, Marie-Desvergne C, Viau C, Maître A (2011) Modeling of the Internal Kinetics of Benzo(a)pyrene and 3-Hydroxybenzo(a)pyrene Biomarker from Rat Data. *Toxicological Sciences* 122(2):275-287 doi:10.1093/toxsci/kfr135
- Heredia Ortiz R, Maître A, Barbeau D, Lafontaine M, Bouchard M (2014) Use of physiologically-based pharmacokinetic modeling to simulate the profiles of 3-hydroxybenzo(a)pyrene in workers exposed to polycyclic aromatic hydrocarbons. *PLoS One* 9(7):e102570-e102570 doi:10.1371/journal.pone.0102570
- Hood DB, Nayyar T, Ramesh A, Greenwood M, Inyang F (2000) Modulation in the developmental expression profile of Sp1 subsequent to transplacental exposure of fetal rats to desorbed benzo[a]pyrene following maternal inhalation. *Inhal Toxicol* 12(6):511-35 doi:10.1080/089583700402897
- Houston JB, Galetin A (2008) Methods for predicting in vivo pharmacokinetics using data from in vitro assays. *Current drug metabolism* 9(9):940-51 doi:10.2174/138920008786485164
- Jagt K, Munn S, Torslov J, Bruijn J (2004) Alternative approaches can reduce the use of test animals under REACH. Report EUR 2
- Kamelia L, de Haan L, Spenkelink B, et al. (2020) The role of metabolism in the developmental toxicity of polycyclic aromatic hydrocarbon-containing extracts of petroleum substances. *J Appl Toxicol* 40(3):330-341 doi:10.1002/jat.3906
- Kamelia L, Louisse J, de Haan L, Rietjens I, Boogaard PJ (2017) Prenatal developmental toxicity testing of petroleum substances: Application of the mouse embryonic stem cell test (EST)

to compare in vitro potencies with potencies observed in vivo. *Toxicol in Vitro* 44:303-312  
doi:10.1016/j.tiv.2017.07.018

Koehl W, Amin S, Staretz ME, et al. (1996) Metabolism of 5-methylchrysene and 6-methylchrysene by human hepatic and pulmonary cytochrome P450 enzymes. *Cancer Res* 56(2):316-24

Li, Zhang, Vervoort, Rietjens, van Ravenzwaay, Louisse (2017a) Use of physiologically based kinetic modeling-facilitated reverse dosimetry of in vitro toxicity data for prediction of in vivo developmental toxicity of tebuconazole in rats. *Toxicology letters* 266:85-93  
doi:10.1016/j.toxlet.2016.11.017

Li H, Flick B, Rietjens IM, Louisse J, Schneider S, van Ravenzwaay B (2016) Extended evaluation on the ES-D3 cell differentiation assay combined with the BeWo transport model, to predict relative developmental toxicity of triazole compounds. *Arch Toxicol* 90(5):1225-37  
doi:10.1007/s00204-015-1541-6

Li H, Zhang M, Vervoort J, Rietjens IM, van Ravenzwaay B, Louisse J (2017b) Use of physiologically based kinetic modeling-facilitated reverse dosimetry of in vitro toxicity data for prediction of in vivo developmental toxicity of tebuconazole in rats. *Toxicol Lett* 266:85-93 doi:10.1016/j.toxlet.2016.11.017

Li Z, Chadalapaka G, Ramesh A, et al. (2012) PAH particles perturb prenatal processes and phenotypes: protection from deficits in object discrimination afforded by dampening of brain oxidoreductase following in utero exposure to inhaled benzo(a)pyrene. *Toxicological sciences : an official journal of the Society of Toxicology* 125(1):233-47  
doi:10.1093/toxsci/kfr261

- Lobell M, Sivarajah V (2003) In silico prediction of aqueous solubility, human plasma protein binding and volume of distribution of compounds from calculated pKa and AlogP98 values. *Mol Divers* 7(1):69-87 doi:10.1023/b:modi.00000006562.93049.36
- Louisse J, Bosgra S, Blaauboer BJ, Rietjens IM, Verwei M (2015) Prediction of in vivo developmental toxicity of all-trans-retinoic acid based on in vitro toxicity data and in silico physiologically based kinetic modeling. *Arch Toxicol* 89(7):1135-48 doi:10.1007/s00204-014-1289-4
- Louisse J, de Jong E, van de Sandt JJ, et al. (2010a) The use of in vitro toxicity data and physiologically based kinetic modeling to predict dose-response curves for in vivo developmental toxicity of glycol ethers in rat and man. *Toxicol Sci* 118(2):470-84 doi:10.1093/toxsci/kfq270
- Louisse J, de Jong E, van de Sandt JJM, et al. (2010b) The Use of In Vitro Toxicity Data and Physiologically Based Kinetic Modeling to Predict Dose-Response Curves for In Vivo Developmental Toxicity of Glycol Ethers in Rat and Man. *Toxicological Sciences* 118(2):470-484 doi:10.1093/toxsci/kfq270
- Louisse J, Gonen S, Rietjens IM, Verwei M (2011) Relative developmental toxicity potencies of retinoids in the embryonic stem cell test compared with their relative potencies in in vivo and two other in vitro assays for developmental toxicity. *Toxicol Lett* 203(1):1-8 doi:10.1016/j.toxlet.2011.02.012
- Marie C, Bouchard M, Heredia-Ortiz R, Viau C, Maitre A (2010) A toxicokinetic study to elucidate 3-hydroxybenzo(a)pyrene atypical urinary excretion profile following intravenous injection of benzo(a)pyrene in rats. *Journal of applied toxicology : JAT* 30(5):402-10 doi:10.1002/jat.1511



- McCallister MM, Maguire M, Ramesh A, et al. (2008) Prenatal exposure to benzo(a)pyrene impairs later-life cortical neuronal function. *Neurotoxicology* 29(5):846-54 doi:10.1016/j.neuro.2008.07.008
- Moreau M, Bouchard M (2015) Comparison of the kinetics of various biomarkers of benzo[a]pyrene exposure following different routes of entry in rats. *Journal of applied toxicology : JAT* 35(7):781-90 doi:10.1002/jat.3070
- Moserova M, Kotrbova V, Aimova D, Sulc M, Frei E, Stiborova M (2009) Analysis of benzo[a]pyrene metabolites formed by rat hepatic microsomes using high pressure liquid chromatography: optimization of the method. *Interdiscip Toxicol* 2(4):239-44 doi:10.2478/v10102-009-0024-0
- Poulin P, Krishnan K (1995) An algorithm for predicting tissue: blood partition coefficients of organic chemicals from n-octanol: water partition coefficient data. *J Toxicol Environ Health* 46(1):117-29 doi:10.1080/15287399509532021
- Poulin P, Theil FP (2000) A priori prediction of tissue:plasma partition coefficients of drugs to facilitate the use of physiologically-based pharmacokinetic models in drug discovery. *J Pharm Sci* 89(1):16-35 doi:10.1002/(sici)1520-6017(200001)89:1<16::Aid-jps3>3.0.Co;2-e
- Prough RA, Patrizi VW, Okita RT, Masters BSS, Jakobsson SW (1979) Characteristics of Benzo(a)pyrene Metabolism by Kidney, Liver, and Lung Microsomal Fractions from Rodents and Humans. *Cancer research* 39(4):1199
- Punt A, Pinckaers N, Peijnenburg A, Louisse J (2021) Development of a Web-Based Toolbox to Support Quantitative In-Vitro-to-In-Vivo Extrapolations (QIVIVE) within Nonanimal Testing Strategies. *Chem Res Toxicol* 34(2):460-472 doi:10.1021/acs.chemrestox.0c00307

- Ramesh A, Hood DB, Inyang F, et al. (2002) Comparative Metabolism, Bioavailability, and Toxicokinetics of Benzo[a]pyrene in Rats After Acute Oral, Inhalation, and Intravenous Administration. *Polycyclic Aromatic Compounds* 22(3-4):969-980  
doi:10.1080/10406630290104121
- Sheng L, Ding X, Ferguson M, et al. (2010) Prenatal polycyclic aromatic hydrocarbon exposure leads to behavioral deficits and downregulation of receptor tyrosine kinase, MET. *Toxicological sciences : an official journal of the Society of Toxicology* 118(2):625-34  
doi:10.1093/toxsci/kfq304
- Sims P (1968) The synthesis of 8- and 9-hydroxybenzo[a]pyrene and the role of the products in benzo[a]pyrene metabolism. *J Chem Soc Perkin 1* 1:32-4 doi:10.1039/j39680000032
- Strikwold M, Spenkelink B, de Haan LHJ, Woutersen RA, Punt A, Rietjens I (2017) Integrating in vitro data and physiologically based kinetic (PBK) modelling to assess the in vivo potential developmental toxicity of a series of phenols. *Arch Toxicol* 91(5):2119-2133  
doi:10.1007/s00204-016-1881-x
- Strikwold M, Spenkelink B, Woutersen RA, Rietjens IM, Punt A (2013) Combining in vitro embryotoxicity data with physiologically based kinetic (PBK) modelling to define in vivo dose-response curves for developmental toxicity of phenol in rat and human. *Arch Toxicol* 87(9):1709-23 doi:10.1007/s00204-013-1107-4
- Strikwold M, Woutersen RA, Spenkelink B, Punt A, Rietjens IM (2012) Relative embryotoxic potency of p-substituted phenols in the embryonic stem cell test (EST) and comparison to their toxic potency in vivo and in the whole embryo culture (WEC) assay. *Toxicol Lett* 213(2):235-42 doi:10.1016/j.toxlet.2012.07.005

- Sun D, Lennernas H, Welage LS, et al. (2002) Comparison of human duodenum and Caco-2 gene expression profiles for 12,000 gene sequences tags and correlation with permeability of 26 drugs. *Pharmaceutical research* 19(10):1400-16 doi:10.1023/a:1020483911355
- Torbert HC (1935) THE EFFECT OF FASTING ON THE SERUM PROTEIN CONCENTRATION OF THE RAT : WITH SPECIAL REFERENCE TO THE QUESTION OF THE EXISTENCE OF AN IMMEDIATELY UTILIZABLE CIRCULATING PROTEIN FRACTION. *J Exp Med* 62(1):1-10 doi:10.1084/jem.62.1.1
- Veignie E, Rafin C, Woisel P, Sahraoui ALH, Cazier F (2002) Metabolization of the polycyclic aromatic hydrocarbon benzo(a)pyrene by a non-white rot fungus (*Fusarium solani*) in a batch reactor. *Polycycl Aromat Comp* 22(1):87-97 doi:Doi 10.1080/10406630210372
- Withey JR, Shedden J, Law FC, Abedini S (1993) Distribution of benzo[a]pyrene in pregnant rats following inhalation exposure and a comparison with similar data obtained with pyrene. *Journal of applied toxicology : JAT* 13(3):193-202 doi:10.1002/jat.2550130310
- Wormley DD, Chirwa S, Nayyar T, et al. (2004) Inhaled benzo(a)pyrene impairs long-term potentiation in the F1 generation rat dentate gyrus. *Cell Mol Biol (Noisy-le-grand)* 50(6):715-21
- Wu J, Ramesh A, Nayyar T, Hood DB (2003) Assessment of metabolites and AhR and CYP1A1 mRNA expression subsequent to prenatal exposure to inhaled benzo(a)pyrene. *International journal of developmental neuroscience : the official journal of the International Society for Developmental Neuroscience* 21(6):333-46 doi:10.1016/s0736-5748(03)00073-x
- Yang SK, Selkirk JK, Plotkin EV, Gelboin HV (1975) Kinetic analysis of the metabolism of benzo(a)pyrene to phenols, dihydrodiols, and quinones by high-pressure chromatography

compared to analysis by aryl hydrocarbon hydroxylase assay, and the effect of enzyme induction. *Cancer Res* 35(12):3642-50

Zhang M, van Ravenzwaay B, Fabian E, Rietjens I, Louisse J (2018) Towards a generic physiologically based kinetic model to predict in vivo uterotrophic responses in rats by reverse dosimetry of in vitro estrogenicity data. *Arch Toxicol* 92(3):1075-1088  
doi:10.1007/s00204-017-2140-5

## **Funding**

This work was supported by Concawe, Belgium ([www.concawe.eu](http://www.concawe.eu)) (grant number: 201506110) and Operationeel Programma Kansen voor West II (EFRO), The Netherlands (KVV-00181).

## **Acknowledgements**

The authors acknowledge dr. Jerry Campbell and dr. Harvey Clewell for their contributions to the development of the model code.

## **Conflicts of interest/Competing interests**

Maartje H. Rietdijk, Danlei Wang, and Ivonne M.C.M. Rietjens declare that they have no conflict of interest. Peter J. Boogaard and Lenny Kamelia are employed by Shell International, a member company of Concawe. Both Prof. Boogaard and dr. Kamelia are totally free (by contract) to freely design and conduct research and express their own scientific opinion without any obligation towards either Shell or Concawe. The current findings are not intended to constitute any product endorsement.

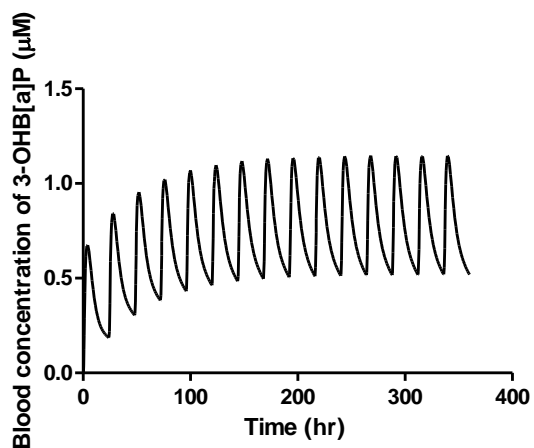
## **Supplementary material 1**

For convenience, the model code for the developed PBK model can be found at:

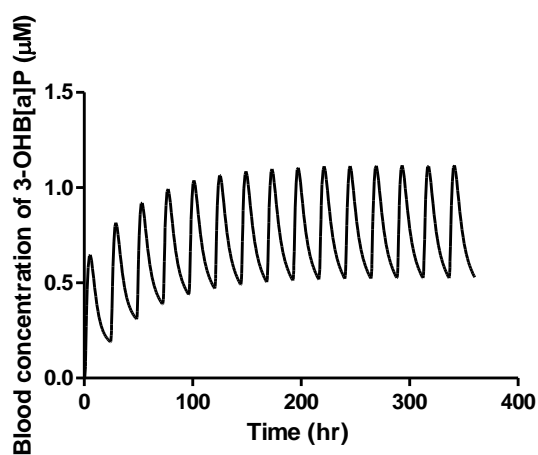
[https://static-content.springer.com/esm/art%3A10.1007%2Fs00204-021-03128-7/MediaObjects/204\\_2021\\_3128\\_MOESM1\\_ESM.docx](https://static-content.springer.com/esm/art%3A10.1007%2Fs00204-021-03128-7/MediaObjects/204_2021_3128_MOESM1_ESM.docx)

## Supplementary materials 2

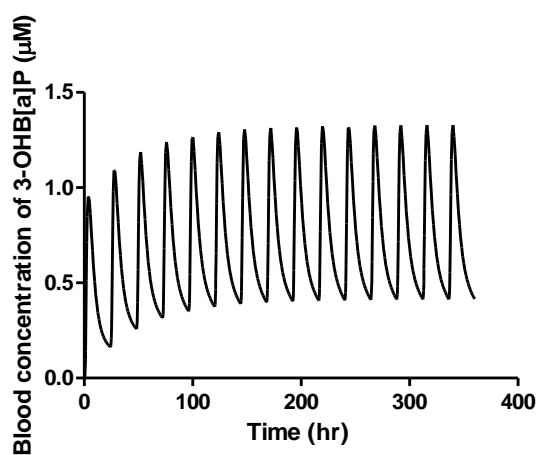
(a)



(b)



(c)



**Figure S1.** Predicted time-dependent blood concentrations of 3-OHB[a]P in rats upon repeated (a) intravenous, (b) intratracheal and (c) oral exposure to 10 mg/kg/day B[a]P in rats.





## **Chapter 6**

### **General discussion and future perspectives**

## **Overview of the main findings**

Foodborne mineral oil aromatic hydrocarbons (MOAH) are an emerging safety concern for human health based on the current occurrence and hazard evaluation. MOAH are not well-defined substances but rather a fraction that can be detected using analytical methods that include chromatographic separation. The presence of MOAH in food could originate from contamination, food contact materials, intended application of mineral oils in processing, or other sources. EFSA estimated that the background exposure via food to hydrocarbons detectable as MOAH accounts of 15-30% of the total intake of mineral oil hydrocarbons (EFSA 2012). The presence of alkyl-substituted PAHs in the MOAH fraction and their structural similarity to some hazardous PAHs makes MOAH of potential concern for genotoxicity, carcinogenicity and developmental toxicity. However, the lack of toxicological data on MOAH and alkyl substituted PAHs seriously hampers hazard and risk characterization.

This thesis provides data on oxidative metabolism and resulting toxicities of a series of selected non- and alkyl-substituted PAHs using in vitro assays. In particular, oxidative metabolic patterns of the selected non- and alkyl-substituted aromatic hydrocarbons mediated by human and rat liver cytochrome P450 enzymes were investigated. The metabolism of the selected alkylated PAHs via aromatic ring and alkyl side chain was characterized reflecting the relative chances in metabolic pathways with potential consequences for bioactivation and detoxification. The effect of monomethyl substitution of PAHs on their mutagenicity was studied in the Ames test. Moreover, an in vitro - in silico alternative testing approach was applied for prediction of the in vivo developmental toxicity of a selected PAH.

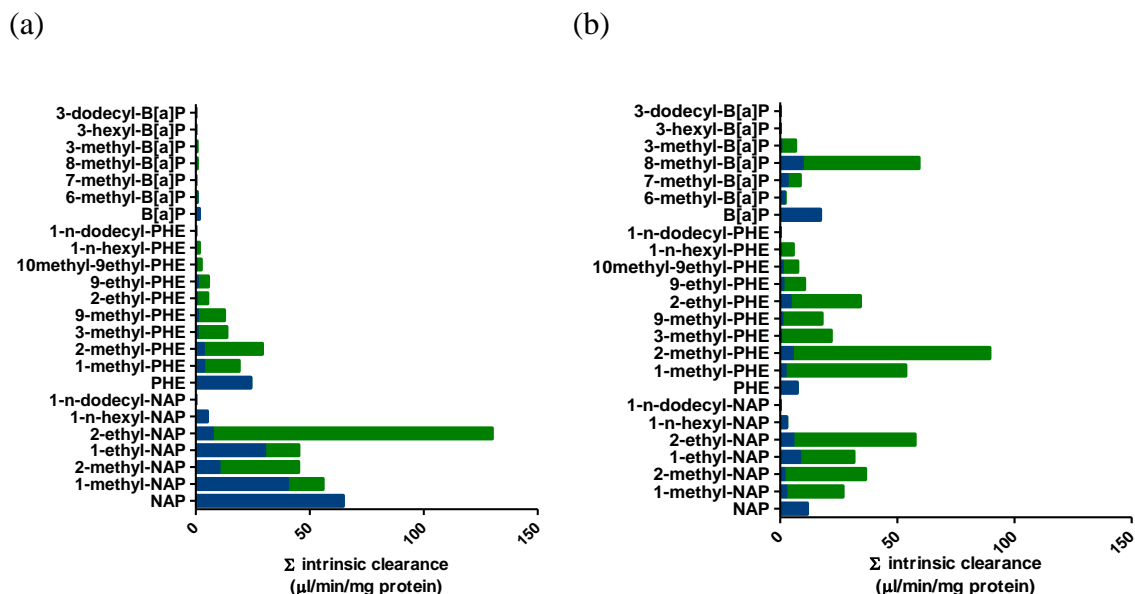
## **The effect of alkyl substitution on oxidative metabolism of aromatic hydrocarbons**

The oxidative metabolism of naphthalene, phenanthrene, benzo[a]pyrene and some of their alkyl substituted analogues was described in **Chapter 2**, **Chapter 3** and **Chapter 4**, respectively, using human liver microsomes (HLM) and rat liver microsomes (RLM). This allowed characterization of the metabolism of the selected model compounds via aromatic ring oxidation as compared to alkyl side chain oxidation (**Figure 1**). On thermodynamic grounds, it was hypothesized that the saturated alkyl side-chain of a substituted PAHs is more easily oxidized than the aromatic ring system. In line with the hypothesis, it was observed that, in general, oxidative metabolism of the short alkyl side-chains ( $\leq C3$ ) of the selected 2-ring, 3-ring and 5-ring aromatic hydrocarbons was preferred over aromatic ring oxidation for both HLM and RLM. This metabolic shift to side-chain oxidation indicates relatively higher chances for excretion and lower chances for bioactivation towards metabolites that might contribute to genotoxicity, carcinogenicity and developmental toxicity. Metabolism of n-hexyl substituted naphthalene, phenanthrene and benzo[a]pyrene resulted in different types of metabolic shifts and included phenols and dihydrodiols (both type of metabolites reflecting aromatic ring oxidation), and side chain hydroxylated metabolites), respectively, based on tentative metabolite identification following incubations with both HLM and RLM. This difference might be due to the different docking approaches between the cytochrome P450 enzymes and the highly substituted aromatic moieties of these model compounds having a different size and structure.

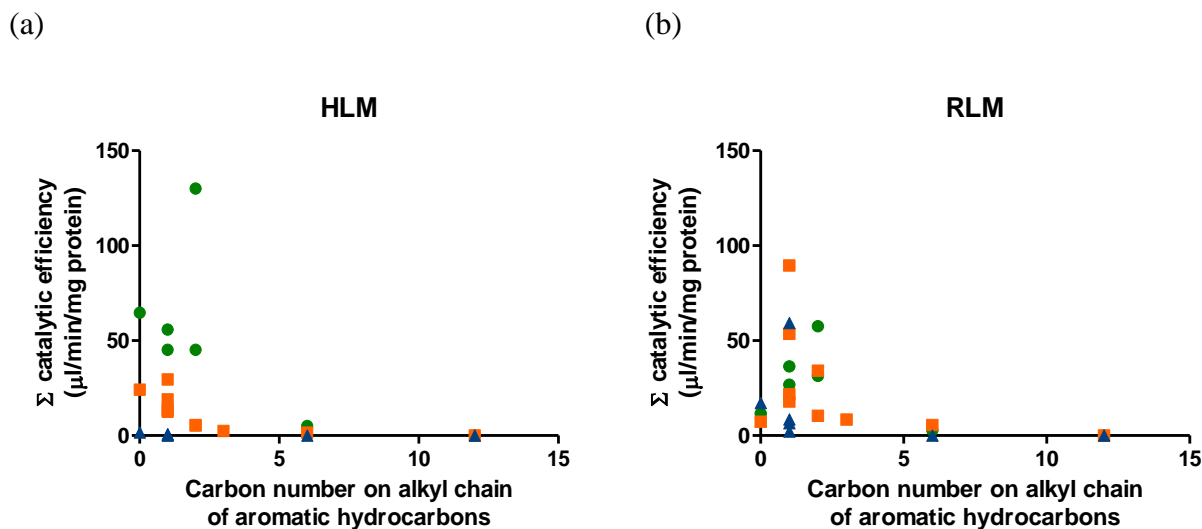
A decrease in overall catalytic efficiency ( $\Sigma Cl_{int}$ ) with elongation of the alkyl chain of the substituted naphthalene, phenanthrene and benzo[a]pyrene was observed (**Figure 2**). Short alkyl substitution ( $< C3$ ) may increase or decrease the overall metabolism of naphthalene, phenanthrene and benzo[a]pyrene. However, a substantial reduction of overall metabolism was observed for the

selected aromatic hydrocarbons that were substituted with side chains with 6 or more carbon atoms. Following incubation with dodecyl (C12) substituted naphthalene, phenanthrene and benzo[a]pyrene with HLM and RLM no metabolic conversion was observed under the experimental conditions applied.

Species difference in the metabolic shift and the metabolite pattern of the selected non-substituted and alkyl-substituted aromatic hydrocarbons between HLM and RLM was also noticed. In most incubations of the selected model compounds, the metabolic shift from aromatic ring oxidation towards preferential aliphatic side chain oxidation was more pronounced with HLM than RLM. An exception for the preference in aromatic ring oxidation observed with 1-methyl-naphthalene and 1-ethyl-naphthalene with HLM could best be ascribed to a difference in metabolic activity of specific CYP isoforms between HLM and RLM (**Chapter 2**). Interestingly, the overall catalytic efficiency for conversion of naphthalene was 2.7- fold higher than that of phenanthrene and 39.7- fold higher than that of benzo[a]pyrene in HLM, while, the overall catalytic efficiency of naphthalene was 1.6-fold higher than phenanthrene and 1.5- fold lower than benzo(a)pyrene in RLM. A grouping effect by aromatic ring number for overall catalytic efficiency of non-substituted and alkyl-substituted aromatic hydrocarbons in HLM was observed but not in RLM (**Figure 2**). Altogether, the rate, regioselectivity and type of P450 mediated metabolism of the non-substituted and alkyl-substituted aromatic hydrocarbons depends on species, as well as on the site and nature of the alkyl substituent.



**Figure 1.** Intrinsic clearance via aromatic ring and alkyl side chain oxidation by (a) HLM (b) RLM for the model compounds of the present thesis. Side chain oxidation: green bars; Aromatic ring oxidation: blue bars. NAP = naphthalene; PHE = phenanthrene; B[a]P = benzo[a]pyrene

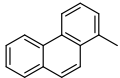
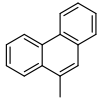
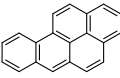
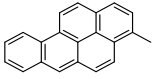
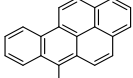
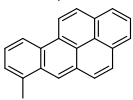
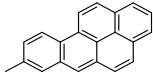


**Figure 2.** Relationship between total catalytic efficiency ( $\Sigma\text{Cl}_{\text{int}}$ ) of alkylated PAHs and the number of carbon atoms on the alkyl side chain in incubations with (a) HLM and (b) RLM. Green dots: phenanthrene and its alkyl substituents; Orange squares: naphthalene and its alkyl substituents; blue triangles: benzo[a]pyrene and its alkyl substituents

## **The effect of alkyl substitution on mutagenicity of PAHs**

The effect of alkyl substitution on mutagenicity of PAHs was assessed in the present thesis using the reverse mutation assay (Ames test). The non-substituted (“naked”) PAHs and monomethylated PAHs among the selected model compounds that tested positive (**Chapter 3 and Chapter 4**) are summarized in **Table 1**. In line with the hypothesis, 1-methyl- and 9-methyl- phenanthrene tested as positive mutagens upon metabolic activation with rat S9 in both tester strain TA98 and TA100, which was related to the fact that in these methylated phenanthrenes the methyl group generates an additional bay region-like structural motif (“fake” bay region). While, non-substituted phenanthrene as well as 2-methyl- and 3-methyl- phenanthrene without this additional “fake” bay region tested negative (**Chapter 3**). All selected non-substituted benzo[a]pyrene and monomethyl substituted benzo[a]pyrenes tested positive towards both tester strain TA98 and TA100. The methyl substitution of benzo[a]pyrene may increase or decrease the mutagenic potency depending the position of the substitution. The observed mutagenic potency of the alkyl substituted benzo[a]pyrene appeared to be not necessarily associated with the number of “fake” bay regions, possibly due to the complexity of the involved metabolic pathways via 4,5-oxide, 7,8-dihydrodiol-epoxide and/or side chain oxidation and their stereoselectivity (**Chapter 4**).

**Table 1.** Mutagenicity of selected non-substituted PAHs and their monomethyl substituents using Aroclor 1254 induced rat S9 and NADPH-generating system as metabolic system in the Ames test in *S. typhimurium* strains TA 98 and TA100. Mutagenic efficacy of each compound was calculated from the maximal increase in the number of revertants divided by that of the solvent control, expressed as fold induction. Mutagenic potency of each compound is presented as the maximum value of the net increase in number of revertants divided by the dose, expressed as revertants per nmol. Only compounds that tested positive in at least one of the tester strains were included.

Compound	Structure	<i>S. typhimurium</i> strain			
		TA98		TA100	
		Mutagenic efficacy	Mutagenic potency	Mutagenic efficacy	Mutagenic potency
1-methyl-phenanthrene		14	1.7	7	4.1
9-methyl-phenanthrene		3	0.6	2	0.9
benzo[a]pyrene		44	69	5	21
3-methyl-benzo[a]pyrene		57	19	8	43
6-methyl-benzo[a]pyrene		100	187	3	8
7-methyl-benzo[a]pyrene		40	39	4	24
8-methyl-benzo[a]pyrene		24	39	7	34

### Proposed relevant metabolic activation pathways of alkyl substituted PAHs

Bioactivation of non-substituted PAHs such as benzo[a]pyrene was extensively studied for its genotoxicity and carcinogenicity and is generally accepted to proceed via the dihydrodiol-epoxide pathway. This thesis provided the metabolic pathways of alkyl-substituted PAHs which may be

responsible for their excretion but also for their genotoxicity, carcinogenicity and developmental toxicity for which the toxicological data are rare. The profiles of oxidative metabolism of the selected alkyl-substituted phenanthrene and benzo[a]pyrene analogues in S9 incubations were studied using the same experimental conditions as applied in the Ames test (**Chapter 3 and Chapter 4**). The possible underlying metabolic pathways included the proposed dihydrodiol-epoxide pathway, formation of a 4,5-oxide, a side chain oxidation and sulfation pathway for genotoxicity and carcinogenicity, and the formation of phenol metabolites that may play a role in the mode of action for developmental toxicity (**Figure 3**).

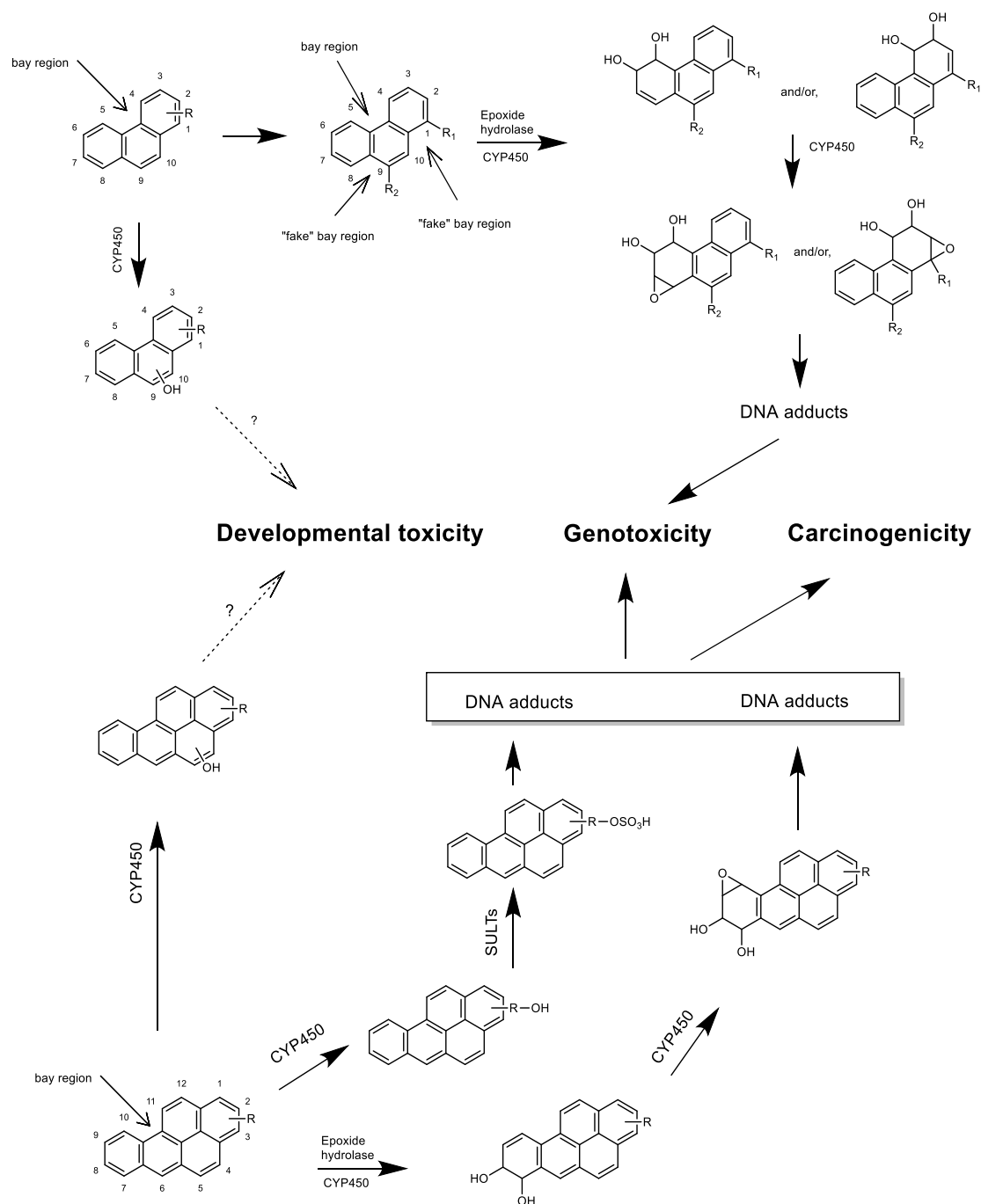
Phenanthrene is the smallest PAH that has a bay region, although it lacks genotoxic and carcinogenic potential (IARC, 2010). Methyl substitution at both the C1 and C9 position (K region) but no other positions of phenanthrene that introduces an additional bay region aromatic motif and induced mutagenicity as observed in Ames test towards tester strain TA98 and TA100. The possible underlying metabolic pathway for genotoxicity of 1-methyl- and 9-methyl-phenanthrene was proposed to be associated with dihydrodiol-epoxide formation, specifically the formation of 3,4- and/or 5,6-dihydrodiol that reflects the formation of the presumed ultimate mutagen 3,4-dihydrodiol-1,2-epoxide and/or 5,6-dihydrodiol-7,8-epoxide (**Figure 3**) (**Chapter 3**). None of the methyl substituted phenanthrenes was found to be an active tumor initiator in mouse skin painting studies, possibly due to the relatively low tumor inducing potency of the formed DNA adducts (LaVoie, Tulley-Freiler et al. 1981).

Two possible metabolic pathways for genotoxicity and carcinogenicity of methyl-substituted benzo[a]pyrene were proposed including the dihydrodiol-epoxide pathway, also relevant for benzo[a]pyrene itself, and side chain hydroxylation followed by sulfation (**Figure 3**) (**Chapter 4**). The skin tumor-initiating activity of some selected methyl substituted benzo[a]pyrenes was



reported for non-alkylated benzo[a]pyrene and 3-methyl-benzo[a]pyrene as being potent, for 6-methyl-benzo[a]pyrene as being weak, while 7-methyl- and 8-methyl-benzo[a]pyrene were inactive (Iyer, Lyga et al. 1980). This is in line with the formation of a 7,8-dihydrodiol, which reflects the formation of the ultimate mutagenic and carcinogenic 7,8-dihydrodiol-9,10-epoxide, from benzo[a]pyrene and its 3-,7- and 6- methyl-substituted analogues, while being negligible for 8-methyl-benzo[a]pyrene,. It is also of interest that it has been reported that the side chain oxidation metabolite of 6-methyl-benzo[a]pyrene is conjugated by sulfotransferases to a DNA reactive sulfate ester of 6-methyl-benzo[a]pyrene that was proven to be the ultimate carcinogen (Cavalieri, Roth et al. 1978, Rogan, Hakam et al. 1983, Stansbury, Flesher et al. 1994). It remains to be elucidated if methyl substitution at non-meso positions can follow the side chain oxidation and sulfation pathway.

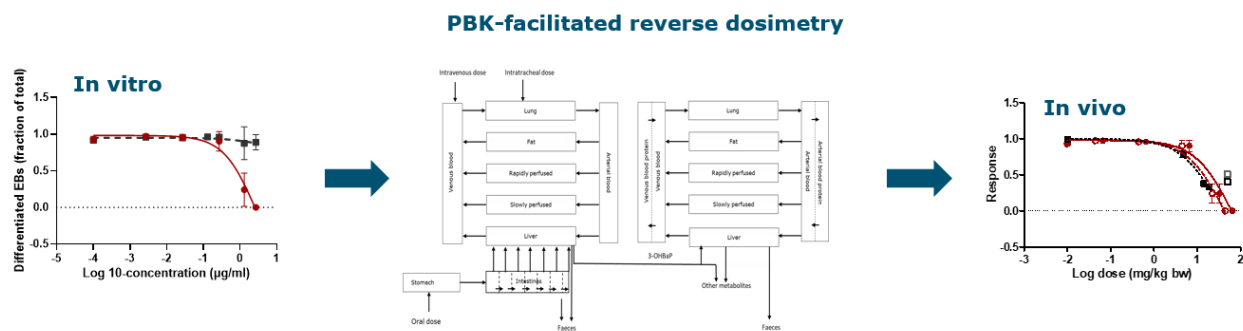
Developmental toxicity of benzo[a]pyrene and phenanthrene needs bioactivation to their phenolic metabolites in some in vitro models (Schrlau, Kramer et al. 2017, Kamelia, de Haan et al. 2020). Phenols were formed as primary metabolites of the selected alkyl substituted PAHs in the metabolism mediated by cytochrome P450 enzymes observed in the present thesis (**Chapter 3 and Chapter 4**). The effect of alkyl substitution of PAHs on the developmental toxicity remains to be elucidated.



**Figure 3.** Proposed possible metabolic pathways for genotoxicity, carcinogenicity and developmental toxicity of alkyl substituted phenanthrene and benzo[a]pyrene. R = CH<sub>3</sub> substitution

## **Physiologically based kinetic (PBK) modeling - facilitated QIVIVE**

The present thesis developed an in vitro-in silico approach to predict in vivo developmental toxicity of benzo[a]pyrene in rats using PBK model facilitated reverse dosimetry. Benzo[a]pyrene needs bioactivation to 3-hydroxy-benzo[a]pyrene by cytochrome P450 enzymes to induce developmental toxicity (Kamelia, de Haan et al. 2020). The PBK model of benzo[a]pyrene via intravenous, intratracheal and oral exposure routes was defined with a sub-model of 3-hydroxy-benzo[a]pyrene with the input of the kinetic parameters derived from metabolic studies (**Figure 4**). The time dependent plasma concentrations of benzo[a]pyrene and 3-hydroxy-benzo[a]pyrene via intravenous, intratracheal and oral exposure routes generated from the developed PBK model were validated by the in vivo kinetic data (Marie, Bouchard et al. 2010, Moreau and Bouchard 2015). The sufficiently validated PBK model was further used together with reverse dosimetry to translate the in vitro concentration-response data for 3-hydroxy-benzo[a]pyrene derived from the embryonic stem cell test (EST) into in vivo dose-response predictions for developmental toxicity upon single and repeated dose exposure. The predicted half maximal effect doses ( $ED_{50}$ ) of benzo[a]pyrene were comparable to the reported  $ED_{50}$  derived from the in vivo dose response data (Bui, Tran et al. 1986, Archibong, Inyang et al. 2002). The developed PBK modeling facilitated a QIVIVE approach as described in this thesis and provides a proof of principle of applying an in vitro-in silico approach for developmental toxicity prediction needed to enable risk assessment based on alternative to animal testing methods.



**Figure 4.** Scheme of the QIVIVE using an in vitro concentration response curve derived from the EST and PBK modelling facilitated reverse dosimetry to predict an in vivo dose response curve for developmental toxicity of benzo[a]pyrene. For details see Chapter 5 of the thesis.

## Literature and future perspectives

### Challenges in hazard assessment of MOAH

For the risk assessment of MOAH, a reference point (RP) cannot be derived for MOE calculation because dose-response data for the carcinogenicity of MOAH are not available also because MOAH is not a chemically defined substance (EFSA 2012). Challenges for the hazard and risk assessment on MOAH that remain to be resolved are discussed in the following sections.

#### 1. MOAH composition

The compounds that appear as MOAH in chromatographic determinations vary in ring number and alkylation degree and this puts challenges for the hazard characterization. The data on metabolism and mutagenicity in this thesis indicated that the ring number, type and position of the alkyl substituents, together affect the metabolism and the subsequent mutagenicity of the non-substituted (“naked”) and alkyl-substituted PAHs. In line with the observations in this thesis, historical studies on dermal carcinogenicity in vivo also suggested the ring number, alkylation degree and position

of the alkyl substituent to influence the tumor-initiating activity of non-substituted (“naked”) and alkyl-substituted PAHs (Iyer, Lyga et al. 1980, Wislocki, Gadek et al. 1980, LaVoie, Tulley-Freiler et al. 1981). Different proportional levels of hazardous PAHs in MOAH may lead to different toxicity outcomes indicating that the hazard characterization of MOAH should be based on the ring number and alkylation degree of the different congeners in the mixture and has therefore to be considered on a case by case basis. In other words, the available data on MOAH for one sample may not be applicable for other samples with similar MOAH characteristics as it may be composed of compounds with different ring-number and alkylation levels of PAHs. Therefore, a systematic RP such as one BMDL<sub>10</sub> value of MOAH may not correctly characterize the hazard of MOAH, which should be determined case by case based on testing of the individual sample.

## **2. The role of biotransformation**

Based on the kinetic data generated in the present thesis and historical studies, the aromatic ring number and alkylation degree of the aromatic hydrocarbons play important roles in their bioactivation and resulting toxicities. The carbon number of the model compounds in the present studies ranged from C<sub>10</sub>-C<sub>32</sub>. The highly alkylated (multi-branched and unbranched) low-ring aromatic hydrocarbons can have as many carbon numbers as short or simple alkylated high-ring aromatic hydrocarbons. They have different physical properties (**Figure 7** in **Chapter 1**) and are converted with different metabolic efficiency and metabolic patterns that subsequently influence the resulting toxicities. In particular, mainly 3-7 ring PAHs with short or simple alkyl side chain substitution in petroleum substances may contribute to the potential genotoxicity, carcinogenicity and developmental toxicity (Agarwal, Shukla et al. 1988, Ingram, Scammells et al. 1994, Concauwe 1996, Mackerer, Griffis et al. 2003, Concauwe 2014, Kamelia, Louisse et al. 2017, Kamelia, de Haan et al. 2019). The long chain alkylated aromatic hydrocarbons ( > C<sub>6</sub> side chain) tested in

**Chapter 2, 3 and 4** showed extremely low metabolic conversion that indicates lower chances on bioactivation and potential toxicities. This observation seems in line with the negative mutagenic effect of octadecyl substituted naphthalene and benzo[a]pyrene derivatives in the reverse mutation assay (Heyst 2019). Furthermore, the results of the reverse mutation assay revealed that also short alkyl substituted PAHs can be mutagenic and bioactivated, specifically 1- and 9- monomethylated phenanthrenes (**Chapter 3**) and 3-, 6-, 7-, 8- monomethylated benzo[a]pyrenes (**Chapter 4**). Therefore, it is of high importance to characterize MOAH in food matrices not only based on ring number but also with respect to the nature and regioselectivity of the alkylation in addition to total MOAH presence. Ring number and alkylation pattern based characterization of MOAH could be achieved to some extent by two dimensional GC×GC-FID (Biedermann and Grob 2009) and possibly nuclear magnetic resonance (NMR), etc. This will allow the exclusion of the “harmless MOAH” and facilitate exposure assessment of the hazardous MOAH fraction.

### **3. Limitation of testing DMSO extracts with bio-systems**

Dimethyl sulphoxide (DMSO) aromatic extracts have been generally used in the in vitro and in vivo bio-systems for the assessment of genotoxicity, carcinogenicity and developmental toxicity of petroleum derived products including mineral oils (Concawe 1994, Concawe 2012, Kamelia 2019). Such bio-systems include the modified Ames test, the mouse skin painting assay, the embryonic stem cell test (EST) and the zebrafish embryonic test (ZET) etc. The petroleum derived oil samples are extracted by DMSO following a standardized method known as IP346 (Standards 1996). The DMSO extracts contain the non-substituted and partially alkylated polycyclic aromatic compounds (PAC), however not the aromatic compounds that are substituted by a long alkyl chain (Carrillo, van der Wiel et al. 2019). This is in line with the present thesis (**Chapter 2, Chapter 3**

**and Chapter 4)** that showed that naphthalene, phenanthrene and benzo[a]pyrene substituted with hexyl- and dodecyl- side chains were no longer dissolved in DMSO. The lack of selectivity of DMSO extraction for PAC with long alkyl side chains may lead to underestimation in the hazard assessment of the petroleum derived products including mineral oils because the unextracted highly alkylated PAC fraction may have an additive effect on toxicities, such as the promotion effect observed in carcinogenicity studies (described in section 5). The sensitivity of the bioassays applied is also of concern since their sensitivity may not always allow detection of a genotoxic or carcinogenic PAC present at a low percentage unless it is a congener with a high potency allowing its detection in an in vitro or in vivo bioassay. False negative results in a bioassay may thus lead to underestimation of the hazard.

#### **4. Matrix effects**

The analytical characterization of MOAH samples is performed based on chromatographic analysis of hydrocarbons in food. MOAH are not chemically defined as individual substances or mixtures. Foodborne MOAH may originate from contamination such as application of unrefined mineral oil and lubricating oil, migration from food contact materials, intentional uses as additives, processing aids, pesticides and others. The complexity of MOAH sources, makes MOAH analysis in food matrices a challenge requiring complex sample preparation, and analysis. The current JRC guideline for monitoring MOAH in food and food contact materials has been based on chromatographic analysis and quantification as total mass fraction of MOAH and cut-off fractions of MOAH by integration of the hump for different molecular weight regions, resulting in quantifications based on the amount of Cx ring PAHs in mg/kg sample (**Table 2**) (Bratinova 2019). Commonly accepted analytical methods include off-line sample preparation or on-line LC-GC-FID. The method for MOAH analysis in different food matrices with cut-off fractions of MOAH

was questioned for its reliability and compatibility (Koster, Varela et al. 2020). The main issue out of many analytical challenges was that the synthetic hydrocarbon polyolefin oligomers, hydrogenated PAHs and other, naturally occurring, substances can co-elute and interfere with the analysis of the MOAH fraction, e.g. carotenoids in the food matrix (Koster, Varela et al. 2020). The carotenoid hump is visible between C<sub>35</sub>-C<sub>40</sub> (total number of carbon) in the chromatogram of MOAH in infant formula samples. Given the importance of analytical reliability for the exposure assessment, the preparation of food samples and the treatment of the food matrices are to be further amended and validated.

**Table 2.** MOAH characterization guideline in food and food contact materials according to JRC report (Bratinova 2019). Symbol “n” means the total number of carbon atoms on both the side chain and the aromatic moiety.

<b>MOAH:</b>
Total MOAH
MOAH $\geq$ n-C <sub>10</sub> to $\leq$ n-C <sub>16</sub>
MOAH $>$ n-C <sub>16</sub> to $\leq$ n-C <sub>25</sub>
MOAH $>$ n-C <sub>25</sub> to $\leq$ n-C <sub>35</sub>
MOAH $>$ n-C <sub>35</sub> to $\leq$ n-C <sub>50</sub>

## 5. Mixture effects

Mixture effects should also be addressed in the hazard assessment of MOAH. The mixture effect of fractionated PAH extracts from jute batching oil (JBO-P) based on ring number was demonstrated in the mouse skin painting study (Agarwal, Shukla et al. 1988). No skin tumor



formation was observed upon 40-day dermal exposure to the individual fractions including “PAH-free fraction”, “2- and 3-ring PAH fraction” and “more than 3-ring PAH fraction”. Surprisingly under the same experimental conditions, all mice showed skin tumors upon 40-week combined dermal exposure to the three fractions. Additionally, the carcinogenic effect was also assessed for each fraction with treatment of a tumor promotor 12-o-tetradecanoyl-phorbol-13-acetate (TPA). Only the “more than 3-ring PAH fraction” induced tumors in all animals with TPA treatment upon 14-week exposure while the other two fractions were negative for tumor initiating potential. Altogether, it suggests that the “more than 3-ring PAH fraction” is potentially carcinogenic in the presence of a tumor promotor. Furthermore, the “less than 3-ring fractions” are not potentially carcinogenic themselves but may act as tumor promoters. However, little is known for the mixture effect for genotoxicity and developmental toxicity. Future focus should also emphasize the potential synergistic and antagonistic effect in the mixture of non-substituted and alkyl-substituted PAHs and petroleum substances for their genotoxicity and developmental toxicity.

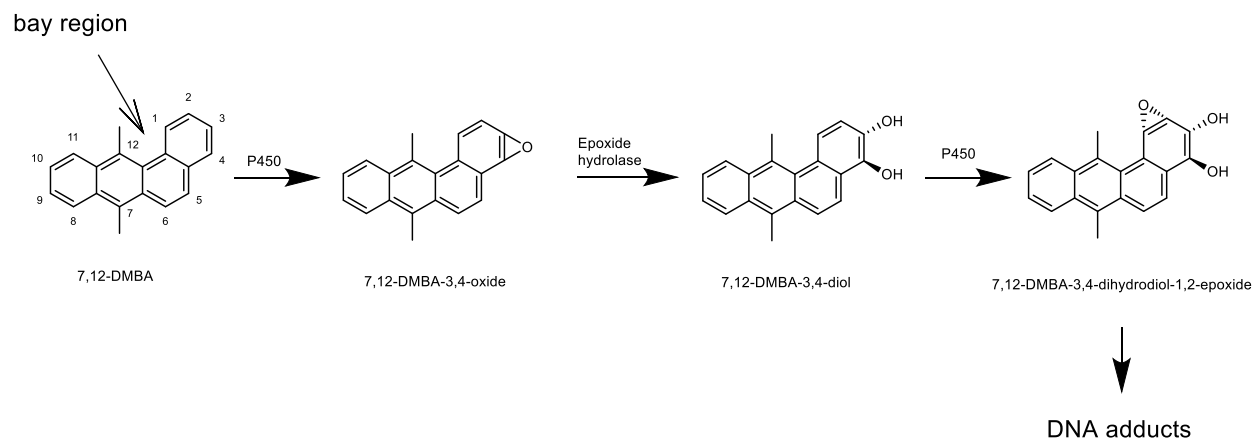
## **6. Use of new approach methodologies (NAMs)**

The European Chemicals Agency (ECHA) proposed a broad concept of New Approach methodologies (NAMs) in regulatory science for hazard assessment (ECHA 2016). The NAMs include “in silico approaches, in chemico and in vitro assays, as well as the inclusion of information from the exposure of chemicals in the context of hazard assessment” (ECHA 2016). Especially the hazard identification and characterization can be performed based on in vivo toxicity data. Thus, modern hazard assessment may be based on the NAM-data obtained from in vitro testing, and in silico models, including data from omics-based endpoints. In particular, the use of in silico alternatives was addressed that can connect to the modern technologies and “big data”, including for example Quantitative Structure Activity Relationships (QSAR), use of the threshold of

Toxicological Concern (TTC) and Read-Across. The next sections discuss some of the aspects related to use of NAM for hazard and risk assessment of alkylated PAHs and/or MOAH.

## **6.1 Metabolism of alkyl substituted PAHs**

The present thesis provided data on oxidative metabolism of aromatic hydrocarbons ranging from 2-ring to 5-ring with non-branched side chains varying from methyl- to dodecyl-substitution using an in vitro approach (**Chapter 3 and Chapter 4**). In line with the hypothesis, the oxidative metabolism of the alkyl substituted aromatic hydrocarbons shifted to the aliphatic side chain at the cost of aromatic ring oxidation. Although it was observed in the present thesis that a multi-branched PAH (10-methyl-9-ethyl-phenanthrene) (**Chapter 3**) showed efficient side chain oxidation over aromatic ring oxidation, it remains to be elucidated if the metabolic shift applies for other multibranched PAHs. Some evidence suggested multi-branched alkylated PAHs such as 7,12-DMBA, 1,4- and 4,10-dimethylphenanthrene being active skin tumor initiators (Wislocki, Gadek et al. 1980, LaVoie, Tulley-Freiler et al. 1981). As an example, genotoxicity and carcinogenicity of 7,12-dimethylbenz[a]anthracene (DMBA) upon bioactivation to an ultimate mutagenic bay-region dihydrodiol-epoxide by cytochrome P450 enzymes was reported (**Figure 5**) (Wislocki, Gadek et al. 1980, Shimada and Fujii-Kuriyama 2004, Shi, Krsmanovic et al. 2011). The reported bioactivation pathway is in line with the proposed metabolic pathways for the genotoxicity of the selected alkyl substituted phenanthrene and benzo[a]pyrene in the present study (**Figure 3**). Therefore, it is of high importance to further investigate the metabolic fate and its potential consequences for the resulting toxicities of multi-branched alkylated PAHs using in vitro based NAM approaches as the ones applied in the present thesis.



**Figure 5.** Reported bioactivation pathway of 7,12-DMBA to a diol-epoxide ultimate carcinogen (Shimada and Fujii-Kuriyama 2004)

The incubation of the selected model compounds with HLM and RLM in the present thesis provided information on how alkyl substitution may affect the metabolic pattern of aromatic hydrocarbons and their relative chances on bioactivation and excretion. In addition to providing information on molecular docking between alkyl substituted aromatic hydrocarbons and cytochrome P450 enzymes, more research on translation of the in vitro findings to the in vivo situation would be logical to consider.

## 6.2 Relevant toxicity of alkyl substituted PAHs

Due to the potential health concerns of MOAH, and the endless number of potential MOAH samples with different constitution, it is of urgent importance to apply NAM alternative testing strategies in testing of the alkylated aromatic hydrocarbons and MOAH under REACH (Registration, Evaluation, and Restriction of Chemical) legislation. Although the present thesis provided data on the effect of alkyl substitution on the metabolism of PAHs characterizing the influence of the alkylation on the potential balance between bioactivation and detoxification,

further toxicity studies on the effect of the alkylation on the ultimate toxicity of alkylated PAHs using validated bioassays are urgently required.

The effect of methyl substitution on the mutagenicity of phenanthrene and benzo[a]pyrene was investigated in **Chapter 3** and **Chapter 4**. In line with the hypothesis, the mutagenicity observed in 1-methyl- and 9-methyl phenanthrene was associated with the formation of the dihydrodiol that may be further metabolized to the ultimate mutagenic dihydrodiol-epoxide at the “fake” bay region (**Figure 3**). The observed mutagenicity of methylated benzo[a]pyrene did not necessarily relate to the hypothesized theory of the extra “fake” bay regions because more than one mode of action may be involved in the mutagenicity of these PAHs (**Figure 3**). The relevant metabolic pathways for genotoxicity and carcinogenicity of methyl substituted benzo[a]pyrene include the dihydrodiol-epoxide pathway, formation of a 4,5-oxide metabolite and/or a side chain oxidation/sulfation pathway. The dominant underlying metabolic pathway for genotoxicity and carcinogenicity of methyl substituted benzo[a]pyrene is still to be elucidated. In addition to the monomethyl substitution of PAHs, the dimethyl- and other multibranched alkylated PAHs are also of interest for further investigation on their mutagenic potential and underlying metabolic pathways in validated chemical- and bio- assays. Validated in vitro testing strategies for genotoxicity include the bacterial reverse mutation test and mammalian cell line based tests such as the chromosome aberration test, the micronucleus test, the gene mutation test using the *Hprt*, *xprt* and thymidine kinase genes (ECHA 2018).

Historical data on dermal carcinogenicity suggested that some methyl substituted PAHs show tumor initiating activity in vivo (**Table 2 Chapter 1**). Also little is known on the effect of the alkyl substitution of PAHs on carcinogenicity upon oral exposure. Chronic toxicity and carcinogenicity of chemicals are typically assessed by in vivo studies according to OECD Test Guideline (TG) 453

that require large number of animals (OECD 2018). EFSA addressed additional considerations for the carcinogenicity testing in rodents to food/feed (EFSA 2013). In vivo testing for carcinogenicity is time-consuming (more than two years) and expensive and it is impossible to perform for the risk assessment of MOAH as MOAH are not a chemically defined substance or mixture and may vary from one sample to another. An alternative testing strategy for carcinogenicity in vitro, the so-called cell transformation assay, was proposed by OECD but is not yet generally accepted (OECD 2007). Such a mammalian cell based assay may be of use for the carcinogenicity screening of alkylated PAHs. In previous studies already concentration response curves were obtained for some of the “naked” PAHs in this cell transformation assay using the BHK 21/CL 13 cell line (Greb, Strobel et al. 1980). The observed in vitro concentration response curves may be further applied in QIVIVE approaches to predict in vivo genotoxicity and carcinogenicity in a quantitative way.

With respect to the endpoint developmental toxicity it is of interest to note that recent studies on a series of PAH-containing extracts from petroleum substances, including mineral oil samples (with a systematic variation in their PAH content), showed that these complex substances were able to induce concentration-dependent in vitro developmental toxicity in the EST to an extent that appeared proportional to their level of 3-7 ring PAHs (Kamelia, Louisse et al. 2017, Kamelia, Louisse et al. 2018, Kamelia, Brugman et al. 2019, Kamelia, de Haan et al. 2019). The effect of alkyl substitution of 3-7 ring PAHs on their developmental toxicity is of interest for the hazard assessment of petroleum substances including MOAH. In the ZET there appeared to be a correlation with the level of 3-5 ring PAHs (Kamelia, Brugman et al. 2019). The application of these NAMs for testing the developmental toxicity hazards of petroleum substances may also prove to be of use for evaluation of alkylated PAHs (Kamelia 2019). Recent results of testing phenanthrene, benz[a]anthracene benzo[a]pyrene and their methyl substituted analogues in the

ZET suggested that the position of the methyl substitution can substantially influence the in vitro developmental toxicity (Wolińska, Brzuzan et al. 2011, Schrlau, Kramer et al. 2017, Jing Fang 2021).

Considering the testing of naked and alkylated PAHs in in vitro bioassays it is of importance to note that bioactivation may be required. This holds not only for genotoxicity but also for their developmental toxicity. Thus testing in the presence of S9 metabolic activation is not only the Ames test, but also coupling of the EST to an exogenous metabolic system is highly recommended for the toxicity evaluation of alkylated PAHs. To what extent the metabolic activation in zebrafish embryo's in the ZET already adequately reflects the metabolic activation required for developmental toxicity remains to be fully established, although there already appears to be a good correlation between the in vitro potency ( $BMC_{50}$ ) in the ZET and the in vivo  $BMDL_{10}$  induced by PAC-containing petroleum substances ( $R^2=0.80$  for increased resorption;  $R^2=0.91$  for live fetuses/litter;  $R^2=0.35$  for fetal body weight) (Kamelia 2019). Studies on the in vitro developmental toxicity of benzo[a]pyrene in the EST however, pointed out that for the EST an exogenous metabolic activation system would be essential, as benzo[a]pyrene which is known to be an in vivo developmental toxin appeared to test negative in the EST while its 3-OH metabolite tested positive. This knowledge was applied for a NAM in the present thesis where the in vivo developmental toxicity of benzo[a]pyrene was predicted by QIVIVE based on the concentration response curve for 3-hydroxy-benzo[a]pyrene in the EST and a PBK model for benzo[a]pyrene kinetics in rats that predicted also plasma and tissue levels of 3-hydroxy-benzo[a]pyrene (**Chapter 5**). The proof of principle thus provided in the present thesis may point at the potential to use this NAM to predict the in vivo developmental toxicity of other PAHs including methylated analogues. To this end also the underlying bioactivation pathway of prenatal developmental toxicity of alkyl substituted PAHs

is to be further investigated. Based on the 3-hydroxy-benzo[a]pyrene bioactivation pathway for benzo[a]pyrene (**Figure 3**), metabolism may also play a role in the developmental toxicity of short alkyl side chain substituted PAHs, a topic that remains to be elucidated. The developmental toxicity of some non-substituted and alkyl-substituted PAHs such as for example dibenz[a,h]anthracene (DBA) for which bioactivation is not required (Kamelia, de Haan et al. 2020) may also be worth further investigation.

### **6.3 PBK modeling-facilitated QIVIVE**

The concept of PBK model facilitated QIVIVE may also be of interest to be applied in the in vivo prediction for genotoxicity or even carcinogenicity of methylated benzo[a]pyrenes. The determined kinetic parameters for metabolism of benzo[a]pyrene and its methylated analogues in vitro (**Chapter 4**) could be applied in PBK models to predict the blood concentration of benzo[a]pyrene or its methylated analogues and their relevant metabolites. As a starting point, a sufficiently validated QIVIVE approach for genotoxicity or carcinogenicity of benzo[a]pyrene is to be developed in mammalian species. The well-validated PBK model of benzo[a]pyrene with a sub-model of 3-hydroxy-benzo[a]pyrene (**Chapter 5**) can serve as a basis for the development of the PBK model for benzo[a]pyrene with a submodel for (+) anti-benzo[a]pyrene-7,8-dihydrodiol-9,10-epoxide (BPDE) (the ultimate genotoxic carcinogen). The PBK model for benzo[a]pyrene with a sub-model for BPDE could be possibly validated with the in vivo time dependent kinetic data in mammalian species. The obtained concentration response curves for genotoxicity and carcinogenicity from the mammalian cell based in vitro testing systems (Section 6.2) can subsequently be translated by the validated PBK model of benzo[a]pyrene with a sub-model for BPDE into in vivo dose response curves using a reverse dosimetry approach that can be ultimately evaluated by in vivo dose response for genotoxicity or carcinogenicity, when available, to set a

proof of principle. Once shown valid for benzo(a)pyrene the approach could also be applied for its analogues without a need for in vivo data.

In a similar way, the concept of PBK model facilitated QIVIVE for prediction of in vivo developmental toxicity may also be applicable to other PAHs for which the in vivo dose response data are not available. The current PBK model facilitated reverse dosimetry of benzo[a]pyrene for the prediction of in vivo developmental toxicity in rats via oral, intravenous and intratracheal exposure was well validated with in vivo kinetic and in vivo dose-response data (**Chapter 5**). The developed model provides a basis to predict in vivo developmental toxicity for other non-substituted ('naked') as well as substituted PAHs that induce developmental toxicity in the EST, either with or without bioactivation (Kamelia, de Haan et al. 2020). Following the reverse dosimetry approach, from the predicted in vivo dose response curve a predicted reference point (RP) for risk assessment such as a benchmark dose (BMD) could be obtained.

#### **6.4 Read-across**

Read-across, theoretically accepted as an alternative testing approach by ECHA, can be used to predict a property or test outcome for a target substance on the basis of a property or test outcome for another structurally related source substance following certain rules (ECHA 2017). Risk assessment of some substances cannot be performed because the in vivo toxicity studies are not available to derive a RP to characterize the hazard. In this case, mode of action (MoA) based read-across could be applied to predict the RP of a target chemical from a structurally related source chemical with an available RP. In the risk assessment of genotoxic carcinogens, including the (alkylated) PAHs that raise such a concern, the Margin of Exposure (MOE) approach is commonly applied where the RP often refers to Benchmark dose level (BMDL<sub>10</sub>).



Previous studies have developed examples of using PBK model facilitated read-across to estimate BMDL<sub>10</sub> values for genotoxic carcinogens. Examples are the definition of a BMDL<sub>10</sub> values for the alkenylbenzenes apiol and elemicin, for which in vivo carcinogenicity data are unavailable, using PBK models to quantify differences in bioactivation and derive BMDL<sub>10</sub> values based on available data for the related compounds safrole (structural analogue for apiol), and estragole and methyleugenol (structural analogues for elemicin) (van den Berg, Punt et al. 2012, Alajlouni, Al\_Malahmeh et al. 2016, Rietjens and Punt 2017).

For complex and variable substances including the compounds that are represented as MOAH, read across from a structurally related analogue may prove too complicated. However, as a proof of principle the concept could be tested for methylated benzo[a]pyrenes using data available for benzo[a]pyrene itself and PBK models to predict the bioactivation of the analogues to the ultimate carcinogenic metabolite. A PBK modeling-based read across approach for estimation of BMDL<sub>10</sub> values for the carcinogenicity of methylated benzo[a]pyrene analogues may then be developed using the predicted level of formation of the ultimate carcinogenic metabolites, such as for example the dihydrodiol epoxide metabolites, as the basis for the read-across and adaptation of the BMDL<sub>10</sub> available for benzo[a]pyrene of 0.07 mg/kg bw per day (EFSA 2008) to a BMDL<sub>10</sub> for the respective analogues.

For the alkyl-substituted PAHs that induce developmental toxicity, the QIVIVE approach reported for benzo[a]pyrene (**Chapter 5**) may be extended to other substituted PAHs. The results of the present thesis already provide kinetic data for metabolism of the alkyl substituted benzo[a]pyrenes (**Chapter 4**) that could be applied in the respective PBK models

In summary, since it is impossible to characterize the hazard of MOAH since it is not a chemically defined substance or mixture, the data gap in toxicity testing of alkyl substituted PAHs and mineral

oil extracts is still to be filled. Some of the NAMs may be applied in future hazard assessment of the MOAH fraction and then drive the risk assessment of MOAH. In vitro bioassays are suggested to facilitate detection of hazards like genotoxicity and developmental toxicity of alkylated PAHs. The resulting concentration response curves for individual alkyl-substituted PAH obtained from in vitro bioassays could be translated via in silico PBK modeling facilitated QIVIVE into in vivo dose response curves (Wang, Rietdijk et al. 2021). Read across from non-substituted PAH to alkylated PAH may also be applicable via well validated PBK models. QSAR models may also be used to predict and assess the genotoxicity and developmental toxicity of the alkyl substituted PAHs (Benigni and Bossa 2019, Kamelia 2019). RPs could be derived from the predicted in vivo dose-response curves for alkyl substituted PAHs that can be subsequently used as a point of departure for the risk assessment of MOAH with consideration of the mixture effect under the Read Across Assessment Framework (RAAF) for multi-constituent substances and UVCBs (substance of Unknown or Variable composition, Complex reaction products and Biological materials) (ECHA 2017). Together with exposure assessment, it will improve the risk assessment of MOAH.

## Concluding remarks

- Short alkyl substitution ( $\leq C3$ ) to PAHs shifts metabolism to the alkyl side chain oxidation at the cost of aromatic ring oxidation.
- The metabolism is hampered with further elongation of the side alkyl chain of PAHs.
- Rate, regioselectivity and type of the P450 mediated metabolism of the non-substituted and alkyl-substituted aromatic hydrocarbons depends on species, as well as on the site and nature of the alkyl substituent.
- Methyl substitution of phenanthrene that introduces an additional “fake” bay region induces mutagenicity possibly via the dihydrodiol-epoxide pathway.
- Methyl substitution of benzo[a]pyrene that introduces additional “fake” bay region(s) may increase or decrease the mutagenic potential with multiple pathways likely contributing to the mutagenicity, such as the dihydrodiol-epoxide pathway, formation of a 4,5-oxide and/or side chain oxidation/sulfation.
- The developed in vitro-in silico QIVIVE approach for prediction of in vivo developmental toxicity of benzo[a]pyrene provides a proof of principle that may be extended to other PAHs including alkyl substituted PAHs and also to other toxicity endpoints.

Overall it is concluded that in vitro and in silico methodologies provide a useful tool to fill gaps in the toxicity data on alkyl substituted PAHs that may also prove to be of use for read across to MOAH.

## Reference

- Agarwal, R., Y. Shukla, S. Kumar and N. K. Mehrotra (1988). "Evaluation of carcinogenic effect of jute batching oil (JBO-P) fractions following topical application to mouse skin." Arch Toxicol **62**(6): 406-410.
- Alajlouni, A. M., A. J. Al\_Malahmeh, R. Kiwamoto, S. Wesseling, A. E. M. F. Soffers, A. A. A. Al-Subeihi, J. Vervoort and I. M. C. M. Rietjens (2016). "Mode of action based risk assessment of the botanical food-borne alkenylbenzene apiol from parsley using physiologically based kinetic (PBK) modelling and read-across from safrole." Food and Chemical Toxicology **89**: 138-150.
- Archibong, A. E., F. Inyang, A. Ramesh, M. Greenwood, T. Nayyar, P. Kopsombut, D. B. Hood and A. M. Nyanda (2002). "Alteration of pregnancy related hormones and fetal survival in F-344 rats exposed by inhalation to benzo(a)pyrene." Reprod Toxicol **16**(6): 801-808.
- Benigni, R. and C. Bossa (2019). "Data-based review of QSARs for predicting genotoxicity: the state of the art." Mutagenesis **34**(1): 17-23.
- Biedermann, M. and K. Grob (2009). "Comprehensive two-dimensional GC after HPLC pre separation for the characterization of aromatic hydrocarbons of mineral oil origin in contaminated sunflower oil." J Sep Sci **32**(21): 3726-3737.
- Bratinova, S. (2019). Guidance on sampling, analysis and data reporting for the monitoring of mineral oil hydrocarbons in food and food contact materials. J. R. Centre.
- Bui, Q. Q., M. B. Tran and W. L. West (1986). "A comparative study of the reproductive effects of methadone and benzo[a]pyrene in the pregnant and pseudopregnant rat." Toxicology **42**(2-3): 195-204.
- Carrillo, J. C., A. van der Wiel, D. Danneels, O. Kral and P. J. Boogaard (2019). "The selective determination of potentially carcinogenic polycyclic aromatic compounds in lubricant base oils by

the DMSO extraction method IP346 and its correlation to mouse skin painting carcinogenicity assays." Regul Toxicol Pharmacol **106**: 316-333.

Cavalieri, E., R. Roth, C. Grandjean, J. Althoff, K. Patil, S. Liakus and S. Marsh (1978). "Carcinogenicity and metabolic profiles of 6-substituted benzo[a]pyrene derivatives on mouse skin." Chem Biol Interact **22**(1): 53-67.

Concawe (1994). "The use of the dimethyl sulphoxide (DMSO) extract by the IP346 method as an indicator of the carcinogenicity of lubricant base oils and distillate aromatic extracts."

Concawe (1996). "Overview of the concawe middle distillate programme."

Concawe (2012). "Use of the modified Ames test as an indicator of the carcinogenicity of residual aromatic extracts ".

Concawe (2014). "Hazard classification and labelling of petroleum substances in the European Economic Area-2014."

ECHA (2016). New Approach Methodologies in Regulatory Science: 65.

ECHA (2017). Current status of regulatory applicability under REACH, CLP and Biocidal products regulations.

ECHA (2017). Read-Across Assessment Framework (RAAF). Considerations on multi-constituent substances and UVCBs.

ECHA (2018). "Three recently approved in vivo genotoxicity test guidelines."

EFSA (2008). "Polycyclic Aromatic Hydrocarbons in Food - Scientific Opinion of the Panel on Contaminants in the Food Chain." EFSA Journal **6**(8): 724.

EFSA (2012). "Scientific Opinion on Mineral Oil Hydrocarbons in Food." EFSA Journal **10**(6): 2704.

EFSA (2013). "Considerations on the applicability of OECD TG 453 to whole food/feed testing." EFSA Journal **11**(7): 3347.

Greb, W., R. Strobel and G. Röhrborn (1980). "Transformation of BHK 21/CL 13 cells by various polycyclic aromatic hydrocarbons using the method of styles." Toxicology Letters **7**(2): 143-148.

Heyst, A. V. (2019). Mineral oil migration from cardboard food contact materials: hazard identification and exposure assessment of the Belgian population. Brussel, Vrije Universiteit Brussel.

Ingram, A. J., D. V. Scammells and K. May (1994). "An investigation of the main mutagenic components of a carcinogenic oil by fractionation and testing in the modified Ames assay." J Appl Toxicol **14**(3): 173-179.

Iyer, R. P., J. W. Lyga, J. A. Secrist, 3rd, G. H. Daub and T. J. Slaga (1980). "Comparative tumor-initiating activity of methylated benzo(a)pyrene derivatives in mouse skin." Cancer Res **40**(4): 1073-1076.

Jing Fang, S. D., Peter J. Boogaard, Ivonne M.C.M Rietjens, Lenny Kamelia (2021). "Developmental toxicity testing of unsubstituted and alkylated 4- and 5-ring polycyclic aromatic hydrocarbons using the zebrafish embryotoxicity test." Submitted to Toxicology in Vitro.

Kamelia, L. (2019). The role of Polycyclic Aromatic Hydrocarbons in Developmental Toxicity of Petroleum Substances. Doctor, Wageningen University.

Kamelia, L., S. Brugman, L. de Haan, H. B. Ketelslegers, I. Rietjens and P. J. Boogaard (2019). "Prenatal developmental toxicity testing of petroleum substances using the zebrafish embryotoxicity test." ALTEX **36**(2): 245-260.

Kamelia, L., L. de Haan, H. B. Ketelslegers, I. Rietjens and P. J. Boogaard (2019). "In vitro prenatal developmental toxicity induced by some petroleum substances is mediated by their 3- to 7-ring PAH constituent with a potential role for the aryl hydrocarbon receptor (AhR)." Toxicol Lett **315**: 64-76.

Kamelia, L., L. de Haan, B. Spenkelink, B. Bruyneel, H. B. Ketelslegers, P. J. Boogaard and I. Rietjens (2020). "The role of metabolism in the developmental toxicity of polycyclic aromatic hydrocarbon-containing extracts of petroleum substances." J Appl Toxicol **40**(3): 330-341.

Kamelia, L., J. Louisse, L. de Haan, A. Maslowska-Gornicz, H. B. Ketelslegers, A. Brouwer, I. Rietjens and P. J. Boogaard (2018). "The Role of Endocrine and Dioxin-Like Activity of Extracts of Petroleum Substances in Developmental Toxicity as Detected in a Panel of CALUX Reporter Gene Assays." Toxicol Sci **164**(2): 576-591.

Kamelia, L., J. Louisse, L. de Haan, I. Rietjens and P. J. Boogaard (2017). "Prenatal developmental toxicity testing of petroleum substances: Application of the mouse embryonic stem cell test (EST) to compare in vitro potencies with potencies observed in vivo." Toxicol In Vitro **44**: 303-312.

Koster, S., J. Varela, R. H. Stadler, J. Moulin, C. Cruz-Hernandez, J. Hielscher, C. Lesueur, J. Roiz and H. Simian (2020). "Mineral oil hydrocarbons in foods: is the data reliable?" Food Addit Contam Part A Chem Anal Control Expo Risk Assess **37**(1): 69-83.

LaVoie, E. J., L. Tulley-Freiler, V. Bedenko and D. Hoffman (1981). "Mutagenicity, tumor-initiating activity, and metabolism of methylphenanthrenes." Cancer Res **41**(9 Pt 1): 3441-3447.

Mackerer, C. R., L. C. Griffis, J. S. Grabowski, Jr. and F. A. Reitman (2003). "Petroleum mineral oil refining and evaluation of cancer hazard." Appl Occup Environ Hyg **18**(11): 890-901.

Marie, C., M. Bouchard, R. Heredia-Ortiz, C. Viau and A. Maitre (2010). "A toxicokinetic study to elucidate 3-hydroxybenzo(a)pyrene atypical urinary excretion profile following intravenous injection of benzo(a)pyrene in rats." J Appl Toxicol **30**(5): 402-410.

Moreau, M. and M. Bouchard (2015). "Comparison of the kinetics of various biomarkers of benzo[a]pyrene exposure following different routes of entry in rats." Journal of Applied Toxicology **35**(7): 781-790.

OECD (2007). Detailed Review Paper on Cell Transformation Assays for Detection of Chemical Carcinogens.

OECD (2018). Test No. 453: Combined Chronic Toxicity/Carcinogenicity Studies.

Rietjens, I. M. C. M. and A. Punt (2017). The use of physiologically based kinetic (PBK) models in the risk assessment of plant genotoxins.

Rogan, E. G., A. Hakam and E. L. Cavalieri (1983). "Structure elucidation of a 6-methylbenzo[a]pyrene-DNA adduct formed by horseradish peroxidase in vitro and mouse skin in vivo." Chem Biol Interact **47**(1): 111-122.

Schrlau, J. E., A. L. Kramer, A. Chlebowski, L. Truong, R. L. Tanguay, S. L. M. Simonich and L. Semprini (2017). "Formation of Developmentally Toxic Phenanthrene Metabolite Mixtures by Mycobacterium sp. ELW1." Environ Sci Technol **51**(15): 8569-8578.

Shi, J., L. Krsmanovic, S. Bruce, T. Kelly, M. Paranjpe, K. Szabo, M. Arevalo, S. Atta-Safoh, F. Debelie, M. K. LaForce, J. Sly and S. Springer (2011). "Assessment of genotoxicity induced by 7,12-dimethylbenz(a)anthracene or diethylnitrosamine in the Pig-a, micronucleus and Comet assays integrated into 28-day repeat dose studies." Environ Mol Mutagen **52**(9): 711-720.

Shimada, T. and Y. Fujii-Kuriyama (2004). "Metabolic activation of polycyclic aromatic hydrocarbons to carcinogens by cytochromes P450 1A1 and 1B1." Cancer Science **95**(1): 1-6.

Standards, I. B. (1996). Determination of Polycyclic Aromatics in Unused Lubricating Base Oils and Asphaltene Free Petroleum Fractions - Dimethyl Sulfoxide Extraction Refractive Index Method.

Stansbury, K. H., J. W. Flesher and R. C. Gupta (1994). "Mechanism of aralkyl-DNA adduct formation from benzo[a]pyrene in vivo." Chem Res Toxicol **7**(2): 254-259.



van den Berg, S. J., A. Punt, A. E. Soffers, J. Vervoort, S. Ngeleja, B. Spenkelink and I. M. Rietjens (2012). "Physiologically based kinetic models for the alkenylbenzene elemicin in rat and human and possible implications for risk assessment." Chem Res Toxicol **25**(11): 2352-2367.

Wang, D., M. H. Rietdijk, L. Kamelia, P. J. Boogaard and I. Rietjens (2021). "Predicting the in vivo developmental toxicity of benzo[a]pyrene (BaP) in rats by an in vitro-in silico approach." Arch Toxicol **95**(10): 3323-3340.

Wislocki, P. G., K. M. Gadek, M. W. Chou, S. K. Yang and A. Y. Lu (1980). "Carcinogenicity and mutagenicity of the 3,4-dihydrodiols and other metabolites of 7,12-dimethylbenz(a)anthracene and its hydroxymethyl derivatives." Cancer Res **40**(10): 3661-3664.

Wolińska, L., P. Brzuzan, M. Wpzyń, M. Góra, M. K. Auczynski, P. Podlasz, S. Kolwicz and A. Piasecka (2011). "Preliminary study on adverse effects of phenanthrene and its methyl and phenyl derivatives in larval zebrafish, *Danio rerio*." Environmental biotechnology **7**: 26-33.



# **Chapter 7**

## **Summary**

Mineral oil aromatic hydrocarbons (MOAH) have been presented as a modern emerging food safety concern by the European Food Safety Authority (EFSA). MOAH is defined as a chromatographic fraction in the analysis of mineral oil hydrocarbons (MOH) in food and does not represent well defined substances or mixtures. The sources of foodborne MOAH include environmental contamination and intentional uses of mineral oils in consumer products or production processes. Some non-substituted PAHs are known to be genotoxic carcinogens and have been extensively studied, however the majority of the compounds represented by MOAH are highly alkylated aromatic hydrocarbons for which the toxicological data are scarce. Potential concerns for genotoxicity, carcinogenicity and developmental toxicity upon MOAH exposure have been raised. However, the lack of toxicological data on related alkyl substituted polycyclic aromatic hydrocarbons (PAHs) seriously hampers a proper hazard assessment and therefore challenges the risk assessment of MOAH.

The present thesis aims at (1) providing data on oxidative metabolism and resulting toxicities of a series of the selected non-substituted and alkyl-substituted aromatic hydrocarbons using in vitro assays and (2) developing a physiologically-based kinetic (PBK) modeling- facilitated quantitative in vitro-in vivo-extrapolation (QIVIVE) approach for prediction of in vivo toxicity of selected PAH. The latter is needed to define data for risk assessment as a proof of principle for using new approach methodologies (NAMs). It was hypothesized (1) that alkylated PAHs will be metabolized preferably on the alkyl side chain rather than on the condensed aromatic rings which can be expected to facilitate their excretion rather than their bioactivation to potentially DNA-reactive metabolites, and (2) that the presence of an additional bay region like aromatic motif introduced by methyl substitution may affect the genotoxic potential of the PAHs.

**Chapter 1** provided the background information of mineral oils that may be present in food and the concept of MOAH. The relevance to public health to the occurrences and the current risk assessment of MOAH were introduced. The aim and hypothesis of the thesis together with relevant methodologies for measurement of oxidative metabolism, mutagenicity and PBK modeling-facilitated QIVIVE were introduced.

**Chapter 2** tested the first hypothesis that, on thermodynamic grounds, alkyl substituents on PAH would be more readily undergo oxidative metabolism than the aromatic rings. The 2-ring aromatic compound naphthalene and a series of its alkylated analogues were used as model compounds. The oxidative metabolism of naphthalene and its methyl-, ethyl-, hexyl- and dodecyl- substituted analogues was studied in microsomal incubations with human liver microsomes (HLM) and rat liver microsomes (RLM) in vitro. The formed metabolites of the model compounds in the microsomal incubations resulting from cytochrome P450 mediated conversions were identified and quantified. In line with the hypothesis, it was shown that short ( $\leq C_2$ ) alkyl chain substitution of naphthalene shifts the metabolism in favor of side chain oxidation at the cost of aromatic ring oxidation. When the alkyl side chain of naphthalene is longer than 6 carbon atoms, the overall metabolism is seriously restricted with no metabolic conversion being observed for dodecylated naphthalene.

**Chapter 3** tested the hypotheses of shifting oxidative metabolism and the influence of additional bay-region like motif on mutagenicity using 3-ring phenanthrene and a series of its alkylated congeners as model compounds. The microsomal cytochrome P450 mediated metabolism of phenanthrene and its methyl-, ethyl-, methyl-ethyl-, hexyl- and dodecyl- substituted analogues was studied with HLM and RLM. In addition to oxidative metabolism, the mutagenicity of phenanthrene and some of its selected monomethylated analogues was tested using the reverse

mutation (Ames) assay. In line with hypothesis, the metabolism of short ( $\leq C3$ ) alkyl chain substituted phenanthrenes shifted to side chain oxidation at the cost of aromatic ring oxidation which was reduced. Elongation of the alkyl side chain reduced the overall metabolism of phenanthrene until no metabolic conversion was observed in dodecylated phenanthrene. Furthermore, the position of the alkylation was shown to affect not only the metabolism but also the resulting mutagenicity of phenanthrene. In line with hypothesis that a “fake” bay-region would influence the mutagenicity of phenanthrene, increasing mutagenicity was observed in cases where the alkyl substituent introduced an additional bay-region like structural motif, in spite of the extra possibilities for side chain oxidation.

**Chapter 4** tested the same hypotheses again using 5-ring benzo[a]pyrene (B[a]P) and its alkylated analogues as model compounds. Metabolism of B[a]P and its methyl-, hexyl-, and dodecyl-analogues was studied in microsomal incubations with HLM and RLM. B[a]P and four selected monomethylated analogues were tested for their mutagenicity in the Ames test. In line with the first hypothesis, the metabolism of methyl substituted B[a]P shifted to aliphatic side chain oxidation at the cost of aromatic ring oxidation. In line with the second hypothesis, methyl substitution influenced the mutagenicity of B[a]P. However, the methylation may appear to increase or decrease the mutagenicity of B[a]P, albeit to only a limited extent, and does not systematically reduce its mutagenicity in spite of the metabolic shift from aromatic to side chain oxidation.

**Chapter 5** provided a proof of concept for applying an in vitro – in silico approach for evaluating developmental toxicity of B[a]P. A PBK model of B[a]P with a sub-model for its main metabolite 3-OHB[a]P in rats was developed including the kinetic parameters derived from metabolic studies. The PBK model based predicted plasma concentrations of B[a]P and 3-OHB[a]P upon intravenous,

intratracheal and oral exposure were evaluated by comparison with literature available in vivo kinetic data. The validated PBK model was further used for reverse dosimetry translating in vitro concentration response data for 3OH-B[a]P obtained in the embryonic stem cell test (EST) to in vivo dose response curves for developmental toxicity of B[a]P upon single and repeated dose exposure via the oral and inhalation routes. The outcome of the predicted ED<sub>50</sub> of B[a]P was in line with the reported ED<sub>50</sub> from literature available in vivo dose response data, thereby showing the adequacy of the NAM.

**Chapter 6** summarized the main findings of the experimental chapters and provided future perspectives for the hazard assessment of MOAH. A systematic effect of alkyl substitution on metabolism of PAHs was demonstrated with the actual size of the effects varying with the alkyl chain length and the PAH and species studied. An overview of mutagenic potency of the tested non-substituted and alkyl-substituted PAHs as well as a discussion of the possible underlying metabolic pathways were provided. Challenges for future hazard assessment of MOAH were discussed and relate to (1) characterization of MOAH composition, (2) the role of biotransformation and bioactivation in the toxicity, (3) limitations of testing DMSO extracts to reflect the potential of MOAH, (4) matrix effects, (5) mixture effects, and (6) the use of new approach methodologies (NAMs).

Overall it is concluded that in vitro and in silico methodologies provide a useful tool to fill gaps in the toxicity data on alkyl substituted PAHs that may also prove to be of use for read across to MOAH.





**Appendix**

**Acknowledgement**

**Biography**

**List of Publication**

**Overview of completed training activities**

## Acknowledgement

My 4-year PhD journey is filled with enormous amounts of exciting, joyful, satisfactory moments. None of these moments and the completion of this thesis could have been achieved without the assistance from the following people.

I would like to express never enough appreciation to my promotors **Prof. dr. ir Ivonne Rietjens** and **Prof. dr. Peter Boogaard**. It is a great honor and pleasure working with both of you throughout my PhD project. Having the opportunity to do research on the emerging food safety topic of 'MOAH' fulfilled my passion and interests in chemistry, biology and public health. In spite of the endless failure and struggle of experiments in the beginning half year of my PhD, I was given enough patience and trust to challenge myself to be an independent and creative researcher. In the rest of my PhD journey, I enjoyed very much your inspiration, guidance, supervision and never ending support although I hardly express my happiness via smiles. Thanks to the well-known Ivonne's characters, I grew to be efficient, effective, logic, precise and direct step by step. Thanks to Peter for his lead in my network and knowledge expansion. I sincerely thank you both for seeing me and helping me in both research and soft skills towards a scientific career.

I would like to extend my sincere gratitude to Concawe, Operationeel Programma Kansen voor West II (EFRO) and China Scholarship Council (CSC) for funding my PhD project. Without the help of **Prof. dr. Albrecht Seidel** (Biochemical Institute for Environmental Carcinogens), my PhD thesis would never have completed in time because of his dedication in synthesis of very unique highly alkylated PAHs. Despite the fact that we never had the chance to meet in person, your strict attitude on science and in depth knowledge on PAHs have never stopped inspiring me. Thank you Albrecht for the lengthy but fruitful discussion and the critical feedback on my work. To **Dr. Juan-Carlos Carrillo** (Shell), thank you for passing your knowledge related to MOSH, MOAH and petroleum substances in every meeting that I enjoyed at Concawe, Shell or EFRO. Additionally, my gratitude extends to **Angelique Groot** (Charles River) for her help in solving the technical bottleneck of the bioassays used in my project.

The co-authors who contributed to my PhD study and publications are highly appreciated. Thank you **Dr. Sebas Wesseling** for always supporting me technically from my master thesis to my PhD thesis at TOX; I enjoyed working with you being my nice lab and cat buddy. To **Ben Bruyneel**, thank you for the serious and hilarious lab time and your expertise in GC-MS that continuously helped me even after you left TOX. To **Maartje Rietdijk**, thank you deeply for your intelligence, the always pleasant discussion, the generous share of your knowledge in PBK modelling and being my buddy in the cell lab. Furthermore, I would like to specially thank my students who shared co-authorship in my chapters including **Annemarijn Brandenburg**, **Effimia Kiachaki**, **Eleni Pardali**, **Jeroen Pool**, **Lulu Wang** and **Viktoria Schramm** for their hard work in lab.

I would like to also acknowledge the opponents in my thesis committee **Dr. J. Louisse, Dr. J.C. Carrillo Palaez, Prof. dr. A.A. Koelmans** and **Prof. dr. H. van Loveren** for taking time to evaluate this thesis with positive feedback.

I'm grateful to our PAClub buddies including **Jing Fang, Maartje Rietdijk** and **Lenny Kamelia** (organizer) who study PACs related topics. Thank you all for the positive discussion, suggestions and inspirations in our regular joint project meeting. Special thanks to Jing and Maartje for your company and help in lab, and I enjoyed so much our talks and the incredible food made by Maartje. To Lenny, thank you for training me for the EST with your excellent skills in the assay and sharing your knowledge on PAHs. I enjoyed our lab talks from research to career. It also reminds me of our great time at Concawe followed with a beer session in Brussels. Our tradition: one publication, one prosecco! Thank you again PAClub buddies for the beautiful memories.

I would like to thank all my colleagues at WUR. **Eric Cuipers** (WFSR), I cannot thank you enough for your involvement in my master internship, for teaching me all the living skills and being my friend. **Dr. Jochem Louisse** (WFSR), thank you for tutoring in my MSc thesis on PBK modelling that helped me a lot, being my MSc internship coordinator, being caring and warm to me. Thank you for always being there. **Vesna Prsic** (VLAG), thank you for listening and helping me in my hardest time of PhD and spending beautiful time together in the TOX-PhD trip in Japan. I would like to first heartfully thank the TOX staffs **Bert, Hans** (van den Berg), **Laura, Sebas** and **Wouter** who generously helped me in the lab growing from a dummy to an experienced researcher from master to PhD, and it has been a pleasure working with you in the practical supervision. **Nico**, thank you for your humor and interests in my topic. **Hans** (Bouwmeester) and **Nynke**, thank you for seeing me as a competent researcher and being impactful colleagues. **Carla, Gerda, Letty** and **Lidy**, thank you for helping arranging administrative work and taking care. **Jing and Wisse**, thank you for your strong support being my amazing paranymphs and office mates. I enjoyed the cakes (especially the 'red celery' cake that impressed me) you both made and the always nice office chat. Appreciation also goes to more of my room 4038 office mates **Alexandra, Bohan, Edith, Felicia, Isaac** for the nice office environment. Thank you the TOX-angle music band that include **Lenny** (Guitar and singer), **Ignacio** (Guitar), **Shuo** (Drummer), **Miaoying** (Egg? lol) and **Koen** (Bass) for the beautiful musical (of course also nice beers) experiences allowing me play accordion again. Furthermore, my gratitude extend to my colleagues at TOX-PhDs for the wonderful memories of lab trips, PhD trip and celebration events such as birthday, Sinterklaas, Christmas and Spring Festival. Thank you **Annelies, Akanksha, Artem, Aziza, Biyao, Diana, Diego, Frances, Gorgia, Ghaliya, Hugo, Ixchel, Jia, Jiaqi, Jin, Jingxuan, Katherina, Katja, Kornphimol, Liang, Lu, Marta, Mebrahtom, Mengying, Menno, Merel, Nina, Qianrui, Qiuhui, Shensheng, Shivani, Shuo, Suparmi, Tessa, Tien, Thijs, Veronique, Weijia, Xiyu, Xukun, Yasser and Yiming** who have been really nice and supportive colleagues and friends. I would like to also thank my other

students **Romy, Yimin, Jeroen** (Berkvens) for working with me in my PhD or other project. I wish you all the best!

I would like to also thank my friends for their support during my PhD journey. **Lintianxiang, Zhan, Zhuang** and **Zulin** thank you for being there no matter if I experienced sadness or happiness, and I enjoyed our dinner and gym time. Thank you, **Jing, Qiuhui** and **Xujun** for your help and memories of travels, food and laughs. **Le, Lili, Mingzhao, Shuang** and **Ziying**, I appreciate our friendship since our MSc in Wageningen. My sincere gratitude also extends to **Arie, Baojian, Bin** (Bao), **Jingyan, Lei** (Ji), **Liangzi, Mutian, Miaoying, Mengying, Qianrui, Ru** (Tian), **Ouyang, Shensheng, Suyeon** and **Yechao** for being my friends who created wonderful memories in my PhD life. **Mingjing**, thank you for designing the cover in the middle of your busiest time of work. My sincere appreciation also extend to **Prof. Xiurong Wang, Dr. Huiping Fan** and **Xiaoshu Huang** who have enlightened me in science during my undergraduate study in Zhengzhou.

最后，我想给我挚爱的父母对我博士和人生的支持以最大的感谢。谢谢爸妈从呼和浩特，到郑州，再到瓦赫宁根一路以来对我每一个决定的支持，理解和牺牲。感谢你们给予我的一切。谨以此书献给我的父亲王谦和母亲刘玉英，爱你们。(Finally, I would like to give the biggest thank to my beloved parents for their supports in my PhD and my life. Thank you for your supports, understanding and sacrifices for every decision I made along the journey from Hohhot to Zhengzhou to Wageningen. Thank you for everything. This book is dedicated to my father Qian Wang and my mother Yuying Liu, with love.)

## **Biography**

Danlei was born on 21<sup>th</sup> September 1992 in Hohhot, Nei Mongol, China. In 2015, Danlei received her Bachelor of Engineering in Food Science and Engineering from Henan Agricultural University (HAU). During her undergraduate study, she did her internship in analytical chemistry at Modern Laboratory Technique Center of HAU. In August 2015, she moved to the Netherlands to follow a master program in Applied Food Safety at Wageningen University and Research (WUR), partly supported by the Holland Scholarship. During her MSc study, she did her thesis entitled “Metabolism and biological effects of imperatorin and risk assessment” at TOX-WUR and her internship entitled “Novel approaches study on the authenticity and safety of gutter oil” at BU Authenticity and Bioassays of Wageningen Food Safety Research (WFSR). After her MSc study, she started her PhD at TOX-WUR with a research topic entitled “Risk assessment on mineral oil aromatic hydrocarbon (MOAH), a novel emerging issue in food safety” in collaboration with Concawe and Operationeel Programma Kansen voor West II (EFRO) also funded by China Scholarship Council (CSC). Danlei has followed the postgraduate education in toxicology (PET) that will allow her to be registered as an European Registered Toxicologist (ERT) after the completion of her PhD study. Currently, Danlei is working as a postdoctoral researcher at TOX-WUR, Wageningen, The Netherlands.

## List of Publication

Wang D., Bruyneel, B., Kamelia, L., Wesseling, S., Rietjens, I.M.C.M., Boogaard, P.J. (2020). In vitro metabolism of naphthalene and its alkylated congeners by human and rat liver microsomes via alkyl side chain or aromatic oxidation. *Chemico-Biological Interactions*, 315: 108905.

Wang D., Rietdijk H. M., Kamelia L., Boogaard, P.J., Rietjens, I.M.C.M. (2021). Predicting the in vivo developmental toxicity of benzo[a]pyrene (B[a]P) in rats by an in vitro-in silico approach. *Archives of Toxicology*, 95: 3323-3340.

Wang D., Schramm V., Pool J., Pardali E., Brandenburg A., Rietjens, I.M.C.M., Boogaard, P.J. (2022). The effect of alkyl substitution on the oxidative metabolism and mutagenicity of phenanthrene. (Submitted to *Archives of Toxicology*)

Wang D., Groot A., Seidel, A., Wang L., Kiachaki E., Boogaard, P.J., Rietjens, I.M.C.M. (2022) The influence of alkyl substitution on the in vitro metabolism and mutagenicity of benzo[a]pyrene. (In preparation)

## **Overview of completed training activities**

### **Discipline specific activities**

Molecular Toxicology	PET	2018
Mutagenesis and Carcinogenesis	PET	2019
Toxicogenomics	PET	2019
Cell Toxicology	PET	2019
Pathobiology	PET	2019
Laboratory of Animal Science	PET	2019
Organ Toxicology	PET	2020

### **Conferences**

60<sup>th</sup> Annual meeting Society of Toxicology (SOT), poster, virtual, 2021

56<sup>th</sup> congress of the European Societies of Toxicology (EUROTOX), poster, Virtual, 2021

### **General courses**

VLAG PhD week	VLAG	2018
The essentials of scientific writing and presentation	WGS	2018
Supervising BSc & MSc thesis students	WGS	2019
Introduction to R	VLAG	2019
Applied statistics	VLAG	2019
Mobilizing your scientific network	WGS	2021
Scientific publishing	WGS	2021

### **Other activities**

Preparation of research proposal	TOX	2018
PhD study tour to Japan	TOX	2018
Scientific presentations	TOX	2018-2021
Environmental toxicology	TOX	2018
Epidemiology and public health	HNE	2018

Approved by the graduate school VLAG

## **Colophon**

The research described in this thesis were conducted with a collaborative project of Wageningen University with Concawe (Project No. 201700093), Operationeel Programma Kansen voor West II (EFRO) (Project No. KVV- 00181) and China Scholarship Council (CSC) (No. 201807720073 to Danlei Wang).

Financial support from Wageningen University for printing this thesis is gratefully acknowledged.

Cover design: Mingjing Li & Danlei Wang

Printed by ProefschriftMaken || [proefschriftmaken.nl](http://proefschriftmaken.nl)



